THE UNIVERSITY
of EDINBURGH

THE UNIVERSITY *of* EDINBURGH
Edinburgh Medical School

Biomedical Sciences

Investigating factors that can influence the rate of neuromuscular junction degeneration in injury and disease

Alannah Jane Mole

A thesis submitted for the degree of PhD

The University of Edinburgh

2021

Declaration

I declare that work presented within this thesis is entirely my own, unless otherwise stated in the text, and has not been submitted for any other degree or qualification.

Alannah Jane Mole

Acknowledgements

There are many people that I would like to acknowledge for their support, advice and guidance throughout my PhD. First and foremost, I would like to thank my supervisor, Dr. Lyndsay Murray. Lyndsay has been an incredible role model and mentor, and has always supported me and made me feel like a valued member of her team. My inspiration to pursue a PhD was founded in the Murray lab, and I am grateful to her for helping me reach this point, and for providing invaluable feedback and opportunities along the way. With Lyndsay's support, I secured my studentship, the award of which and for additional associated opportunities, I would like to thank the Anatomical Society. I also thank other members of my thesis committee, Professor Richard Ribchester and Dr. Karen Smillie, for their time and interest in my work. Similar thanks are extended to Dr. Kosala Dissanayake for her assistance.

I thank current and previous members of the Murray lab for their support, both professionally and personally. Special thanks to Natalie Courtney for inspiring me to pursue a PhD, and for her support throughout. Thanks also to Rachel Kline for her help with proteomics, and for her unforgettable company at conferences. To current members of the Murray lab - Laura, Nithya and Vicky - I thank you for your support along the way. I also thank members of the Paxton Lab who have completed our amazing office group: particular thanks to Jeremy for his unwavering support, and also to Hamad, Christina and Bastiaan. I have made friends for life in our office, and cannot thank you all enough - it would not have been the same without you! I would additionally like to thank members of the Gillingwater lab; in particular, Rachel, Dinja and Leire for their help. I also recognise the hard work and patience of technical staff.

Finally, I thank all of my friends and family, who have wholeheartedly supported my endeavours and shown great interest in my work. To my mum and dad, who have always encouraged me to follow my ambitions and provided me with so many opportunities. Also, to my sister, Amy, for keeping me sane throughout. I thank you all for supporting me, and for helping me to keep calm in the tough times, and to celebrate the good!

Abstract

Axonal and synaptic degeneration occur in response to nerve injury and during neurodegenerative disease. Traumatic nerve injury leads to rapid fragmentation of the distal axon and loss of synaptic terminals in a process known as Wallerian degeneration (WD). This is morphologically distinct from some motor neuron diseases, like Spinal Muscular Atrophy (SMA), where axons gradually retract, or die-back, from the motor endplate. Identifying and understanding factors that can influence the rate of degeneration is of significant clinical and biological importance, to facilitate our knowledge of the mechanisms of neurodegeneration and to aid in the identification of novel therapeutic targets. Factors that can change the speed of axonal and synaptic breakdown are interesting, as targeting these could represent an approach to slow or prevent breakdown in disease. The work contained within this thesis aims to identify factors that can alter the rate of synaptic degeneration in morphologically distinct types of synaptic degeneration, including following injury, during disease and during postnatal development. Using an *ex vivo* model of peripheral nerve injury, it is apparent that synaptic withdrawal is slower during early postnatal development, and that this delay is progressively lost over time. For example, significantly more neuromuscular junctions (NMJs) remain fully occupied in the cranial muscle preparations at postnatal day (P) 15 than P25. Intermuscular variability was also found to be a feature of WD, with less synaptic retraction evident in the abdominal preparations compared to cranial muscles. Importantly, differences in synaptic responses to injury were not consistent with patterns of neuromuscular vulnerability that have been previously described in mouse models of SMA, which is caused by a lack of survival motor neuron protein (Smn). To further investigate the relationship between SMA and WD, nerve injury was induced in preparations from the $Smn^{2B/-}$ mouse model of SMA. In a disease-resistant muscle (rostral band of levator auris longus), where there is minimal denervation, the level of synaptic loss in response to injury is similar to wild-type, suggesting that loss of Smn alone is not sufficient to influence rates of WD, suggesting that WD is Smn-independent. However, in a disease-vulnerable muscle with ongoing degeneration (transversus abdominis), the level of synaptic loss in response to injury is significantly increased, with the

percentage of denervated endplates increasing by 33% following injury. Thus, the presence of dying-back pathology appears to accelerate synaptic loss. Next, analysis of two independent proteomic datasets highlighted that there are changes in mitochondrial proteins during postnatal development that correlate with increases in synaptic vulnerability following injury during this time frame. Expanding this analysis to assess mitochondrial-associated protein levels and mitochondrial DNA levels in a range of different muscles revealed that although there are global changes in mitochondrial proteins across development, complex I levels do not correlate with differences in the synaptic response to injury. There is evidence, however, that increases in complex I in nerve may underlie intermuscular differences. The final part of this work was to determine whether reductions in P53, a factor that is involved in cell death processes, could alter the rate of synaptic loss under different scenarios. Application of the *ex vivo* model, and immunohistochemical and transcriptional analysis in an inducible P53-knockout mouse model demonstrated that postnatal reduction in P53 has no effect on the rate of synaptic loss following injury, during a die-back, or during development, suggesting P53-independence. Overall, the expanded *ex vivo* model and workflows described here represent powerful tools with which to study factors or pathways that can influence the rate of synaptic degeneration under different physiological scenarios. This will provide insight into mechanistic commonalities in synaptic degeneration that could ultimately facilitate the identification of a common therapeutic target in a range of neurodegenerative conditions.

Lay Abstract

Motor neurons are the wires of the body that send signals that arrive in the spinal cord from the brain to muscles to instruct them to move. If these wires become damaged, either by injury or in disease, then these signals are interrupted, and communication breaks down. When wires are cut or damaged, they break down very quickly. However, in diseases, like some motor neuron diseases, wires pull away gradually from the muscle without breaking up, almost as if they are being reeled back in. Although we know that these types of breakdown look very different under the microscope, it is unclear how the processes that regulate breakdown relate to each other. This work aims to better understand this relationship and identify factors that can influence the speed of breakdown in different scenarios. Factors that can change the speed of breakdown are interesting, as targeting these could represent a treatment to slow or prevent breakdown in disease. Here, I firstly expanded an experimental model that allows us to take different muscles and the wires that connect them from mice, and artificially maintain them. To isolate the muscle from the body, the wire must be cut, thereby mimicking an injury. I found that wire breakdown was much slower in very young mice compared to adults. However, breakdown rates varied in different muscles; while some wires maintained their connections well, others had very little remaining after the same amount of time. Also, when an underlying disease condition was present, in this case a motor neuron disease, the rate of breakdown after injury was accelerated. This suggests that the underlying processes responsible for breakdown are shared. Next, I looked at part of the cell that specialises in energy production called mitochondria, to determine if changes in energy processing can explain slower rates of breakdown in younger animals. Although I did not identify a strong connection with age, there was evidence that some changes in mitochondria in the wire itself could explain variations between muscles. I then considered P53, a factor linked to cell death. If this death factor is involved in regulating the rate of breakdown, then reducing it should slow breakdown. Using a mouse where this death factor is reduced, P53 reduction was found to have no effect on the rate of breakdown after injury, during disease, or during normal development, suggesting it is not involved.

Table of Contents

List of Figures

General Introduction and Materials and Methods

Chapter 1

Chapter 2

Chapter 3

Appendices

List of Tables

List of Abbreviations

ABBREVIATION	EXPANSION
AAL	Adductor auris longus
AAP	Amyloid precursor protein
AC3	Activated caspase-3
ACh	Acetylcholine
AICAR	5-Aminoimidazole-4-carboxamide ribotide
ALS	Amyotrophic lateral sclerosis
ANOVA	Analysis of variance
AS	Auricularis superior
ATP	Adenosine triphosphate
BAX	B cell lymphoma-associated X
BSA	Bovine serum albumin
BTX	Bungarotoxin
Ca^{2+}	Calcium ion
cDNA	Complementary DNA
CI	Complex I
CII	Complex II
CIII	Complex III
CIV	Complex IV
CV	Complex V
CNS	Central nervous system
DAVID	Database for annotation, visualisation and integrated discovery
DL	Deep lumbrical
DNA	Deoxyribonucleic Acid
DRG	Dorsal root ganglion
eEF1A2	Eukaryotic translation elongation factor 1 alpha 2
EGTA	Ethylene glycol tetraacetic acid
ELISA	Enzyme-linked immunosorbant assay
ETC	Electron transport chain
FAD	Flavin adenine dinucleotide
FDA	Food and Drug Administration
FMN	Flavin mononucleotide
GSH	Glutathione
LALc	Levator auris longus (caudal band)
LALr	Levator auris longus (rostral band)
M	Molar
mg	Milligram
mL	Millilitre

mm	Millimeter
mM	Millimolar
MND	Motor neuron disease
mRNA	Messenger RNA
mtDNA	Mitochondrial DNA
NAC	N-acetylcysteine
NAD	Nicotinic adenine dinucleotide
NF	Neurofilament
NGF	Nerve growth factor
NMDA	N-methyl-D-aspartate
NMJ	Neuromuscular Junction
NMN	Nicotinamide mononucleotide
Nmnat	Nucleotide transferase
OCT	Optimal cutting temperature compound
OXPHOS	Oxidative phosphorylation
P	Postnatal (e.g. postnatal day 15 = P15)
PBS	Phosphate buffered saline
PCR	Polymerase chain reaction
pmn	Progressive motor neuronopathy
PNS	Peripheral nervous system
Prnp	Prion protein gene
qPCR	Quantitative polymerase chain reaction
RNA	Ribonucleic acid
ROCK	Rho-kinase
ROS	Reactive oxygen species
RT-qPCR	Quantitative reverse transcription polymerase chain reaction
SARM1	Sterile alpha and TIR motif containing 1
SEM	Standard error of the mean
SMA	Spinal Muscular Atrophy
SMN/*Smn*	Survival motor neuron gene (HUMAN/murine)
SMN/Smn	Survival motor neuron protein (HUMAN/murine)
SMN1	Survival motor neuron 1
SMN2	Survival motor neuron 2
SOD1	Superoxide dismutase 1
SOD2	Superoxide dismutase 2
SV2	Synaptic vesicle protein 2
TS	Triangularis sterni
TVA	Transversus abdominis
Ube1	E1-ubiquitin activating enzyme
Ube4b	Ubiquitination factor E4B
WD	Wallerian degeneration

Wld^S	Wallerian degeneration slow
Wst	Wasted
WT	Wild-type
μL	Microlitre
μM	Micrometer

General Introduction

Motor neurons are vulnerable to degeneration following physical or chemical injury, and across a range of neurodegenerative diseases. The descending motor tracts that permit voluntary movement involve upper and lower motor neurons. Upper motor neurons carry signals from the motor cortex to the brainstem or ventral horn of the spinal cord (Bear et al., 2007). Signals are then received by lower motor neurons (α-motor neurons), which transmit signals peripherally to the target muscle in order to elicit a coordinated contraction (Bear et al., 2007). The lower motor neuron cell body resides in the ventral horn of the spinal cord, and transmits signals along the axon to the presynaptic terminal of the neuromuscular junction (NMJ).

The NMJ represents a critical interface between the motor neuron nerve terminal and the muscle, and is the major focus of this thesis. The presynaptic component of the NMJ contains vesicles loaded with the neurotransmitter, acetylcholine (ACh) for electrochemical signalling (Hirsch, 2007). The presynaptic terminal also contains complex networks of microtubules involved in the transport and re-uptake of neurotransmitters from the synaptic cleft. The postsynaptic component of the NMJ consists of clustered nicotinic ACh receptors, or motor endplate, located within the membrane of the muscle fibre, that are responsible for receiving acetylcholine that diffuses across the synaptic cleft (Sine, 2012, Hirsch, 2007). In nerve injury scenarios, and in a range of motor neuron diseases, the NMJ is widely recognised as an early and significant pathological target (Murray et al., 2008a, Kariya et al., 2008, Martinez-Hernandez et al., 2013, Wadman et al., 2012, Wishart et al., 2006, Martineau et al., 2018).

Depending on the original insult, motor neurons can degenerate in morphologically distinct ways, although the mechanisms underlying degeneration remain largely unknown. Wallerian degeneration (WD) and dying-back neuropathies are two well-known processes that ultimately lead to axonal degeneration, and are the primary degenerative pathologies that I will examine throughout this work. WD occurs

following a variety of insults, such as after nerve transection (axotomy). Following separation of distal elements from the soma, WD is characterised by spontaneous and rapid fragmentation of the distal axon and presynaptic terminal, followed by degradation and clearance by phagocytosing cells (Waller, 1851) (Fig. 1). Dissecting the mechanisms of WD in humans is challenging, and nerve injury models have therefore been extensively utilised in an attempt to elucidate the mechanisms of degeneration following injury. Since the timing and origin of the original insult is a known factor, it allows us to examine the course of nerve degeneration in both acute and latent phases of degeneration. This also facilitates identification of molecular changes that may be responsible for degenerative events. The discovery that some models with spontaneous or transgenic modifications have different rates of WD following injury has accelerated research and enhanced our understanding of the mechanisms of WD.

In contrast, dying-back neuropathy does not involve fragmentation, and is seen during many neurodegenerative diseases, including some motor neuron diseases (MNDs) like Amyotrophic Lateral Sclerosis (ALS) and Spinal Muscular Atrophy (SMA) (Cavanagh, 1964). Dying-back pathology is characterised as a progressive and retrograde retraction of the presynaptic terminal from the NMJ (Fig. 1) (Murray et al., 2008a, Cavanagh, 1964, Raff et al., 2002, Gillingwater and Ribchester, 2003). The most well-known and common form of MND is ALS. In ALS, both upper and lower motor neurons are affected, with symptoms including limb paralysis, dysphagia, dysarthria and respiratory weakness (Chio et al., 2009). There is currently no cure for ALS, with median survival from onset to death reported to be between 20-48 months; less than 10% of ALS patients survive more than 10 years (Chio et al., 2009). Patients with ALS invariably develop respiratory weakness, with death often a result of pulmonary complications. Much research is currently focussed on determining the aetiology and mechanisms of cell death in this disease, however in ALS, the majority of cases are described as being sporadic, meaning that the cause, or causes, of disease are unknown, which presents challenges. On the other hand, SMA is a purely inherited childhood motor neuron disease that affects lower motor neurons only. The genetic underpinnings of SMA have been well-defined, and this has facilitated the generation

of a number of animal models that can be used to investigate the timing and mechanisms of motor neuron degeneration. This understanding has accelerated the development of a number of therapies that are now available, with clinical trials showing promising improvements in motor function and survival (Hagenacker et al., 2020, Mercuri et al., 2017, Ratni et al., 2018, Mendell et al., 2017b, Mendell et al., 2017a). In the work I present here, I use an intermediate mouse model of SMA, which I will describe in greater depth in the following sections, to ask whether similar mechanisms could be responsible for NMJ loss in different degenerative scenarios. Overall, using models of neurodegeneration where the genetics and/or timing of pathological onset is known provides an opportunity to investigate mechanisms of neurodegeneration.

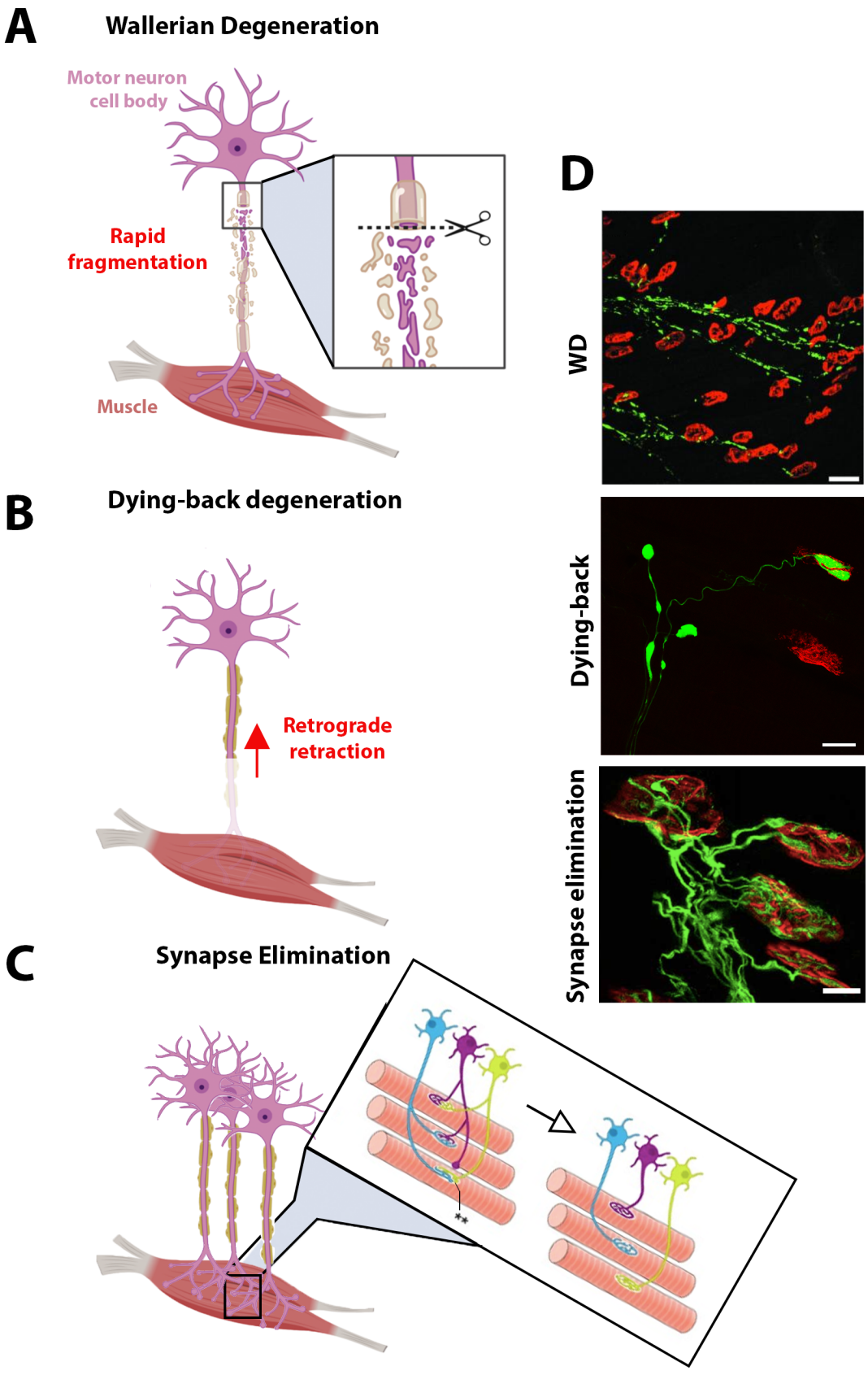
A
Wallerian Degeneration
Motor neuron cell body
Rapid fragmentation
Muscle
B
Dying-back degeneration
Retrograde retraction
C
Synapse Elimination
D
WD
Dying-back
Synapse elimination

Figure 1: Overview of the morphology of different types of axonal and synaptic degeneration. (**A**) Schematic of Wallerian degeneration (WD) which can be induced by transection nerve injury; this results in rapid fragmentation along the length of the distal axon. (**B**) Schematic of dying-back pathology which occurs in some motor neuron diseases like Spinal Muscular Atrophy (SMA); it is characterised by a progressive and retrograde retraction. The presynaptic terminal dissociates from the postsynaptic motor endplate and the axon withdraws. (**C**) Schematic to show developmental synapse elimination. During development, an excess number of synapses are formed, and motor endplates are predominantly polyinnervated (indicated by **). During early postnatal development, excess synapses are eliminated, and exuberant branches are 'pruned' away. A monoinnervated, mature neuromuscular system is thereby established. (**D**) Micrographs demonstrating different types of nerve degeneration under different physiological scenarios. NMJs are labelled with antibodies against neurofilament (NF, green) and synaptic vesicle protein 2 (SV2, green), and α-bungarotoxin (BTX, red). Top panel: WD micrograph showing catastrophic axotomy-induced fragmentation of axonal and synaptic compartments in the deep lumbrical muscles from P25 wild-type mice 24 hr after tibial nerve transection. Scale bar: 50μm. Adapted from Murray et al., 2008b (Copyright permissions obtained (license number can be provided on request). Central panel: micrograph showing an example of dying-back pathology in the transversus abdominus muscle of the *Smn*$^{2B/-}$ mouse model of SMA at a late-symptomatic time point (P18). Endplates that are devoid of innervation are described as being 'vacant'. Scale bar: 20μm. Bottom panel: across early postnatal development, excess synapses are eliminated, and the NMJ shifts from being predominantly polyinnervated to a monoinnervated structure. In this micrograph from a P7 wild-type mouse, you can see examples of endplates with multiple axonal inputs, and in the bottom right corner, an example of an endplate that is monoinnervated. Scale bar: 10μm. Adapted from Tomas et al., 2017. Copyright permissions obtained (license not required). Schematics were generated using Biorender© and Adobe photoshop software, and based on Murray et al., 2008b, Tomas et al., 2017, Lanuza et al., 2018.

Axonal and synaptic loss are also important features of normal development, both centrally and peripherally. The NMJ has long been used to investigate synaptic development and function as it is easily accessed (Sanes and Lichtman, 2001). In neonatal animals, skeletal muscle fibres receive multiple axonal inputs, with NMJs therefore being described as being polyinnervated (Lichtman and Colman, 2000). Across the first 2-3 weeks of life, synapses compete for resources and inactive synapses are eliminated until just one remains (Tapia et al., 2012, Lichtman and Colman, 2000, Sanes and Lichtman, 2001, Wyatt and Balice-Gordon, 2003). In this way, connectivity becomes refined and specific, and a mature monoinnervated neuromuscular system is established, where functional motor units consist of a motor neuron and the skeletal muscle fibres that it innervates (Fig. 1). Unlike in disease, only specific axonal branches are removed, as opposed to the entire motor neuron. The mechanisms by which such refined and segmented degeneration occurs are unclear. It should be noted that debate exists over the use of degenerative terminology when describing normal, postnatal synapse elimination. Here, I have chosen to view elimination of select axonal branches as a regulated, degenerative process, and therefore my work, and relating studies, are presented from this perspective.

Despite morphological differences between degenerative pathologies, it remains unclear whether mechanistic commonalities exist between different forms of axonal and synaptic degeneration. There is evidence to support that WD and dying-back pathways may share common molecular features (Conforti et al., 2014), however there is other work that provides scope to hypothesise that distinct mechanisms exist. Much debate therefore exists in the field as to whether mechanistic convergence or divergence exists. Identification of differentiating or common factors that can influence the rate of degeneration under different contexts is critical if we are to dissect degenerative mechanisms and identify therapeutic targets to slow or prevent neurodegeneration in a range of pathophysiological scenarios. In the following sections, I will provide overviews of the morphology, molecular features and animal models available to study synaptic loss in the contexts of traumatic injury, disease and development, and summarise what is known about the extent of their mechanistic similarities and differences.

1.1 Traumatic nerve injury: an overview

Peripheral nerve injury is common in both humans and animals, and can have potentially severe and irreversible physiological and functional consequences. Peripheral nerves are vulnerable to injury which can be caused by insult, including traumatic or chemical injury. Peripheral nerve injuries have an incidence estimated between 13 and 23 per 100,000 people annually (Li et al., 2014), and present many challenges for patients that can range from mild discomfort to lifelong impairment of motor, sensory or autonomic functions, depending on the severity of the insult (Menorca et al., 2013, Hussain et al., 2020). The most common peripheral neuropathies are traumatic in origin. Seddon classification is used to grade traumatic injuries into three categories depending on severity, which were later subdivided further by Sunderland; the Seddon and Sunderland grading system remain in use to classify traumatic nerve injuries into categories based on the presence of demyelination, extent of axonal damage and extent of damage to connective tissues of the nerve (Menorca et al., 2013, Seddon, 1943, Seddon et al., 1943, Seddon, 1948, Sunderland, 1951, Chhabra et al., 2014, Caillaud et al., 2019, Hussain et al., 2020). Nerve injury models have been invaluable to efforts to better understand mechanisms of degeneration, since the origin and timing of insult are known, and the temporal and molecular course of nerve degeneration can be studied and dissected. In Chapter 1, I will expand upon and apply an *ex vivo* model of peripheral nerve injury to examine levels of NMJ loss after insult, therefore it is important to appreciate what is already known with regard to the morphological and molecular changes that are associated with WD, and the models that are already used in the field.

1.1.1 Changes in synaptic and axonal morphology following traumatic injury

The earliest characterisation of the neuronal response to traumatic injury can be found in descriptions by Waller in 1851 (Waller, 1851). Using severed frog hypoglossal and glossopharyngeal nerves, Waller described extensive neuronal fragmentation that occurs distal to the injury site, whilst the proximal portions are retained for a longer period of time (Waller, 1851). These characteristics are now widely recognised as a

process termed ‘Wallerian degeneration’ (WD). WD is a conserved, active and highly regulated process that occurs in response to different insults, including traumatic injury, but also is seen in some disease scenarios, such as in Multiple Sclerosis (Casanova et al., 2003, Ciccarelli et al., 2003, Simon et al., 2000b, Zerres and Rudnik-Schoneborn, 1995, Gillingwater and Ribchester, 2001, Llobet Rosell and Neukomm, 2019).

Morphologically, WD is characterised by rapid axonal and synaptic fragmentation, a loss of organelles and plasma membranes, a breakdown in the myelin sheath and phagocytosis of axonal and synaptic debris by Schwann cells and macrophages (Beirowski et al., 2005, Beirowski et al., 2004, Conforti et al., 2014, Waller, 1851, Gillingwater and Ribchester, 2001). Distinct molecular events have also been described that consist of both acute and latent phases (Wang et al., 2012). Within the first 5-30 min following transection, an injured axon enters an acute, degenerative phase that is primarily calcium (Ca^{2+})-dependent. During the immediate acute phase, Ca^{2+}- and calpain-dependent processes result in the cleavage of axonal neurofilament and microtubule components (Wang et al., 2012). This is followed by a latent phase during which initially, the distal severed stump maintains electrical activity and morphological integrity (Miledi and Slater, 1968, Lunn et al., 1989, Tsao et al., 1994, Ribchester et al., 1995, Gillingwater et al., 2002). Within 24-48 hr after injury in mice electrical conductivity fails and, the axon disintegrates distally from the point of injury (Beirowski et al., 2005, Beirowski et al., 2004). Axonal fragments are then degraded and cleared by phagocytic cells, including macrophages and Schwann cells that influx the injury site (Wang et al., 2012, Saxena and Caroni, 2007, Beirowski et al., 2005). Schwann cells can also secrete growth factors that promote regeneration of the disintegrated nerve terminal (Gillingwater and Ribchester, 2001).

Any circumstance in which the rate of axonal and synaptic degeneration is altered, presents an opportunity to investigate the molecular mechanisms of WD and may help in the identification of therapeutically useful targets. In this respect, using mice to model peripheral nerve injury has provided valuable insight. Investigating mechanisms of axonal degeneration in WD is undoubtedly easier than in diseases

where the aetiology of pathology is often undefined; in injury models, the origin and timing of degenerative triggers are known, thereby facilitating investigation of subsequent molecular events. Identifying factors that can influence the rate of degeneration after injury will help to advance our understanding of degenerative mechanisms, which could also be important during cell death in disease scenarios.

1.1.2 Animal models to investigate the mechanisms of Wallerian degeneration

Much of our knowledge regarding the mechanisms of WD is based on how specific mutations influence the rate of axonal degeneration in animal models. Studies attempting to elucidate the molecular mechanisms of WD have been aided by the discovery of mouse models in which the rate of WD following injury is altered. Injury models are particularly useful to investigate the progression and molecular events that follow nerve insult, as the origin and timing of the injury can be controlled.

A key finding that has accelerated study into the mechanisms of WD is that acute and latent degenerative periods following injury can be extended by the spontaneous Wallerian degeneration slow (*Wld*^{S}) mutation. The *Wld*^{S} mutation was fortuitously discovered in C57BL/6J mice, and was mapped as a tandem triplication of an 85-kb repeating unit distally on chromosome 4 (Coleman et al., 1998). Mack et al., subsequently demonstrated that the gene responsible for conferring the slow WD phenotype is a chimeric gene that contains the 5' end of ubiquitination factor E4B (Ube4b), and a murine gene that is identical to the human nucleotide transferase 1 gene (NMNAT1) (Mack et al., 2001). Fusion of these genes results in the production of a unique and stable protein isoform of the nicotinamide adenine dinucleotide (NAD)-synthetic enzyme, Nmnat1 (Mack et al., 2001). In mammals, there are three isoforms of NMNAT that include nuclear NMNAT1, cytoplasmic NMNAT2 and mitochondrial NMNAT3, which catalyse NAD synthesis from nicotinamide mononucleotide (NMN) and adenosine triphosphate (ATP). Mitochondrial depolarisation results in reduced NMNAT2 synthesis and axonal transport, resulting in decreased NMNAT2 levels (Loreto et al., 2020). After injury, levels of NMNAT2 decline sharply, triggering fragmentation and axonal degeneration (Beirowski et al., 2005, Beirowski et al., 2009,

Babetto et al., 2010, Gilley and Coleman, 2010, Gilley et al., 2013, Milde et al., 2013, Di Stefano et al., 2015). It is thought that *Wld*^{S} confers protection to injured axons by maintaining axonal NMNAT activity by substituting for cytosolic NMNAT2 (Conforti et al., 2009, Beirowski et al., 2009, Avery et al., 2009, Gilley and Coleman, 2010).

The *Wld*^{S} mutation confers ten-fold delays in WD following axotomy; in contrast to wild-type axons, transected *Wld*^{S} axons remain structurally intact and functional for up to two weeks *in vivo*, with protection being dose-dependent (Mack et al., 2001, Beirowski et al., 2005, Beirowski et al., 2004, Wong et al., 2009). Isolated distal axons also maintain electrical and synaptic activity; they are capable of conducting action potentials, synapses can release neurotransmitters, and synaptic vesicle recycling continues for several days (Ribchester et al., 1995, Tsao et al., 1994, Gillingwater et al., 2002, Miledi and Slater, 1968, Lunn et al., 1989). This delay is apparent when *Wld*^{S}-expressing nerves are exposed to traumatic, chemical and pathological insult (Oyebode et al., 2012). Protection conferred by *Wld*^{S} is age-dependent, with mice over the age of 4 months appearing to demonstrate wild-type patterns of degeneration (Perry et al., 1992, Tsao et al., 1994, Gillingwater et al., 2002, Crawford et al., 1995). Similar delays are also seen centrally following chemical or pathological insult in *Wld*^{s} mice (Oyebode et al., 2012). *Wld*^{S} mutants have been widely used and represent an invaluable tool to study the mechanisms of WD. I will use preparations isolated from *Wld*^{S} mice in Chapter 1 to optimise an *ex vivo* model of nerve injury.

A similar, protective phenotype is observed in the Sterile Alpha and TIR motif containing 1 (*SARM1*) knockout mouse. *SARM1* was identified in a genetic screen undertaken in *Drosophila* that sought to identify loss of function mutations that could delay axonal degeneration following antennal ablation (Osterloh et al., 2012). SARM1 is critical to the WD pathway, with *Sarm1* knockout found to phenocopy *Wld*^{S} gene expression, delaying *in vivo* axonal degeneration for over two weeks post-axotomy (Osterloh et al., 2012). Until relatively recently, the mechanisms by which SARM1 promotes axonal degeneration were unclear. In 2016, Sasaki et al., demonstrated that in response to injury, SARM1-deficient axons exhibit similar NAD^{+} levels to those present in wild-type controls (Sasaki et al., 2016). Since NAD^{+} loss is associated with

degeneration, it was suggested that SARM1 might be involved with regulating NAD^+ levels. Further work *in vitro* confirmed that SARM1 can hydrolyse NAD^+ directly, and is therefore intimately involved with NAD^+ metabolism and WD pathway (Essuman et al., 2017). Wld^S (NAD^+ synthesis) and SARM1 (NAD^+ degradation) are recognised to have opposing effects on WD, and have been extensively utilised to investigate degenerative pathways.

Experimental models have provided an invaluable tool with which to study nerve injury, which is not possible clinically, however a major limitation when studying WD *in vivo* is the accessibility and reproducibility of nerve injuries. A limited number of muscles have therefore been studied, with the majority of work focussed on the deep lumbrical muscles, due to ease of access of the tibial/sciatic nerve in the hindlimb. Recent work has generated an *ex vivo* model that facilitates study of the mechanisms of nerve injury (Brown et al., 2015). Work by Brown et al., used an *ex vivo* model to model peripheral nerve injury in nerve/muscle preparations from the mouse hindlimb. Consistent with *in vivo* work, this group demonstrate that Wld^S can delay WD, with 54% innervation remaining in Wld^S muscles, compared to just 12% innervation remaining in wild-type muscles after 25-30 hr (Brown et al., 2015).

Work in both Wld^S and *SARM1* knockout models have attempted to identify molecular differences that might be responsible for regulating the rate of axonal degeneration following injury. Work in both models has implicated mitochondria as playing an important role in WD; proteomic analysis undertaken in Wld^S mice has identified several proteins relating to mitochondrial stability and degeneration (Wishart et al., 2007). After injury, mitochondrial motility is preserved in axons expressing Wld^S in *Drosophila* (Avery et al., 2012). Additionally, ultrastructural studies have reported morphological changes in mitochondria after injury, including mitochondrial swelling, that is thought to be a result of opening of the mitochondrial permeability transitioning pore; activation of this pore is considered a key event in axonal degeneration (Barrientos et al., 2011). By utilising animal models where the rate of WD is altered, a number of modulators have been identified, however attempts to integrate and understand degenerative pathways remain limited. Identifying factors that can regulate

the rate of axonal and synaptic degeneration, and crucially, how axonal degeneration differs mechanistically in different physiological scenarios, is key to targeting neurodegeneration in the contexts of injury and disease.

1.1.3 Molecular mechanisms of Wallerian degeneration

Animal models have permitted us to dissect apart the mechanisms that underlie different phases of axonal and synaptic degeneration following injury. Morphologically, there are proposed to be at least three distinct phases of axonal degeneration: an acute degenerative phase affecting the proximal and distal stumps of the axon immediately after injury; a latent period where the distal axon maintains its morphology and remains excitable; and an abrupt, granular degenerative phase where the axonal skeleton distal to the injury site rapidly fragments. In this section, I will provide a brief overview of some the molecular events that are thought to underlie different phases of WD (for review see Wang et al., 2012).

In vivo, real-time imaging has revealed that within the first 5 to 30 minutes following injury, portions immediately proximal and distal to the injury site rapidly recede in either direction (Kerschensteiner et al., 2005). This is followed by the slower formation of dystrophic bulbs at the terminals of transected ends due to an accumulation of axoplasmic organelles, due to ongoing axonal transport (Griffin et al., 1995). Ca^{2+} influx is considered a critical event in initiating acute axonal degeneration; Ca^{2+} blockade can prevent intra-axonal rises in Ca^{2+}, thereby attenuating the progression of acute degeneration. The addition of Ca^{2+} ionophores has been shown to increase the number of injured axons undergoing acute axonal degeneration (Knoferle et al., 2010). Ca^{2+} influx activates the serine-theonine protease calpain, which can cleave axonal neurofilament and other microtubule-associated components (Billger et al., 1988, Johnson et al., 1991, Kampfl et al., 1996). Pharmacologic inhibition of calpain can reduce short distance degeneration in spinal cord axons following injury, highlighting calpain activity as a modulator of the acute phase (Schlaepfer and Bunge, 1973, George et al., 1995). Ca^{2+} influx also triggers autophagic processes (Knoferle et al., 2010). The acute phase of degeneration is thought to promote cytoskeletal

restructuring and formation of growth cones that aids in regenerative efforts (Spira et al., 2003). Clearing space at the lesion site is thought to facilitate glial cell proliferation to create an environment more conducive to regeneration. *Wld*^{S} can delay the onset of acute degeneration, suggesting that this phase forms part of WD mechanisms (George et al., 1995, Knoferle et al., 2010).

This is followed by a latent phase that occurs around 24 to 48 hr after injury, during which axons remain morphologically intact and excitable for brief periods of time (Wang et al., 2012). Transected motor neurons are capable of producing action potentials even 24 hr after injury *in vivo*, although evoked potentials and the velocity of conduction decays with time (Moldovan et al., 2009). Both retrograde and anterograde transport also continue in the distal axon during this time (Smith and Bisby, 1993). Similar to the acute phase, in the latent phase, increases in intra-axonal calcium also occur. Axonal degeneration can be delayed for up to 4 days by culturing neurons in a reduced calcium media, or by using a chelating agent, like ethylene glycol tetraacetic acid (EGTA), with a high affinity for Ca^{2+}. Complimenting this, increasing Ca^{2+} can induce degeneration in uninjured neurites (Schlaepfer and Bunge, 1973, George et al., 1995). The addition of Ca^{2+} can abolish protection conferred by *Wld*^{S} (Glass et al., 1994*)*. Calcium-dependent activation of calpain is also considered a key event in the latent phase, however, although inhibition delays the progression of axon degeneration for 12-24 hr *in vitro*, it does not prevent WD (Glass et al., 1994, Wang et al., 2000). This suggests that other, as of yet unidentified, pathways are involved in cytoskeletal breakdown in WD.

Two hypotheses have emerged to explain the mechanisms that can ultimately signal and initiate axonal degeneration. The first is that there is a 'death signal' that involves a series of kinases that promote axonal degeneration. Genetic or pharmacologic inhibition of kinases have been shown to protect axons from injury if administered within the first 3 hr after injury (Miller et al., 2009). It remains unclear whether increased kinase activity can induce spontaneous degeneration or abolish protection conferred by *Wld*^{S}. The second hypothesis is that nerve injury disrupts axonal transport or expression of axonal trophic factors, resulting in levels dropping below the critical

threshold required to support normal axon integrity and functioning (Wang et al., 2000). Trophic withdrawal has been shown to lead to cleavage and secretion of amyloid precursor protein (APP), a precursor of β-amyloid protein and marker of axonal damage (Coleman, 2005). APP ultimately triggers B cell lymphoma-associated X (BAX)-dependent, caspase-6-mediated cytoskeletal breakdown (Nikolaev et al., 2009). Gilley and Coleman recently demonstrated that inhibition of protein translation at the cell body, but not in the axon, can lead to degeneration in uninjured neurites (Gilley and Coleman, 2010). Thus, it is the synthesis of protein in the soma and delivery to the axon that appears to be critical to axon viability, as opposed to local translation. This group further demonstrated that Nmnat2 was required for axon survival, and that following axotomy, or blockade of axonal transport, expression of Nmnat2 declines rapidly; Nmnat2 turnover time was found to correlate with the period between axonal injury and the appearance of axonal blebbing (Beirowski et al., 2004). Depletion of Nmnat2 can induce degeneration in uninjured axons, whilst overexpression of Nmnat2 can delay degeneration of wild-type axons for up to 48 hr (Gilley and Coleman, 2010, Yan et al., 2010). Blockade of the ubiquitin-proteasome system has also been shown to delay degeneration following injury for up to 3 days *in vivo* (Watts et al., 2003). Since the primary function of the proteasome system is to regulate protein turnover, this is thought to promote axonal survival either by maintaining transport or by preventing degradation of survival factors. Nmnat2 turnover has been shown to be dependent on proteosome activity (Gilley and Coleman, 2010), further supporting the trophic withdrawal hypothesis.

The final phase of axonal degeneration is the granular degeneration phase that occurs around 72 hr after injury, and is characterised by catastrophic, asynchronous fragmentation (Wang et al., 2012). Following axotomy, axonal degeneration proceeds anterogradely, whereas after a nerve crush, axons degenerate retrogradely (Beirowski et al., 2005). Notably, in WD, loss of neuromuscular transmission is recognised as an early event following a range of insult (Brown et al., 2015, Beirowski et al., 2005, Ribchester et al., 1995, Miledi and Slater, 1970, Winlow and Usherwood, 1975). The ability of axons to degenerate in either direction challenges the trophic withdrawal hypothesis. Interestingly, *Wld*^{S} axons only degenerate anterogradely regardless of

lesion type (Beirowski et al., 2005). This suggests that rather than *Wld*^{S} simply conferring a slower rate of WD, that degenerative processes may in fact be distinct, with blockade of WD via *Wld*^{S} ultimately leading to the activation of a different degenerative pathway. Granular degeneration is accompanied by glial influx, which primarily includes astrocytes, macrophages and, in the peripheral nervous system (PNS), Schwann cells, which facilitate the clearance of axonal debris (Wang et al., 2012). Glial influx is thought to play a key role in facilitating regeneration attempts by the proximal axon (Liu et al., 2019). Following fibre tract or optic nerve crush lesion in the central nervous system (CNS), where macrophages are virtually excluded from entry, no spontaneous regeneration occurs (Horner and Gage, 2000, David and Ousman, 2002). *In vivo* tracking of macrophages has shown that macrophages enter crushed peripheral nerves with a proximodistal gradient that begins at the lesion site, and remain stationary (Bendszus and Stoll, 2003). Targeting of macrophages has been proposed as a way to improve peripheral nerve regeneration, however the underlying regulatory mechanisms of macrophage activation, polarisation and subtype transformation to promote repair and regeneration remain poorly understood (Liu et al., 2019).

1.2 Dying-back pathology: an overview

Motor neurons are recognised as pathological targets in neurodegenerative diseases, such as motor neuron diseases, however the morphology of degeneration is distinct from that which occurs following injury. Motor neuron disease is an umbrella term that encompasses a range of neuromuscular conditions where motor neurons in the brainstem and spinal cord are primary pathological targets (Bede and Pradat, 2019). Motor neuron diseases, such as ALS and SMA, are described as 'dying-back' neuropathies, due to the characteristic way in which synapses and axons withdraw retrogradely from the motor endplate (Cavanagh, 1964). During a die-back, the presynaptic terminal of the motor neuron gradually withdraws from the NMJ, and the distal portion of the nerve terminal forms a bulb, known as a retraction bulb. This retraction leaves the motor endplate devoid of innervation (Gillingwater and Ribchester, 2003, Murray et al., 2008a).

Neurodegenerative diseases have diverse and often unknown aetiologies, and are an extensive and heterogenous group of conditions. This presents challenges when attempting to identify and characterise common molecular factors or pathways that are involved in dying-back pathology. Identifying common molecular mechanisms that are responsible for regulating dying-back pathology is therefore difficult, with most groups focussing on understanding a specific disease. Our in-depth knowledge of the genetic underpinnings of SMA has facilitated the development of several murine models which can be used to study the pathogenesis and progression of dying-back pathology. Ultimately, this may aid in the identification of common targets that could prove useful in modifying the progress of degeneration in a range of different diseases. In Chapters 1 and 3, I will use the *Smn*$^{2B/-}$ mouse model of SMA to investigate factors that can alter the rate of NMJ degeneration, therefore in the following sections, I will summarise the genetics of SMA, animal models that are widely used, and the morphology and mechanisms of motor neuron pathology.

1.2.1 Spinal Muscular Atrophy: an overview

The childhood motor neuron disease, SMA, is a monogenic and devastating, autosomal recessive condition that is characterized by the loss of lower alpha motor neurons from the ventral horn of the spinal cord, proximal muscle atrophy and paralysis (Lunn and Wang, 2008). SMA remains the leading genetic cause of infant mortality, with the commonly reported incidence of SMA being between 1 in 6000 - 10,000 live births (Lunn and Wang, 2008). More recently, a study seeking to estimate the worldwide incidence of SMA has suggested that incidence lies between ~1 in 3900 and ~1 in 16,000 (Verhaart et al., 2017).

SMA is caused by homozygous disruption of the telomeric survival motor neuron 1 (SMN1) gene, located on chromosome 5q13, that ultimately disrupts the production of survival motor neuron (SMN) protein which is critical for motor neuron survival. More than 98% of patients have a homozygous disruption of *SMN1* by deletion, rearrangement or mutation (Lefebvre et al., 1995, Hahnen et al., 1995). Full-length SMN protein contains 294 amino acids, and, despite its name, is expressed ubiquitously and is required by all cells and tissue types (Lefebvre et al., 1995, Giavazzi et al., 2006, Battaglia et al., 1997, Chaytow et al., 2018). Since SMN is ubiquitously expressed, it is unclear why motor neurons are particularly vulnerable to reductions. Smn is suggested to have multiple functions, with the best described being in pre-messenger ribonucleic (RNA) splicing (Singh and Singh, 2018, Chaytow et al., 2018, Coady and Lorson, 2011, Workman et al., 2012). A complete lack of SMN is embryonically lethal, however, in humans, a paralogous 'back-up' gene, *SMN2*, exists. An inverted duplication in *SMN1* has resulted in a centromeric copy of the gene, which is termed *SMN2*. *SMN1* and *SMN2* both contain 9 exons and 8 introns with differences at 5 bases, however, it is a critical C to T transition within exon 7 of *SMN2* that disrupts the exon splicing enhancer site, leading to alternative splicing and skipping of exon 7 (Singh and Singh, 2018). As a result, only around 10% of protein produced by this gene is full-length and functional, with the majority of *SMN2* products exhibiting an exon 7 exclusion that results in a non-functional, truncated protein (SMNΔ7) that is targeted for degradation (Singh and Singh, 2018, Kolb and Kissel, 2015) (Fig. 2).

Consequently, in SMA, there is reduced expression of functional, full-length SMN protein which cannot support normal functioning of the neuromuscular system. This leads to motor neuron degeneration, muscular paralysis and, in severe cases, death before 2 years of age (Zerres and Rudnik-Schoneborn, 1995). The *SMN2* gene can modify disease severity and patient presentation, depending on its copy number, where higher copy number is associated with reduced disease severity (Wirth et al., 2006b, Wirth et al., 2006a, Wirth et al., 2006c). In this respect, SMN2 has been described as a phenotypic modifier, and has been the focus of therapeutics, as a higher copy number leads to higher SMN levels in the body, and can extend survival (Prior et al., 2009, Jedrzejowska et al., 2008, Elsheikh et al., 2009). The role of SMN2 as a phenotypic modifier is most profoundly seen in patients that lack *SMN1* yet, due to increased *SMN2* copy number, are asymptomatic (Jedrzejowska et al., 2008, Zheleznyakova et al., 2011). Other phenotypic modifiers have also been described, for example, work by Oprea et al., has demonstrated that expression of plastin 3, an actin-binding protein that is important for axogenesis, can modify disease phenotype (Oprea et al., 2008). Thus, although *SMN1* is the primary disease-causing gene, other genetic factors can also influence how disease manifests.

Clinically, SMA is divided into different sub-types, depending on severity and onset of disease (Fig. 2). Type 0 is very severe with antenatal onset, and a life expectancy of under 6 months, whereas Type 3 and 4 are milder, with adult onset and life expectancy extending into adulthood. As expected, SMN2 copy number is linked to disease severity; more severe patients typically have fewer copies of SMN2 (Fig. 2) (Calucho et al., 2018, Zerres and Rudnik-Schoneborn, 1995, Kolb and Kissel, 2015, Lunn and Wang, 2008). Our understanding of the genetic underpinnings of SMA has accelerated our ability to develop effective therapies to treat this devastating disease. Therapeutic strategies to increase SMN protein in motor neurons have primarily focussed on enhancing the effectiveness of the *SMN2* 'back-up' gene, however gene replacement therapy is also available for young patients. There are currently three approved treatments for SMA, and many more that are in clinical trials (summarised in Table 1).

Despite major advances in therapeutics for SMA, complementary strategies will likely be required to ensure long-term, normal functioning. It is unclear whether SMN-based treatments confer complete rescue, therefore delayed symptoms may appear. Since available therapies are new and the first treated cohorts have not yet reached adulthood, it is unclear what other pathology may manifest as patients age. Although we have targeted motor neuron-related aspects of the disease, other symptoms could become apparent (Shababi et al., 2014, Hamilton and Gillingwater, 2013); adjunctive therapies will therefore likely be important in years to come. Overall, despite therapeutic advances in SMA, continued investigation is critical to understand pathogenesis and progression.

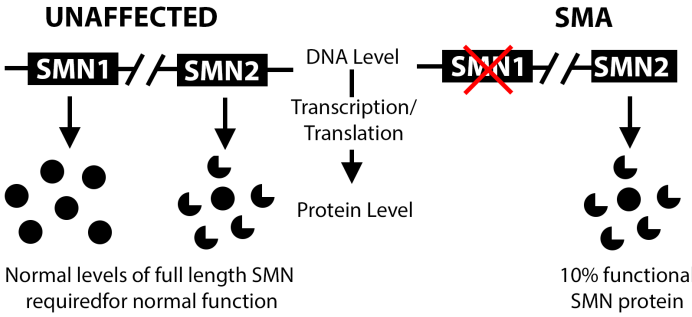

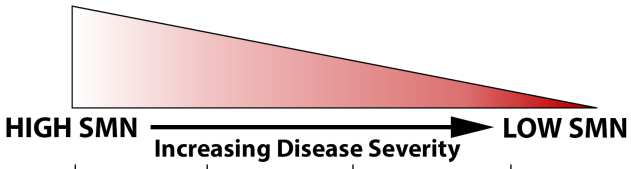

Clinical Phenotype	Normal	Type 4	Type 3	Type 2	Type 1	Type 0
Age of onset	-	10-30 years	>18 months	6-18 months	<6months	Prenatal
Typical SMN2 copy number	1-8	≥4	3-4	2-3	1-3	1
Life expectancy without intervention	-	Adult	Adulthood	>2 years	<2 years	<6 months
Level of function achived	-	Walk through adulthood	Walking (may lose mobility with time)	Sit indpendently	Sit with support	None

Figure 2: SMA is caused by a loss of SMN protein, with disease severity dependent on SMN2 copy number. This figure provides an overview of the genetics and prognoses in SMA. Complete loss of SMN is embryonically lethal, however in humans, a second gene, *SMN2* produces around 10% functional, full-length protein. This is due to a C to T base transition within exon 7 of *SMN2*, that leads to alternative splicing and exclusion of exon 7, and the favoured production of a truncated protein that is non-functional and targeted for degradation: SMNΔ7. *SMN2* is a phenotypic modifier; a higher copy number of *SMN2* leads to more full-length SMN protein, and reduced disease severity. The different clinical phenotypes of SMA and associated onset, functional effect and prognoses are summarised in this table. (Calucho et al., 2018, Zerres and Rudnik-Schoneborn, 1995, Kolb and Kissel, 2015, Lunn and Wang, 2008).

Table 1: Table summarising key therapies that are currently approved by the Food and Drug Administration (FDA) or are being tested in clinical trials for the treatment of SMA. Table obtained from CureSMA.org (as of 2nd September 2020, available at: https://www.curesma.org/treatment/).

Name	Stage	Marketed/Developed By	Type of Therapy	Who Can Take it
Spinraza	FDA-approved	Biogen	SMN-enhancing	All ages and types.
Zolgensma	FDA-approved	AveXis/Novartis	SMN-enhancing	Patients with SMA up to 2 years of age.
Evrysdi	FDA-approved	Genentech/Roche	SMN-enhancing	Adults and children 2 months of age and older.
Reldesemtiv	Phase 2 trial completed	Cytokinetics/Astellas	Non-SMN (muscle drug)	Trials have tested the drug on patients with SMA types 2, 3 and 4 who are age 12 or older.
LMI070	Phase 2 trial ongoing	Novartis	SMN-enhancing	Infants with SMA type 1.
AVXS-101 (IT)	Phase 1 trial ongoing	AveXis/Novartis	SMN-enhancing	Currently being tested on children 6 months to 5 years of age with 3 copies of SMN2.
SRK-015	Phase 2 trial ongoing	Scholar Rock	Non-SMN (muscle drug)	Individuals between 2 and 21 who have SMA type 2 or 3.

1.2.2 Animal models of SMA

Due to limited availability of suitable patient material, detailed analyses of cellular pathology, particularly across time, in SMA patients is restricted, particularly at time points that do not reflect the end-stage of disease (Monani and De Vivo, 2014). Much work has therefore been undertaken in animal models. SMA is unique to humans, as other species lack *SMN2* (Rochette et al., 2001). Null mutations in SMN genes are lethal (Monani, 2005), therefore genetic modification has been undertaken in a number of different species to generate SMA-like models.

Drosophila *(Drosophila melanogaster)* models of SMA are useful for genetic mapping, and when undertaking large-scale screens for modifiers of disease due to their rapid reproductive cycle, propensity to produce large numbers of progeny, remarkable gene and pathway conservation and ease and speed of genetic manipulation (McGurk et al., 2015). For example, *Drosophila* have been used to investigate a range of patient-derived SMN missense mutations and their associated phenotypes, demonstrating a wide range of severities and pathology that is consistent with phenotypes found in SMA patients (Spring et al., 2019). Zebrafish (*Danio rerio*) represent a rapidly developing and transparent vertebrate model that demonstrate conservation of genes implicated in neurodegenerative diseases and physiological processes involved in morphogenesis and maintenance of the nervous system (Bandmann and Burton, 2010, Becker and Rinkwitz, 2012, Xi et al., 2011). Transgenic zebrafish are easily and rapidly generated, as eggs are accessible and relatively easy to manipulate, and fish have a short generation time (Chen et al., 2016). Other work has also generated SMA-like models in zebrafish pharmacologically, for example the administration of an antisense oligonucleotides into embryos can inhibit the translation of target messenger RNA (mRNA). It has been shown that this can reduce Smn protein by over 60% and results in abnormal axonal morphology (McWhorter et al., 2003). Although undoubtedly useful, translating findings from such basic models can present challenges.

A number of transgenic mouse models with a range of severities are also available to study the pathophysiology of SMA (Bebee et al., 2012). Mice also have just one copy of the SMN gene, which poses a challenge when attempting to generate models that recapitulate SMA disease pathology. Complete knockout of the Smn gene (*Smn*$^{-/-}$) is embryonically lethal (Schrank et al., 1997), however a number of transgenic mouse models have been generated. Whilst knockout of exon 2 or 7 is embryonically lethal, insertion of an SMN2 human transgene on this background has permitted the establishment of severe models of SMA. The *Smn*$^{-/-}$*;SMN2* mouse possesses 2 copies of the SMN2 transgene on a null murine background, and survives between 4-6 days (Monani et al., 2000). The additional insertion of an SMN allele without exon 7 (*SMNΔ7*) onto this severe background can extend life to around 13.5 days (Le et al., 2005) (Fig. 3). The phenotypically similar 'Hsieh-Li' or Taiwanese mouse, also possesses 2 copies of SMN2 on a null background that survives between 8-10 days (Hsieh-Li et al., 2000). Although invaluable, such severe models offer a limited timeframe to study the development and progression of SMA pathology.

The more recent development of a new allele of the mouse gene, Smn2B, has led to the generation of the *Smn*$^{2B/-}$ mouse model, which will be used in my work. The *Smn*$^{2B/-}$ mouse has around 15% normal levels of Smn protein, and represents an intermediate mouse model of SMA (DiDonato et al., 2001, Hammond et al., 2010, Bowerman et al., 2012). The Smn2B allele consists of a 3 nucleotide substitution in the exon splicer enhancer region within exon 7 of the murine SMN gene, with the resultant model exhibiting reduced levels of full-length Smn protein (DiDonato et al., 2001, Hammond et al., 2010). Unlike in other models, no human transgenes are inserted, and rather it is the lack of murine Smn protein that disrupts motor neuron function and ultimately leads to progressive loss of lower motor neurons and skeletal muscle atrophy (Bowerman et al., 2012). In our hands, this model has a lifespan of around 21 days, with symptom onset around P10. Symptoms observed by us, and others, include weight loss, smaller body size, smaller ears, smaller tail and motor weakness when compared to control littermates (Courtney et al., 2019, Bowerman et al., 2012) (Fig. 3).

The extended pre-symptomatic time window available in the *Smn*$^{2B/-}$ model when compared to other models, facilitates study of the temporal and molecular pathological events of a die-back that ultimately lead to motor neuron death. Not all muscles are equally affected in SMA; some muscles are known to be vulnerable, whilst others described as being more resistant to pathology (Murray et al., 2008a). This provides a useful tool, which I will exploit throughout this thesis, that may help us to determine what factors might be responsible for such differences between muscles. Overall, the *Smn*$^{2B/-}$ mouse model represents a useful model of a die-back, which will not only facilitate our understanding of motor neuron pathology in SMA, but may translate to other diseases where dying-back morphology is a pathological hallmark. More widely, this will facilitate comparison to other degenerative processes and assist us to better categorise degenerative processes in different scenarios.

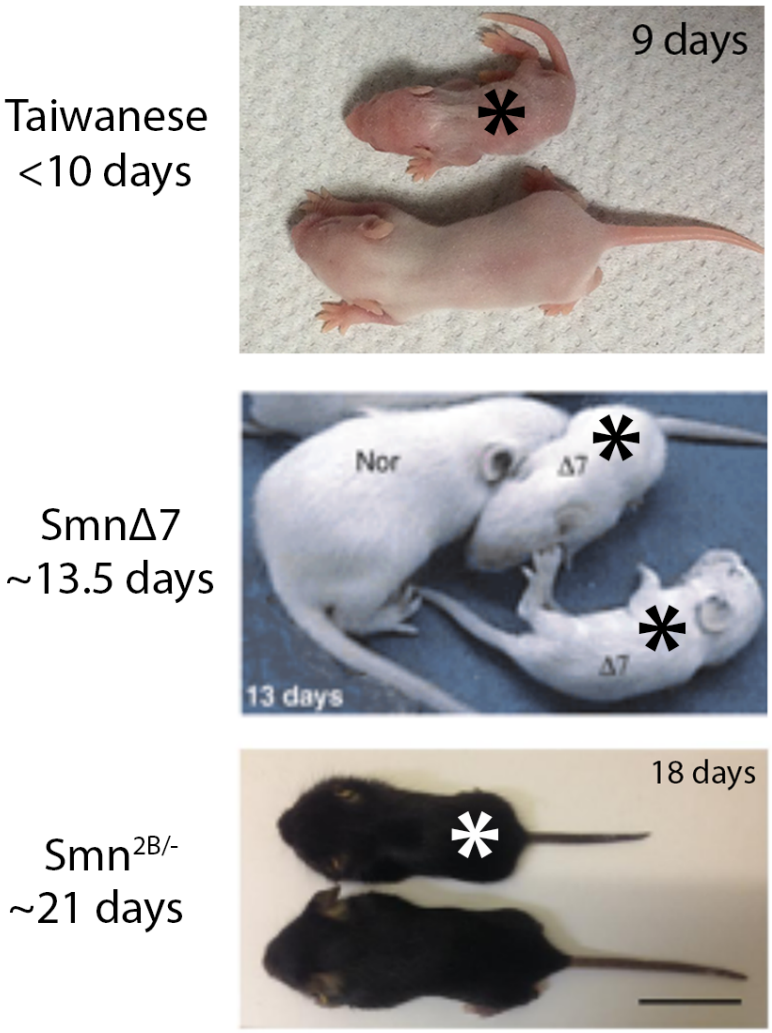

Figure 3: Photographs showing mouse models of SMA at late-symptomatic stages. **(A)** Taiwanese mouse (top) compared to littermate control (bottom) at postnatal day (P) 9. SMA-like pups have a lifespan <10 days. This image was kindly provided by the Gillingwater group, and taken by Dr. Hannah Shorrock. (**B**) *SmnΔ7* mice at P13, denoted by 'Δ7' (right), compared to a littermate control (left). Adapted from Le et al., 2005. This mouse has an average lifespan of around 13.5 days. Copyright permissions obtained (license number can be provided on request). (**C**) *Smn*$^{2B/-}$ mouse (top) compared to littermate control (bottom). This was taken by myself at P18 in the Murray laboratory. Scale bar = 2cm. In our hands, this model has a lifespan of around 21 days. Note that for Taiwanese and *SmnΔ7* mice, date of birth is considered P1, whilst for *the Smn*$^{2B/-}$ line, date of birth is considered P0. In all cases, SMA-like pups are indicated by a black or white *.

1.2.3 Dying-back morphology and mechanisms in SMA

The NMJ - the main focus of this thesis - is widely recognised as an early and significant pathological target in SMA in both human patients and animal models (Kariya et al., 2008, Murray et al., 2008a, Martinez-Hernandez et al., 2013, Wadman et al., 2012). NMJs are lost early in the disease process, with denervation in muscles evident prior to symptom onset (Murray et al., 2008a). Morphologically, synaptic and axonal degeneration in SMA proceeds by a dying-back mechanism; the presynaptic terminal and distal axon progressively withdraw from the post-synaptic endplate of the muscle in a retrograde direction without fragmentation (Murray et al., 2008a). The distal portion of the axon gradually retracts, and a retraction bulb forms distally; this leaves NMJs on skeletal muscle devoid of innervation (Kariya et al., 2008). Features of dying-back pathology include pre-synaptic accumulation of neurofilaments, endplate abnormalities and denervation, loss and shrinkage of motor neuron cell bodies, axonal loss in ventral roots and muscle fibre atrophy (Goulet et al., 2013, Tisdale and Pellizzoni, 2015).

In mouse models of SMA, not all motor neuron populations are equally affected; some have been found to be more vulnerable to degeneration than others, even at late stages of disease, and are described as being selectively vulnerable (Murray et al., 2008a). Selective vulnerability is seen in patients and in mouse models of SMA. For example, in patients, the lower limb and proximal musculature have been found to be more affected than the upper limb and distal musculature (Dubowitz, 1999). In patients, whilst the intercostal muscles display significant pathology, the diaphragm and facial muscles are comparatively spared. In the *Smn*$^{2B/-}$ mouse, neuromuscular pathology is extensive in transversus abdominis (TVA) muscle, yet the rostral band of levator auris longus (LALr) or deep lumbrical (DL) muscles are largely spared (Murray et al., 2008a). In other mouse models of SMA, selective vulnerability and resistance have also been described, although in more severe models, the pattern of susceptibility appears to vary (Thomson et al., 2012). This observation has been exploited to identify potential modifiers of motor neuron health (Kline et al., 2017, Murray et al., 2015, Boyd et al., 2017). It should be noted that although more variable in pattern, selective

vulnerability is also described in ALS, and a number of studies have similarly exploited intermuscular differences to investigate factors that can influence the rate of synaptic and axonal degeneration in ALS, to try and better understand degenerative mechanisms (Brockington et al., 2013, Hedlund et al., 2010, Kaplan et al., 2014). Recently, a cross-species comparison of transcriptional screens from SMA and ALS, identified candidate phenotypic modifiers, and identified alpha-synuclein as a common modifier of pathology in motor neuron disease (Kline et al., 2017). It is unclear whether selective vulnerability is a unique feature to dying-back degeneration, or whether intermuscular differences are present in other types of injury-induced or developmentally regulated degeneration. Overall, identifying intermuscular differences represents a powerful tool to investigate factors that can influence the rate of degeneration. Throughout this thesis, I identify, refer to and use intermuscular differences in the rate of NMJ loss as a tool to examine factors that could regulate synaptic stability.

In SMA, molecular changes have been detected at pre-symptomatic time points, prior to the onset of NMJ pathology or symptoms (Murray et al., 2015). RNA sequencing on motor neurons from the spinal cord has identified upregulations in transcripts that are involved with apoptotic signalling at a pre-symptomatic time point, including transcripts that are associated with P53 signalling, a factor involved in apoptotic regulation (Murray et al., 2015). RNA sequencing has identified changes that indicate that dysregulation of synaptogenesis and other transcriptome abnormalities are also present prior to the onset of NMJ pathology (Murray et al., 2015, Zhang et al., 2008, Zhang et al., 2013). Post-symptomatic transcriptional changes have also been described in transcripts that are involved with splicing, such as chondrolectin, in the *SmnΔ7* mouse model (Baumer et al., 2009). Work in a zebrafish model of SMA has exploited differences in vulnerability between motor neuron pools to assess differences in their bioenergetic profiles. This has revealed differences in the basal molecular profiles between muscles that correlate with selective vulnerability *in vivo* (Boyd et al., 2017). Targeting of phosphoglycerate kinase 1 was found to modulate motor neuron vulnerability, where knockdown induced synaptic degeneration in wild-type zebrafish, and pharmacological activation rescued motor axon phenotypes in the

SMA model (Boyd et al., 2017). Whilst the role of apoptotic pathways in motor neuron death in SMA is widely appreciated, the role of pro-apoptotic pathways at the synapse and in the axon that influence can synaptic retraction are less clear. Further work is required to identify factors and pathways that can modify the rate of synaptic and axonal withdrawal during a die-back, which could have broader implications across a range of other conditions where synaptic retraction is a pathological feature.

1.3 Postnatal maturation of the neuromuscular system

In the mature, adult neuromuscular system, the NMJ is innervated by a single motor axon, and is therefore described as being monoinnervated. This one-to-one connection ensures robust neurochemical transmission; every action potential that arrives in the terminal of the motor neuron triggers action potentials in all of the muscle fibres that it innervates, facilitating coordinated muscle contraction (Shi et al., 2012, Lichtman and Colman, 2000). The NMJ is widely utilised experimentally to investigate synaptic development and function due to its large size and ease of accessibility (Sanes and Lichtman, 2001). At birth, the NMJ is highly polyinnervated: each NMJ receives multiple axonal inputs (Lichtman and Colman, 2000). The development of precise connectivity between the motor neuron and skeletal muscle fibre involves spatially defined removal of exuberant neuronal processes (Tapia et al., 2012). Across early postnatal development, excess synapses are removed or 'pruned', until just one connection remains, which is then strengthened and maintained throughout life (Lichtman and Colman, 2000, Sanes and Lichtman, 2001). Much work has attempted to define what determines the success of one synapse over another, with activity and competition thought to be key factors. Terminals compete with neighbouring synaptic sites for post-synaptic resources and ultimately, inactive sites are eliminated and withdrawn (Wyatt and Balice-Gordon, 2003). The mechanisms by which such selective degeneration occur remains largely unclear. In terms of morphology, synapse elimination has been compared to a die-back, however it is unclear whether similar pathways are utilised. Throughout this thesis, I examine synaptic stability across development: in Chapter 1, I consider whether synaptic maturity can influence the rate of synaptic degeneration after injury; in Chapter 2, I ask whether changes in

mitochondrial dynamics across development can alter synaptic stability; and in Chapter 3, I examine whether reductions in P53, a factor involved in apoptotic cell death, can delay synaptic maturation. An appreciation of the morphology and mechanisms of developmental synapse elimination is therefore also pertinent.

1.3.1 Morphology and mechanisms of synapse elimination

Many studies have sought to provide mechanistic insight into the process of synapse elimination in the CNS, in various brain regions, however, developmental synapse elimination has been most extensively characterised and is best understood at the developing rodent NMJ. This is largely due to the peripheral location of the NMJ which makes it accessible, but also due to its simple architecture, large size, and ease of functional readout in response to presynaptic axonal stimulation (muscle contraction) (Lee, 2020). The first anatomical descriptions of the presence of multiple axonal inputs in young animals date back to observations by Tello, a student of Ramon y Cajal (Tello, 1907). This was later functionally confirmed through intracellular recordings of neonatal rat muscle fibres, which revealed that in early postnatal life, most end-plate potentials were complex and a summation of multiple inputs, but that these simplified during the second week of life, to resemble that of the adult (Redfern, 1970). Unlike in disease scenarios, during synapse elimination, only select axonal branches are pruned without cellular death.

Several cellular mechanisms have been proposed to underlie this process, with competing hypotheses emerging to explain mechanisms of axonal withdrawal. The first is that exuberant processes degenerate by axonal fragmentation. Ultrastructural similarities with WD have been described in *Drosophila*, and this includes fragmentation, aberrant mitochondria, high cytoplasmic density and clumping of synaptic vesicles (Watts et al., 2004, Watts et al., 2003). Similar features have been described across the neuron, with a combination of morphological and molecular studies also showing that severing the dendritic tree from the cell body, results in subsequent fragmentation in a process that is thought to be dependent on local caspase activity (Williams et al., 2006, Williams and Truman, 2005, Kuo et al., 2006). Glial cells have also been shown to localise to severed dendrites, however their precise role

remains unclear (Han et al., 2011). Much of this work has been undertaken in *Drosophila*. In *Wld*^{s} mice, synapse elimination proceeds normally, suggesting that distinct mechanisms may exist (Gillingwater et al., 2003, Parson et al., 1997, Gillingwater et al., 2006).

A second hypothesis is that axonal branches undergo retrograde retraction, in a similar way as occurs during a die-back; axonal retraction involves the reabsorption of axons and processes into the proximal axon without fragmentation. The presence of retraction bulbs, that are also characteristic of dying-back pathology, and lack of degenerative features have supported this (Rosenthal and Taraskevich, 1977). Long-term 2-photon imaging across the first 3 weeks of postnatal development to image axons in the murine neocortex, has demonstrated that pruning proceeds by retraction of small axon branches (Portera-Cailliau et al., 2005). It is possible that different types of axons may utilise different modes of pruning, depending on length (Luo and O'Leary, 2005). Other work has proposed that synapse elimination may proceed by a distinct mechanism altogether, in a processed termed 'axosome shedding' (Bishop et al., 2004). Bishop et al., 2004 suggest that as axons are eliminated, they shed membrane bound remnants, to expose 'axosomes' that are dense with synaptic organelles at their tips, which are then engulfed by Schwann cells.

Activity-dependent competition has been proposed as a key factor regulating synaptic elimination at the NMJ, with only the most active inputs prevailing. This is supported by the finding that blocking activity can prevent synaptic elimination (Costanzo et al., 2000). Trophic deprivation, particularly of nerve growth factor (NGF), is a well-known model for investigating axonal pruning and the mechanisms of neuronal apoptosis (Maor-Nof and Yaron, 2013, Geden and Deshmukh, 2016). Trophic factors, such as NGF, are critical regulators of axonal maintenance and survival, with withdrawal of trophic support found to activate pro-apoptotic pathways (Sanes and Lichtman, 1999, Harrington and Ginty, 2013). It has been suggested that presynaptic inputs compete for muscle-derived trophic signals; indeed, a lack of trophic support can induce synapse elimination (Goda and Davis, 2003, Sanes and Lichtman, 1999, Huang and Reichardt, 2001). Recent work has implicated glutamatergic transmission

in influencing neuromuscular synapse elimination. Work by Personius et al., 2016 has shown that N-acetylaspartylglutamate that is released from the motor nerve terminal, is converted to glutamate which can bind and activate N-methyl-D-aspartate (NMDA) receptors, leading to Ca^{2+} influx. This group demonstrated that developmental synapse pruning can be delayed by reducing NMDA receptor activation or expression, or by reducing production of glutamate (Personius et al., 2016). Conversely, the addition of exogenous NMDA was shown to accelerate synapse elimination (Personius et al., 2016). Overall, the molecular regulators of neuronal remodelling remain largely unclear, however due to morphological similarities, there has been much debate as to the extent of mechanistic overlap or divergence between different types of axonal and synaptic degeneration.

1.4 Mechanistic commonalities and divergence in morphologically distinct forms of synaptic and axonal degeneration

Despite morphological distinctions between different forms of degeneration, it remains unclear how degenerative pathways relate mechanistically. A diverse range of triggers can ultimately result in neuronal death, and this presents a challenge when attempting to define common degenerative mechanisms. Whilst some work supports the hypothesis that WD and die-back pathways share common mechanisms, other work indicates that distinct mechanisms exist (Gillingwater and Ribchester, 2003, Coleman, 2005, Conforti et al., 2014, Wang et al., 2012, Yaron and Schuldiner, 2016, Mi et al., 2005). Much of the debate over the extent of convergence and divergence in degenerative mechanisms has arisen from conflicting results in mouse models of disease that express *Wld*^{S}.

Support for mechanistic commonality can be seen in cases where *Wld*^{S} is capable of delaying degeneration in models that exhibit a die-back. In a mouse model of progressive motor neuronopathy (*pmn),* it has been shown that the *Wld*^{S} gene product can prevent axonal degeneration, rescue motor neuron number and size, delay deficits in retrograde transport, attenuate symptoms and extend life span (Ferri et al., 2003). In myelin protein zero mice, used to model of charcot-marie-tooth disease, *Wld*^{S} also significantly delays dying-back processes (Samsam et al., 2003). This suggests that

there are mechanistic links between dying-back pathology and WD. Several mechanistic convergence points have been suggested, including: increased intra-axonal Ca^{2+}, impaired axonal transport from the cell body and mitochondrial failure (Coleman, 2005). Changes in mitochondrial dynamics have been linked to changes in the rate of synaptic and axonal degeneration in different physiological scenarios. Proteomic studies investigating synaptic stability in *Wld*^{S} have identified mitochondria as playing an important role in the progression of WD (Wishart et al., 2007). Wishart et al., identified 8 mitochondria-localised proteins that were significantly altered at *Wld*^{S} synapses that are thought to be important in conferring the delayed *Wld*^{S} phenotype. In line with this, blocking the mitochondrial permeability pore can phenocopy protection that is conferred by *Wld*^{S} (Barrientos et al., 2011). Other studies also support that mitochondrial changes are critical in the procession of axonal degeneration, including reports of enhanced levels of mitochondrial proteins at the NMJ during a die-back in SMA mice and altered mitochondrial morphology including rounding and elongation (Neve et al., 2016). Up-regulations of mitochondrial proteins between P10 and P26 of postnatal development have also been described, that correlate with accelerations in synaptic loss following insult across this time frame (Murray et al., 2011).

However, in other models with dying-back pathology, *Wld*^{S} fails to attenuate synaptic and axonal loss. For example, *Wld*^{S} fails to delay degeneration in some mouse models of ALS and SMA (Kariya et al., 2009, Vande Velde et al., 2004, Fischer et al., 2005, Rose et al., 2008). In the superoxide dismutase 1 (SOD1) mouse model of ALS, the presence of *Wld*^{S} fails to delay disease onset, ameliorate motor neuron death, or prevent synaptic and axonal degeneration (Vande Velde et al., 2004). Work by Fischer et al., also reports that *Wld*^{S} presence fails to mitigate motor axon loss in SOD1 mice (Fischer et al., 2005). In *SMNΔ7* mice, *Wld*^{S} does not improve the synaptic phenotype (Kariya et al., 2009, Rose et al., 2008). Work in *Wld*^{S} mutants has also demonstrated that the normal rate of postnatal synapse elimination is unaffected (Parson et al., 1997), again suggesting that distinct mechanisms exist.

There is evidence to suggest that the presence of dying-back pathology may delay WD, which could suggest that mechanisms of a die-back and WD oppose each other. For example, *Wasted* (*Wst*) mice carry a spontaneous mutation that abolishes the expression of eukaryotic translation elongation factor 1 alpha 2 (*eEF1A2)*. Loss of this factor triggers dying-back neuropathy (Murray et al., 2008b). It has been shown that whilst loss of *eEF1A2* significantly inhibits the initiation and progression of WD, it is required to prevent dying-back pathology at the NMJ (Murray et al., 2008b). In neonatal mice, synaptic and axonal degeneration in response to traumatic or hypoxic nerve injury is slower than in adult mice in the DL muscles (Murray et al., 2011). Resistance to WD gradually declines between 2-3 weeks of age until adult levels of vulnerability to injury are established (Murray et al., 2011). The delay in injury-induced synaptic degeneration observed in this time window coincides with the period of time during which extensive remodelling and synapse elimination is ongoing, supporting the hypothesis that opposing mechanisms exist. Collectively, these data indicate that mechanisms underlying dying-back pathology in these scenarios are distinct from those responsible for WD, and those in other models where rates of degeneration can be modified by the presence of Wld^S.

The debate as to whether independent cascades exist remains ongoing; it is unclear whether morphological distinctions in axonal degeneration also translate to mechanistic distinctions. A better understanding of factors that can modify the rates of degeneration in different physiological scenarios will help us to better categorise degeneration and identify therapeutics which could have applications across a range of neurodegenerative diseases.

1.5 Thesis aims

The work contained within this thesis aims to explore factors that can influence the rate of degeneration under different degenerative scenarios, including following injury, during disease and during postnatal development. Despite distinct morphologies in response to various stimuli, the mechanisms of synaptic degeneration and how they relate to one another remain largely unknown. Understanding factors that can influence the rate of degeneration is of critical importance if we are to identify and develop therapies to target neurodegeneration in different contexts.

Chapter 1

Aims:

1) To expand, optimise and explore an *ex vivo* model of peripheral nerve injury to study a range of different muscles that have not previously been looked at in the context of WD
2) To apply the *ex vivo* model to investigate the impact of underlying dying-back pathology on the progression of WD

Rationale:

Previous work has indicated that rates of WD are developmentally regulated in the deep lumbrical muscles of the mouse (Murray et al., 2011), however it is unclear if this is unique to these muscles. Expansion of an *ex vivo* model of peripheral nerve injury will permit the inclusion of other muscle preparations, including those that are relevant to disease. Application of this *ex vivo* assay will permit the inclusion of preparations from mouse models that exhibit different synaptic pathologies, thereby providing a useful tool to investigate how these backgrounds can influence WD.

Hypotheses:

1) An *ex vivo* model can be expanded to investigate synaptic loss following injury in a range of different muscles
2) Increases in the rate of degeneration during postnatal development will be a common feature across different muscles
3) Selective vulnerability of muscles is a feature of WD
4) The presence of dying-back pathology will delay synaptic loss following injury

Chapter 2

Aims:

1) To analyse two independent proteomic datasets to determine whether mitochondrial alterations in the murine proteome are common during early postnatal development
2) To investigate whether changes in mitochondrial number or complex protein levels correlate with differences in synaptic vulnerability during early postnatal development or between muscles/nerves

Rationale:

In mice, neonatal NMJs are significantly more resistant to nerve injury than those in the adult (Murray et al., 2011). Across the first 3 weeks of life, the rate of WD progressively increases until adult rates of degeneration are achieved (Murray et al., 2011). Within this developmental time frame, increases in mitochondrial proteins have also been reported that appear to coincide with accelerations in synaptic loss (Kline et al., 2019, Kim et al., 2019). Pharmacological manipulation of complex I has been shown to alter the rate of synaptic degeneration (Kline et al., 2019). It is unclear whether changes in mitochondrial protein expression can similarly explain differences in the synaptic response to injury in other muscles, either temporally or regionally. Understanding how mitochondrial biology changes across this transitional, postnatal time window in a range of muscles and nerve will help us to better understand factors that can influence synaptic vulnerability.

Hypotheses:

1. Consistent increases in mitochondrial-associated proteins will be revealed through analyses of two independent proteomic screens
2. Increases in mitochondrial content will positively correlate with patterns of developmental regulation that are seen following injury
3. Increases in mitochondrial content will positively correlate with increased synaptic vulnerability to injury in muscles that display greater vulnerability to synaptic loss following nerve injury
4. Increases in Complex I of the respiratory chain will positively correlate with patterns of developmental regulation that are seen following injury
5. Increases in Complex I of the respiratory chain will positively correlate with selective vulnerability to synaptic loss that is seen following nerve injury

Chapter 3

Aims:

1) To investigate the role of P53 in morphologically distinct types of synaptic and axonal degeneration
2) To assess whether reduced levels of P53 can influence the expression of synaptic genes

Rationale:

P53 is a transcript that plays a role in cell death, however its role in synaptic and axonal degeneration is unclear. Upregulation of P53-associated transcripts in response to reduced Smn are well-documented in the literature (Murray et al., 2015, Baumer et al., 2009, Jangi et al., 2017, Staropoli et al., 2015, Zhang et al., 2008). Previous work has indicated that postnatal reductions in P53 can reduce NMJ loss in a mouse model of SMA, however P53 reduction failed to extend lifespan or improve motor function (Courtney et al., 2019). A more comprehensive analysis across different muscles is required to assess whether reductions in P53 can uniformly improve synaptic retention. Previous work has indicated that P53 is present at synapses (Gilman et al., 2003) and that P53 signalling increases in the distal nerve following injury despite separation from the cell body (Yao et al., 2013), suggesting that P53 may play a role in synaptic

degeneration in WD. Application of the *ex vivo* model in this case will allow us to assess whether P53 plays a role in regulating synaptic loss following injury. Pro-apoptotic pathways have been implicated in synapse elimination, particularly in trophic withdrawal models (Maor-Nof et al., 2016). Investigating whether P53 reductions can delay axonal pruning *in vivo* will provide a better indication of the role of pro-apoptotic pathways.

Hypotheses:

1. Reductions in P53 will delay synaptic loss following injury in wild-type mice
2. Reductions in P53 will delay synaptic loss in a mouse model of SMA
3. Reductions in P53 will delay synapse elimination during normal postnatal development
4. P53-related transcripts will be dysregulated in a mouse model of SMA
5. P53 reduction will alter the expression of synaptic genes that are thought to be regulated by P53, including *Bin1, Picalm* and *Mef2c*

1.6 Ethics statement

All animal procedures were performed in accordance with UK Home Office and institutional guidelines.

1.7 Mouse Maintenance

Throughout this thesis, a number of murine models are used to investigate factors that can influence the rate of synaptic degeneration under different physiological conditions. These models are described under the relevant headings of this section, however a brief overview of their applications is provided here.

Firstly, an *ex vivo* model of peripheral nerve injury was optimised using adult preparations from a well-characterised mouse model where synaptic loss is known to be slower after injury (Wld^S). Next, preparations from MCos1 mice - referred to as wild-type mice – were introduced to expand the *ex vivo* model to permit the inclusion a range of different muscles. For these experiments, I chose to examine the time frame of P15 to P25, as the rate of synaptic degeneration following injury progressively increases during this developmental time period in the deep lumbrical muscles (Murray et al., 2011). This time frame was also used to examine changes in mitochondrial proteins across development to ask whether changes in mitochondrial dynamics could be responsible for conferring developmental delays in synaptic degeneration. To study synaptic loss in a disease scenario, I utilised the $Smn^{2B/-}$ mouse model of SMA at time points P15 or P18, as these time points represent late-symptomatic or end-stage disease respectively. I also used a P53-floxed mouse model to look at the role of P53 in synaptic degeneration under different scenarios. To look at an injury scenario, I used *ex vivo* preparations from P53-floxed mice at P18 and P25, since we would expect to observe differential and robust synaptic loss following injury at these points. To look at a disease scenario, I used P53-floxed $Smn^{2B/-}$ mice, and

assessed the level of synaptic innervation remaining in different muscles at disease end-stage (P18). Finally, to investigate synapse loss that occurs during normal development or when P53 is depleted, I evaluated levels of mono- or polyinnervation remaining at P10 or P14, since the maturation of the neuromuscular system is thought to occur across the first few weeks of life. These models are detailed below.

1.7.1 Wld^s mice – Wallerian degeneration slow model

C57BL6/*Wld*^{s} adult mice were group housed in individually ventilated cages under pathogen-free conditions with *ad libitum* access to food and water, on a 12:12 light/dark cycle within animal facilities at the University of Edinburgh. These mice were maintained and kindly provided by Professor Richard Ribchester to assist with optimising the *ex vivo* system.

1.7.2 MCos1 mice – wild-type mice

C57BL6/J MCos1, herein referred to as wild-type mice, were group housed in individually ventilated cages under pathogen-free conditions, with *ad libitum* access to food and water, on a 12:12 light/dark cycle within animal facilities at the University of Edinburgh. Wild-type mice of either sex were sacrificed between P15 and P25, as this is the time frame during which developmental regulation of WD has previously been described (Murray et al., 2011). When lumbrical muscle preparations were harvested only, animals were sacrificed by cervical dislocation and death was confirmed by severing a major artery. When cranial/abdominal preparations were harvested, these animals were sacrificed by an inhalational overdose of anaesthetic (isofluorane) and death was confirmed by severing the carotid artery.

1.7.3 Smn$^{2B/-}$ mice – an intermediate mouse model of SMA

C57BL/6 Smn$^{2B/2B}$ and Smn$^{+/-}$ mice were maintained in individually ventilated cages under pathogen-free conditions, with *ad libitum* access to food and water, on a 12:12 light/dark cycle within animal facilities at the University of Edinburgh. The *Smn*$^{2B/-}$ mouse is an intermediate mouse model of the childhood motor neuron disease, SMA that exhibits dying back pathology. The *Smn2B* allele consists of a three-nucleotide substitution in the exon enhancer region within exon 7 of the murine *Smn* gene. The resultant mouse has reduced levels of full-length, endogenous SMN protein which leads to progressive loss of lower motor neurons (DiDonato et al., 2001; Hammond et al., 2010; Bowerman et al., 2012). Symptom onset is at around P10, and, in our hands, this model has a lifespan of around 21 days. *Smn*$^{2B/-}$ mice of either sex were sacrificed at P18 by inhalational overdose of anaesthetic (isofluorane) and death was confirmed by severing the carotid artery.

1.7.4 P53-floxed mice

This colony was established in the Murray Lab after kind donation by Dr. Luke Boulter and Dr Kevin Myant (University of Edinburgh). Mice were group housed in open cages, with *ad libitum* access to food and water, on a 12:12 light/dark cycle within animal facilities at the University of Edinburgh. These mice have been described in depth by our lab previously (Courtney et al., 2019, see co-author paper provided in Appendix 3 for reference). For work investigating the role of P53 in disease scenarios, mice were maintained in breeding pairs that were made up of an Smn$^{2B/2B}$;P53$^{fl/fl}$ and Smn$^{+/-}$;P53$^{fl/fl}$;CAG-Cre^{+} mice, to produce Smn$^{2B/-}$;P53$^{fl/fl}$;CAG-Cre^{+}, herein referred to as P53-floxed Smn$^{2B/-}$, and Smn$^{2B/+}$;P53$^{fl/fl}$;CAG-Cre^{+} controls. Controls from these breeding pairs also produce the equivalent Cre^{-} controls, yielding a total of 4 experimental genotypes. P53-floxed Smn^{2B-} mice and control littermates of either sex were sacrificed by rising CO_2 and death was confirmed by severing the carotid artery. P53 lines consisting of Smn$^{+/+}$;P53$^{fl/fl}$;Cre^{+} mice and Smn$^{2B/-}$;P53$^{fl/fl}$;Cre^{+}, referred to herein as P53-floxed wild-type or P53-floxed Smn$^{2B/-}$ mice were also maintained. Mice for *ex vivo* experiments were sacrificed by an inhalational overdose of anaesthetic

(isofluorane) and death was confirmed by severing the carotid artery, whilst those sacrificed for other work were sacrificed by rising CO_2 and death was confirmed by severing the carotid artery.

1.8 Genotyping

1.8.1 DNA Extraction

DNA was extracted from tail tips or ear notches by digestion in 500μL of lysis buffer composed of 0.5M EDTA, 1M Tris- HCl, 1M NaCl, 10% SDS in ddH_2O and 2.5μL of Proteinase K (1mg/mL) for 24 hr at 55°C. DNA was precipitated using isopropanol and washed in duplicate with 70% ethanol. After drying, DNA was re-suspended in either 200μL or 50μL of ddH_2O for tail tips and ear notches respectively, and could be nanodropped if required. DNA was stored at -20°C.

An alternative method was also applied in some cases if genotyping was required more quickly; this could be undertaken on the same day. In these cases, DNA was extracted from tail tips or ear notches by digestion in 600μL or 300μL of 50mM NaOH respectively. These were then heated to at least 95°C for 10 minutes. DNA was precipitated using 1M Tris-HCl (pH 8.0). After microfuging for 6 minutes, the supernatant was transferred to a new eppendorf and DNA was stored at -20°C.

1.8.2 PCR Protocols

For identification of appropriate genotypes and maintenance of breeding pairs, four PCR protocols were required. The relevant primer sequences pertaining to these protocols are detailed in Table 2, and master mix components and temperature cycles are provided in Tables 3-12. For ease, a summary of the expected band sizes is provided in Figure 4.

The Smn^{2B} protocol was used to identify the presence or lack of the Smn^{2B} allele. The *Smn2B* allele was identified by a band at 700bp. This protocol used an Invitrogen PCR Kit. 9μL of master mix (Table 3) was added to 1μL of DNA and set to a pre-programmed temperature cycle (Table 5). The $Smn^{+/-}$ protocol was used to identify the presence or absence of the Smn null allele. The null Smn allele was identified by a band at 500bp, whilst the wild-type Smn allele was identified at 800bp. This protocol used an Invitrogen PCR Kit. 10μL of master mix (Table 5) was added to 2μL of DNA and set to a pre-programmed temperature cycle (Table 6). The Cre protocol was used to identify whether a mouse was Cre positive or Cre negative. This protocol used an Invitrogen PCR Kit. 10μL of master mix (Table 7) was added to 2μL of DNA and set to a pre-programmed temperature cycle (Table 8). The P53 protocol was used to identify the presence or absence of the P53-floxed allele. This protocol used a KAPA PCR Kit. 26.5μL of master mix (Table 9) was added to 2μL of DNA and set to a pre-programmed temperature cycle (Table 10).

For analyses of Cre-mediated recombination in P53-floxed mice, PCR was performed on genomic DNA extracted from tail tips (Note that visualisation of this result can be seen in Chapter 3, Results, Figure 3.1). This protocol used an Invitrogen PCR Kit. 9μL of master mix (Table 11) was added to 1μL of DNA and set to a pre-programmed temperature cycle (Table 12). This protocol was used to identify the presence of the recombined allele. The recombined allele was identified by a 612bp product.

Table 2: PCR Primer Sequences

Protocol	*Primer Sequence*
Smn^{2B}	F: 5'AACCTCCGGGTCCTCCTTCCT R: 5'TTTGGCAGACTTTAGCAGGGC
$Smn^{+/-}$	F Common: 5'CTCCGGGATATTGGGATTG R Wild-type: 5'TTTCTTCTGGCTGTGCCTTT R Mutant: 5'GGTAACGCCAGGGTTTTCC
Cre	F Control (*interleukin-2*): 5'-CTAGGCCACAGAATTGAAAGATCT R Control (*interleukin-2)*: 5'-GTAGGTGGAAATTCTAGCATCATC F Cre: 5'TTAATCCATATTGGCAGAA R Cre: 5'CAGGCTAAGTGCCTTCTCT
P53-floxed	F P53-wild-type: 5'-CTCAGCAGTAAGGAAGACA R P53-wild-type: 5'-CCATGAGACAGGGTCTTGC F P53-floxed: 5'-CTGTGCCCTCCGTCCTTTT R P53-floxed: 5'-GGCTGCAGATAACTTCGTATAGCAT
P53-floxed recombined allele	P53-intl-fwd: 5′-CACAAAAACAGGTTAAACCCA P53-int10-rev: 5′-GAAGACAGAAAAGGGGAGGG

Table 3: 2B Protocol Master Mix Components

Reagent	**Volume (*μ*L)/sample**
Water	7.2
Buffer	1.0
$MgCl_2$	0.3
dNTPs (Invitrogen)	0.2
'2B Forward' Primer	0.1
'2B Reverse' Primer	0.1
Taq	0.1

Table 4: 2B Protocol Temperature Cycle

Step Number and Temperature (°C)	**Time**
1. 94°C	3 minutes
2. 94°C	45 seconds
3. 58°C	45 seconds
4. 72°C	45 seconds
REPEAT STEPS 2-4 35X	
5. 72°C	5 MINUTES
6. 4°C	HOLD

Table 5: $Smn^{+/-}$ Protocol Master Mix Components

Reagent	**Volume (μL)/sample**
Water	4.85
Buffer	0.97
$MgCl_2$	0.48
dNTPs (Invitrogen)	0.24
'Forward Common' Primer	1.60
'Wild Type Reverse' Primer	1.20
'Mutant Reverse' Primer	0.60
Taq	0.05

Table 6: $Smn^{+/-}$ Protocol Temperature Cycle

Step Number and Temperature (°C)	**Time**
1. 94°C	3 minutes
2. 94°C	30 seconds
3. 58°C	1 minute
4. 72°C	1 minute
REPEAT STEPS 2-4 35X	
5. 72°C	2 MINUTES
6. 4°C	HOLD

Table 7: Cre Protocol Master Mix Components

Reagent	**Volume (μL)/sample**
Water	3.25
Buffer	1.2
$MgCl_2$	0.48
dNTPs (Invitrogen)	0.24
'Control Forward' Primer	1.2
'Control Reverse' Primer	1.2
'Cre Forward' Primer	1.2
'Cre Reverse' Primer	1.2
Taq	0.03

Table 8: Cre Protocol Temperature Cycle

Step Number and Temperature (°C)	**Time**
1. 95°C	3 minutes
2. 95°C	30 seconds
3. 51.7°C	1 minute
4. 72°C	1 minute
REPEAT STEPS 2-4 35X	
5. 72°C	2 minutes
6. 10°C	HOLD

Table 9: P53-floxed Protocol Master Mix Components

Reagent	**Volume (μL)/sample**
Water	10.9
Buffer (KAPA)	5
Enhancer (KAPA)	5
dNTPs (KAPA)	0.5
Wild-type Forward Primer	1.25
Wild-type Reverse Primer	1.25
P53-floxed Forward Primer	1.25
P53-floxed Reverse Primer	1.25
Taq (KAPA Robust2G)	0.1

Table 10: P53-floxed Protocol Temperature Cycle

Step Number and Temperature (°C)	**Time**
1. 94°C	2 minutes
2. 94°C	20 seconds
3. 65°C	15 seconds
4. 68°C	10 seconds
REPEAT STEPS 2-4 10x	
5. 94°C	15 seconds
6. 60°C	15 seconds
7. 72°C	10 seconds
REPEAT STEPS 6-8 28X	
8. 72°C	10 minutes
9. 4°C	HOLD

Table 11: P53-floxed recombined allele Protocol Master Mix Components

Reagent	**Volume (μL)/sample**
Water	7.2
Buffer	1
$MgCl_2$	0.3
dNTPs (Invitrogen)	0.2
P53-intl-fwd	1.2
P53-intl-rev	1.2
Taq	1.2

Table 12: P53-floxed recombined allele Protocol Temperature Cycle

Step Number and Temperature (°C)	**Time**
1. 94°C	30 seconds
2. 58°C	30 seconds
3. 72°C	50 seconds
REPEAT STEPS 2-4 30x	
4. 4°C	HOLD

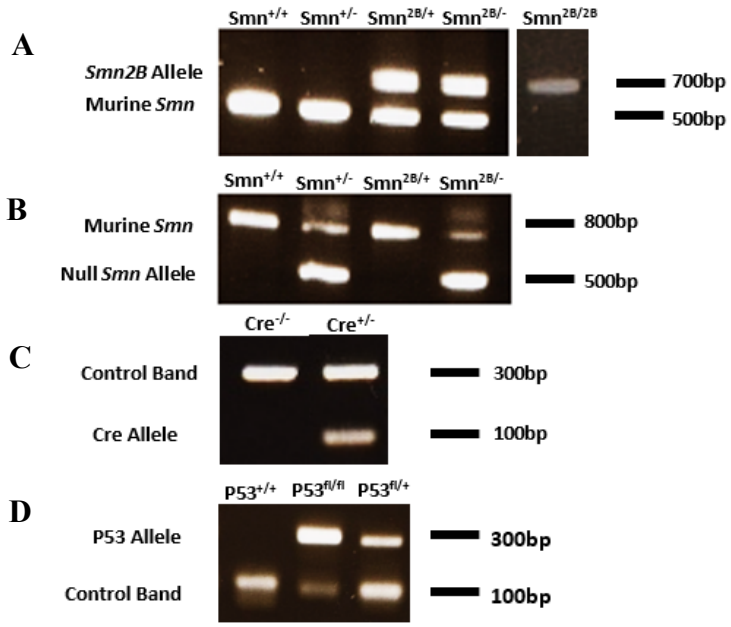

Figure 4: Genotyping results and expected band sizes. (**A**) Resulting possibilities following the Smn2B protocol. This protocol can be used to determine if a mouse is $Smn^{2B/+}$ or $Smn^{+/+}$. Note that this protocol cannot be used to differentiate between $Smn^{2B/+}$ and $Smn^{2B/-}$, therefore an additional protocol is required as shown in B. (**B**) Resulting possibilities after following the $Smn^{+/-}$ protocol. This protocol can be used to determine if a mouse carries the null allele. (**C**) Resulting possibilities after following the Cre protocol. This protocol can be used to determine if a mouse is Cre positive. (**D**) Resulting possibilities after following the P53-floxed protocol. This protocol can be used to confirm the presence of a floxed allele. Note that this protocol cannot distinguish copy number, for which further qPCR analysis is required. Breeding for homozygosity was undertaken by previous members and so copy number analyses were not required for this work (Courtney et al., 2019).

1.9 qPCR

Mitochondrial DNA analyses, and P53 DNA recombination analyses were undertaken using quantitative polymerase chain reaction (qPCR). DNA was extracted from tissues by conventional extraction methods (see Materials and Methods, *1.8.1 DNA Extraction,* for details) and concentration was determined using a nanodrop. All samples were loaded at concentration of 10ng/μL. Primer sets were custom-made (Sigma) and selected based on previous work by Puente et al., 2014 and Marino et al., 2000 (Table 13). To test primer efficacy, standard curves were generated from two-fold dilution series of mixed sample DNA. Relative gene expression was calculated using the $2^{-\Delta\Delta cT}$ formula and normalised to *H19* or *Gapdh* for mitochondrial analysis (see Table 13 for primer sequences). Genes used for normalisation are detailed in figure legends.

1.10 RT-qPCR

Transcriptional analysis were undertaken using quantitative reverse transcription (RT-qPCR). RNA from spinal cords was extracted using an RNeasy Kit (Qiagen), according to manufacturer's instructions and concentration determined using a nanodrop. Reverse transcription (RT) was performed using the QuantiTect Reverse Transcription Kit (Qiagen), according to manufacturer's instructions, and complementary DNA (cDNA) was used at a concentration of 10ng/μL. A CFX96 Touch Real-Time PCR Detection System machine (Bio-Rad) was used. RT-qPCR analyses was undertaken using PrimePCR SYBR Green assays for mouse. Pre-optimised primers based on descriptions by Merlo et al., 2014 were used to target *Bin1*, *Mef2c* and *Picalm* (primers available to purchase as SYBR® Green Assays for mouse from Bio-rad). Relative gene expression was calculated using the $2^{-\Delta\Delta cT}$ formula and normalised to *Actin*, *Gapdh* and *Ywhaz* (see Table 13 for normalisation primer sequences). Genes used for normalisation are detailed in figure legends.

Table 13: qPCR primer sets

Target	*Primer Sequence*
*Mitochondrial-encoded NAD2 (*herein referred to as *mtDNA)*	F: 5' CCCATTCCACTTCTGATTACC R: 5'ATGATAGTAGAGTTGAGTAGCG
H19	F: 5'GTACCCACCTGTCGTCC R: 5'GTCCACGAGACCAATGACTG
P53-recombined allele	F: 5′-CACAAAAACAGGTTAAACCCA R: 5′-GAAGACAGAAAAGGGGAGGG
Gapdh	F: 5' CGTCCCGTAGACAAAATGGT R: 5'TTGATGGCAACAATCTCCAC
Actin	F: 5'CCGTCAGGCAGCTCATAGCTCTTC R: 5'CTGAACCCTAAGGCCAACCGT
Ywhaz	F: 5'TTGATCCCC AATGCTTCGC R: 5'CAGCAACCTCGGCCAAGTAA

1.11 Tamoxifen dosing to induce P53 recombination

Pups expressing the P53-floxed allele and control littermates were dosed using a modified oral gavage for neonates with 80mg/kg Tamoxifen (Sigma) dissolved in corn oil to a concentration of 20mg/mL. Note that tamoxifen treatment was initiated prior to P5, as this time point precedes evidence of *P53* pathway activation in the spinal cord in $Smn^{2B/-}$ mice (Courtney et al., 2019). P53-floxed $Smn^{2B/-}$ mice and controls were treated at P4 and 5, and were sacrificed at P15. P53-floxed wild-type mice were treated for three consecutive days; for the *ex vivo* study, these were treated at P4, 5 and 6 and for the synapse elimination study, these were treated at P1, 2 and 3. Pups were monitored after dosing to ensure that they maintained condition, that maternal care was resumed, and that pups continued to thrive. If over 10% of the maximum recorded body mass was lost over a period of 48 hours, then the animal was humanely sacrificed.

1.12 *Ex vivo* explant preparation

Deep lumbrical (DL), cranial and abdominal nerve/muscle explants were gross dissected as described previously (Murray et al., 2010, Murray et al., 2014, Brown et al., 2015) in Hepes-buffered saline composed of NaCl (137 mM), KCl (5 mM), $CaCl_2 \cdot 2H_2O$ (2 mM), $MgCl_2 \cdot 6H_2O$ (1 mM), glucose (5.6 mM) and Hepes (5 mM) with pH corrected to 7.4. Nerves (sciatic, facial or intercostal) were severed at a consistent point, and distal nerve portions with attached musculature were pinned to dental wax and suspended in oxygenated mammalian physiological saline containing: NaCl (120 mM), KCl (5 mM), $CaCl_2 \cdot 2H_2O$ (2 mM), $MgCl_2 \cdot 6H_2O$ (1 mM), $NaH_2PO_4 \cdot 2H_2O$ (0.4 mM), $NaHCO_3$ (23.8 mM), glucose (5.6 mM), gentamicin (50 mg/ml, Thermo Fisher) and kanamycin (100 mg/ml, Thermo Fisher) in a 30 mL bijou tube. The bijou lid was modified, with two 0.8 mm needles, one needle clipped short, above the buffer level, to act as a pressure valve. A length of 0.50 mm tubing (VWR) sufficient to reach the bottom of the receptacle was attached to the other needle to provide a constant supply of 95/5% O_2/CO_2 to equilibrate the saline, at a perfusion rate of approximately 5 mL/min. The bathing solution was equilibrated for approximately 30 min before adding the sample. The receptacle containing the nerve/muscle explant was then incubated in a 30°C water bath for 24 hr (Fig. 5). Temperature was monitored during this period using a digital thermometer (Fisher Traceable Digital Thermometer with stainless steel probe).

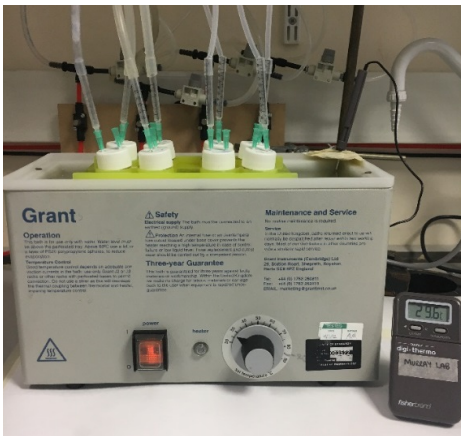

Figure 5: Ex vivo rig setup. Receptacles containing mammalian physiological saline (see Materials and Methods, *1.12 Ex vivo explant preparation* for composition), and a suspended tissue sample pinned to dental wax were suspended in a water bath, with gas supply (95/5% O_2/CO_2) and air vent to relieve pressure as shown. Temperature was monitored by digital thermometer via a probe that was secured in the bath.

1.13 Non-*ex vivo* tissue collection

For non-*ex vivo* morphological work, abdominal and cranial preparations were fixed immediately for 15 min. Muscles of interest were microdissected in 1x phosphate buffered saline (PBS) as described previously (Murray et al., 2010, Murray et al., 2014, Brown et al., 2015) (Fig. 6), in preparation for immunostaining. Any tissue that was collected for protein or transcriptional analyses were snap frozen immediately, to reduce the chance of post-mortem changes.

To assess the level of P53 reduction, heart, tibialis anterior muscle, liver, and spinal cords, were collected from P15 *Smn*$^{2B/+}$ and *Smn*$^{2B/-}$ P53-floxed and control mice and fixed immediately for 60 min (heart), 15 min (muscle), overnight (liver) or for 4 hr (spinal cord). Embedding and sectioning preparation, and immunohistochemistry for different tissues are detailed below and were kindly provided by Victoria Zimmel:

Heart: Following thorough washing with 1xPBS, hearts were equilibrated in 30% sucrose solution before embedding in 50% optimal cutting temperature compound

(OCT) and 15% sucrose in 1xPBS. Forceps were used to suspend the hearts vertically with the apex at the bottom of the mould, and great vessels at the top, before snap freezing over dry ice. Hearts were sectioned on Leica cryostat at 10μM, with sections collected at 160μM intervals from the middle third of the heart on Superfrost® Plus slides (Thermo Fisher). Slides were stored at -20°C prior to staining. In preparation for staining, slides were mounted onto Shandon coverplates (Thermo Fisher) in 1xPBS and placed in Shandon sequenza (Thermo Fisher) slide rack at room temperature.

Tibialis anterior muscle: Following thorough washing with 1xPBS, tibialis anterior muscles were equilibrated in 30% sucrose solution before embedding in 50% OCT and 15% sucrose in 1xPBS over dry ice. Muscles were sectioned on Leica cryostat at 10μm, with sections collected at 100μm intervals from the middle third of the muscle on Superfrost® Plus slides (Thermo Fisher). Slides were stored at -20°C prior to staining. In preparation for staining, slides were mounted onto Shandon coverplates (Thermo Fisher) in 1xPBS and placed in Shandon sequenza (Thermo Fisher) slide rack at room temperature.

Liver: Fixed livers were embedded in paraffin wax in preparation for sectioning on a microtome at 8μm. Antigen retrieval was performed using citric acid buffer (10mM sodium citrate; 0.05% Tween 20; with pH adjusted to 6); slides were immersed in a staining rack in a water bath at 95-100°C for around 30 min. The staining dish was removed from the water bath and allowed to cool at room temperature for around 25 min. In preparation for staining, slides were mounted onto Shandon coverplates in 1xPBS and placed in sequenza and washed with 1xPBS for 10 min.

Spinal Cord: Spinal cords were equilibrated in 30% sucrose in 1xPBS for 24-48 hours. Samples were then embedded in moulds in embedding solution composed of 50% OCT and 15% sucrose in 1xPBS. Samples were snap frozen over dry ice. Tissue was sectioned longitudinally on a Leica cryostat at 20°C at 10μm thickness. Sections were collected at 50μm intervals on Superfrost Plus slides (Thermo Fisher). Slides were stored at -20°C prior to staining. In preparation for staining, slides were mounted onto

Shandon coverplates (Thermo Fisher) in 1xPBS and placed in Shandon sequenza (Thermo Fisher) slide rack at room temperature.

1.14 Immunohistochemistry

For *ex vivo* tissue, after 24 hr incubation in oxygenated mammalian physiological saline, muscle preparations were fixed immediately in 4% paraformaldehyde (EMS) for 15 min. For all other tissue, muscle preparations were dissected and fixed immediately in 4% paraformaldehyde (EMS) for 15 min. Muscles were then washed in PBS. Muscles of interest were microdissected as described previously (Murray et al., 2010, Murray et al., 2014, Brown et al., 2015) (Fig. 6), and permeabilised in 2% Triton-X-100-PBS (Sigma; PBT) for 30 min on a rocking platform at room temperature. Blocking solution (4% bovine serum albumin [BSA]/1% PBT) was applied for 60 min followed by primary antibodies against synaptic vesicle protein 2 (SV2) and neurofilament (NF) (SV2, 1:100; 2H3, 1:50 respectively, both from Developmental Studies Hybridoma Bank) in blocking solution, and left to incubate at 4°C on a rocking platform for 24 hr. Preparations were then washed three times for 5 min with PBS. Secondary antibody (anti-mouse, Alexa Fluor 488, Stratech, 1:250 in 1×PBS) was added to each well and incubated in the dark at room temperature for a minimum of 4 hr. Muscles were washed three times in 1 × PBS for 5 min, and incubated with tetramethylrhodamine-conjugated α-bungarotoxin (TRITC-BTX; Thermo Fisher, 1:250) for 20 min. Muscles were washed in PBS and whole-mounted on glass slides with Mowiol® (Calbiochem) and cover-slipped. Slides were stored in the dark at 4°C.

For activated caspase-3 cell staining, slides that were mounted in sequenza were washed with 400μL of 1xPBS and then permeabilised for 30 min with 400μL of 2% Triton X-100 (Sigma) in PBS. Sections were blocking with 400μL of 1% Triton X-100, 4% BSA (Sigma) in PBS. 300μL of rabbit anti-active caspase-3 (BD Bioscience) primary antibody (1:200 in block) was added and slides were incubated at 4°C overnight. Slides were washed in triplicate with PBS, before incubation with secondary antibody (AlexaFluor 488 donkey anti-rabbit IgG, Life Technologies, 1:250

in block) in the dark for 2 hr. Slides were washed in triplicate with PBS for 10 minutes each. 400μL of 4', 6-diamidino-2-phenylindole (DAPI) (DAPI, 1:1000, in 1xPBS) was then added for 10 min in the dark. Following triplicate washing with PBS, slides were once again mounted in Mowiol® and cover-slipped. Slides were stored in the dark at 4°C.

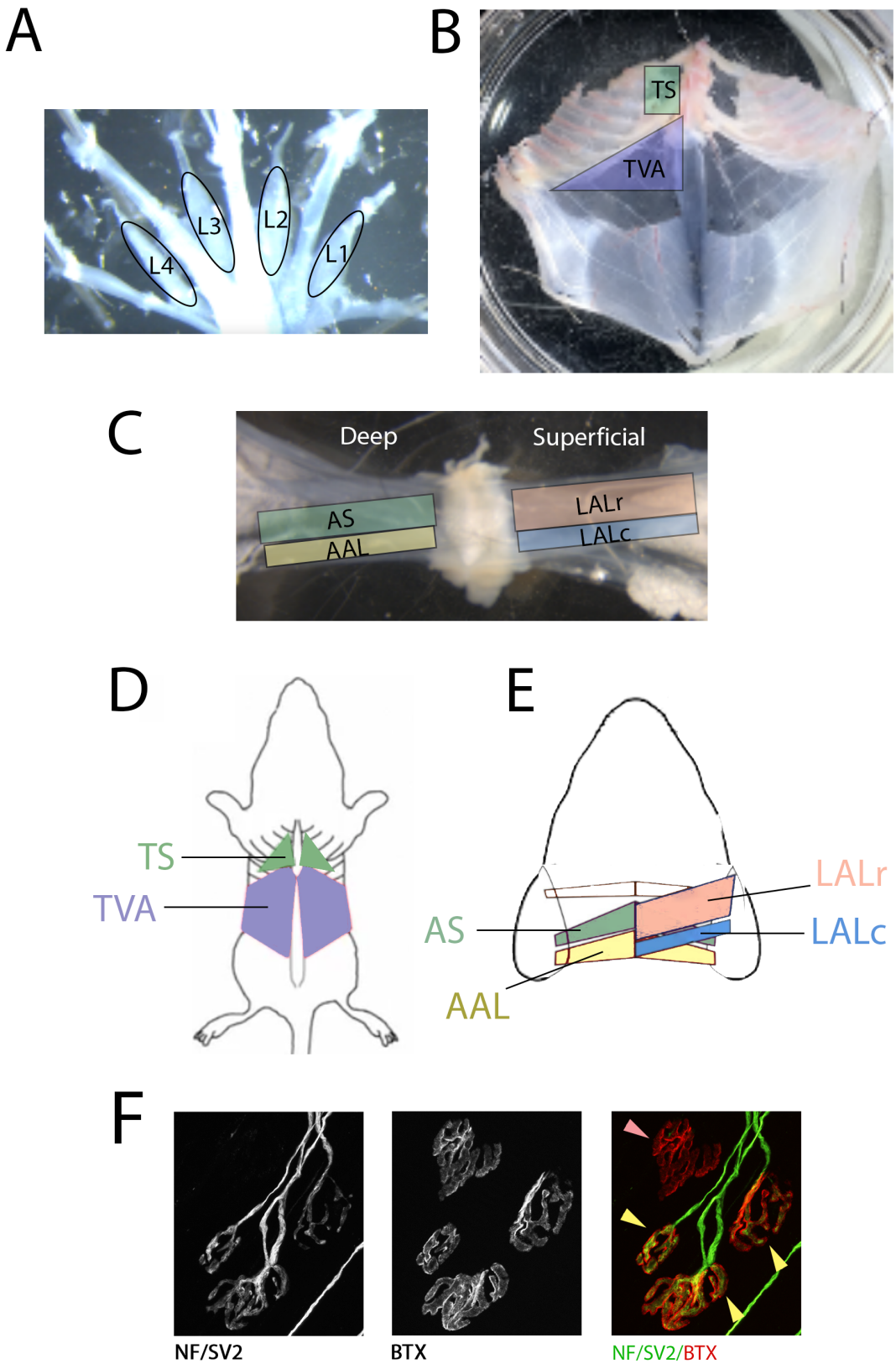
A
L4
L3
L2
L1
B
TS
TVA
C
Deep
Superficial
AS
AAL
LALr
LALc
D
TS
TVA
E
LALr
AS
LALc
AAL
F
NF/SV2
BTX
NF/SV2/BTX

Figure 6: Muscles of interest that were microdissected and quantified following fixation. (**A**) Deep lumbrical muscle preparation after removal of flexor digitorum brevis, with lumbrical muscles 1-4 highlighted by black rings. (**B**) Thoracoabdominal preparation with the superficial layer of external oblique and rectus abdominis muscles removed to expose the deeper muscles of interest. Superior portion of transversus abdominis (TVA) and triangularis sterni (TS) muscles highlighted. (**C**) Cranial muscle preparation with cranial muscles of interest highlighted. Deeper muscles – auricularis superior (AS) and adductor auris longus (AAL) – and superficial muscles – rostral and caudal bands of the levator auris longus (LALr/LALc respectively) are highlighed. (**D-E**) Schematics to show the anatomical positions of muscles of interest from thoracoabdominal and cranial regions respectively. (**F**) NMJs labelled with antibodies against neurofilament (NF, green) and synaptic vesicle protein 2 (SV2, green), and α-bungarotoxin (BTX, red). The yellow arrowheads highlight endplates that would be quantified as 'full', whereas the pink arrowhead indicates a vacant endplate, where apposition between the pre-synaptic terminal and the motor endplate has been lost (see Materials and Methods, *1.17 Quantification and statistical analyses* for further detail of categorisation).

1.15 Quantitative fluorescent western blotting

Levels of Complex I-V in muscle and Complex I, IV and V in nerve were determined by quantitative fluorescent western blotting, following protocols as described previously (Huang et al., 2019). Muscles were collected bilaterally and pooled from 2 animals to ensure adequate protein yield, and included: LALr/LALc/AS combination of cranial muscles; AAL cranial muscle; TVA/TS combination of thoracoabdominal muscles. Nerves were collected bilaterally and pooled from 2 animals, and included sciatic/tibial nerve and intercostal nerves (x15 intercostal nerves in total). Brain (halved along the longitudinal fissure) with cerebellum removed, and spinal cord (halved along the midline) were also harvested. Spinal cord was removed via application of needle pressure applied from the rostral end (note that results relating to central tissue can be found in Appendix 4). All tissue were snap-frozen on dry ice prior to extraction. In brief, tissue was thawed and homogenised in ice-cold PBS with

Dounce homogeniser (VWR) and extracted in RIPA lysis and extraction buffer (ThermoFisher) with 1% Halt protease inhibitor cocktail (ThermoFisher). Protein concentration was determined by micro-BCA assay (Pierce Biosystems). Samples were diluted to load 30µg of protein in 10µL of deionised water and 5µL of NuPage® LDS Sample buffer (4X) (Invitrogen) and run on a NuPAGE™ Novex™ 4-12% Bis-Tris protein gel (Invitrogen) before transfer to a PVDF membrane using an iBlot2® transfer system (ThermoFisher).

To determine total protein concentration as a loading control, membranes were incubated in 5mL of REVERT fluorescent total protein stain (Licor) for 5 minutes and washed twice with REVERT was solution (Licor). Total protein stain was scanned whilst still wet using an Odyssey imaging system (Licor) with Image Studio Lite software (Licor). The membrane was then blocked with Odyssey blocking buffer (Licor) for 30 minutes at room temperature, before overnight incubation with primary antibody of Total OXPHOS (1:1000) (Abcam) in 5mL Odyssey blocking buffer at 4°C. This OXPHOS cocktail contains 5 mouse antibodies, one against each CI subunit NDUFB8, CII-30kDa, CIII-Core protein 2, CIV subunit 1, and CV alpha subunit as a premixed cocktail. These subunits have the benefit in that they are labile when the complex is not assembled. Membranes were incubated in secondary solution containing IRDye 680RD donkey anti-mouse IgG (H + L) antibody (Licor) at 1:5000 in Odyssey blocking buffer for 1 hr at room temperature. Membranes were dried and stored at 4°C prior to imaging and analysis. For measurement and analysis, Image Studio Lite software was used to analyse intensities of area-constant total protein banding against background. Quantification of bands was undertaken on the 700nm channel, and normalised to total protein. Readouts were exported to Microsoft Excel for normalisation. All statistical analyses and graph generation was performed on Graphpad Prism 8 software. Statistical significance was considered when $p \leq 0.05$.

1.16 DAVID Analysis

Proteomic datasets were obtained from that of Kline et al., 2019 and Kim et al., 2019, however all analyses presented here were undertaken by myself. Note that I am a co-author on the Kline et al., 2019 paper, which is provided in Appendix 2 for reference. Proteins exhibiting a consistent up-regulation in muscle from P12 to P24, regardless of magnitude of change, were submitted as a gene list and converted to Database for Annotation, Visualisation and Integrated Discovery (DAVID) identifications using the DAVID 6.7 *Mus musculus* database. For a more in depth description of using DAVID bioinformatic resources for gene list analyses and manipulation, readers are directed to Huang et al., 2009 (Huang da et al., 2009). In brief, converted gene lists were analysed using the Functional Annotation Clustering tool, in DAVID Bioinformatics Resources (Version 6.7) to produce a list of functional annotations. Functional annotations are ranked by an enrichment score. An enrichment score of >1.3 in DAVID is equivalent to $p < 0.05$, which is considered to be statistically significant.

1.17 Quantification and Statistical Analyses

Quantification of NMJ occupancy or maturity status was undertaken by fluorescent microscopy at ×40 magnification. The investigator was blinded to the age, genotype and treatment of muscles. A minimum of two (deep lumbrical, TS) or three (LALr, LALc, AS, AAL, TVA) fields of view and 50 NMJs were sampled per muscle (average of 118 motor endplates per muscle). Fields of view were chosen at random from across the entire muscle using bungarotoxin staining only, to ensure a fair representation of the entire muscle and to reduce the chance of bias for innervated areas. Previously optimised criteria for NMJ quantification were applied to quantify the percentage of fully occupied endplates (Murray et al., 2013, Murray et al., 2015, Murray et al., 2011, Murray et al., 2008a, Thomson et al., 2012, Sleigh et al., 2014a, Sleigh et al., 2014b, Brown et al., 2015, Comley et al., 2016, Kline et al., 2017, Courtney et al., 2019, Osman et al., 2019). In brief, fully occupied endplates were defined as complete apposition between the pre-synaptic terminal and the motor endplate (see Fig. 6F for examples). This has been expressed as a percentage of the total number of endplates

quantified for each muscle, with the remainder of endplates displaying synaptic withdrawal, appearing either only partially occupied (where only part of the ACh receptor cluster is covered by a pre-synaptic terminal) or vacant (where no pre-synaptic staining is evident at the ACh receptor cluster). An example of the occupancy criteria implemented to categorise NMJs can be seen in Fig. 6F. For NMJ maturation, the number of axonal inputs to the motor endplate were quantified, and expressed as a percentage of the total number of endplates included for analysis.

Quantification of activated caspase-3 (AC3) positive cells was undertaken blind to genotype on a Leica DMi8 fluorescent microscope with LAS X software at x40 magnification, and images were stitched together to create a whole section image in Adobe Photoshop. The absolute number of AC3 positive cells were counted and averaged from a minimum of three slides to give the mean number of cells per section, per replicate. Quantification of AC3 staining in different tissues were undertaken and provided by lab members: Victoria Zimmel (heart/liver), Mohammad Omar Khan (muscle), and Dr. Alison Thomson (spinal cord).

All analyses were collated into Microsoft Excel before exporting to GraphPad Prism 8 software for statistical analysis with *n* numbers referring to the number of muscles or biological replicates analysed. Statistical tests are detailed in the legend of the relevant graphs to which they refer. Data were tested for normality using a Shapiro–Wilk test. Data that were normally distributed were tested using one-way analysis of variance (ANOVA) with post-hoc Tukey correction, or two-way ANOVA with post-hoc Sidak correction or unpaired t-test with post-hoc Welch correction. In groups that were not normally distributed, Kruskal–Wallis tests with Dunn's post-hoc or, when one group has been normalised to 1, a one-sample t-test with comparison to a hypothetical value of 1 were applied. All data are presented as mean values ± standard error of the mean (SEM). Differences were considered significant when $p < 0.05$.

Micrographs are projections of Z-image stacks collected on a Nikon A1R FLIM confocal microscope and were adjusted for overall image brightness and contrast only using ImageJ (downloadable from https://imagej.nih.gov/ij/) and

Adobe Photoshop CS6 software (licence purchased from https://www.adobe.com/uk/products/).

Chapter 1 : Expansion and exploration of an *ex vivo* model of Wallerian degeneration

1.18 Chapter overview and principle findings

In this chapter, I aimed to expand, optimise and explore an *ex vivo* model of peripheral nerve injury in a range of different muscles that have not been looked at in this context previously. Here, I examined the level of synaptic loss across time in different muscles, and investigated the impact of underlying pathology on the rate of synaptic loss following injury.

Principle Findings

- *Ex vivo* modelling of peripheral nerve injury is possible in a range of muscles
- Synaptic loss increases with age in the cranial muscles
- Differences in the level of synaptic loss following injury does not correlate with synaptic maturity
- Synaptic loss is minimal in the thoracoabdominal muscles following injury
- Patterns of synaptic vulnerability are distinct from those that occur in a die-back
- WD is Smn-independent
- The presence of a die-back can accelerate synaptic loss following injury

1.19 Introduction

Motor neurons are vulnerable to degeneration following physical or chemical injury and in a range of neurodegenerative diseases. Damaged axons and synapses degenerate in morphologically distinct ways depending on the nature of the original trauma. Following injury, spontaneous and rapid fragmentation occurs along the length of the injured axon in a characteristic process known as Wallerian degeneration (WD) (Waller, 1851, Beirowski et al., 2004, Beirowski et al., 2005, Conforti et al., 2014). In WD, the cytoskeleton is disassembled and granular degeneration proceeds distal to the injury site (reviewed by Wang et al., 2001). This is morphologically distinct from degeneration that occurs during peripheral neuropathies, such as ALS and SMA. In some forms of motor neuron disease, axons retrogradely retract away from the synaptic region and are described as 'dying-back' (Cavanagh, 1964). An example of dying-back pathology can be seen in the childhood motor neuron disease, SMA, where a lack of survival motor neuron (SMN) protein leads to the progressive loss of lower motor neurons (Lefebvre et al., 1995, Rodrigues et al., 1995). Despite morphological distinctions between WD and dying-back pathology, the degree of mechanistic divergence remains unclear. Understanding the degree to which morphologies also relate to different mechanisms would provide a powerful tool to better categorise different types of neurodegeneration and will potentially facilitate the identification of novel therapeutic targets.

Attempts to decipher the mechanisms of synaptic and axonal degeneration have been facilitated by model systems in which the degenerative rate is altered. For example, the discovery of the Wallerian Degeneration slow (*Wld*^{s}) mutation, so called for its ability to delay axonal and synaptic degeneration, has been instrumental in developing our understanding of the mechanisms of WD (Lunn et al., 1989, Ribchester et al., 1995, Mack et al., 2001, Wang et al., 2001, Gillingwater et al., 2004, Gillingwater et al., 2002, Gillingwater et al., 2006, Coleman and Freeman, 2010). *Wld*^{s} confers tenfold delays in the rate of WD following axotomy in mice (Coleman, 2005); expression of *Wld*^{s} is sufficient to protect the structural integrity of wild-type axons for up to two weeks *in vivo* (Mack et al., 2001). Indeed, the fortuitous discovery of *Wld*^{s} mutant

mouse, has been pivotal to much work that has sought to elucidate the mechanisms of WD (Lunn et al., 1989) (see *General Introduction 1.1.2* for more detail on *Wld*^{s}). In brief, pathways that regulate WD are thought to be activated by the loss of axonal, labile nicotinamide mononucleotide adenylyl-transferase 2 (NMNAT2), a nicotinamide adenine dinucleotide (NAD)-synthesising enzyme. Following injury, levels of axonal NMNAT2 decline within a few hours when transport or synthesis are impaired (Gilley and Coleman, 2010). Endogenous NMNAT2 has been reported to prevent spontaneous degeneration of healthy axons, and it is thought that *Wld*^{s} may therefore substitute for NMNAT2 loss after axon injury (Gilley and Coleman, 2010). Similar delays in the rate of WD have also been reported when Sterile Alpha and TIR motif-containing 1 (*Sarm1*), is knocked out. In both Drosophila and mice, *Sarm1* knockout also confers protection that phenocopies *Wld*^{s} (Osterloh et al., 2012), and appears to either operate independently or downstream of NMNAT2 (Gilley et al., 2015). These models have been invaluable in developing our understanding of the putative mechanisms of WD.

Recent work has revealed that rates of axonal and synaptic degeneration also can be influenced by postnatal age. Significant differences in the response of neonatal versus adult mice to peripheral nerve injury and hypoxic insult have been reported (Murray et al., 2011). In young adult mice (P25), tibial nerve lesion results in a loss of motor nerve terminals within the deep lumbrical (DL) muscles, with just 3% of motor endplates remaining innervated after 24 hr (Murray et al., 2011). In contrast, in mice aged less than 2 weeks of age, the rate of degeneration is much slower, with 86% of endplates remaining innervated after 24 hr (Murray et al., 2011). Synaptic loss in response to injury therefore appears to be regulated during postnatal development in the DL muscles. Neonatal, murine NMJs also remain structurally intact following exposure to an *ex vivo* model of hypoxia reperfusion injury, with over 99% of endplates remaining fully occupied in P2 murine TVA, compared with just 4% in adult mice (Murray et al., 2011).

Differential rates of degeneration have been reported between different motor neurons pools in humans and in mouse models of motor neuron disease (Bowerman et al.,

2012). This difference in relative vulnerability has been used as a tool to identify transcripts and pathways which can modify the rate of degeneration (Hedlund et al., 2010, Brockington et al., 2013, Kaplan et al., 2014, Comley et al., 2015, Murray et al., 2015, Kline et al., 2017, Boyd et al., 2017). Properties that are intrinsic to the motor neuron may therefore regulate the rate of axon degeneration. Understanding the properties of different groups of motor neurons should better inform us of the mechanisms of axon degeneration.

Due to the limited numbers of muscle that have been studied in detail, it remains unclear whether there is any variability in the rate of synaptic loss that occurs following injury in different muscles. Similarly, it remains unclear whether developmental resistance to injury is unique to DL preparations. Investigating synaptic degeneration following injury in different muscles *in vivo* presents challenges; for example, the precise and reproducible nerve injury required is difficult in nerves like the facial nerve that are not as easily accessible as the sciatic nerve. Furthermore, some muscles, such as the abdominal and thoracic muscles, are innervated by multiple spinal nerves, meaning consistent and complete denervation is experimentally challenging. Determining how different pools of motor neurons respond to injury and how this response changes during postnatal development would provide a useful tool to investigate the factors that regulate WD, and how this relates to other types of axonal and synaptic degeneration.

Here, we optimised and expanded an *ex vivo* assay to assess the level of synaptic degeneration in cranial and thoracoabdominal musculature following nerve injury. This was achieved by using an *ex vivo* model of axon injury, where the nerve is transected, and the distal portion along with the musculature that it innervates are removed and maintained in oxygenated solutions for 24 hr. Cranial muscle/facial nerve and abdominal muscle/intercostal nerve preparations were introduced from different postnatal time points. These muscles have not previously been maintained in this way, and so this system was optimised to permit their inclusion. The *ex vivo* setup was established within our laboratory and optimised using sciatic nerve/deep lumbrical muscle preparations from *Wld*^{s} mice to confirm that the system could reproduce results

described in the literature (Brown et al., 2015, Kline et al., 2019). I then optimised this system for *ex vivo* maintenance of a range of other muscles, which involved precise dissection and the resolution of issues including bacterial infection and contamination. Antibiotics were introduced to prevent bacterial growth, and were found to have no effect on the level of synaptic loss following injury in the cranial muscles. For the first time, a range of cranial and thoracoabdominal muscles were maintained. It was found that there is a developmental delay in synaptic withdrawal following injury in all cranial muscles. Interestingly, some muscles (such as adductor auris longus; AAL) showing significantly greater loss than other muscles of the same age (such as levator auris longus; LAL). Furthermore, synaptic degeneration was consistently and dramatically reduced in the thoracoabdominal muscles compared to the cranial muscles. Together these data suggest that factors intrinsic to the muscle/motor neuron affect the degree of synaptic degeneration following injury. It was shown that increased monoinnervation – used as an indicator of maturational status of the muscle – did not correlate increased levels of synaptic loss, although differences in the level of mono- and polyinnervation were seen across different muscles. Comparison of the degree of synaptic loss following injury with the degree of synaptic loss in a mouse model of SMA, revealed strikingly different patterns. This suggests that the factors which affect the rate of synaptic degeneration following injury are not the same as those which affect the vulnerability of motor neurons to SMA. Finally, by exposing muscles from the mouse model of SMA to the *ex vivo* model of nerve injury, it was shown that the presence of SMA-induced synaptic pathology significantly increases synaptic loss following injury.

1.20 Results

1.20.1 Preliminary ex vivo assay optimisation

An *ex vivo* model of peripheral nerve injury has previously been used to investigate levels of innervation and synaptic function in the DL muscles following tibial nerve injury in *Wld*^{s} and wild-type mice (Brown et al., 2015, Gillingwater et al., 2002, Mack et al., 2001, Kline et al., 2019, Murray et al., 2011). Here, the aim was to setup and optimise a new *ex vivo* system that would facilitate the expansion of *ex vivo* modelling into muscles that have not previously been characterised following peripheral nerve injury. Levels of synaptic loss following sciatic nerve injury are well-characterised in *Wld*^{s} DL muscles; for example, Brown et al., 2015, reported that after 24 hr *ex vivo* at 32°C, the majority of synapses remained functional and around 54% of motor endplates remained innervated (Brown et al., 2015). Preliminary work to test the system therefore firstly involved maintaining DL nerve/muscle preparations from adult *Wld*^{s} mice at 32°C for 24 hr and quantifying the level of innervation remaining. Preparations maintained *ex vivo* in the 'new setup' were compared to equivalent preparations that were maintained in a 'pre-optimised setup' that has been utilised extensively in previous work by Professor Richard Ribchester. Access to the pre-optimised setup to prepare equivalent preparations was kindly provided by Professor Richard Ribchester. This comparison aimed to replicate previous findings to validate the new *ex vivo* setup (Brown et al., 2015). For *ex vivo* preparation techniques see Materials and Methods, *1.12 Ex vivo explant preparation*.

However, initial trials with the new setup yielded problems. Most notably, there was a distinct, and unexpected, loss of muscle fibre integrity, with preparations often disintegrating within the receptacle. Muscles also had a globular appearance and texture, with immunohistochemistry (when possible) revealing a lack of innervation that was not consistent with previous work in *Wld*^{s} DL muscles. Initially, it was hypothesised that muscle breakdown could be due to the presence of paraformaldehyde fixative residue on equipment or tools. As tools had also used in fixed tissue dissection, it was possible that contamination had occurred. To address this, new tools were purchased, and separate space and equipment was designated for

non-fix work. Pinning tension on the muscle was also reduced to ensure that muscles remained in a natural position. These measures did not improve the outcome, and it was concluded that there must be other factors influencing assay viability. An odour was also identified from specimens, therefore it was next hypothesised that bacterial contamination might be compromising the system. Indeed, the introduction of the antibiotics gentamicin and kanamycin (50 mg/ml, and 100 mg/ml, respectively) into the physiological buffer resolved all integrity issues. From this point, antibiotics were included in the oxygenated solution.

After *Wld*^{s} sciatic nerve/DL muscle preparations were maintained for 24 hrs at 32°C, DL muscles in the pre-optimised setup remained 89.72±2.67% innervated, whilst DL muscles in the new setup remained 84.54±3.57% innervated (Fig. 1.1). No significant differences in innervation were therefore seen between setups, indicating that these were comparable (Unpaired t-test; $p > 0.25$).

To further validate this as an *ex vivo* model of nerve injury, sciatic nerve/DL muscle preparations were maintained from adult wild-type mice. For this work, a maintenance temperature of 30°C was selected for wild-type experiments, which was expected to produce robust degeneration in adult preparations. Previous publications show that the majority of endplates are denervated in wild-type murine DL muscles after 24 hr *ex vivo* (Brown et al., 2015). Previous work has also reported that the rate of synapse loss is impacted by developmental age (Kline et al., 2019, Murray et al., 2011). I was able to replicate this finding in wild-type murine DL muscles at P15 versus adult (6-7 weeks old) (Fig. 1.2). As expected, reduced levels of synaptic loss were seen in younger animals following nerve injury in the DL muscles, with the percentage of fully occupied endplates found to be 77.68 ± 10.85% at P15 compared to 1.08 ± 1.08% in adult mice (Fig. 1.2).

To assess whether antibiotics can influence synaptic degeneration, the percentage of fully occupied endplates were quantified following the inclusion of gentamicin and kanamycin in the oxygenated mammalian physiological saline after *ex vivo* maintenance of cranial muscle preparations at 30°C for 24 hr. Antibiotics had no

significant influence on the levels of innervation in any cranial muscle (Two-way ANOVA with Sidak correction; $p > 0.2$). I conclude that the presence of antibiotics has no significant effect on synaptic loss in response to injury (Fig. 1.3).

Overall, I have optimised the *ex vivo* system of nerve injury, and it was evident that this had capacity for expansion to a range of other muscles.

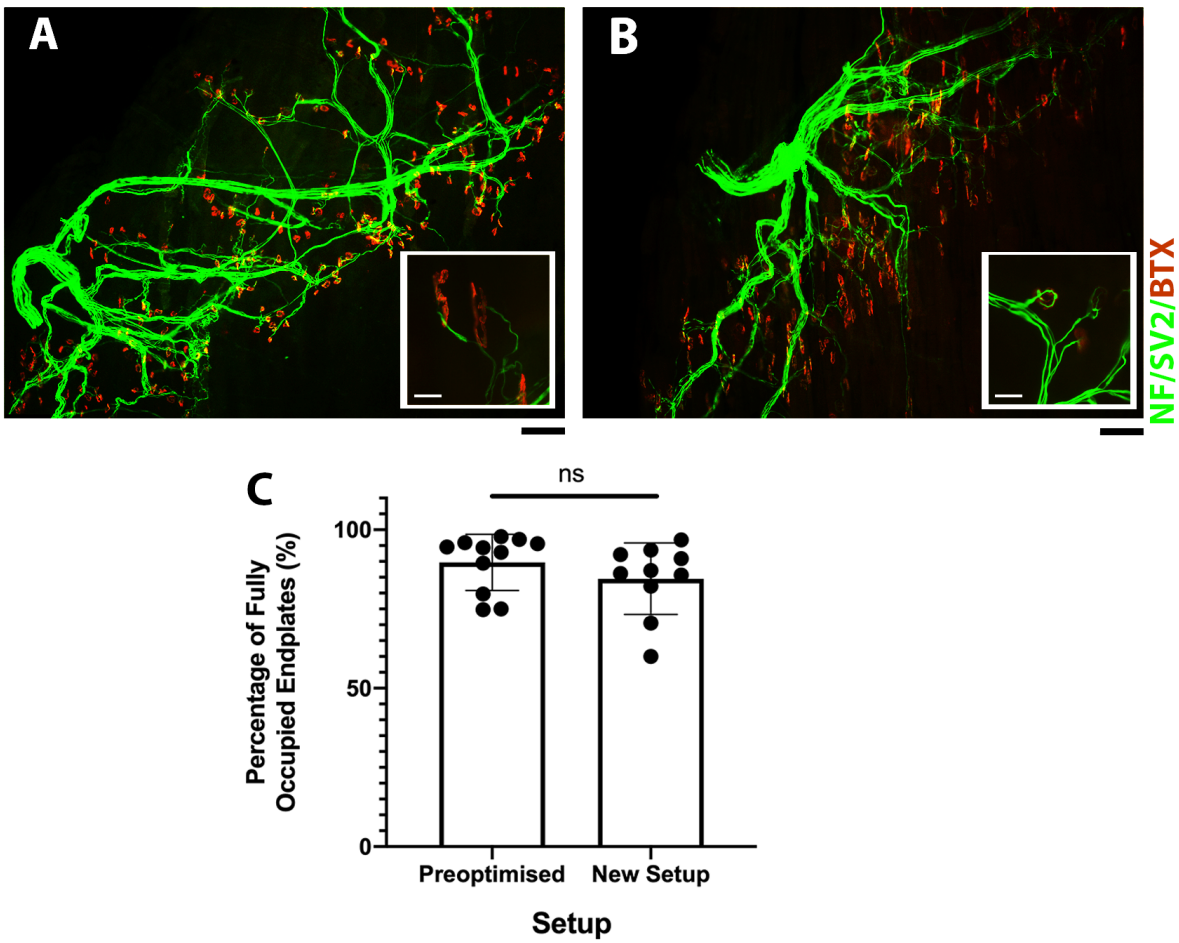

Figure 1.1: Following optimisation of a new ex vivo system, adult Wld^S DL muscle/nerve explants can be maintained at 32°C as expected, with high levels of innervation remaining after 24 hr. (**A-B**) Micrographs with higher magnification insets from one plane of focus obtained by standard fluorescent microscopy to show innervation remaining in DL muscles of *Wld^s* mice after measures to reduce the possibility of fixative contamination and excessive tension, and after antibiotic introduction in the new setup (**A**) and preoptimised setup (**B**). NMJs are labelled with antibodies against neurofilament (NF, green) and synaptic vesicle protein 2 (SV2, green), and α-bungarotoxin (BTX, red). Black scale bar: 100μm, white scale bar: 20μm. (**C**) Quantification of the percentage of fully occupied endplates remaining in the DL muscles following *ex vivo* nerve injury and maintenance at 32°C. There is no significant difference in the percentage of fully occupied endplates between setups. Ns = not significant, $p > 0.25$; Unpaired t-test with Welch's correction. Pre-optimised, n = 11 and new setup, n = 10 muscles. Error bars represent mean ± SEM.

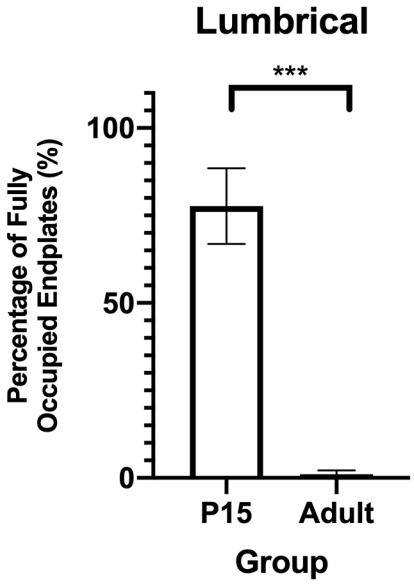

Figure 1.2: Developmental regulation is present in the DL muscles of wild-type mice following injury and ex vivo at 30°C for 24 hr. The percentage of fully occupied endplates in DL muscles at P15 and in adults (6-7 weeks old) were quantified, where age refers to the age of the animal at the time of dissection. Note that developmental regulation of synapse loss is evident, with significantly less fully occupied endplates seen in adult mice following injury. ***$p < 0.001$; Unpaired t-test with Welch's correction. N = 6, 3 muscles at P15 and adult time points respectively. Error bars represent mean ± SEM.

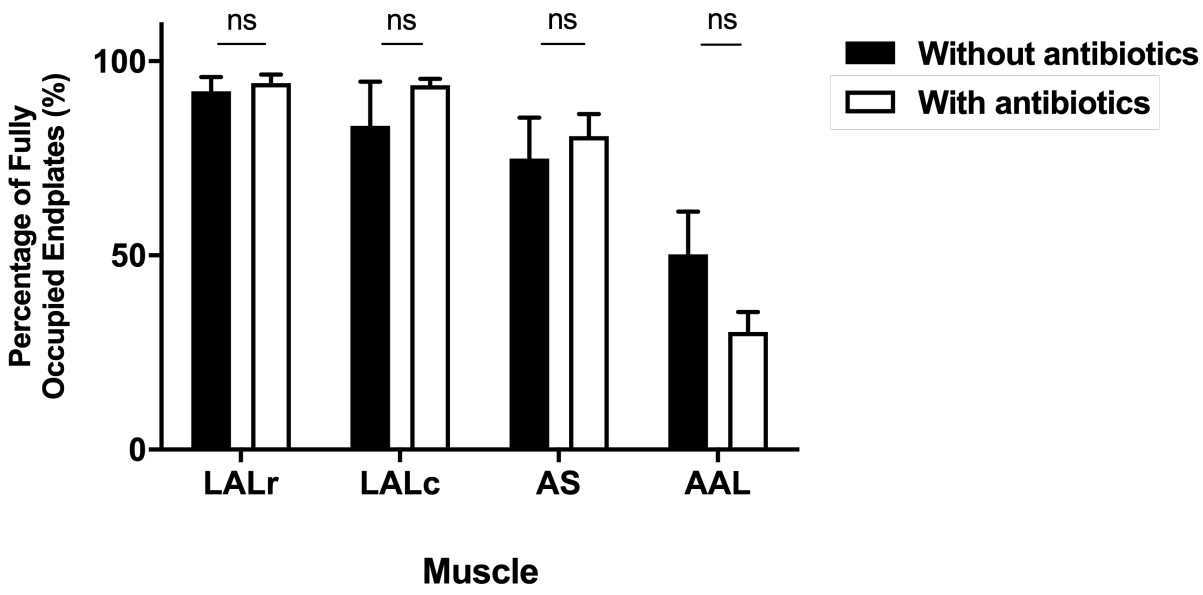

Figure 1.3: The introduction of antibiotics has no effect on the level of synapse loss in response to ex vivo injury at P15 in wild-type cranial muscles when maintained at 30°C for 24 hr. Quantification of the percentage of fully occupied endplates remaining with and without antibiotics in a range of cranial muscles (levator auris longus rostral/caudal band [LALr/c], auricularis superior [AS] and abductor auris longus [AAL]). Note that there is no significant difference in the percentage of fully occupied endplates remaining after *ex vivo* nerve injury in preparations suspended in oxygenated solution with or without antibiotics in any muscle. Ns = not significant, $p > 0.2$; Two-way ANOVA with Sidak correction. N = 4 muscles in all cases. Error bars represent mean ± SEM.

1.20.2 Synaptic loss following injury is developmentally regulated and non-uniform in the cranial muscles of the mouse

It remains unclear whether developmental regulation of synaptic loss in response to injury is unique to the DL muscles or whether developmentally regulated delays in synaptic withdrawal also occurs in other muscle preparations. Rates of synaptic withdrawal following injury were therefore examined during the critical time window of P15–P25, using an *ex vivo* model of nerve injury (see Materials and Methods, *1.12 Ex vivo explant preparation* for details). Nerve-muscle preparations comprising facial nerve (CN VII) branches innervating the cranial musculature (comprising rostral and caudal bands of levator auris longus [LALr/LALc, respectively], abductor auris longus [AAL] and auricularis superior [AS]) were isolated and maintained in oxygenated physiological solution at 30°C for 24 hr. It was hypothesised that synapse loss would be slower in younger mice, and that the level of synaptic loss would differ between different muscles. This was tested this by analysing the percentage of fully occupied endplates following 24 hr exposure to the *ex vivo* model of nerve injury at different postnatal ages.

The percentage of fully innervated or 'occupied' endplates remaining in immunostained muscles from P15–P25 mice, 24 hr after ex vivo nerve injury were quantified (Fig. 1.4 to 1.5). Note that all ages refer to the age at dissection. The data show that postnatal age affected the degree of synapse loss in all preparations analysed (Fig. 1.4 to 1.5). For example, at P15, the LALr remained highly innervated, with 77.05 ± 7.05% (mean ± SEM) of endplates covered by motor nerve terminals. As expected, levels of innervation 24 hr after injury declined with age to 58.75 ± 6.06% innervation in preparations from mice aged P18, to 13.81 ± 10.4% aged P21, and 7.53 ± 2.84% aged P24/5. The LALc and AS muscles followed similar patterns. However, significantly more denervated endplates in AAL were seen from the outset, with only 23.56 ± 3.85% innervation remaining at P15. This declined with mouse age to 21.02 ± 4.96% at P18, whereas less than 1.3% innervation remained at P21 and P24/5 (Fig. 1.5). As both AAL and LAL are homogeneously fast twitch muscles, and AS predominantly slow twitch, these differences cannot be attributed to fibre type. This

data suggests that there are other intrinsic properties of nerve or muscle that influence the rate of synaptic degeneration during postnatal development.

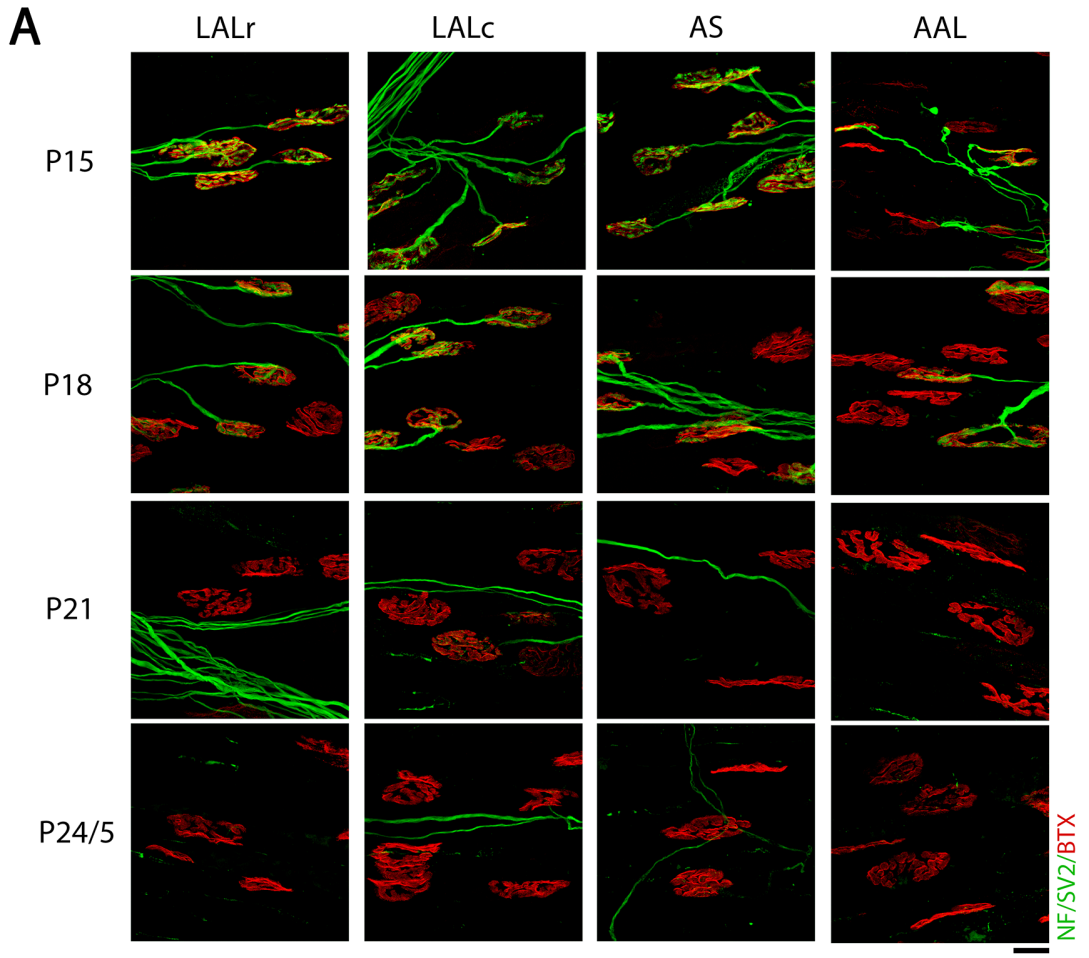

Figure 1.4: Levels of synaptic loss following injury are developmentally regulated and non-uniform in cranial muscles of the mouse. (**A**) Confocal micrographs showing NMJs labelled with antibodies against NF (green) and SV2 (green), and BTX (red) from cranial muscles (levator auris longus rostral/caudal band [LALr/c], abductor auris longus [AAL], auricularis superior [AS]) that have been maintained *ex vivo* at 30°C for 24 hr. Postnatal age refers to the age of the animal at the time of dissection. Scale bar: 20μm.

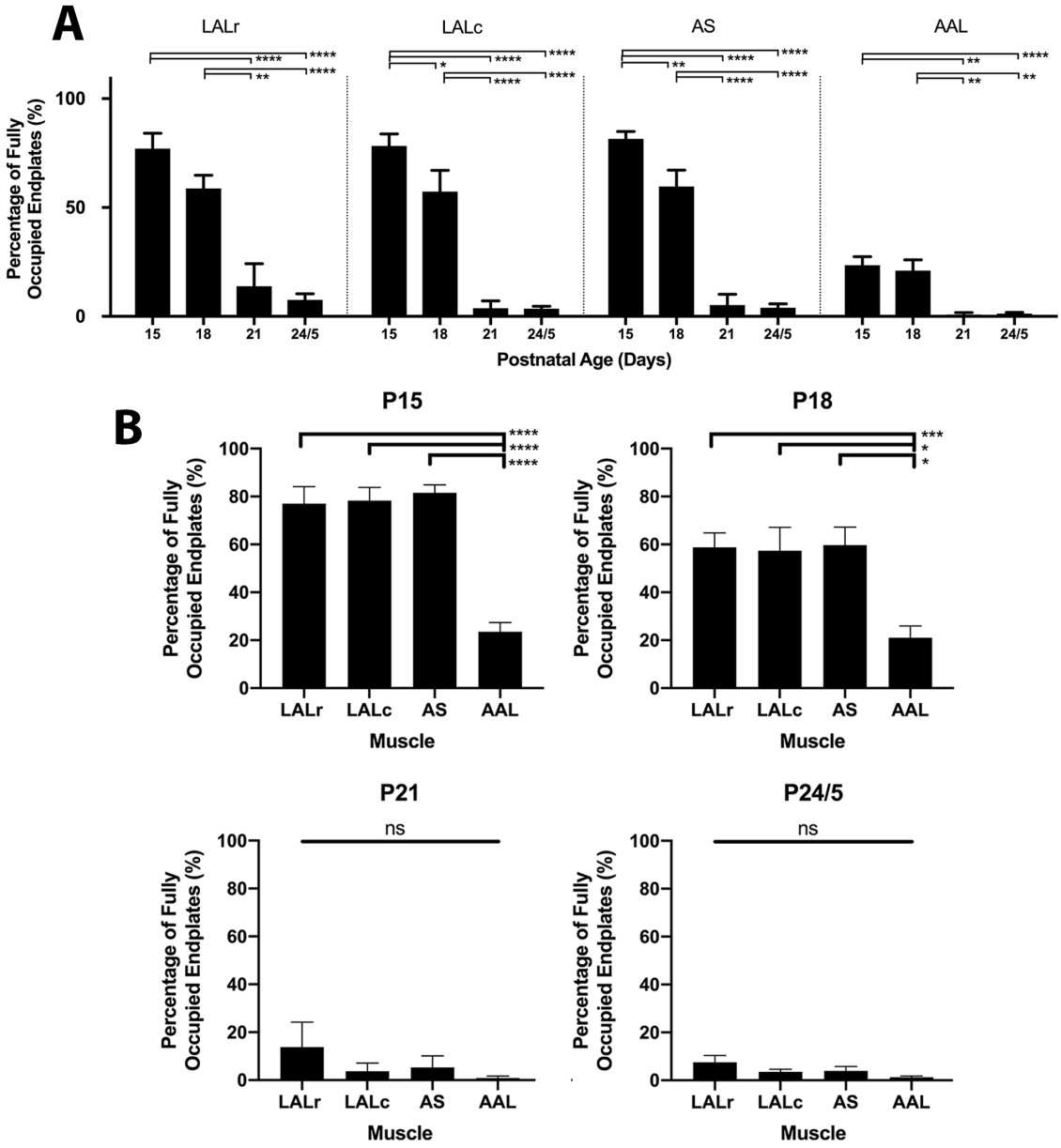
A
LALr
LALc
AS
AAL
Percentage of Fully Occupied Endplates (%)
Postnatal Age (Days)
15
18
21
24/5
B
P15
P18
P21
P24/5
Muscle
LALr
LALc
AS
AAL
ns

Figure 1.5: Quantification of the percentage of fully innervated NMJs remaining after injury and ex vivo maintenance at 30°C for 24 hr. (**A**) Quantification of the percentage of fully innervated motor endplates in cranial muscle bands between P15 and P24/5. Note that the percentage of fully occupied endplates decreases as postnatal age increases, supporting the finding that the response to injury is developmentally regulated. (**B**) Quantification of the percentage of fully occupied endplates in cranial muscles grouped by postnatal age at the time of *ex vivo* nerve injury. Note that there is a significant reduction in the percentage of fully occupied endplates in the AAL at both P15 and P18 time points in comparison to all other muscles. *p < 0.05, **p < 0.01, ***p < 0.001, ****p < 0.0001; one-way ANOVA with Tukey's correction. All comparisons where no statistical result is shown were not significantly different. N = 10 at P15 and P24/5; n = 18/6 for the LALr/all other muscles at P18; and n = 4/5 at P21 for the AAL/all other muscles. Error bars represent mean ± SEM.

1.20.3 Levels of synaptic loss are uniformly reduced following injury in the thoracoabdominal muscles of the mouse

Data thus far suggest that the rate of synaptic loss is slower in younger animals in a range of muscles. However, differences between the rates of synaptic withdrawal observed in the AAL at different time points, led us to ask whether there would be similar differences within thoracoabdominal musculature. To investigate the response to injury in these muscles, TVA and TS muscles were examined 24 hr after ex vivo nerve injury using the same protocol as for cranial muscles. In contrast to cranial preparations, both the TVA and TS showed high levels of NMJ innervation across all time points analysed (Fig. 1.6). There was no significant difference in the percentage of fully occupied endplates at any time point; in all cases, the muscle remained over 77% innervated (one-way ANOVA with Tukey correction, $p \geq 0.09$) (Fig 1.6).

Taken together, the data indicate that there are properties intrinsic to the muscle, and/or motor neuron, that can influence the extent of synaptic withdrawal in response to injury during the postnatal period. In this case, there must be properties that are intrinsic to the throacoabominal muscles (and/or nerves that serve these muscles) that

are responsible for conferring significant and remarkable delays to synaptic withdrawal. The thoracoabdominal *ex vivo* preparation therefore represents an intriguing model system to further discern the factors and mechanisms that that govern rates of synaptic degeneration after injury.

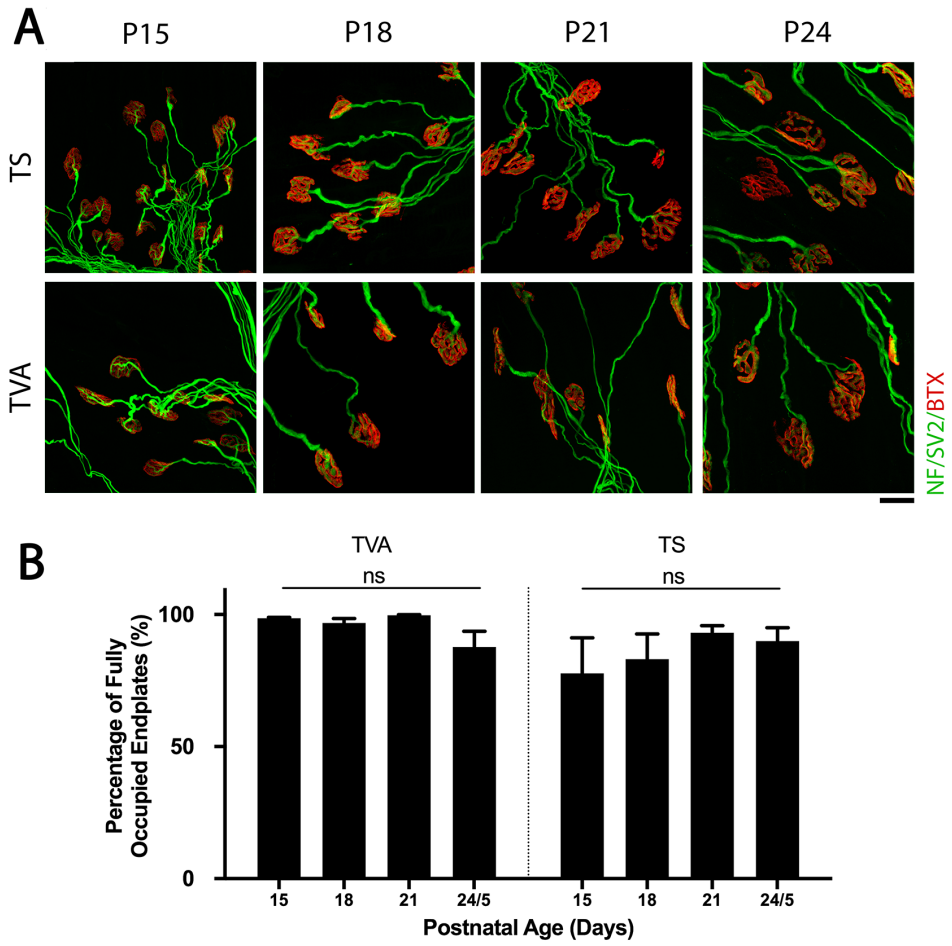

Figure 1.6: Minimal synaptic loss is observed following injury across all time points analysed in thoracoabdominal musculature. (**A**) Confocal micrographs showing NMJs labelled with antibodies against neurofilament (NF, green) and synaptic vesicle protein 2 (SV2, green), and α-bungarotoxin (BTX, red) from transversus abdominis [TVA] and triangularis sterni (TS) muscles which have been maintained *ex vivo* at 30°C for 24 hr. Postnatal age refers to the age of the animal at the time of dissection. Note that the majority of endplates remain fully occupied at all ages examined. Scale bar: 20μm. (**B**) Quantification of the percentage of fully innervated motor endplates after *ex vivo* nerve injury in the TVA and TS at P15, P18, P21, and P24/5. The percentage of fully occupied endplates remains high across all time points and there is no significant difference within muscles at any time point. Ns = not significant, $p \geq 0.09$; one-way ANOVA with Tukey's correction. TVA, n = 6, 18, 4, and 6 muscles, at P15, 18, 21, and 24/5, respectively, and n = 6, 6, 6, and 4 in the TS at P15, 18, 21, and 24/5, respectively. Error bars represent mean ± SEM.

1.20.4 Synaptic loss following injury is minimal in the thoracoabdominal muscles at 32℃

Thoracoabdominal musculature/intercostal nerve preparations showed resistance to WD across all time points analysed. However, the extent of this resistance remained unclear. Previous work by Brown et al., 2015 has shown that after 24 hr exposure at 32°C, the majority of endplates lack innervation in the hindlimb muscles of wild-type (WT) animals (Brown et al., 2015). Based on previous findings that have shown the rate of WD to be temperature-dependent (Tsao et al., 1999), it was hypothesised that raising the temperature would lead to robust synapse loss. To further test the response of the thoracoabdominal explants, the *ex vivo* temperature was therefore raised to 32°C.

Remarkably, it was found that raising the temperature had no effect on the level of synaptic innervation remaining in the thoracoabdominal musculature (Fig 1.7) (Unpaired t-test with Welch's correction, $p > 0.15$ and $p > 0.25$ for TVA and TS respectively). At 30°C, 87.66 ± 6.03% and 89.98 ± 5.06% of endplates remained fully innervated, and at 32°C, 97.75 ± 1.46% and 97.10 ± 1.72% of endplates remained fully innervated after 24 hr in the TVA and TS muscles respectively (Fig. 1.7). The thoracoabdominal muscles therefore demonstrate a remarkable resistance to WD. These muscles therefore represent intriguing candidates to further investigate factors capable of conferring this comparative protection and regulating axonal and synaptic degeneration.

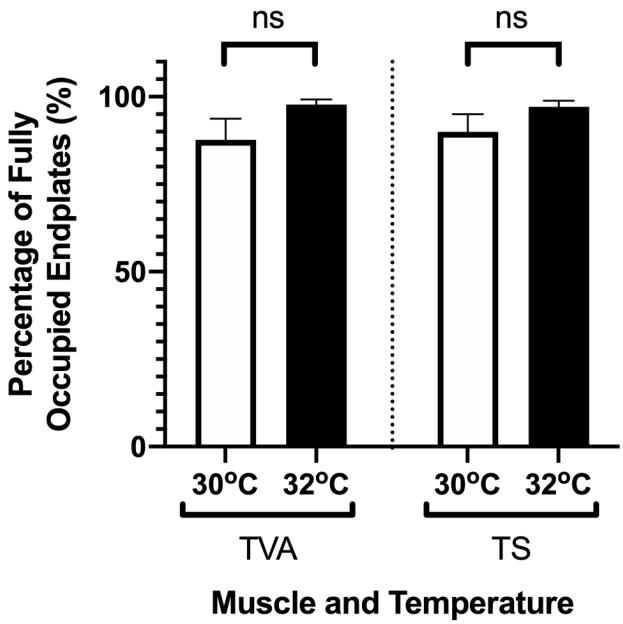

Figure 1.7: Minimal synaptic loss is observed following injury and ex vivo at 30 or 32°C in the thoracoabdominal muscles of wild-type mice at P25. Quantification of the percentage of fully innervated motor endplates after *ex vivo* nerve injury and maintenance at 30 or 32°C in the transversus abdominis [TVA] and triangularis sterni [TS] muscles, where P25 refers to the age of the animal at the time of dissection. Note that an increase in temperature has no significant effect on the percentage of fully occupied endplates in either muscle. Ns = not significant, $p > 0.15$ for TVA and $p > 0.25$ for TS; unpaired t-test with Welch's correction. At 30°C in TVA, n= 6; for all other groups n=4 muscles. Error bars represent mean ± SEM.

1.20.5 An increase in synaptic maturation does not correlate with synaptic vulnerability to injury

It is clear that some muscles exhibit significantly more synaptic loss than others in response to injury. In general, increases in age lead to progressively more synaptic loss following injury across this time window. Increased synaptic loss therefore appears to temporally correlate with the maturation of the neuromuscular system which occurs across the first 2-3 weeks of life. During this time, extensive remodelling occurs as neuromuscular junctions shift from being predominantly polyinnervated structures, to a mature monoinnervated neuromuscular system that prevails into adulthood. This

raises the question as to whether differences in maturational rates might contribute to the differential responses to injury. It was hypothesised that muscles that reach maturity at an earlier time point would be more vulnerable to synaptic loss following injury. If this is true, muscles that demonstrate more profound synaptic loss after injury, such as the AAL, would be expected to mature at an earlier timepoint in development. It follows that the AAL would be predicted to exhibit higher levels of monoinnervation at P10 than the other cranial muscles. In line with this, it would also be expected that muscles with comparable resistance after injury, such as the TVA/TS, would have higher degrees of polyinnervation.

Contrary to this however, in wild-type mice at P10, it was found that muscles that exhibit extensive synapse loss in response to injury, such as the AAL, had significantly lower levels of monoinnervation than muscles that are comparatively resistant, like the TVA. To exemplify, AAL was 49.18 ± 2.67% monoinnervated, whilst the TVA was 82.94 ± 2.65% monoinnervated (Fig. 1.8). Significant differences were also seen in levels of monoinnervation between LALr and LALc, and between LALc and AS, despite these muscles exhibiting similar profiles in response to injury (Fig 1.8). This suggests that increased maturity does not explain incidences of increased synaptic loss following injury. In fact, there is a trend towards the opposite, with muscles that are more mature appearing to exhibit less synaptic loss following injury.

Overall, despite significant intermuscular differences in the level of polyinnervation across muscles at P10, it is concluded that increased NMJ maturity does not correlate with increased synaptic vulnerability to injury.

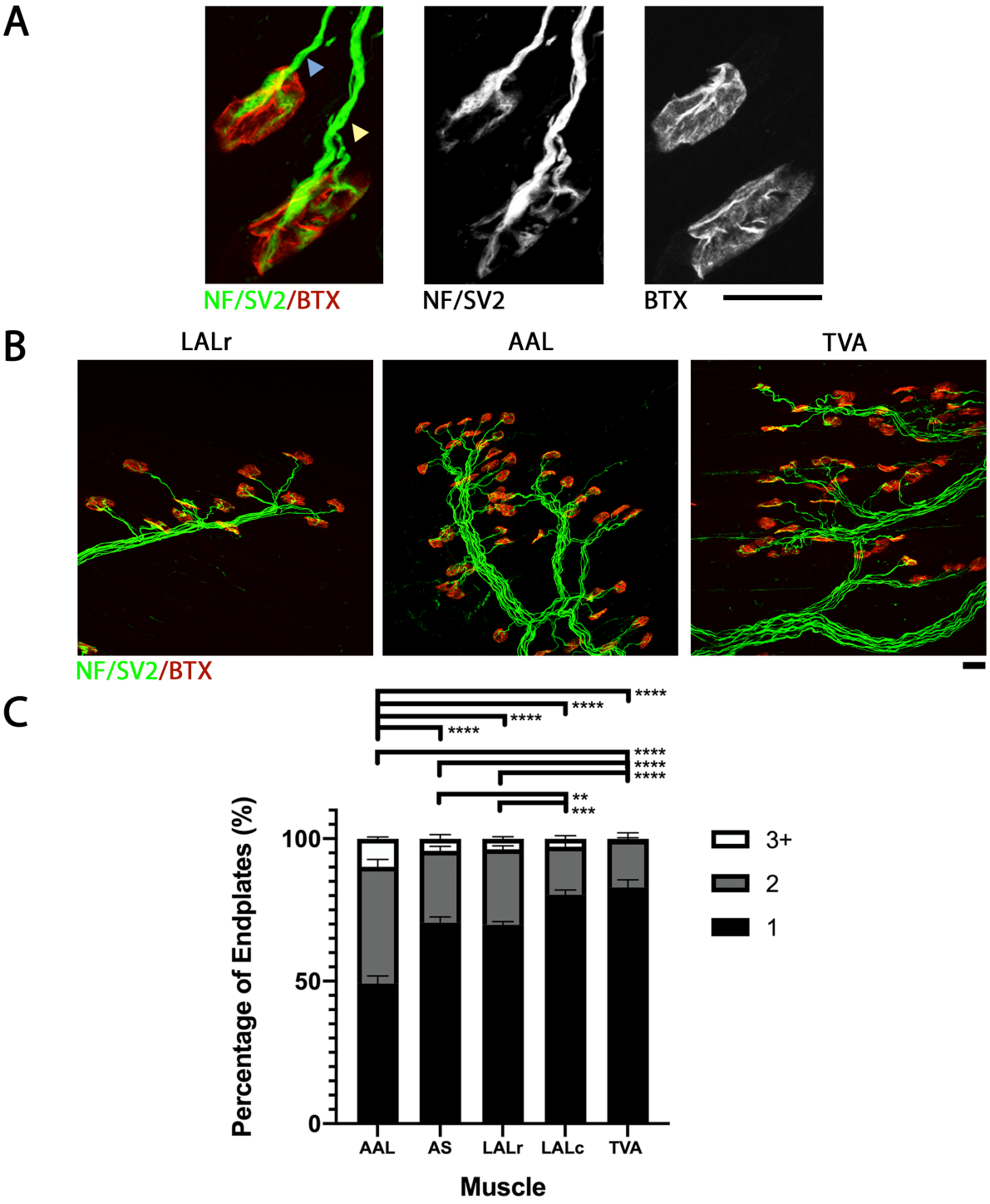
A
NF/SV2/BTX
NF/SV2
BTX
B
LALr
AAL
TVA
NF/SV2/BTX
C
****
****
****
****
****
****
**
***
Percentage of Endplates (%)
100
50
0
AAL
AS
LALr
LALc
TVA
Muscle
3+
2
1

Figure 1.8: Neuromuscular junction maturity in wild-type mice varies between different muscles at P10, but does not correlate with synaptic vulnerability to injury. Note that here, NMJ maturity is defined by the number of axonal inputs to motor endplates, where 1 input (monoinnervation), represents mature NMJs (See Materials and Methods, *1.17 Quantification and statistical analysis* for details). (**A**) Confocal micrograph showing example NMJs to exemplify criteria for input quantification. NMJs are labelled with antibodies against neurofilament (NF, green) and synaptic vesicle protein 2 (SV2, green), and α-bungarotoxin (BTX, red). The blue arrowhead highlights an input that would be considered 'monoinnervated', whereas the yellow arrowhead indicates multiple inputs (in this case, 2) that would be considered 'polyinnervated'. Scale bar: 20μm. (**B**) Confocal micrographs showing innervation of AAL, LALr and TVA in wild-type animals at P10. Again, NMJs are labelled with antibodies against neurofilament (NF, green) and synaptic vesicle protein 2 (SV2, green), and α-bungarotoxin (BTX, red). Scale bar: 20 μm. (**C**) Quantification of the percentage of motor endplates with 1, 2 or more than 3 axonal inputs in a range of wild-type muscles at P10. Statistics refers to the single input (monoinnervation) group only. It is important to bear in mind that NMJs of the AAL have already been shown to be more vulnerable to injury than those of LALr or TVA at younger age points (See Chapter 1, Results, *Figure 1.5*). Note that there are significant differences in NMJ maturity across different muscles. Statistics refer to endplates receiving 1 input only where **p = 0.005, ***p < 0.001 ****p < 0.0001. All comparisons where no statistical result is shown were not significantly different. Two-way ANOVA with Sidak correction was used. N = 8 muscles per muscle group. Error bars: mean ± SEM.

1.20.6 Patterns of differential synaptic stability in Wallerian degeneration contrast with patterns of vulnerability in a mouse model of Spinal Muscular Atrophy

Variability in the levels of synaptic degeneration between different muscles, has previously been reported in mouse models of motor neuron disease. For instance, in the *Smn*$^{2B/-}$ mouse model of SMA, the TVA muscle is highly vulnerable and displays high levels of synaptic loss, whereas the LALr and AAL muscles are relatively spared, with little synaptic loss even at late stages of disease (Murray et al., 2015). To investigate how synaptic stability differs between disease and injury, levels of innervation remaining in muscles from end-stage (P18) *Smn*$^{2B/-}$ mice *in vivo* were compared with levels of innervation remaining in homologous muscles from wild-type animals after *ex vivo* nerve injury. This provided insight into how synaptic responses differ following these distinct insults.

In line with previous work undertaken by Murray et al., 2015, here the LALr and AAL of *Smn*$^{2B/-}$ mice were largely spared from dying-back neuropathy *in vivo*, with over 98% of motor endplates remaining fully innervated at P18 (Fig. 1.9 and 1.10). Contrasting this, 24 hr after *ex vivo* nerve injury in P18 wild-type mice, the LALr was 47.23 ± 2.58% innervated and the AAL only 21.02 ± 4.96% innervated (Fig. 1.10). These cranial muscles therefore appear to be more vulnerable to injury than in an SMA mouse model (Mann–Whitney *U*-test, $p \leq 0.0007$). Also in line with descriptions by Murray et al., in the *Smn*$^{2B/-}$ model, the TVA is vulnerable to dying-back pathology in vivo, with 62.11 ± 3.78% innervation remaining at P18, compared with 99.54 ± 0.29% innervated in wild-type age-matched mice 24 hr after ex vivo nerve injury (Fig. 1.10). This suggests that the TVA exhibits less extensive synaptic loss following injury than in an SMA mouse model (Mann-Whitney *U* test, $p = 0.0002$). Thus, the factors responsible for determining relative synaptic stability following both nerve injury and SMA appear to be distinct.

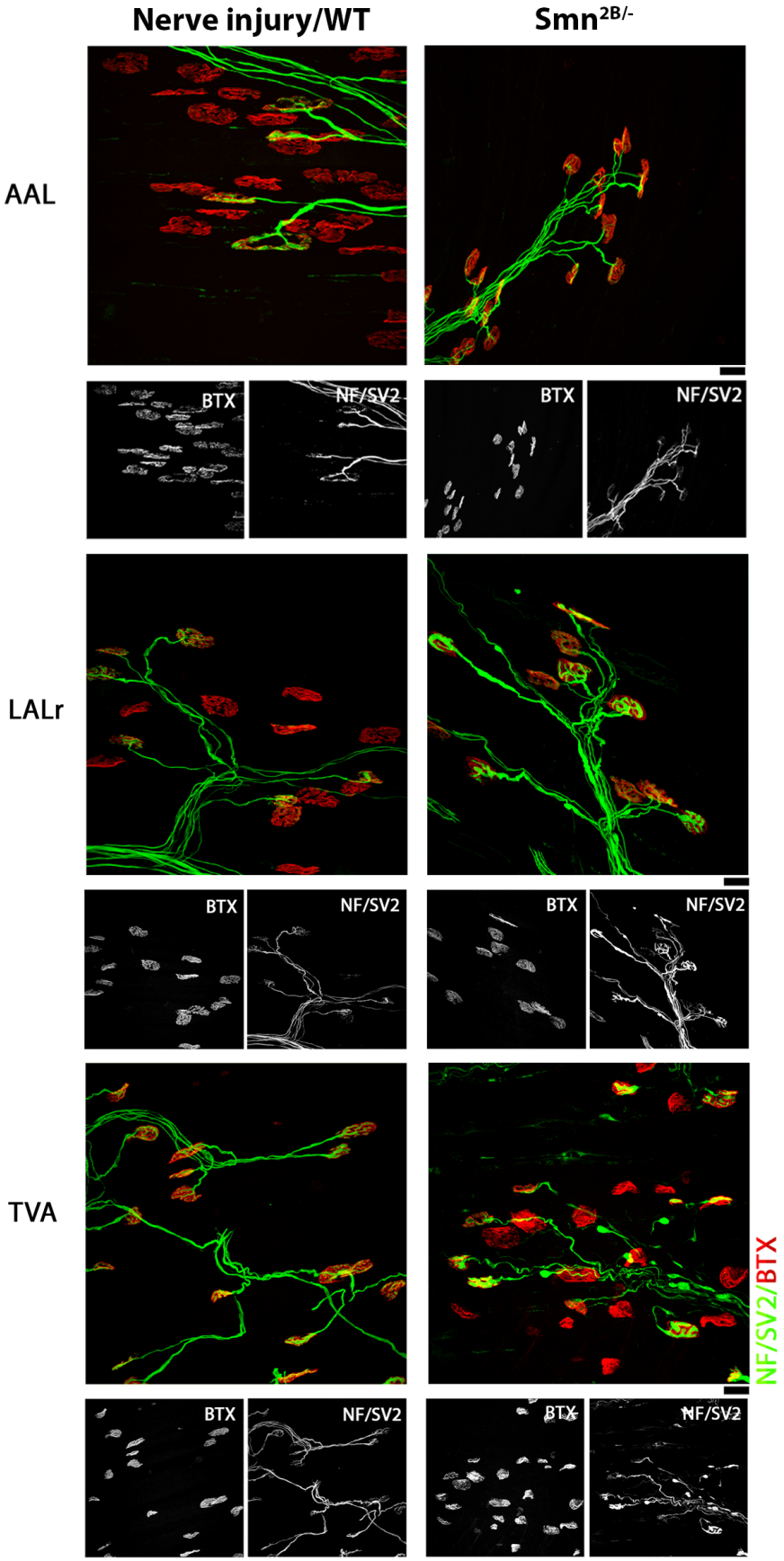
Nerve injury/WT
Smn2B/-
AAL
LALr
TVA
BTX
NF/SV2
NF/SV2/BTX

Figure 1.9 : Confocal micrographs that show differences in synaptic loss in response injury or disease conditions. NMJs are labelled with antibodies against neurofilament (NF, green) and synaptic vesicle protein 2 (SV2, green), and α-bungarotoxin (BTX, red) showing innervation of abductor auris longus (AAL), levator auris longus rostral band (LALr), and transversus abdominis (TVA) following *ex vivo* nerve injury in wild-type (WT) animals at P18 (Nerve injury/WT group) and under disease conditions from *Smn*$^{2B/-}$ mice at P18 (Smn$^{2B/-}$ group). Nerve/muscle explants from the 'nerve injury' group were maintained *ex vivo* at 30°C for 24 hr. Scale bar: 20μm.

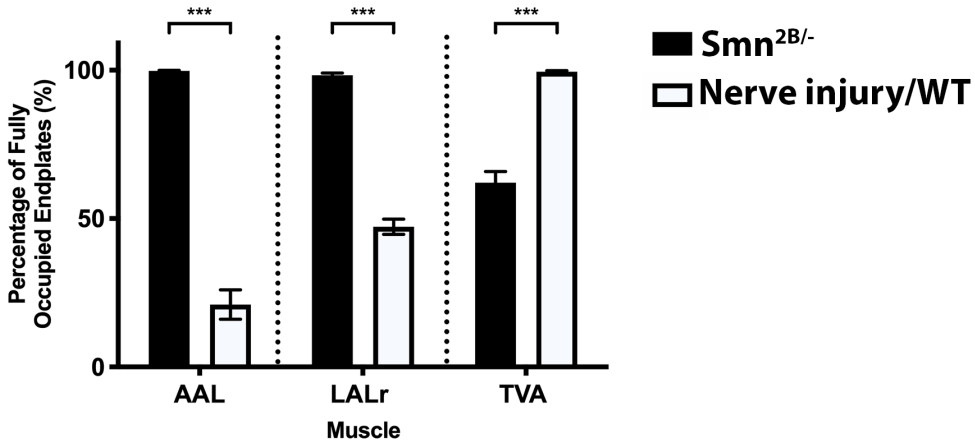

Figure 1.10: Quantification of the percentage of fully innervated NMJs remaining in injury or disease conditions. Quantification of the percentage of fully innervated motor endplates in the AAL, LALr, and TVA after *ex vivo* nerve injury in WT vs. *Smn*$^{2B/-}$ mice reveals opposing patterns of synaptic loss. In the *Smn*$^{2B/-}$ mouse, the LALr and AAL cranial muscles are spared from degeneration in comparison to the TVA muscle. Following *ex vivo* nerve injury, LALr and AAL show high levels of synapse loss, whereas the TVA appears preserved. Ns = not significant, ***$p < 0.001$; Mann–Whitney U-test. Note that for the AAL, n = 9, 6; for the LALr, n = 8, 6; and for the TVA, n = 10, 6 muscles for *Smn*$^{2B/-}$ and nerve injury/WT groups, respectively. Error bars represent mean ± SEM.

1.20.7 Reduced **Smn** *levels do not influence the incidence of synaptic withdrawal following injury in the LALr cranial muscle of the mouse*

Previous work in Smn-independent motor neuron diseases, like ALS, have indicated that Smn could be a disease modifier. For example, SOD1 mutant mice with genetic reductions in Smn display a more severe phenotype, whilst overexpression of Smn has been shown to ameliorate the ALS phenotype (Turner et al., 2009, Turner et al., 2014), suggesting SMN can modify synaptic stability. I therefore asked whether reductions in SMN levels could influence synaptic loss after injury. To address this, cranial nerve/muscle preparations were isolated and maintained from wild-type mice and from $Smn^{2B/-}$ mice. In $Smn^{2B/-}$ mice, cranial muscles are classified as selectively resistant, in that even at end-stage of disease, there is no synapse loss evident (Fig. 1.11). Therefore, these muscles have reduced Smn levels but no resultant synaptic loss. Levels of denervation in the LALr were compared under three conditions: LALr from wild-type after *ex vivo* nerve injury; LALr from $Smn^{2B/-}$; and LALr from $Smn^{2B/-}$ after *ex vivo* nerve injury.

In this disease-resistant muscle, as described above, minimal denervation was found *in vivo* in $Smn^{2B/-}$ mice, with 98.28 ± 0.79% of endplates remaining fully occupied. In wild-type mice, as expected, *ex vivo* nerve injury induced extensive denervation, with 47.12 ± 4.08% of endplates remaining fully occupied. In muscles from $Smn^{2B/-}$ mice subject to *ex vivo* nerve injury, it was found that the level of synaptic loss was comparable to wild-type levels, where 58.55 ± 3.53% of endplates remaining fully occupied (Kruskal-Wallis with Dunn's correction, $p = 0.031$; Fig. 1.11). It was concluded that in the LALr, where synapse loss due to Smn deficiency is minimal, the synaptic loss caused by nerve injury is not altered. As Smn levels are reduced in this model, despite the lack of NMJ pathology, it follows that Smn levels do not affect synaptic withdrawal following nerve injury.

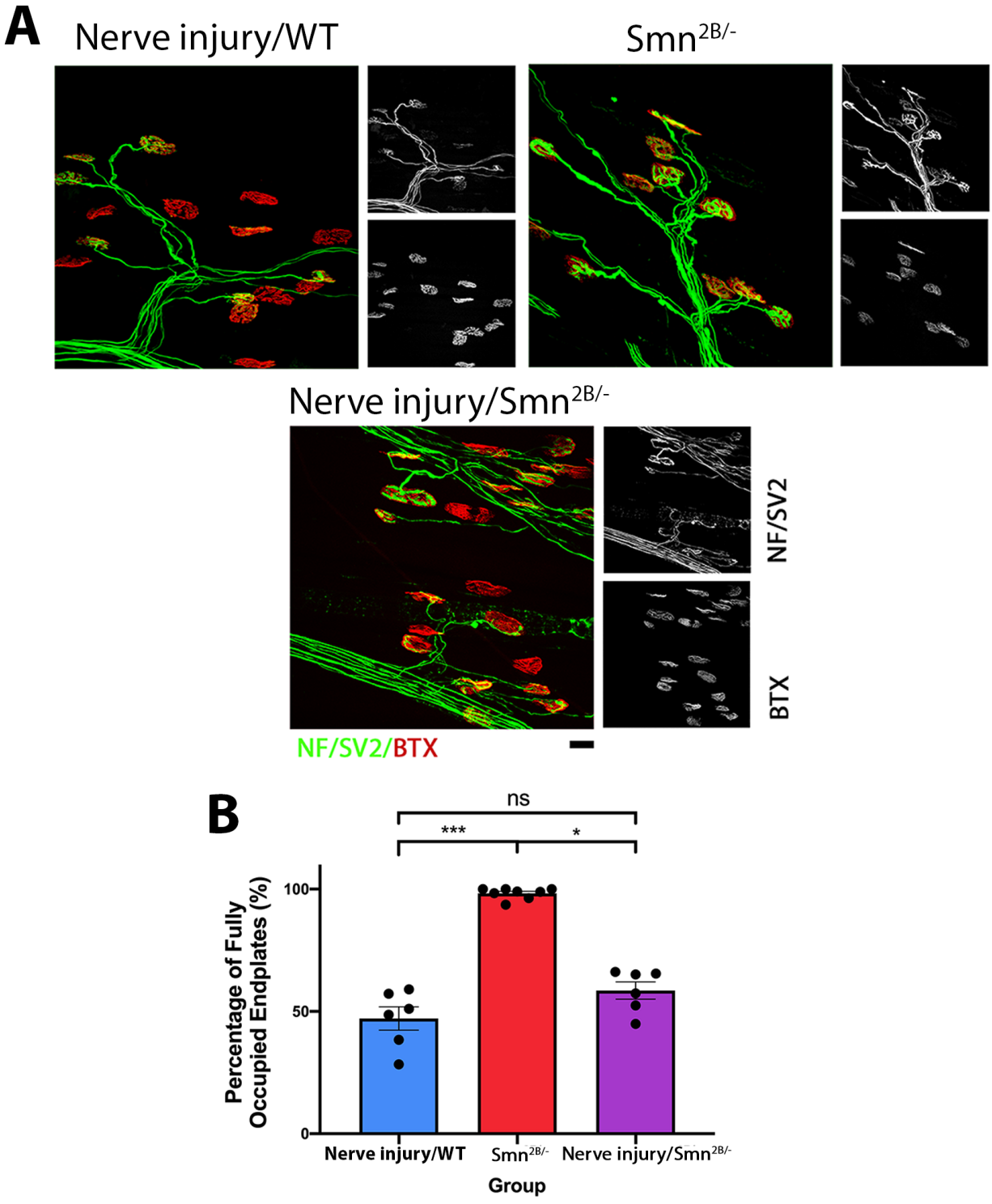
A
Nerve injury/WT
Smn2B/-
Nerve injury/Smn2B/-
NF/SV2
BTX
NF/SV2/BTX
B
ns
***
*
Percentage of Fully Occupied Endplates (%)
100
50
0
Nerve injury/WT
Smn2B/-
Nerve injury/Smn2B/-
Group

Figure 1.11: Reduced SMN levels have no effect on the level of synaptic degeneration following injury in the LALr cranial muscle of the mouse. (**A**) Confocal micrographs showing NMJs labelled with antibodies against neurofilament (NF, green) and synaptic vesicle protein 2 (SV2, green), and α-bungarotoxin (BTX, red) from levator auris longus rostral band [LALr] in wild-type animals after ex vivo nerve injury (nerve injury/WT), in $Smn^{2B/-}$ mice and in $Smn^{2B/-}$ mice after ex vivo nerve injury (nerve injury/ $Smn^{2B/-}$). In nerve injury/WT and nerve injury/ $Smn^{2B/-}$ conditions, LALr muscles were maintained ex vivo at 30°C for 24 hr. Scale bar: 20μm. (**B**) Quantification of the percentage of fully occupied endplates in LALr in nerve injury/WT, $Smn^{2B/-}$, and nerve injury/$Smn^{2B/-}$ conditions. The percentage of fully occupied endplates after nerve injury in $Smn^{2B/-}$ mice is not significantly different than after nerve injury in wild-type animals. *$p < 0.05$, ***$p < 0.001$, ns = not significant. For all comparisons with the $Smn^{2B/-}$ group, Kruskal–Wallis with Dunn's correction was used to account for non-normally distributed data; otherwise, a one-way ANOVA with Tukey's correction was used. Note that $n = 6, 8, 6$ for the nerve injury/WT, $Smn^{2B/-}$ and nerve injury/ $Smn^{2B/-}$ groups, respectively. Error bars: mean ± SEM.

1.20.8 The presence of dying-back pathology increases the level of synaptic loss following injury in the TVA muscle of the mouse

Previous work has shown that dying-back pathology can delay WD (Murray et al., 2008b). Therefore, to investigate the relationship between synaptic loss that occurs in injury versus disease, I also investigated whether there was any alteration in the level of synaptic loss following injury in the presence of dying-back pathology. The TVA muscle of the $Smn^{2B/-}$ mouse model exhibits high levels of synaptic pathology, including denervation, pre-synaptic swelling, and post-synaptic shrinkage at end-stages of disease (P18). Levels of denervation in the TVA were compared under three conditions at P18: TVA from wild-type after *ex vivo* nerve injury; TVA from $Smn^{2B/-}$; and TVA from $Smn^{2B/-}$ after *ex vivo* nerve injury.

It was found that *ex vivo* nerve injury of the TVA muscle from $Smn^{2B/-}$ mice resulted in a significant reduction in the percentage of fully occupied endplates, to 29.22 ± 6.23% in comparison with wild-type TVA with *ex vivo* nerve injury (99.54 ± 0.29% of endplates fully innervated, Kruskal–Wallis with Dunn's correction, $p < 0.0001$) and to $Smn^{2B/-}$ in vivo (61.45 ± 3.98% of endplates fully innervated, Kruskal-Wallis with Dunn's correction, $p = 0.0001$) in isolation (Fig. 1.12). Overall, as it has already been established that Smn reduction alone is not sufficient to increase levels of synaptic loss, it follows that the increase in synapse loss observed here is induced by the presence of disease-induced synaptic pathology.

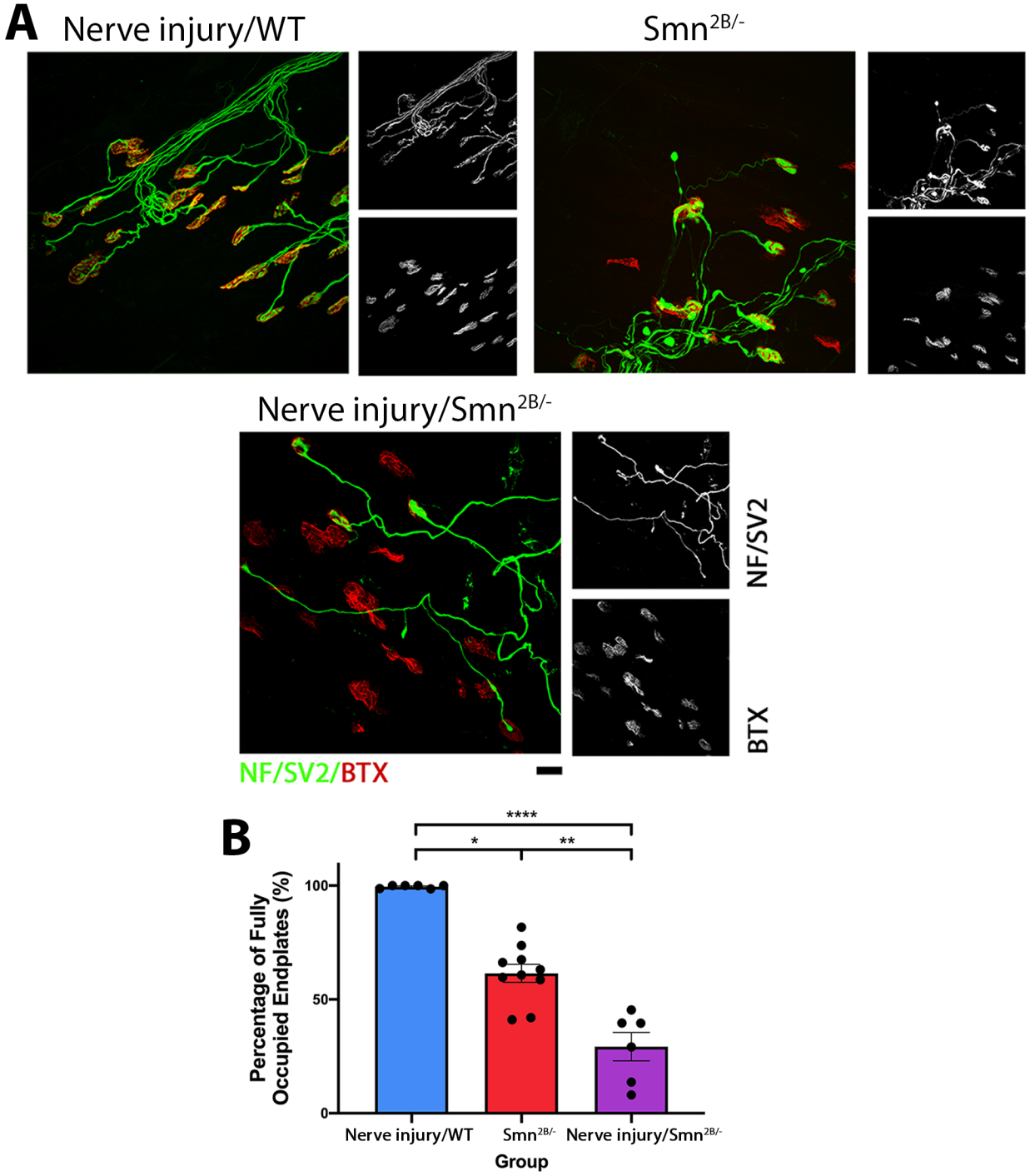
A
Nerve injury/WT
Smn2B/-
Nerve injury/Smn2B/-
NF/SV2
BTX
NF/SV2/BTX
B
****
*
**
Percentage of Fully Occupied Endplates (%)
100
50
0
Nerve injury/WT
Smn2B/-
Nerve injury/Smn2B/-
Group

Figure 1.12: Presence of synaptic pathology in the Smn$^{2B/-}$ mouse significantly amplifies the level of synaptic loss induced by injury in the TVA muscle. (**A**) Confocal micrographs showing NMJs labelled with antibodies against neurofilament (NF, green) and synaptic vesicle protein 2 (SV2, green), and α-bungarotoxin (BTX, red) from transversus abdominis (TVA) at P18 in wild-type animals after *ex vivo* nerve injury (nerve injury/WT), in the *Smn*$^{2B/-}$ mice, and in *Smn*$^{2B/-}$ after *ex vivo* nerve injury (nerve injury/*Smn*$^{2B/-}$) conditions, respectively. In *ex vivo* conditions, TVA muscles were maintained ex vivo at 30°C for 24 hr. P18 refers to the postnatal age of the animal at the time of dissection. Scale bar: 20μm. (**B**) Quantification of the percentage of fully occupied endplates in the TVA in nerve injury/WT, *Smn*$^{2B/-}$, and nerve injury/*Smn*$^{2B/-}$ conditions. The percentage of fully occupied endplates following injury in *Smn*$^{2B/-}$ mice was significantly increased in comparison with either wild-type injury or *Smn*$^{2B/-}$ conditions in isolation. *$p < 0.05$, ***$p = 0.0001$, ****$p < 0.0001$. For all comparisons with the nerve injury/WT group, Kruskal–Wallis with Dunn's correction was used to account for non-normally distributed data, otherwise a one-way ANOVA with Tukey's correction was used. Note that n = 6, 10, 6 muscles for the nerve injury/WT, *Smn*$^{2B/-}$, and nerve injury/*Smn*$^{2B/-}$ groups, respectively. Error bars: mean ± SEM.

1.20.9 Journal of Anatomy Publication Declaration

Some work presented within this chapter has been published as a paper in the Journal of Anatomy entitled: *The rate of Wallerian degeneration following injury is influenced by postnatal maturity, motor unit specific properties and the presence of underlying pathology in mice* (Mole et al., 2020). A copy of this publication is provided in Appendix 1.

1.21 Discussion

1.21.1 Overview of Results

Here, an *ex vivo* assay has been optimised and applied to investigate rates of synaptic withdrawal following traumatic nerve injury in a range of muscles that have not been examined in this context previously. Optimisation of an *ex vivo* assay demonstrated a capacity for this model of peripheral nerve injury to be expanded to a range of muscles that have not been examined previously. Applying this model found that increasing postnatal age led to a progressive decline in the level of innervation remaining following injury in the cranial muscles, suggesting that synaptic stability is developmentally regulated in these muscles. It has also been shown that levels of synaptic loss are non-uniform in the cranial muscles, with a significant increase in the rate of synaptic withdrawal in response to injury in the AAL at younger ages when compared with other cranial muscles. Remarkably high levels of innervation persisted in the thoracoabdominal muscles after injury across P15–P25, and this preservation remained evident even at 32°C. Results suggest that muscle and/or motor neuron intrinsic properties can affect synaptic stability following injury. Analyses of NMJ maturational status did not reveal a correlation between increased maturity and increased synaptic loss following injury, although there was a trend towards muscles with less mature NMJs being more susceptible to synaptic loss. Furthering this, comparison of the patterns of relative synaptic stability following injury to the patterns of synaptic vulnerability in a mouse model of SMA suggests that the factors which affect synaptic stability following injury are distinct from those in peripheral neuropathies such as SMA. By exposing a muscle from a mouse model of SMA that is resistant to dying-back pathology to the *ex vivo* nerve injury assay, it was found that synaptic loss in response to injury is SMN-independent. Furthermore, exposure of a muscle with ongoing dying-back pathology to the assay has demonstrated that the presence of dying-back pathology accelerates the rate of synaptic loss in response to injury. Overall, I have provided and characterised a model system of peripheral nerve injury in a range of different muscles that will facilitate the investigation of factors that can alter rates of synaptic degeneration temporally and regionally. I have also provided

an indication of downstream, mechanistic convergence in degenerative mechanisms in injury and disease scenarios; this could ultimately aid in the identification of common targets to slow synaptic degeneration under different physiological conditions.

1.21.2 Synaptic stability following injury is governed by properties that are intrinsic to the muscle and/or motor neuron

This work suggests that synaptic withdrawal in response to injury is influenced by developmental age in a range of muscles that can now be maintained *ex vivo*. Across all four cranial muscles analysed, there was a marked increase in the incidence of denervated endplates with increasing postnatal age. These findings are in line with previous work that has shown that following either peripheral nerve injury or hypoxic insult, resistance is gradually lost across the first few weeks of life as the muscle transitions to adult levels of vulnerability (Murray et al., 2011). Furthermore, some muscles, like the AAL, reach adult levels of degeneration at an earlier time point, whereas others, such as the TVA, remain comparatively stable following injury, even at P25 (Murray et al., 2011). This suggests that postnatal maturity as well as properties specific to the muscle and/or motor neuron, are capable of regulating synaptic degeneration following injury. The expansion of the *ex vivo* model of peripheral nerve injury to allow the inclusion of a range of different muscles that respond differently will provide an opportunity to discern mechanisms and regulators of synaptic degeneration in injury and disease.

Various genetic mutations have been shown to alter the rate of WD in animal models, and have increased our understanding of the mechanisms of WD. As mentioned previously, this includes *Wld*^{s} and SARM1 knockout, both of which can delay axonal and synaptic degeneration significantly after injury (Lunn et al., 1989; Ribchester et al., 1995; Mack et al., 2001; Wang et al., 2001; Gillingwater et al., 2002, 2004, 2006; Coleman, 2005; Coleman and Freeman, 2010; Gilley and Coleman, 2010; Osterloh et al., 2012; Di Stefano et al., 2015; Gilley et al., 2015). Work presented here highlights the presence of differential responses both at different ages and between different

muscles. It is interesting to note that subcellular, compartmental differences have also been reported in the response to injury within the central nervous system, suggesting that differential responses to injury may also feature centrally (Sajadi et al., 2004). Such differences in degenerative rates can help us to discern the factors that might govern the rate of synaptic degeneration and identify novel targets aiming to slow neurodegeneration.

Differences in synaptic vulnerability in motor neuron disease have been exploited to investigate the underlying factors that may be responsible making motor neurons vulnerable in motor neuron disease. Transcriptional profiling of differentially vulnerable motor neurons has helped identify transcripts and pathways which can modify the rate of degeneration (Hedlund et al., 2010; Brockington et al., 2013; Kaplan et al., 2014; Comley et al., 2015; Murray et al., 2015; Boyd et al., 2017; Kline et al., 2017). Work by Hedlund et al., 2010 in rats has highlighted that there are transcriptome level differences in populations of motor neurons that are generally spared in conditions like ALS and SMA (Hedlund et al., 2010). Similar findings have also been shown in mouse model of SMA, where comparative gene expression profiling of vulnerable and resistant populations of motor neurons has found that a modified bioenergetic profile, particularly relating to mitochondrial biogenesis (which will be discussed further in Chapter 2), can modulate motor neuron vulnerability (Boyd et al., 2017). Through cross-species comparisons, the Murray laboratory has also highlighted that differential gene expression can commonly modify neurodegenerative phenotypes (Kline et al., 2017). In this work, alpha-synuclein and stathmin 1 were identified as phenotypic modifiers of pathology in motor neuron diseases. Importantly, when levels of alpha-synuclein or stathmin 1 were increased, disease severity was reduced and NMJ pathology ameliorated (Kline et al., 2017; Villalon et al., 2019). Overall, it is clear that identifying factors that can modify the rate of synaptic and axonal degeneration is invaluable in the search for targets that can modify the rate of neurodegeneration. This emphasises the value of the expanded *ex vivo* model as a tool to identify and investigate factors that can modify the rate of synaptic and axonal degeneration. Any factor that can alter the degenerative rate represents an opportunity to study the mechanisms of degeneration in both disease and injury.

Here it has been shown that muscle and/or motor neuron-specific properties are another factor that can influence the rate of synaptic loss, with responses varying between muscles. This is unlikely to be attributed to muscle fibre type. For example, both LAL and AAL are predominantly fast twitch muscles, but they display a marked difference in synaptic stability following injury (Erzen et al., 2000; Murray et al., 2008a, 2010a, 2010b). Intermuscular differences in maturational status do exist, as evidenced by differences in the level of mono- and polyinnervation across different muscles, however it remains unclear whether differences in NMJ maturity could be directly responsible for determining susceptibility to synaptic loss following injury. In wild-type rats and in *Wld*^{s} mice, the rate of synaptic loss has been shown to be dependent on nerve stump length, with failure of neuromuscular transmission occurring more rapidly when nerve stump length is shorter (Slater, 1966; Ribchester et al., 1995). However, the differences reported here cannot be attributed to differences in nerve stump length, as stump length is the same for all of the cranial muscles.

A promising avenue which may explain the differing synaptic stability following injury in different muscles at different postnatal ages, is differences in mitochondrial bioenergetics. In a recent study, profiling of the nerve and muscle proteome in tibial nerve/lumbrical muscles between P12 and P24, highlighted a consistent up-regulation in proteins involved with mitochondrial bioenergetics in both muscle and nerve. Interestingly, similar profiles have been observed in the tibialis anterior muscle, and during postnatal development of the heart (Puente et al., 2014; Kim et al., 2019). Importantly, in our previous work it was also shown that inhibition of complex I of the mitochondrial respiratory chain could slow axon degeneration, whereas pharmacological activation of oxidative phosphorylation accelerated synaptic degeneration (Kline et al., 2019). It will be important to investigate mitochondrial bioenergetics in the range of ages and muscles investigated in this study, to determine whether this can explain the differences in synaptic stability observed. This will help identify factors responsible for conferring rate differences and will provide insight into the mechanisms of synaptic degeneration. This may further aid in the identification of targets to manipulate the rate of degeneration. The role of mitochondria in influencing the rate of synaptic loss following injury will be considered in Chapter 2.

1.21.3 To what extent do mechanistic commonalities exist between synaptic withdrawal in injury and dying-back neuropathy?

Following traumatic injury in the *Smn*$^{2B/-}$ mouse model of SMA, I assessed the influence on the level of synaptic loss. Selective vulnerability is a known feature in this disease model, therefore both die-back-resistant (LALr) and die-back-vulnerable (TVA) muscles were studied (Murray et al., 2015). As synaptic withdrawal after injury was amplified in the presence of a die-back, it is concluded that the presence of dying-back pathology can increase synaptic loss in following injury.

Initially, these results are perhaps surprising based on previous work where the presence of dying-back pathology has reduced synaptic loss and axon fragmentation following nerve injury. For example, *Wasted* (*Wst*) is a spontaneous, autosomal recessive mutation in which the gene encoding translation factor eEF1A2 is deleted (Shultz et al., 1982). *Wst* mice display a dying-back neuromuscular phenotype and have a lifespan of around 30 days (Shultz et al., 1982, Newbery et al., 2005, Murray et al., 2008b). It has been found that whilst loss of translation elongation factor eEF1A2 causes dying-back pathology at the NMJ, loss of this factor can also delay the initiation and progression of WD following axotomy of the tibial nerve (Murray et al., 2008b). This is in contrast to my findings where the presence of a die-back neuropathy accelerated WD. Therefore, although differing requirements for eEF1A2 expression may represent a mechanistic distinction between injury-induced degeneration and dying-back pathology, work presented here suggests that there may be convergence in degenerative pathways further downstream.

Commonalities between WD and dying-back neuropathies have been reported in animal models of motor neuron disease. For example, *Wld*^{S} has been found to be protective in some motor neuron disease and peripheral neuropathy models, suggesting that there may be some convergence between degenerative mechanisms. Similarly, in mice with progressive motor neuronopathy, *Wld*^{S} expression also delays dying-back pathology (Ferri et al., 2003). It is worth noting that protection conferred by *Wld*^{S} during dying-back neuropathy is not universal. Work in *SOD*/*Wld*^{S} mice, a

mouse model of ALS, has shown that this levels of motor axon loss remain unaffected, although modest delays in NMJ degeneration and prolonged survival were reported (Fischer et al., 2005). Similarly, work undertaken by Velde et al., has also evidenced that *Wld*^{S} cannot slow disease onset, motor neuron death, axonal degeneration or reduce synapse loss in a mouse model of ALS (Vande Velde et al., 2004). In mouse models of SMA, the *Wld*^{S} gene did not alter the onset or progression of disease phenotype (Rose et al., 2008, Kariya et al., 2009). Delays in neurodegeneration have been reported in a number of other diseases however, including animal models of Parkinson's and demyelinating diseases that possess the *Wld*^{S} mutation (Sajadi et al., 2004, Conforti et al., 2014).

Several similarities have also been highlighted at the cellular level between WD and dying-back pathology, including poor axonal transport, mitochondrial dysfunction, and an increase in intra-axonal calcium (reviewed by Coleman, 2005; Conforti et al., 2014). Our recent proteomic work in mice has also identified alterations in mitochondrial bioenergetics that coincide with delays in the change in level of synaptic loss in response to injury during postnatal development in the hindlimb (Kline et al., 2019, see Appendix 2 for co-author paper). Furthermore, we demonstrated that Complex I inhibition could delay WD, and pharmacological activation of oxidative phosphorylation accelerated WD (Kline et al., 2019). Targeting bioenergetic pathways by enhancing mitochondrial bioenergetics has also been found to rescue motor axon defects in a model of SMA (Boyd et al., 2017). Alterations in mitochondrial dynamics may therefore represent a promising, and perhaps uniting factor in WD and dying-back neuropathy. The role of mitochondria will be considered in Chapter 2.

Overall, the *ex vivo* system optimised and described here will provide a valuable model to aid in the identification of factors that are capable of influencing the rate of neurodegeneration under different physiological conditions. Anything that can alter the rate of degeneration can inform of mechanism, therefore the range of muscles now available for study and characterised in terms of WD present intriguing opportunities to further study the mechanisms and regulators of synaptic degeneration. Ultimately

this could aid in the identification of targets that are common across multiple diseases, and that may slow degeneration under different physiological conditions.

Chapter 2 : **Role of mitochondria in regulating postnatal delays in Wallerian degeneration**

1.22 Chapter overview and principle findings

This chapter aimed to examine changes in mitochondrial proteins and number during early postnatal development, where rates of synaptic degeneration following injury progressively accelerate. Here, I analysed two independent proteomic screens and highlighted key changes in mitochondrial proteins across the first few weeks of life. I then examined mitochondrial protein levels in a range of other muscles and nerve to determine if similar patterns of changes in mitochondrial proteins could be observed. Overall, I sought to investigate whether changes in mitochondrial proteins or number correlated with accelerations in the rate of synaptic degeneration across development, or between different muscles.

Principle Findings

- Analyses of two independent proteomic screens reveal that mitochondrial proteins increase across postnatal development.
- These increases in mitochondrial proteins can be accounted for by an increase in mitochondrial number in nerve, but not in muscle.
- Expanding analysis to include a range of nerves and muscle reveals changes in mitochondrial complex protein levels do not correlate with the rate of synaptic degeneration during postnatal development.
- Comparison of muscles with differential rates of synaptic degeneration reveals that the rate of degeneration does not correlate with changes in mitochondrial number in either muscle or nerve.
- Comparison of nerves with differential rates of synaptic degeneration reveals a correlation with complex I levels.

1.23 Introduction

As discussed and expanded upon in Chapter 1, previous work has demonstrated that there are age-dependent accelerations in the rate of synaptic withdrawal in the deep lumbrical muscles following traumatic injury of the sciatic nerve (Murray et al., 2011). To better understand what factors might be responsible for determining the rate of synaptic withdrawal, in a recent paper where I am a co-author, we recently profiled proteomic changes during postnatal developmental in sciatic nerve and DL muscles from P12 to P24 (Kline et al., 2019) (see Appendix 2). In this paper, a tandem mass-tagging proteomic approach was used and protein changes were identified in both muscle and nerve that correlated with accelerations in synaptic degeneration across this early developmental period (Kline et al., 2019). Previously, using network-based software and functional annotation of upregulated clusters in DAVID, we identified consistent increases in proteins pertaining to mitochondria, oxidation/reduction and the electron transport chain across this time period. Using pathway analysis software, specific enrichments and convergence on components pertaining to complexes I and IV were identified (Kline et al., 2019).

The hypothesis that mitochondrial changes are therefore responsible for accelerations in axon degeneration was further supported through pharmacological manipulation of oxidative phosphorylation. Pharmacological inhibition of complex I (CI) through the application of rotenone was found to be axoprotective to dorsal root ganglion (DRG) neurons in culture following axon injury, whilst up-regulation of basal oxidative phosphorylation through the application of 5-Aminoimidazole-4-carboxamide ribotide (AICAR) was found to accelerate synaptic degeneration (Kline et al., 2019). It therefore appears that an increase in mitochondrial proteins correlates with the acceleration in the rate of synaptic degeneration in the DL muscles during postnatal development. If mitochondrial changes are responsible for the acceleration in synaptic degeneration, then these changes should be consistent and robust, and present in other nerves and muscles. This therefore provides a platform from which I now ask whether changes in mitochondrial proteins correlate with alterations in synaptic stability in other muscles or nerves following injury.

Structurally, mitochondria are composed of a matrix that is surrounded by an inner and outer mitochondrial membrane that are separated by an intermembrane space. The outer membrane separates the mitochondrion from the cytosol. The inner mitochondrial membrane is folded to form cristae, which is where the electron transport chain (ETC) is housed. The ETC is essential for cellular respiration and the production of ATP, the energy currency of the cell. The ETC is composed of a series of multi-subunit complexes, complexes I-IV and ATP synthase (herein referred to as complex V), and mobile, electron transporters that are responsible for accepting and transferring electrons. The assembled components and supercomplexes are the basis of ATP production during oxidative phosphorylation (Fig. 2.1).

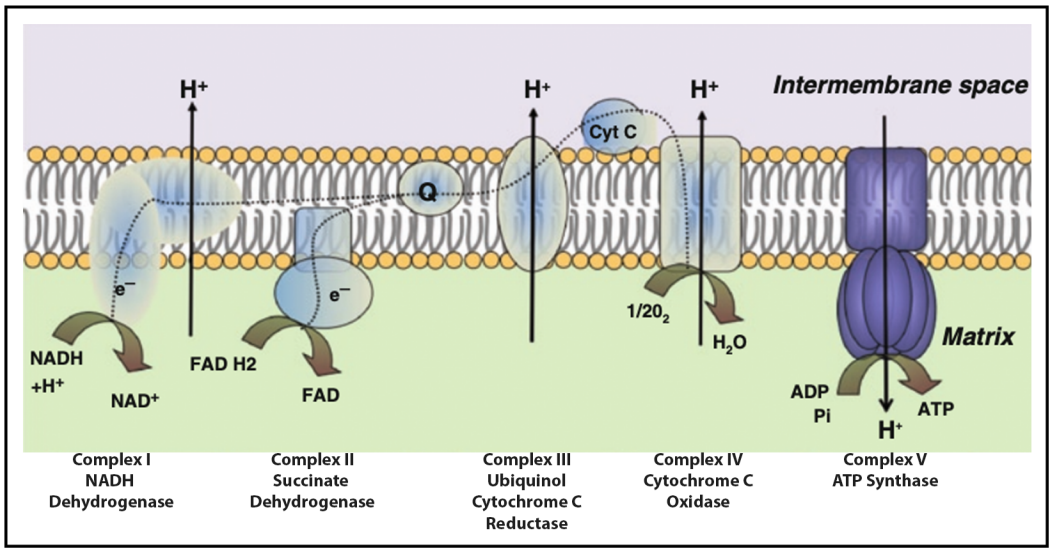

Figure 2.1: Schematic of the mammalian electron transport chain (ETC) on the inner mitochondrial membrane. In the presence of NADH. H^+ or $FADH_2$, energy substrates arising as products from the metabolism of glucose, electrons are transferred through a series of enzyme complexes, complex I-IV (CI-IV). To provide a simplified overview, CI (NADH dehydrogenase) and CII (succinate dehydrogenase), accept electrons from NADH or FADH respectively. Both CI and CII transfer electrons onto Coenzyme Q (ubiquinone, labelled here as Q). Electrons are then passed onto CIII (ubiquinol cytochrome c reductase), then cytochrome c (labelled here as Cyt C). Complex IV (cytochrome c oxidase) is the final enzyme in the series, where the final electron receptor, oxygen, is reduced to water. As electrons are transferred, protons are extruded from the cell, thereby establishing an electrochemical gradient. This gradient is then used by ATP synthase (often referred to as Complex V), to generate energy in the form of ATP. This overall process is referred to as oxidative phosphorylation, since it culminates in the phosphorylation of ADP to ATP. Note that the membrane-bound enzymes are complex and composed of multiple subunits; this schematic does not show this supramolecular complexity. Schematic reproduced from Benard et al., 2011, with copyright permissions (license number can be provided on request) (Benard et al., 2011).

The transfer of electrons through the ETC is not 100% efficient; some electrons are transferred to O_2, thereby generating reactive oxygen species (ROS). Endogenous ROS are mainly produced by mitochondria, and are an inevitable by-product of oxygen metabolism. ROS can include: superoxide anions (O_2•-), hydrogen peroxide (H_2O_2), and hydroxyl radicals (OH•). At low concentrations, ROS are thought to play key signalling roles in proliferation, hypoxia adaptation and cell fate determination (Sena and Chandel, 2012). However, excessive production of ROS can have harmful and irreversible effects on lipids, proteins and nuclear acids. It is well recognised that elevated intracellular ROS can lead to oxidative stress that results in DNA damage and even cell death (Cross et al., 1987, Vendemiale et al., 1999, Simon et al., 2000a). ROS overproduction has also been linked as being both causative and a consequence of disease, for example mitochondrial defects and ROS have been implicated in axon degeneration, including in WD (Barrientos et al., 2011, Villegas et al., 2014, O'Donnell et al., 2013, Park et al., 2013, Calixto et al., 2012). In our previous work, inhibition of CI, which is known to be a major ROS producer (Brand, 2010, Zhao et al., 2019, Kowaltowski et al., 2009), prevented axotomy-induced elevations in ROS and was shown to be axoprotective (Kline et al., 2019). Mitochondrial depolarisation in the absence of physical injury can similarly induce axonal death through WD pathways (Loreto et al., 2020). In work by Press and Milbrandt, the application of antioxidants was shown to confer axonal protection from rotenone-induced axonal degeneration (Press and Milbrandt, 2008). Other work has also suggested that anitoxidants may prove therapeutically useful to counteract oxidative damage and toxicity in disease scenarios (Sherer et al., 2003, Testa et al., 2005). This further supports the hypothesis that ROS-mediated damage plays a key role in determining the neuronal response to injury and implicates mitochondrial dysfunction as a key factor in determining axonal and synaptic health.

Additionally, there is a growing body of evidence that implicates mitochondria as playing a role in axonal and synaptic degeneration. Proteomic profiling have highlighted mitochondrial dysfunction as an important factor in regulating synaptic stability and vulnerability in the pathogenesis of neurodegenerative diseases (Llavero Hurtado et al., 2017, Luiro et al., 2006, Graham et al., 2017). This is particularly true

of diseases where the synapse is an early pathological target, such as Parkinson's disease (Ferrer et al., 2012), Alzheimer's disease (Lee et al., 2012, Du et al., 2010), and Batten disease (Luiro et al., 2006). In mouse models of SMA, mitochondrial dysfunction has been implicated as playing a role in disease pathogenesis, with both structural and functional defects having been described prior to symptom onset (Miller et al., 2016). In mutant SOD1 mice, widely used as a mouse model of ALS, protein aggregation, enhanced oxidative stress and excitotoxicity have been implicated in the process of motor neuron degeneration (Martin et al., 2007). Structural defects in mitochondria have also been described in ALS patients in skeletal muscle, liver and spinal motor neurons (Menzies et al., 2002), with markers of oxidative stress and ROS damage also reportedly elevated (Beal, 2002). Considering the abundance of evidence implicating mitochondrial dysfunction in disease, it is unsurprising that mitochondria are thought to play a fundamental role in axonal and synaptic degeneration under pathophysiological conditions.

There is increasing evidence that implicates mitochondrial changes as an important aspect of normal development. In rats, it has been shown that whilst mitochondria are arranged individually and parallel to the muscle fibre at birth, by 2 months of age, these form a highly connected, and grid-like network that facilitates rapid energy distribution (Bakeeva et al., 1981, Glancy et al., 2015). Proteomic work by Kim et al., has profiled proteomic changes in developing tibialis anterior muscle that are thought to be important for the formation of this mature mitochondrial network (Kim et al., 2019). Kim et al., highlight an upregulation of proteins that are associated with mitochondrial bioenergesis and oxidative phosphorylation across development. Across P1-P42 of postnatal development, Kim at al., not only demonstrate morphological changes in the orientation of muscle mitochondrial network configuration, but also detail changes in mitochondrial-associated protein expression. This group profile changes in cytochrome c oxidase, complex IV (CIV), subunits, assembly factors, mitophagy-associated proteins and antioxidants to ultimately conclude that proteins involved in mitochondrial biogenesis and oxidative phosphorylation are upregulated throughout muscle development. Cytochrome c oxidase (CIV) plays a pivotal role in mitochondrial energetics; work by Larsen et al.,

has previously highlighted that CIV shows a strong association with oxidative capacity in human skeletal muscle (Larsen et al., 2012). CIV is also the last enzyme in the respiratory chain, and is therefore considered as a major regulation site for oxidative phosphorylation (Li et al., 2006). In the Kim et al., study, developmentally-regulated transitions in mitochondrial biology are discussed in the context of the establishment of a mature mitochondrial network; alterations in mitochondria are suggested to represent a metabolic shift towards mitochondria that are specialised to meet postnatal, cellular energy demands. Although this work clearly recognises that the mitochondrial proteome is dynamic during development, it remains unclear how this relates to alterations in synaptic stability. Focussing on the postnatal time frame where developmental regulation is a feature (in this dataset this refers to P1-P21), and drawing comparisons to the Kline et al., dataset, will therefore provide better insight into the role of mitochondria across this critical and transitional time period.

Other work has also implicated mitochondria as playing an important role in postnatal development. In 2015, Puente et al., undertook a temporal analysis to better understand factors that can regulate the loss of regenerative capacity in cardiomyocytes postnatally in mice (Puente et al., 2014). This work focused on the first week of life, where there is a shift from a hypoxic, embryonic environment where cardiomyocytes primarily utilise anaerobic glycolysis as their energy source, to the mature, adult state where cardiomyocytes primarily utilise oxygen-dependent mitochondrial oxidative phosphorylation as their energy source. Within this early time frame, there are marked increases in ROS, oxidative DNA damage and DNA damage response markers (Puente et al., 2014). Postnatal hypoxemia, ROS scavenging and inhibition of DNA damage response were also shown to prolong the proliferative period of cardiomyocytes (Puente et al., 2014). Across the first two weeks of development, mitochondrial number – indicated by increased mitochondrial DNA (mtDNA) copy number – and complexity were shown to significantly and linearly increase across time. Levels of mtDNA have previously been used as a biomarker of mitochondrial content (Malik and Czajka, 2013, Puente et al., 2014, Quiros et al., 2017). Such changes in mitochondrial biology, and the associated increase in ROS production during this time

frame, indicate an important role for mitochondria in postnatal development however, it remains unclear if similar temporal shifts are also seen in neural tissue.

Overall, a major question that emerges is whether changes in mitochondrial protein expression can also explain differences in the synaptic response to injury in other muscles, either temporally or regionally. In our previous work, proteomic analyses were limited to CI and IV, therefore a more comprehensive analyses of the Kline et al., proteomic dataset would provide insight into how mitochondrial proteins change during this transitional period. A range of proteins originally profiled by Kim et al., will be examined in the Kline et al., dataset, and considered in the context of synaptic stability after injury. Note that synaptic withdrawal responses were described in Chapter 1, and for ease of referral are summarised in Table 14. Kim et al., originally consider an extended postnatal time period, however this is not specific to the transitional time window in which synaptic stability is altered. To facilitate comparison and begin to look for correlations with rates of synaptic loss, here, I will only time points up to and including P24 were considered. Notably, both the Kline et al., and Kim et al., proteomic screens are limited in that they only looked at one muscle, therefore comparing and expanding upon this to investigate patterns of change in mitochondrial proteins in other muscles at a range of different time points, will provide an indication of whether temporal and regional differences in mitochondria might influence the rate of synaptic withdrawal following injury.

In this chapter, I subjected proteomic datasets to new analyses and highlight increases in mitochondrial protein abundance across the first 3 weeks of life that correlate with accelerations in synaptic degeneration following injury across early postnatal development. I found that increases in mitochondrial proteins correlated with an increase in mtDNA in muscle but not in nerve, suggesting that increased mitochondrial number could account for the increase in mitochondrial proteins in muscle. To determine if changes in mitochondria could explain the alterations in the rates of synaptic degeneration, I analysed mitochondrial complex protein levels and mtDNA content in cranial and thoracoabdominal musculature, and in sciatic and intercostal nerves across the time period of P12 to P24. In contrast with findings from the proteomic analysis, I found that changes in mitochondrial complex protein levels or

mitochondrial number were not consistent with previous reports, and therefore could not account for regional or temporal changes in the rate of synaptic degeneration. However, interestingly, in nerve increases in complex I did correlate with differential rates of synaptic degeneration. Overall, despite initially promising indications from proteomics that mitochondrial changes could be responsible for accelerations in synaptic degeneration in muscle, this pattern is not substantiated, suggesting that other factors must be involved in regulating the degenerative rate.

Table 14: Summary table showing the rates of synaptic withdrawal at postnatal days 15 and 24 in a range of different muscles following ex vivo nerve injury and maintenance at 30°C in muscle. Note that • denotes muscles served by the facial nerve, whilst * denotes those served by intercostal nerves.

Muscle	**P15**	**P24**
AAL •	Fast	Fast
LALr •	Slow	Fast
LALc •	Slow	Fast
AS •	Slow	Fast
TVA *	Slow	Slow
TS *	Slow	Slow

1.24 Results

1.24.1 Proteomic comparisons highlight changes in mitochondrial proteins that coincide with developmental regulation

Raw proteomic data gathered from our previous work in deep lumbrical muscles (Kline et al., 201), and a raw proteomic dataset made available by Kim et al., in tibialis anterior muscle (Kim et al., 2019), were subjected to new analysis with the aim of undertaking a comprehensive analysis of the changes in mitochondrial proteins occurring during postnatal development. Note that whilst these datasets were collected as part of other studies, the analyses and comparisons presented here have been undertaken by myself. In both studies, isolated and pooled regions of nerve or muscle were digested and extracted from each age point, and a tandem mass tagging approach was implemented. Here, I performed functional clustering of up-regulated proteins in both data sets using open source DAVID software. This revealed a significant overlap in the most highly enriched functional clusters in both Kline et al., and Kim et al., datasets, with mitochondria emerging as the most significantly enriched cluster, with scores of 152.52 and 33.93 respectively (Fig. 2.2). Notably, the majority of functional clusters that were identified in these analyses pertained to aspects of mitochondrial function. Note that a DAVID score of >1.3 is equivalent to $p < 0.05$, and so all of the clusters listed are significantly enriched.

A

Up from P12-P24
Kline et al., 2019

Cluster Name	Enrichment Score
Mitochondrion	152.52
Mitochondrial inner membrane	44
Oxidation reduction processes	27.1
Carbon metabolism	14.21
Nucleotide/ATP binding	9.77
Sarcoplasmic reticulum	9.02
Electron carrier activity/Flavoprotein	8.55
Fatty acid/lipid metabolism	8.44
Troponin	6.76
Iron-sulfur cluster binding	6.36

B

Up from P1-P42
Kim et al., 2019

Cluster Name	Enrichment Score
Mitochondrion	33.93
Carbon metabolsm/glycolysis	17.35
Mitochondrial inner membrane	12.5
Tricarboxylic acid cycle/pyruvate metabolism	9.04
Oxidation-reduction process/activity	5.92
Mitochondrial acetyl-coA biosyntheic process from pyruvate	4.34
Cytochrome-c oxidase activity	4.2
Ubiquinone/NADH dehydrogenase activity	3.78
Carbohydrate metabolitic process/glycogen metabolism	3.57
Fructose and mannose metabolism	3.56

Figure 2.2: Top 10 most significantly enriched functional clusters identified by DAVID analysis across the postnatal time periods analysed from two independent proteomic screens. Note that in deep lumbrical muscles (**A**) and in tibialis anterior muscle (**B**), analysis of proteins consistently upregulated across P12-24 or P1-42 respectively, reveals an enrichment of processes relating to mitochondria and oxidative phosphorylation. Note the many commonalities between independent screens. Functional annotations are ranked by a DAVID enrichment score, where a score of >1.3 in DAVID is equivalent to $p < 0.05$.

Our previous work primarily focussed on characterising and validating changes in CI levels and activity across P12 to P24 (Kline et al., 2019, Appendix 2). Here, I expanded this analysis to include subunits from different complexes to gain a broader overview of ETC activity within this time frame. This included profiling five different subunits across P12-P24: CI subunit NDUFB8 (NADH: Ubiquinone oxidoreductase subunit B8), an accessory subunit of CI; complex II (CII) subunit SDHB (Succinate dehydrogenase complex iron sulfur subunit B), an iron-sulfur protein subunit of CII; complex III (CIII) subunit UQCRC2L (Ubiquinol-cytochrome c reductase core protein 2), a key assembly component of CIII; CIV subunit COX II, the second subunit of CIV; and complex V (CV) subunit ATP5A (ATP synthase F1 subunit alpha), a component of the catalytic core of mitochondrial membrane ATP synthase. Here, these subunits have also been profiled in the Kim et al., dataset across P1 to P21. In line with previous work, it was hypothesised that increases in CI subunit expression would be seen in both datasets. Since it has previously been shown that oxidative activity increases across the postnatal period, it was also hypothesised that other complex subunits would also be upregulated across these time periods. Consistent with these hypotheses, it was found that CI subunit expression increased with age in both cases (Fig. 2.3), as did expression of all other complex subunits across P12-P24 and P1-P21 in the Kline et al., and Kim et al., datasets respectively. Notably, CI showed the strongest correlation when both datasets are considered. Since CI is recognised as a major ROS producer (Giachin et al., 2016, Telford et al., 2009), it is hypothesised that increases in CI will be a key and common factor in determining the synaptic response to injury both across time in other muscles.

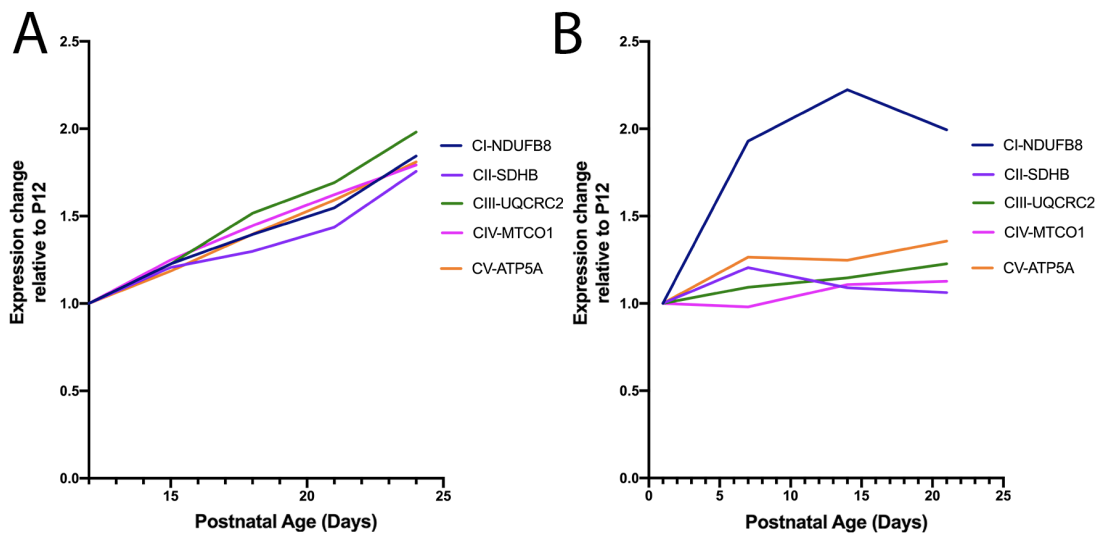

Figure 2.3: Relative fold change of oxidative phosphorylation (OXPHOS)-related subunits in developing muscles across early postnatal development. Changes of individual OXPHOS subunit proteins are shown across postnatal development of the deep lumbrical muscles relative to P12 (A) or tibialis anterior muscle relative to P1 (B). (**A**) Line graph showing expression fold change in subunits of CI-V of the electron transport chain from P12-P24 in the deep lumbrical muscles. Note that increases are seen across time in all subunits. N = 5 mice, with 20 muscles per timepoint, with timepoints including P12, P15, P18, P21 and P24 (raw data available: Kline et al., 2019) (**B**) Line graph showing expression fold change in subunits of CI-V of the electron transport chain from P1-P21 in tibialis anterior muscle. Note that increases are seen across time in all subunits, although this is most pronounced in CI. N = 4 mice, with 3-5 pooled tissues, with timepoints P1, P7, P14 and P21 (raw data available: Kim et al., 2019).

Kim et al have previously described upregulations of cytochrome c oxidase subunits (CIV) between P1 and P42 (Kim et al., 2019). I therefore examined subunits identified by Kim et al., within our own dataset, and re-examined data provided by Kim to focus on the time period of P1 to P21, the period of postnatal development when synaptic stability is altered. It was hypothesised that there would be progressive increases in cytochrome c oxidase subunit protein levels between P12 and P24 in our dataset. Consistent upregulations in cytochrome c oxidase subunit protein levels were seen in both datasets. 13 common subunit proteins were identified (Fig. 2.4). Of these, 10

proteins were consistently upregulated across time (Fig. 2.3). Three notable and common exceptions were seen, that can be attributed to developmentally regulated isoform switches that occur. Cox4 has two isoforms: isoform 1 (Cox4i1), which increases with age, and isoform 2 (Cox4i2) which decreases. In early development, Cox6a also undergoes an isoform switch from isoform 1 (liver isoform) to isoform 2 (heart isoform). The third exception is seen in Cox7a, which also has heart (Cox7a1) and liver (Cox7a2) isoforms. Heart isoforms are seen to increase across time, whilst the liver isoform declines (Fig. 2.4). Such isoform switches are important for regulation of a number of regulatory processes including enzyme activity and energy production (Malek et al., 2018). Overall, comparable patterns are seen in both datasets, with progressive increases in cytochrome c oxidase subunits being evident. This provides further support for the hypothesis that changes in the mitochondrial proteome during postnatal development are important in determining and influencing synaptic stability following injury.

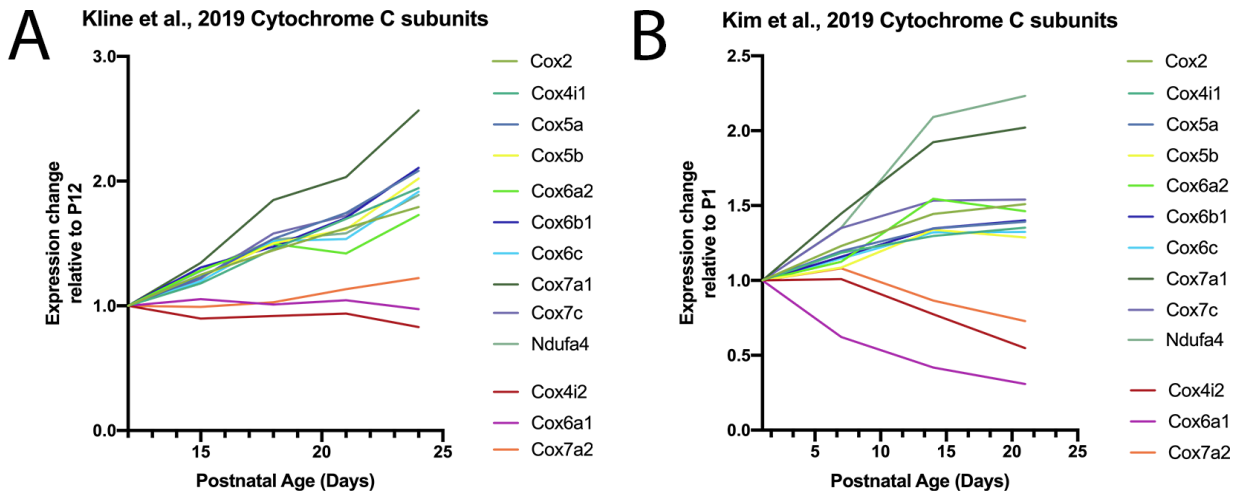

Figure 2.4: Relative fold change of cytochrome c oxidase proteins in developing muscles across early postnatal development. Changes of individual cytochrome c oxidase subunit proteins are shown across postnatal development of the deep lumbrical muscles relative to P12 (**A**) and tibialis anterior muscle relative to P1 (**B**). For deep lumbrical muscles, n = 5 mice, with 20 muscles per timepoint, with timepoints including P12, P15, P18, P21 and P24 (raw data available: Kline et al., 2019); for tibialis anterior muscles n = 4 mice, with 3-5 pooled tissues, with timepoints P1, P7, P14 and P21 (raw data available: Kim et al., 2019). Note that many similar increases are seen in cytochrome c oxidase protein changes between different muscles.

Previous work has shown that following axonal injury, ROS levels rise rapidly (O'Donnell et al., 2013). I was interested in whether factors that act to counteract ROS, including antioxidants and flavoproteins, were also upregulated across this time frame. I therefore mapped profiles of antioxidants and flavoproteins up to and including P24 (Fig. 2.5 and Fig. 2.6 respectively). Analyses of major antioxidant-related proteins revealed upregulations in three common, major antioxidants in both datasets: SOD2, GSTk1 and mitochondrial GPX (Fig. 2.5). Common decreases were seen in Catalase and IDH2. In addition, proteomic analyses of flavoproteins revealed consistent increases across time (Fig. 2.6). Flavoproteins are mainly localised to mitochondria, again implicating mitochondrial changes as influencing synaptic stability within this period.

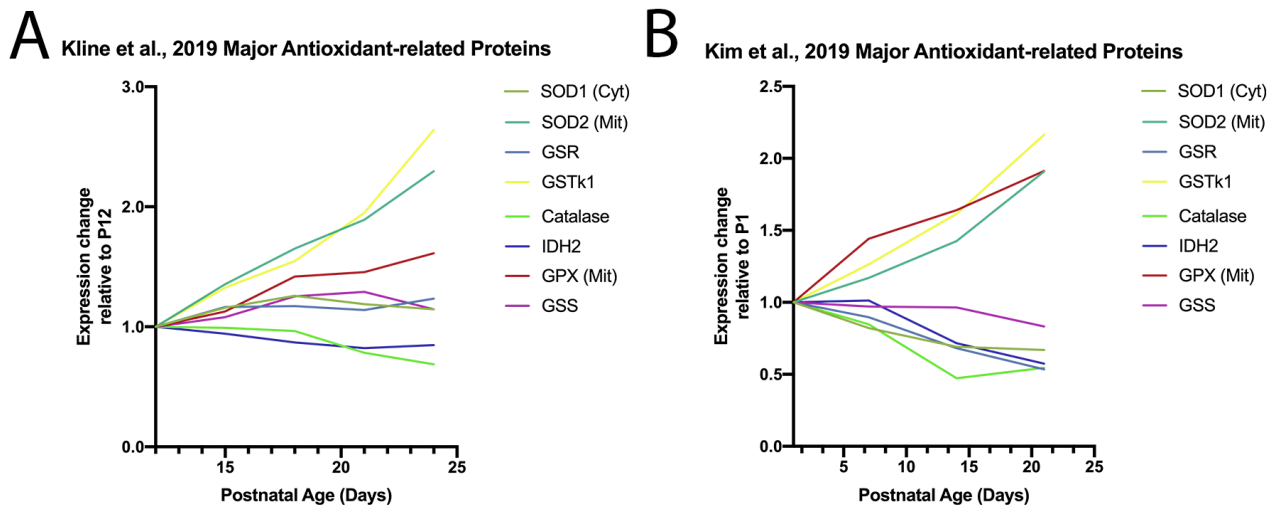

Figure 2.5: Relative fold change of major antioxidant-related proteins in developing muscle across early postnatal development. Changes of major antioxidant proteins are shown across postnatal development in the deep lumbrical muscles relative to P12 (**A**) and tibialis anterior muscle relative to P1 (**B**). For deep lumbrical muscles, n = 5 mice, with 20 muscles per timepoint, with timepoints including P12, P15, P18, P21 and P24 (raw data available: Kline et al., 2019); for tibialis anterior muscles n = 4 mice, with 3-5 pooled tissues, with timepoints P1, P7, P14 and P21 (raw data available, Kim et al., 2019).

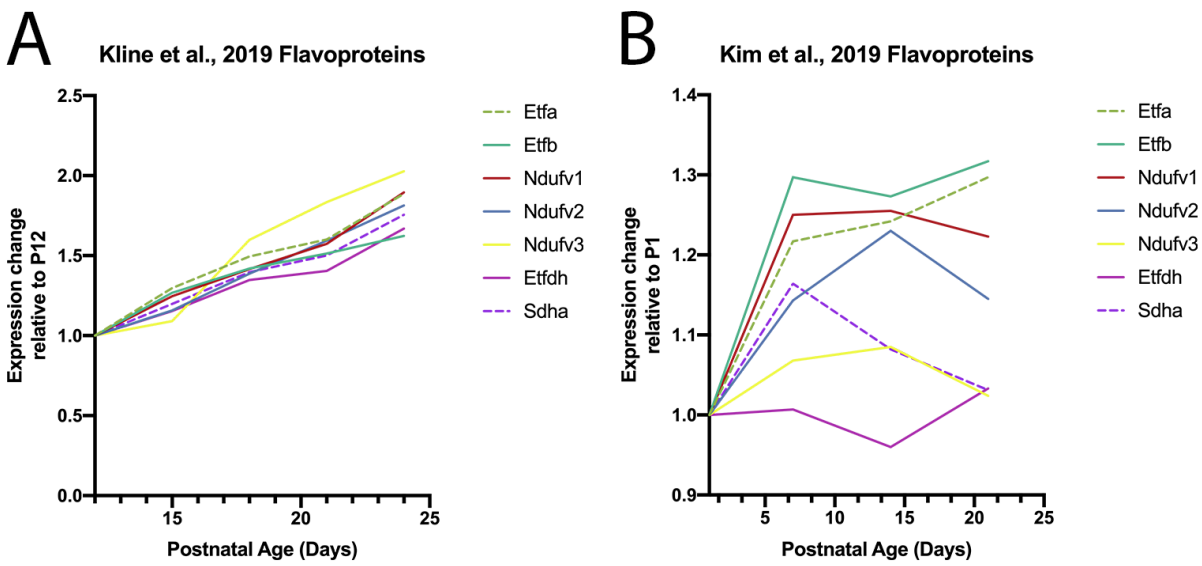

Figure 2.6: Relative fold change of flavoproteins in developing muscles across early postnatal development. Changes in individual flavoprotein proteins are shown across postnatal development of the deep lumbrical muscles relative to P12 (**A**) and tibialis anterior muscle relative to P1 (**B**). Note that flavoproteins levels generally increase across the first three weeks of life, and always increase by P24 (**A**) or P21 (**B**) relative to the earliest time point. For deep lumbrical muscles, n = 5 mice, with 20 muscles per timepoint, with timepoints including P12, P15, P18, P21 and P24 (raw data available: Kline et al., 2019); for tibialis anterior muscles n = 4 mice, with 3-5 pooled tissues, with timepoints P1, P7, P14 and P21 (raw data available: Kim et al., 2019).

These comparisons were also undertaken in sciatic nerve, using the Kline et al., raw dataset. Note that nerve data was not gathered in the Kim et al., study, therefore this is not included here. In nerve, although there are fluctuations during development, overall there are similar upregulations in proteins as described in muscle. For example, for cytochrome c oxidase subunit analysis, there are similar increases in the majority of proteins if the general trend from P12 to P24 is considered (Fig. 2.7, A). Cox6a2 and Cox7a1 show the most profound increases, which is consistent with isoform switching that is seen in muscle. Similar upregulations are also seen in the major antioxidants SOD2, GSTk1 and GPX in nerve. IDH2 is similarly decreased in nerve as it is in muscle, however catalase levels are seen to increase in nerve (Fig. 2.7, B). When considered generally, flavoprotein levels increase from P12 to P24 in nerve,

despite greater oscillations observed at intermediate time points (Fig. 2.7, C). Finally, oxidative phosphorylation (OXPHOS) subunits also follow a similar trend, with general increases from P12 compared to P24, despite intermediate time point oscillations (Fig. 2.7, D).

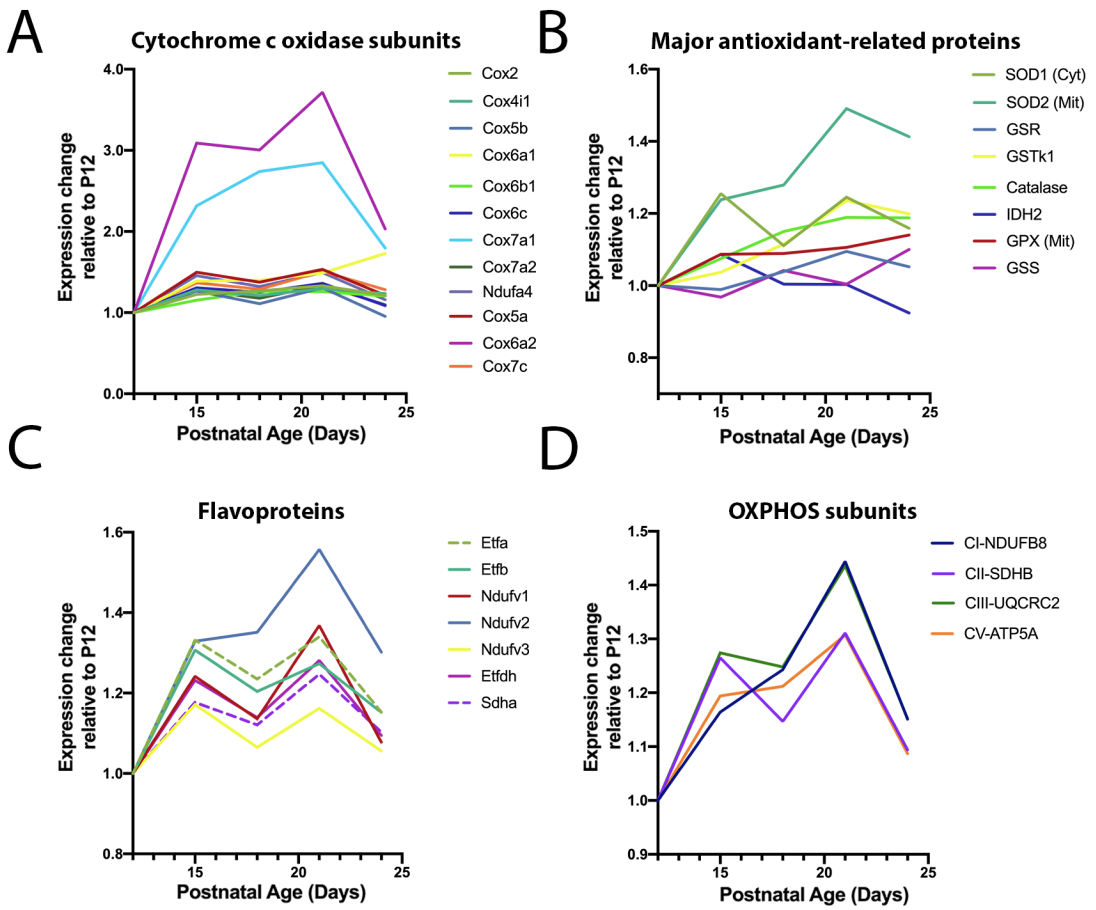

Figure 2.7: Relative fold changes of mitochondrial-associated proteins in sciatic nerve across early postnatal development. All changes are expressed relative to P12. (**A**) Relative fold change of cytochrome c oxidase subunit proteins in developing nerve. (**B**) Relative fold change of major antioxidant-related proteins in developing sciatic nerve. (**C**) Relative fold change of flavoproteins in developing sciatic nerve. Note that at P24, there are consistently higher levels of flavoproteins compared to P12, despite intermediate oscillations. (**D**) Relative fold change in individual oxidative phosphorylation (OXPHOS) subunit proteins across postnatal development in the sciatic nerve. Changes in different subunits of CI-V of the electron transport chain are shown from P12-P24. CIV subunit is not detected in nerve in this proteomic screen. Note that increases are seen from P12 to P24 in all subunits, despite intermediate time point oscillations. N = 5 mice, with 10 nerves per timepoint, with timepoints including P12, P15, P18, P21 and P24 (raw data available: Kline et al., 2019).

Overall, there appear to be consistent upregulations in mitochondrial-associated proteins across time in the deep lumbrical and tibialis anterior muscles and in sciatic nerve across independent proteomic screens, which coincide temporally with the acceleration in the rate of axon degeneration following injury. There appear to be global changes in mitochondrial proteins that are not restricted to a specific subset of proteins. This provides strong rationale to hypothesise that alterations in the mitochondrial proteome during postnatal development may influence the rate of synaptic loss following injury in other muscles. It remains unclear whether such alterations in mitochondrial protein level are a result of an increase in the total mass of mitochondria, i.e. a change in mitochondrial number, or due to increased mitochondrial activity. An assessment of mitochondrial content in subsequent analyses would provide insight into this.

1.24.2 Increases in mitochondrial content in nerve, but not muscle, can explain increases in protein expression and direct the rate of synaptic loss following injury

To provide insight into whether proteomic changes could be due to increases in mitochondrial number, mtDNA – a biomarker of mitochondrial content – was assessed by qPCR. Recent work by Puente et al., has used mtDNA copy number as an indicator of mitochondrial content, with temporal correlations seen between mtDNA and the shift from glycolytic to mitochondrial, oxidative phosphorylation during early postnatal development (Puente et al., 2014). To firstly validate the use of mtDNA as an indicator of mitochondrial content, I used qPCR to compare mtDNA levels between a slow- (type I) oxidative and fast- (type II) twitch glycolytic muscle, since it is known that these have different numbers of mitochondria (Picard et al., 2012). Slow-twitch muscles like soleus, would be expected to have higher numbers of mitochondria than fast-twitch muscles like gastrocnemius. In line with this, it was found that mtDNA levels were significantly higher in soleus than in gastrocnemius, suggesting a positive correlation between mtDNA and mitochondrial number (Fig. 2.8).

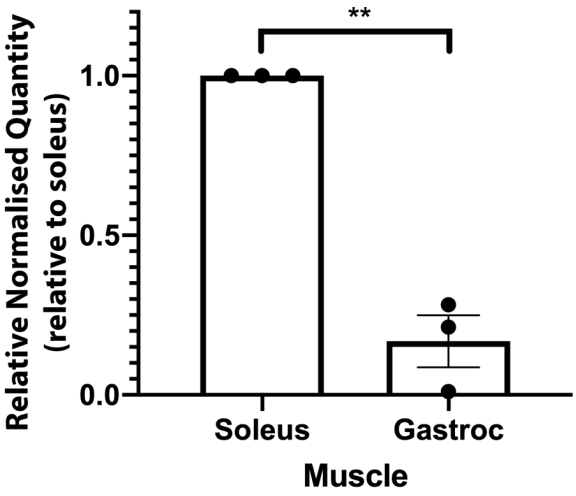

Figure 2.8: Quantification of mtDNA levels as determined by qPCR and $2^{-\Delta\Delta CT}$ method in soleus and gastrocnemius at P25 in wild-type mice. Note that, as expected, mtDNA is significantly higher in soleus, a slow-twitch muscle, than in gastrocnemius, a fast-twitch muscle. This suggests that mtDNA can be used to indicate mitochondrial number. This shows relative normalised quantity of mtDNA as determined by $2^{-\Delta\Delta CT}$ method. Data is normalised to H19 and expressed relative to soleus. ** p = 0.0095; One-sample *t*-test. In both groups, n = 3 biological replicates. Error bars represent mean ± SEM.

Next, this qPCR approach was used to ask whether mitochondrial content changed from P15 to P24 in sciatic/tibial nerve, and whether increases in mtDNA might therefore explain observed increases in mitochondrial protein expression. In sciatic/tibial nerve, the relative quantity of mtDNA was seen to increase significantly with age, increasing by 0.67 fold from P15 to P24 (One sample *t*-test, $p = 0.0058$) (Fig. 2.9). In nerve, differences in mitochondrial content correlate with protein expression changes over time, suggesting that increases in mitochondrial number could be responsible for proteomic upregulations in mitochondrial proteins.

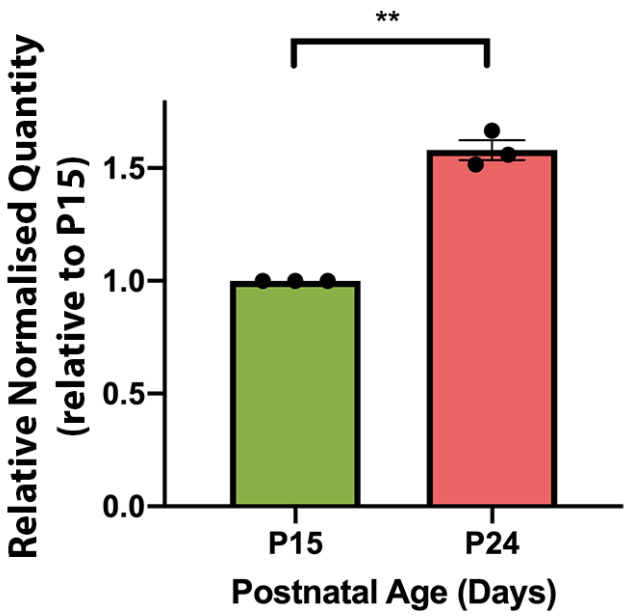

Figure 2.9: Quantification of mtDNA levels as determined by qPCR and $2^{-\Delta\Delta CT}$ method in sciatic/tibial nerve at P15 and P24 in wild-type mice. For ease of interpretation, preparations that have been found to degenerate faster following injury are represented by pink bars, whilst those that are comparatively slower are represented by green bars. Data is expressed normalised to H19, and expressed relative to P15. Note that a significant increase in relative quantity of *mtDNA* is detected in sciatic/tibial nerve from P15 to P24. ** p = 0.0058; one sample *t*-test. N = 3 biological replicates. Error bars represent mean ± SEM.

However, when changes in mitochondrial content was examined from P15 to P24 in LALr/c/AS pooled muscles, it was found that there were no significant changes in mtDNA levels (One sample *t*-test; $p > 0.98$) (Fig. 2.10). This suggests that developmental regulation of synaptic withdrawal following injury cannot be attributed to alterations in mitochondrial content in these muscles.

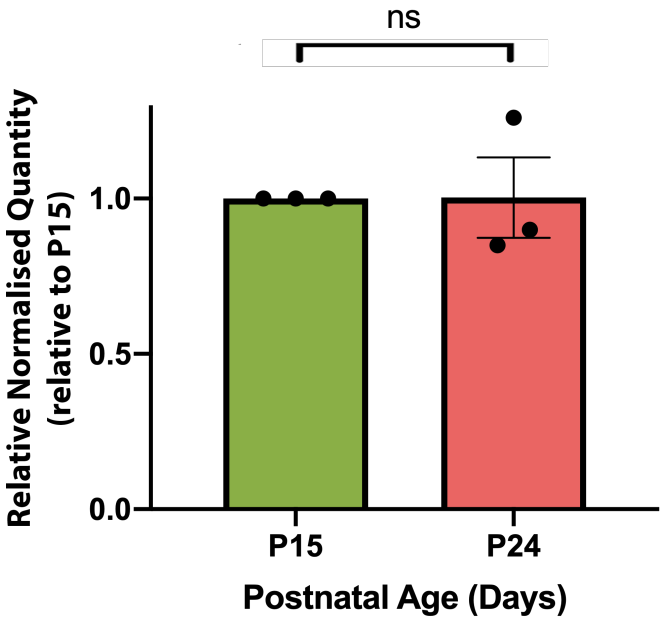

Figure 2.10: Quantification of mtDNA levels as determined by qPCR and $2^{-\Delta\Delta CT}$ method at P15 and P24 in LALr/c/AS pooled muscles from wild-type mice. For ease of interpretation, preparations that have been found to degenerate faster following injury are represented by pink bars, whilst those that are comparatively slower are represented by green bars. Data is expressed normalised to H19, and relative to P15. Note that no significant changes in mtDNA are detected. Ns = not significant, $p > 0.98$; one sample *t*-test. At both time points, n = 3 biological replicates. Error bars represent mean ± SEM.

1.24.3 Changes in mitochondrial proteins and content do not correlate with differences in vulnerability across development in other muscles

If mitochondrial changes account for the developmentally regulated alterations in the rate of synaptic degeneration, then it follows that similar changes in mitochondrial proteins would be seen in other nerves and muscles. To expand analysis of mitochondrial proteins into other muscles, quantitative fluorescent western blotting was applied to quantify levels of CI protein in the cranial and thoracoabdominal musculature, and in sciatic/tibial and intercostal nerves. To provide an overview of this transitional period, three time points were analysed: P15, P19 and P24. It was hypothesised that, since the cranial muscles follow a similar developmental profile as the DL in response to injury (See Chapter 1, *Results, 1.20.2*), that there would be similar increases in CI protein levels with increasing age. Since the thoracoabdominal muscles show minimal synaptic loss in response to injury within this timeframe (See Chapter 1, *Results, 1.20.3*), it was hypothesised that protein levels in this group would remain constant. Overall, it was predicted that higher levels of CI, would correlate with greater vulnerability to synaptic loss.

An antibody cocktail was used that targets subunits from each complex within the respiratory chain, thereby providing a better overview of ETC activity within this time frame. These subunits were: CI subunit NDUFB8 (NADH: Ubiquinone oxidoreductase subunit B8), an accessory subunit of CI; CII subunit SDHB (Succinate dehydrogenase complex iron sulfur subunit B), an iron-sulfur protein subunit of CII; CIII subunit UQCRC2L (Ubiquinol-cytochrome c reductase core protein 2), a key assembly component of CIII; CIV subunit COX II, the second subunit of CIV; and CV subunit ATP5A (ATP synthase F1 subunit alpha), a component of the catalytic core of mitochondrial membrane ATP synthase. Note that protein extracted from muscles were grouped in ways that reflected differential *ex vivo* responses, as have been described in Chapter 1 (see Table 14 for summary): the LALr/c/AS were grouped together, AAL was considered on its own, and TVA/TS were grouped together.

It was found that regardless of which muscle group is selected (LALr/c/AS; AAL or TVA/TS), CI protein levels fail to correlate with patterns of synaptic stability following injury; CI protein levels do not increase between P15 and P24 in any case (Fig. 2.11, Fig 2.12 and Fig. 2.13) (Two-way ANOVA with Sidak correction, $p > 0.06$). Moreover, no convincing trends towards an increase were identified in any of the other complex subunits analysed. If anything, trends towards a decrease were more prevalent in many cases. A similar lack of association was observed in nerve (Fig. 2.14).

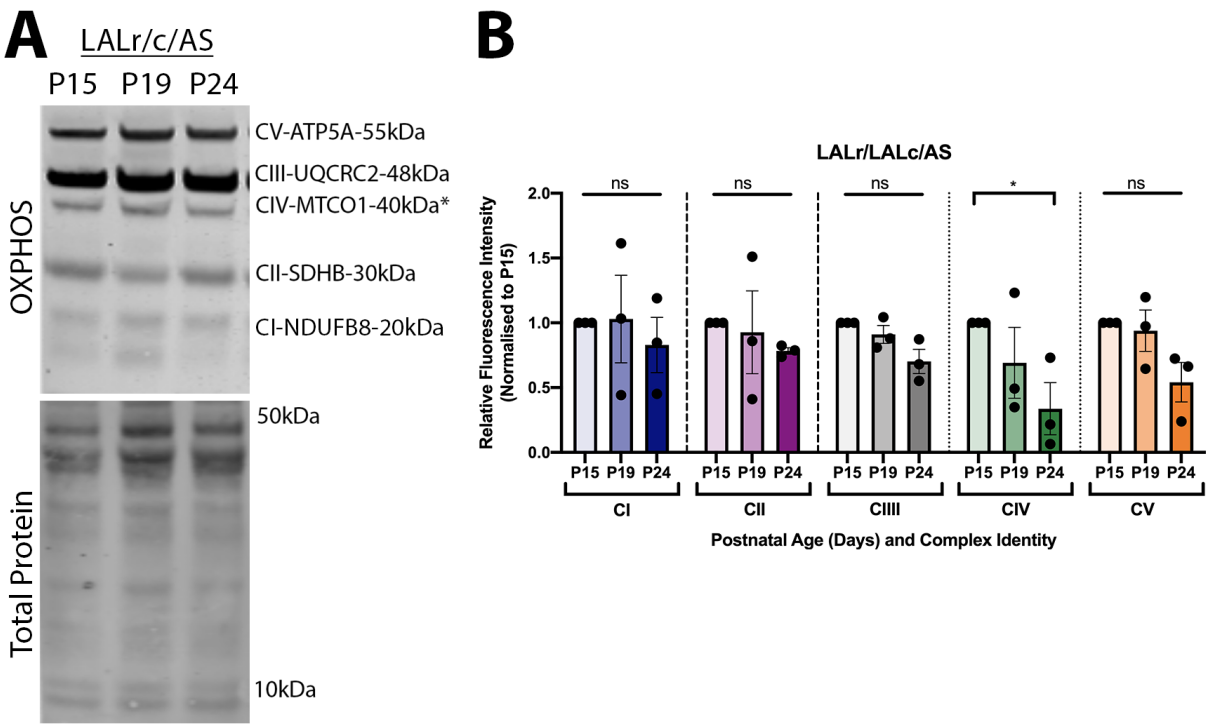

Figure 2.11: Analysis of respiratory chain complex subunit protein levels across P15-24 fails to reveal any significant increases across time in pooled LALr/c/AS muscles from wild-type mice. (**A**) Western blot result using antibodies against Complex I, II, III, IV and V subunits on muscle from P15, P19 and P24 mice, with total protein staining used as a loading control. (**B**) Quantification of western blot against different complex subunits. Data is expressed normalised to loading control and relative to levels at P15. Note that no increases in protein levels are seen across time. Ns = not significant, $p > 0.15$, * $p = 0.027$; two-way ANOVA with Sidak correction. For each time point, n=3 biological replicates. Error bars represent mean ± SEM.

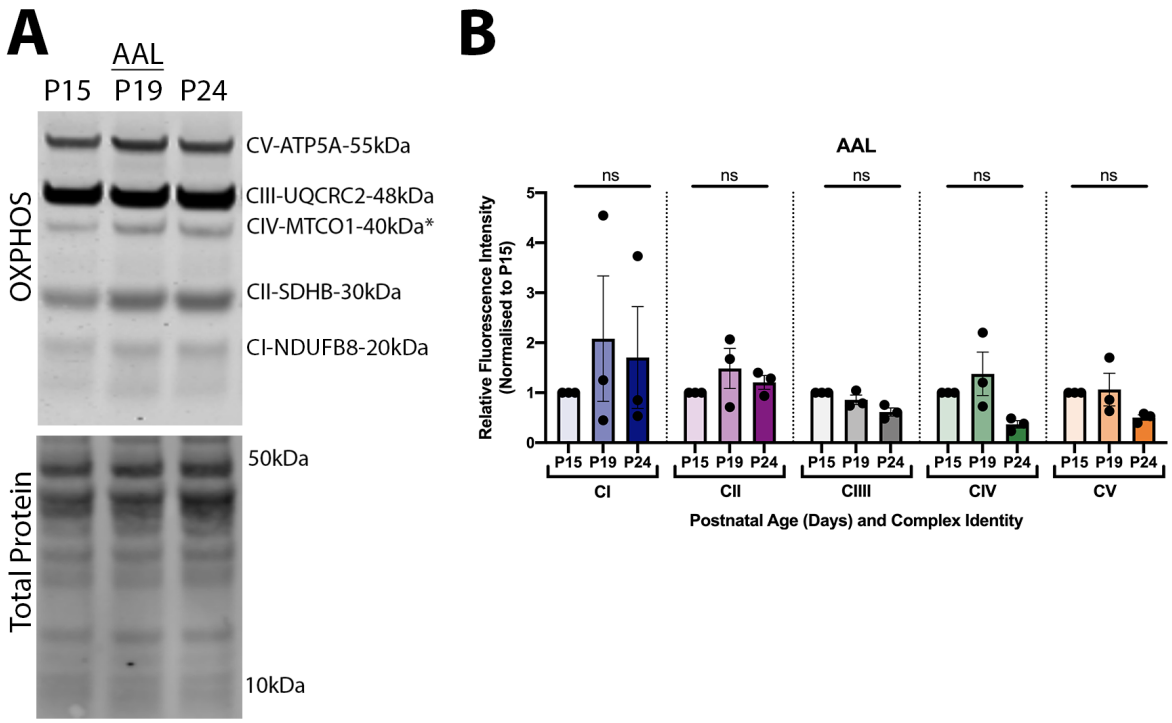

Figure 2.12: Analysis of respiratory chain complex subunit protein levels across P15-24 fails to reveal any significant increases across time in AAL from wild-type mice. (**A**) Western blot result using antibodies against Complex I, II, III, IV and V subunits on muscle from P15, P19 and P24 mice, with total protein staining used as a loading control. (**B**) Quantification of western blot against different complex subunits. Data is expressed normalised to loading control and relative to levels at P15. Note that no increases in protein levels are seen across time. Ns = not significant, $p > 0.22$; two-way ANOVA with Sidak correction. For each time point, n=3 biological replicates. Error bars represent mean ± SEM.

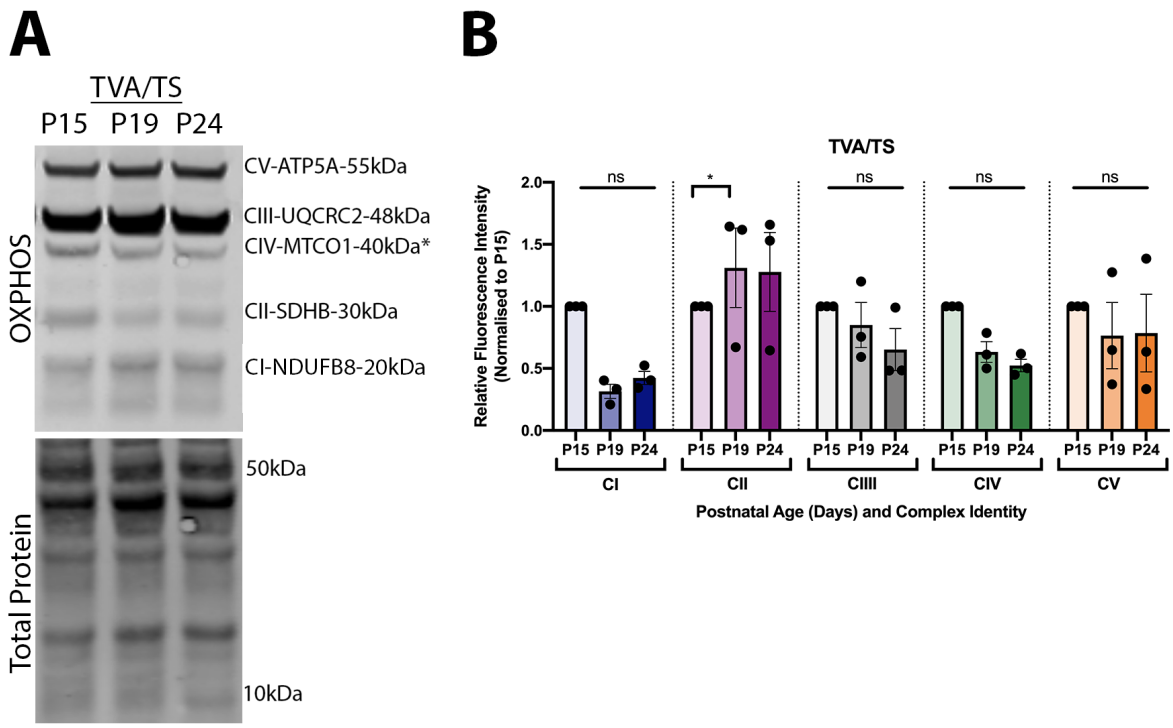

Figure 2.13: Analysis of respiratory chain complex subunit protein levels across P15-24 fails to reveal significant increases in complex I levels across time in pooled TVA/TS muscles from wild-type mice. There is also a lack of convincing increases in other complexes. (**A**) Western blot result using antibodies against Complex I, II, III, IV and V subunits on muscle from P15, P19 and P24 mice, with total protein staining used as a loading control. (**B**) Quantification of western blot against different complex subunits. Data is expressed normalised to loading control and relative to levels at P15. Note that no increase in CI is seen, and that the majority of other complex subunit proteins also fail to show increases. Ns = not significant, $p > 0.06$, * $p = 0.024$; two-way ANOVA with Sidak correction. For each time point, n=3 biological replicates. Error bars represent mean ± SEM.

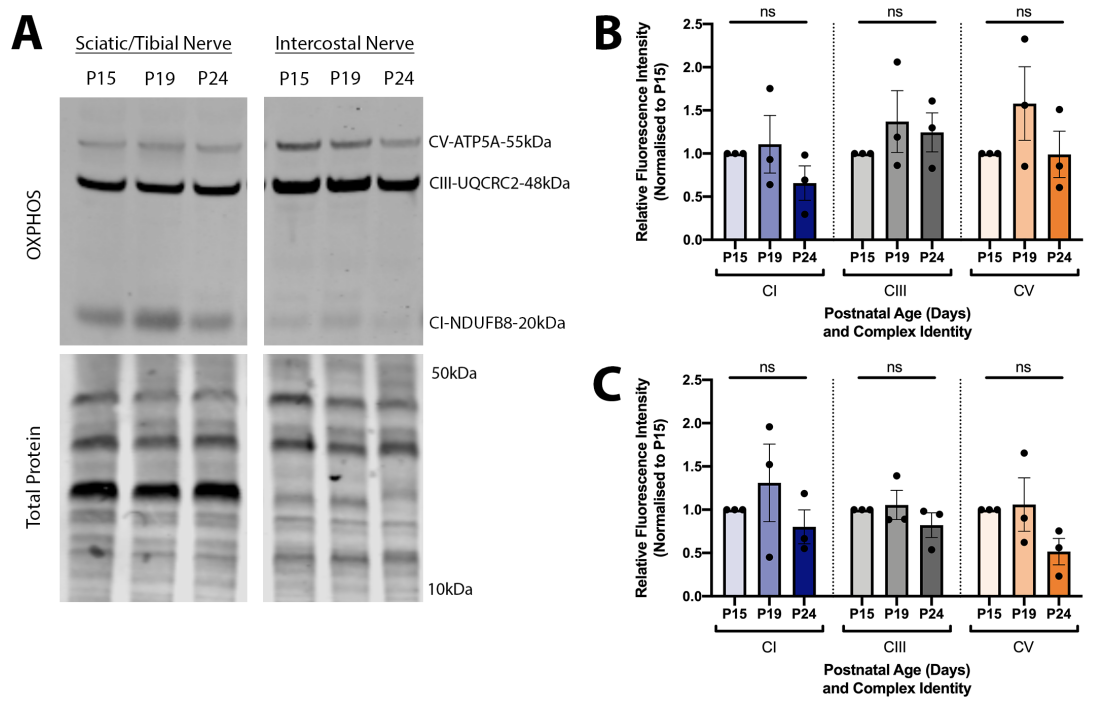

Figure 2.14: Analysis of respiratory chain complex subunit protein levels across P15-24 fails to reveal significant increases in either sciatic/tibial nerve or intercostal nerve from wild-type mice. (**A**) Western blot result using antibodies against Complex I, II, III, IV and V subunits on muscle from P15, P19 and P24 mice in sciatic/tibial nerve (left) and intercostal nerve (right), with total protein staining used as a loading control. Note that in both nerves only CI, III and IV bands are detected (**B**) Quantification of western blot against different complex subunits in sciatic/tibial nerve. Data is expressed normalised to loading control and relative to levels at P15. Note that no increases in protein levels are seen across time. Ns = not significant, $p > 0.31$; two-way ANOVA with Sidak correction. Error bars represent mean ± SEM. (**C**) Quantification of western blot against different complex subunits in intercostal nerve. Data is expressed normalised to loading control and relative to levels at P15. Note that no increases in protein levels are seen across time. Ns = not significant, $p > 0.23$; two-way ANOVA with Sidak correction. In all cases, n=3 biological replicates. Error bars represent mean ± SEM.

1.24.4 Changes in mitochondrial proteins and DNA do not correlate with differences in vulnerability between different muscles

It was next important to determine whether mitochondrial changes could contribute to muscle-specific differences. When considering the results contained within this section, it is important to keep in mind the injury-response profiles that have been described in Chapter 1. To briefly summarise, the LALr, LALc and AS cranial muscles have a characteristic profile of developmental regulation, with increased synaptic loss occurring with age. The AAL shares a similar profile, but is significantly more affected at earlier time points than the other cranial muscles, suggesting it is more vulnerable to loss earlier in development. Meanwhile, the abdominal muscles show comparatively slower rates of synaptic loss across all time points. Here, it was hypothesised that muscles that are more vulnerable to synaptic loss following injury would have higher levels of CI.

Firstly, using western blotting, regional differences in CI-V protein levels were analysed at P15, P19 and P24. Since it was found in Chapter 1, that the AAL was significantly more denervated following injury at P15 than any of the other muscles, it was anticipated that CI levels would be higher in the AAL at this time point. However, this was not the case: it was found that CI levels were not higher in the AAL at any age, and even showed significantly reduced levels compared to the TVA/TS at P15 and P19 (Fig. 2.15). In general, when other complexes are considered, the AAL fails to show a convincing trend towards an increase at any age. Although CII is higher in the AAL at P19 and P24 when compared to the TVA/TS, at P15, no difference in protein levels are detected despite differences in the synaptic response to injury. Thus, although developmental changes are present, these do not correlate with patterns of synaptic stability.

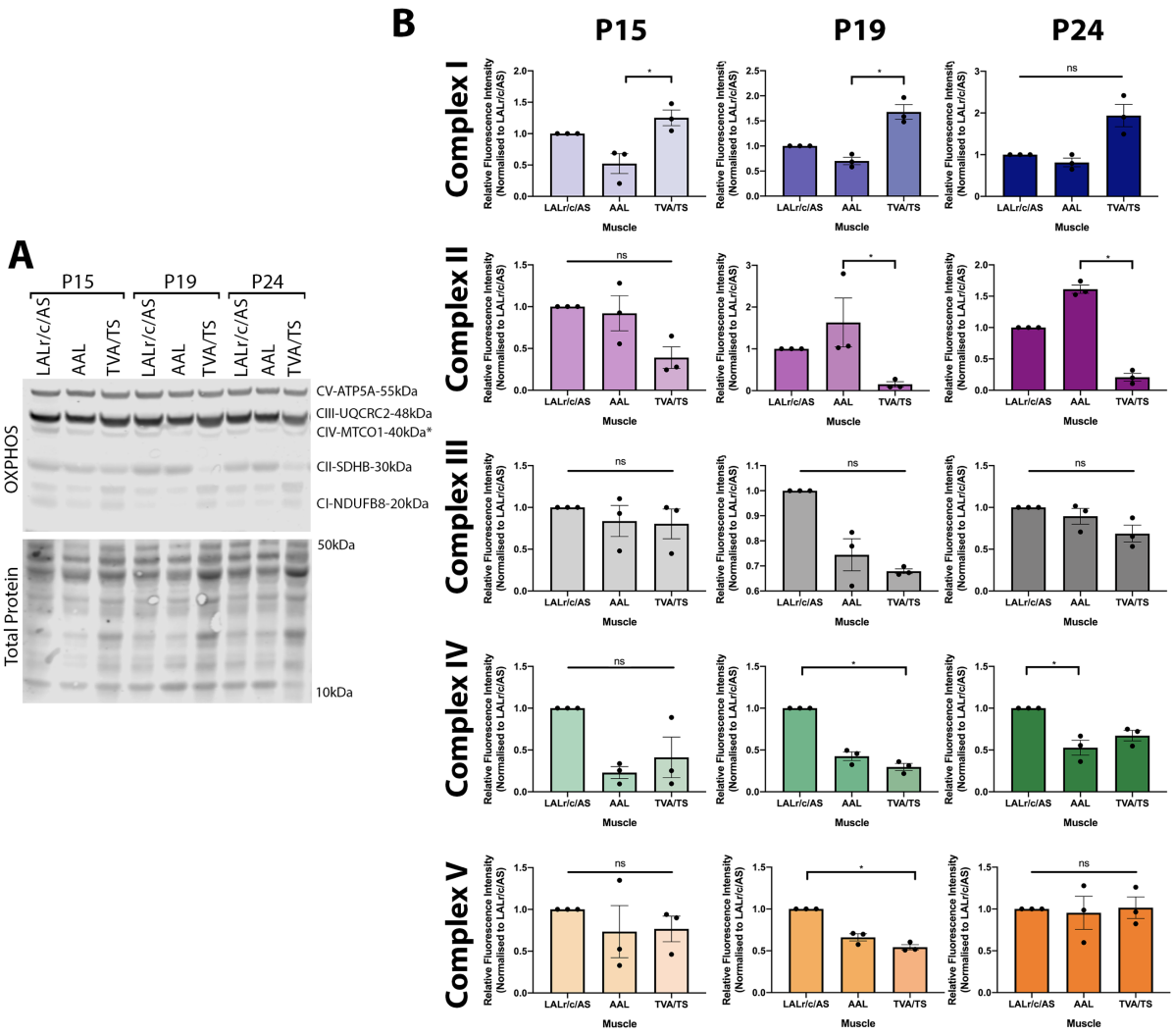
A
P15
P19
P24
LALr/c/AS
AAL
TVA/TS
OXPHOS
CV-ATP5A-55kDa
CIII-UQCRC2-48kDa
CIV-MTCO1-40kDa*
CII-SDHB-30kDa
CI-NDUFB8-20kDa
Total Protein
50kDa
10kDa
B
Complex I
Complex II
Complex III
Complex IV
Complex V
Relative Fluorescence Intensity (Normalised to LALr/c/AS)
Muscle
ns

Figure 2.15: Analysis of respiratory chain complex subunit protein levels across different muscles from wild-type mice fails to reveal increases that are consistent with patterns of synaptic vulnerability in response to injury. (**A**) Western blot result using antibodies against Complex I, II, III, IV and V subunits on pooled LALr/LALc/AS muscle, AAL muscle and pooled TVA/TS muscle from P15, P19 and P24 mice, with total protein staining used as a loading control. (**B**) Quantification of western blot against different complex subunits in pooled LALr/LALc/AS muscle, AAL muscle and pooled TVA/TS muscle. Data is expressed normalised to loading control and relative to levels in LALr/LALc/AS. Note that with the exception of CII, no significant increases in protein levels are seen in more vulnerable muscles. CII does show increases at P19 and P24, however since differences in vulnerability are already prevalent in this muscle at P15 (see Chapter 1, *Results, 1.20.2* for profiling), differences do not appear to be consistent with alterations in synaptic stability. Ns = not significant, $p > 0.07$, * $p < 0.05$; Kruskal Wallis with Dunn's correction. In all cases, n=3 biological replicates. Error bars represent mean ± SEM.

Next, it was asked whether increases in CI protein levels correlated with differences in the response to injury in nerve. It was hypothesised that CI levels would be higher in the sciatic/tibial nerve, since the muscles served by this nerve exhibit greater synaptic loss than those served by the intercostal nerve. At all timepoints, there were significantly higher CI protein levels in the sciatic/tibial nerve than the intercostal nerve, with the sciatic/tibial nerve found to have up to 5X relative fluorescence intensity (One sample t-test; $p < 0.02$) (Fig. 2.16). Contrasting this, in CIII and V, there was a consistent trend towards an increase in protein levels in the intercostal nerve when compared to the sciatic/tibial nerve (Fig. 2.16).

Overall, in nerve, there are clear and significant differences in CI protein levels that correlate with differences in the rates of synaptic withdrawal after injury.

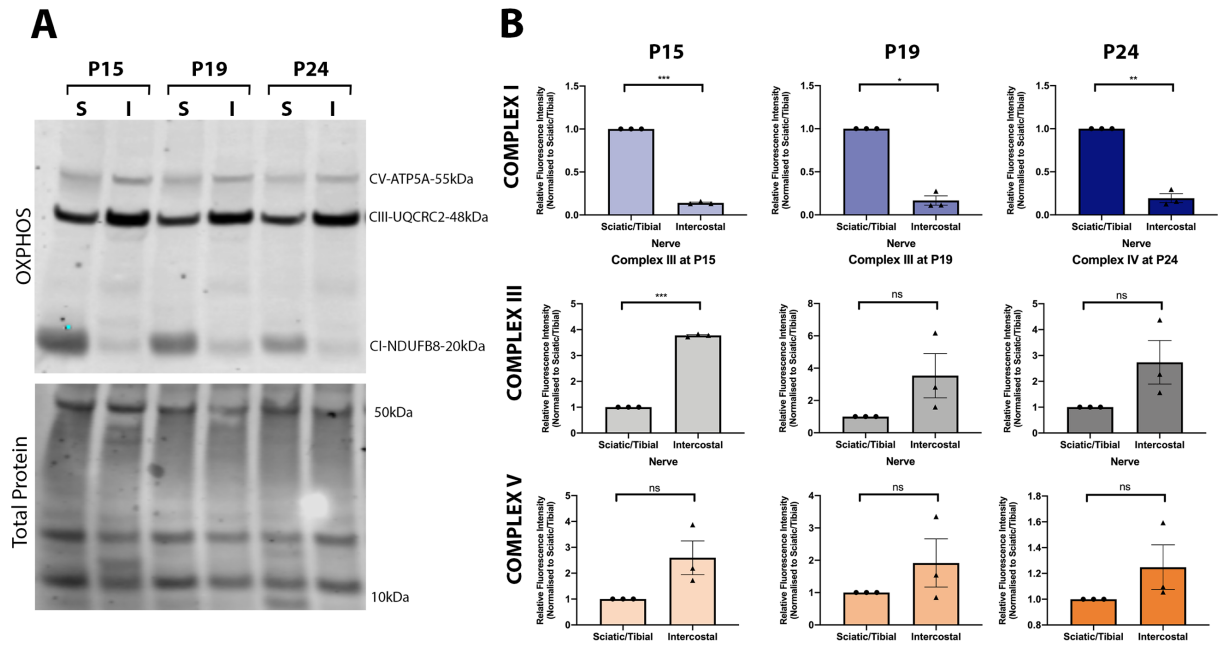

Figure 2.16: Analysis of respiratory chain complex subunit protein levels in sciatic/tibial and intercostal nerves from wild-type mice reveals increases in CI protein level that correlate with increases in the rate of synaptic withdrawal after injury. (**A**) Western blot result using antibodies against Complex I, II, III, IV and V subunits on sciatic/tibial nerve (S), and intercostal nerve (I) from P15, P19 and P24 wild-type mice, with total protein staining used as a loading control. Note that in both nerves only CI, III and IV bands are detected. (**B**) Quantification of western blot against different complex subunits in sciatic/tibial nerve versus intercostal nerve at P15, 19 and P24. Data is expressed normalised to loading control and relative to levels in sciatic/tibial nerve. Note that whilst increases in CI are seen at P19 and P24 in the sciatic/tibial nerve, this difference is also seen at P15, when similar synaptic responses to injury are observed. This suggests that although differences are present, these do not explain developmentally-regulated alterations to synaptic stability following injury. Ns = not significant, $p > 0.13$, * $p < 0.02$, ** $p < 0.005$, *** $p = 0.0001$; One-sample *t*-test. In all cases, n=3 biological replicates. Error bars represent mean ± SEM.

The final part of this work was to determine whether regional differences in mitochondrial number correlated with patterns of synaptic stability following injury in nerve or muscle. Comparison of mtDNA levels in intercostal nerve versus sciatic/tibial nerve revealed no significant differences at P24 (One sample *t*-test; $p > 0.98$). Altered mtDNA levels in nerve therefore do not correlate explain differential rates of degeneration following injury (Fig. 2.17). For ease of interpretation preparations that have been found to degenerate more rapidly following injury are represented by pink bars, whilst those that are comparatively slower are represented by green bars.

In muscle, no significant difference was detected in mtDNA levels between the LALr/c/AS and the AAL at P15 (Fig. 2.18, A). Note that the LALr/c/AS muscles show significantly less synaptic loss following injury than the AAL at P15 (refer to Chapter 1, *Results 1.20.2*, or Table 14 for summary). This suggests that altered mitochondrial number does not correlate with differential rates of degeneration following injury across different muscles. At P24, the TVA/TS has minimal synaptic loss following injury, whilst the LALr/c/AS muscles exhibit profound synaptic loss (Fig. 2.18, B). When considered in isolation, increases in mtDNA content initially appear to correlate with reduced synaptic stability; the more vulnerable muscle group (LALr/c/AS) has higher mtDNA at P24. However, when taken together with the P15 data, this correlation is not consistent, and therefore remains unconvincing. Overall, although global differences in mtDNA levels are detected, these do not correlate with patterns of synaptic stability.

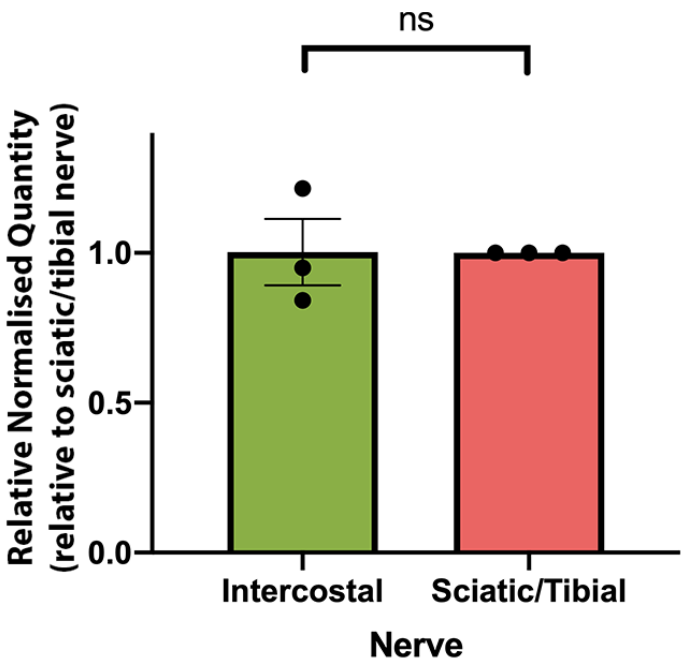

Figure 2.17: Quantification of mtDNA levels as determined by qPCR and $2^{-\Delta\Delta CT}$ method in nerve at P24 in wild-type mice. For ease of interpretation, preparations that have been found to degenerate faster following injury are represented by pink bars, whilst those that are comparatively slower are represented by green bars. Here, the relative quantity of mtDNA in intercostal nerve versus sciatic/tibial nerve at P24 has been quantified. Note that no significant difference is detected between different nerves at P24. Data is expressed normalised to *Gapdh*, and expressed relative to sciatic/tibial nerve. ns = not significant, $p > 0.98$; one sample *t*-test. n = 3 biological replicates and error bars represent mean ± SEM.

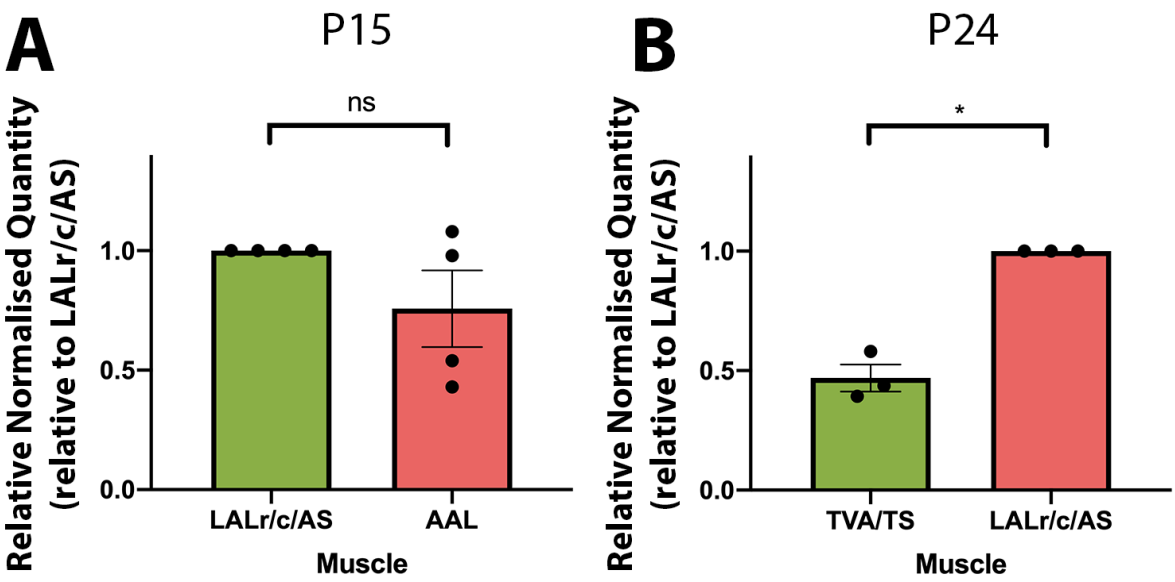

Figure 2.18: Comparison of regional differences in relative quantity of mtDNA as assessed by qPCR and $2^{-\Delta\Delta CT}$ method in different muscles in wild-type mice. For ease of interpretation, preparations that have been found to degenerate faster following injury are represented by pink bars, whilst those that are comparatively slower are represented by green bars. (**A**) Relative normalised quantity of mtDNA in LALr/LALc/AS pooled muscles versus AAL at P15. Data is expressed normalised to H19, and relative to LALr/LALc/AS. Note that no significant changes in mtDNA are detected. Ns = not significant, $p > 0.22$; one sample *t*-test. (**B**) Relative normalised quantity of mtDNA in pooled TVA/TS muscles versus pooled LALr/LALc/AS muscles at P24. Data is expressed normalised to H19, and relative to LALr/LALc/AS. Note that mtDNA levels are significantly reduced in the TVA/TS compared to the LALr/c/AS at P24. * $p = 0.01$; one sample *t*-test. At P15, n = 4 and at P24, n = 3 biological replicates. Error bars represent mean ± SEM.

1.25 Discussion

1.25.1 Overview of results

Here, analyses of two independent proteomic datasets revealed increases in mitochondrial proteins that correlate with accelerations in synaptic degeneration following injury across early postnatal development. I found that these increases could be attributed to increases in mitochondrial number in nerve, but not in muscle. However, changes in mitochondrial complex protein levels failed to correlate with accelerations in the rate of synaptic degeneration across development in a range of other muscles and nerve. Differential rates of synaptic degeneration also failed to correlate with changes in mitochondrial number in either muscle or nerve, although changes in complex I in nerve did correlate with patterns of selective vulnerability. Overall, although there are global changes to the mitochondrial proteome during early postnatal development, changes in mitochondrial proteins fail to correlate with accelerations in rates of synaptic degeneration following injury across this time window. There is some evidence however to support that changes in complex I in nerve could underlie intermuscular differences in the rate of synaptic degeneration following injury.

1.25.2 Accelerations in synaptic degeneration cannot be attributed to changes in mitochondrial proteins in muscle across early postnatal development

I initially demonstrated a strong and promising correlation between increases in mitochondrial proteins and accelerations in the rate of synaptic degeneration following injury across early postnatal development. All five mitochondrial complexes, as well as other key mitochondrial-associated proteins, consistently increased in deep lumbrical and tibialis anterior muscles. In previous work in both scenarios of health and disease, mitochondrial alterations have been associated with altered synaptic stability (Llavero Hurtado et al., 2017, Luiro et al., 2006, Graham et al., 2017, Kline et al., 2019, Kim et al., 2019). Early proteomic studies investigating synaptic stability in *Wld*^{S} identified mitochondria as playing an important role in conferring the delayed *Wld*^{S} phenotype (Wishart et al., 2007). This is further supported by studies showing

that inhibition of the mitochondrial permeability pore can phenocopy protection that is conferred by *Wld*^{S} expression (Barrientos et al., 2011). In drosophila models, and in *Wld*^{S} mice, it has been proposed that *Wld*^{S} can prevent axon degeneration by increasing mitochondrial motility and by enhancing the capacity of mitochondrial calcium buffering. This buffering prevents elevations in calcium that are thought to trigger axon degeneration, and has been considered as a mechanism of WD suppression (Avery et al., 2012). Mitochondrial dysfunction is also recognised as a common feature in many neurodegenerative disorders where synapses are early pathological targets (Llavero Hurtado et al., 2017, Luiro et al., 2006, Graham et al., 2017). In mouse models of SMA, structural and functional defects in mitochondria have been described pre-symptomatically (Miller et al., 2016). Increased levels of mitochondrial proteins, and altered mitochondrial morphology have been described at the NMJ during a die-back in SMA mice (Neve et al., 2016). In a mouse model of ALS, accumulations of mitochondria have been reported in motor neurons, along with higher levels of ROS than their wild-type counterparts, further supporting a role for mitochondrial dysfunction in the process of motor neuron degeneration (Martin et al., 2007). Structural defects in mitochondria have been described in ALS patients in skeletal muscle, liver and spinal motor neurons (Menzies et al., 2002), with markers of oxidative stress and ROS damage also reportedly elevated (Beal, 2002). Based on our proteomic work and work by others, the hypothesis that mitochondrial changes could be responsible for determining synaptic stability in the context of postnatal development was therefore well-founded.

However, when I expanded these analyses to assess mitochondrial complex protein levels and number in a range of other muscles, this was not substantiated. I found that changes in mitochondrial complex I-V protein levels failed to correlate with accelerations in the rate of synaptic degeneration across development in LALr/c/AS, AAL or TVA/TS muscles. I therefore considered what could explain such disparity in other muscles. Firstly, I considered whether the technique applied was sensitive enough to detect alterations in mitochondrial proteins. However, since changes in complex I protein levels are evident in work undertaken by Kline et al., where similar

methods are implemented, it is unlikely that technique sensitivity is masking changes (Kline et al., 2019).

Perhaps disparity could instead be due to differences in the developmental profile of different muscles. Postnatal changes in mitochondrial content have been described previously, with previous work indicating that metabolic remodelling in cardiac tissue occurs during early postnatal life and is triggered by the transition from a hypoxic environment *in utero*, to an oxygen-rich postnatal environment (Puente et al., 2014, Neary et al., 2014). Across the first week of life, Puente et al., describe a transition from glycolytic metabolism to aerobic metabolism, with ROS, oxidative DNA damage and DNA damage response markers all increasing within this time frame (Puente et al., 2014). It is possible that different tissues undergo metabolic remodelling at different rates or at different developmental time points. Further work to characterise mitochondrial maturation across a range of muscles at earlier time points (<P12), may provide insight into whether maturation of mitochondrial networks occurs at an earlier time point in development. Interestingly, I also demonstrated a lack of correlation between increases in mitochondrial complex proteins, number or activity in spinal cord and brain across P12 to P24, providing further evidence that published patterns of mitochondrial increases across this window do not bear out in other tissues (see Appendix 4, Figures A1 and A2). A more comprehensive temporal characterisation of mitochondrial changes in a range of different muscles would help us to better understand the impact of postnatal, metabolic shifts on synaptic vulnerability.

It is important to note that not all aspects of mitochondrial biology were considered. Additional assessment of changes in mitochondrial morphology and/or activity in early postnatal development in a range of muscles would also help to further strengthen the conclusion that mitochondria are not responsible for altering rates of synaptic degeneration during early postnatal development. Mitochondrial morphology could be assessed by electron microscopy, whilst activity could be assessed through enzyme-linked immunosorbant assay (ELISA) assay, or by assessing the effect of CI stimulants of inhibitors, such as AICAR or rotenone, on the level of synaptic loss after injury. If the conclusion that mitochondrial changes are not responsible for determining

developmental delays in WD is corroborated, then additional proteomic profiling and pathway analysis could be performed in muscles like the LALr and TVA, to identify other changes or differences in the proteome that could explain the differences in the rate of WD across this transitional developmental window. Following this, we could undertake a proteomic comparison of these outputs with the DL proteomic with the aim of identifying intermuscular commonalities that might be responsible for altering synaptic stability.

1.25.3 Postnatal accelerations across time and selective vulnerability are regulated by distinct factors

These data suggest that mitochondrial changes in nerve correlate with differential vulnerability. In Chapter 1, I demonstrated that muscles served by the intercostal nerve (TVA/TS) show a remarkable and consistent resistance to WD across the developmental time window of P12 to P24, whilst muscles served by the sciatic/tibial nerve (DL) show progressive acceleration in synaptic degeneration across the same time window (Murray et al., 2011). When I examined levels of mitochondrial proteins across time in either sciatic/tibial nerve or intercostal nerve, no significant increases in complex I protein levels were seen. However, CI levels were significantly higher in the sciatic/tibial nerve when compared to the intercostal nerve directly at different time points, indicating that differences in the rate of synaptic degeneration in different muscles can be attributed to increases in CI protein levels. Notably, differences were not present in muscle, suggesting that changes in nerve may be more important in determining degenerative rate. These findings suggest that different factors may be responsible for determining synaptic vulnerability in the contexts of development versus selective vulnerability.

These data suggest that intermuscular differences in synaptic vulnerability to injury can be explained by an increase in CI protein levels. Whilst CI changes in nerve at the protein level do correlate with accelerations in synaptic degeneration, we did not detect an increase in mtDNA, suggesting that increases in CI are unlikely to be due to increases in mitochondrial number. It is possible that increases in protein level are

rather due to increased mitochondrial activity. This could be assessed in future by ELISA, or by pharmacologically manipulating CI activity. Previous work has demonstrated that the CI inhibitor, rotenone, is axoprotective in dorsal root ganglion primary cultures (Kline et al., 2019). We have also previously utilised AICAR to pharmacologically upregulate oxidative phosphorylation in an *ex vivo* scenario, where AICAR accelerated the rate of NMJ degeneration in the DL muscles (Kline et al., 2019). AICAR is capable of upregulating oxidative metabolism through acting as an agonist of adenosine monophosphate kinase (Golubitzky et al., 2011, Jager et al., 2007). Testing the effect of CI inhibition or upregulation in a range of different muscles would help to reveal whether altered CI activity is responsible for conferring intermuscular differences in the rate of synaptic degeneration.

Across postnatal development, I did not find any correlation between mitochondrial complex protein levels or number and accelerated rates of synaptic degeneration. The factors that are responsible for determining postnatal vulnerability may therefore be distinct from those which regulate selective vulnerability. Further work is required to determine the extent of divergence, as well as identifying what other factors might be involved however returning to proteomic outputs may provide some insight. In both proteomic screens, we identified carbon metabolism as a common and significantly upregulated functional cluster. One-carbon metabolism, mediated by folate cofactor, supports many physiological processes that include nucleotide biosynthesis, DNA methylation, and redox defence (Ducker and Rabinowitz, 2017). These processes are critical components of cell and tissue homeostasis. Although the importance of folate metabolism is well-recognised in embryonic development, very little is known about the regulation of one-carbon metabolism in muscle during postnatal development, therefore profiling changes over early postnatal development may reveal whether alterations correlate with accelerations in synaptic degeneration,

Proteomic data also suggest that proteins involved with ROS neutralisation increase across postnatal development in muscle. ROS, oxidative DNA damage and DNA damage response markers have all been shown to increase across early postnatal development following the transition from a hypoxic *in utero* environment, to an

oxygen-rich postnatal environment (Puente et al., 2014). Increases in ROS induce cell cycle arrest of postnatal cardiomyocytes, which can be delayed by pharmacological inhibition of the DNA damage response pathway or ROS scavenging (Puente et al., 2014). Could alterations in ROS handling be responsible for delays in WD during postnatal development? Mouse models have been created to investigate the effect of altering endogenous levels of mitochondrial oxidative stress by modulating the function of superoxide dismutase 2 (SOD2). SOD2 is a key component of the antioxidant defence system against superoxide radicals (Birben et al., 2012). SOD2 is localised to the inner mitochondrial matrix, specifically at sites of superoxide production from the ETC. When oxygen diffuses into mitochondria, it can be converted to superoxide as a by-product of oxidative phosphorylation. SOD2 converts superoxides into hydrogen peroxide which can then diffuse from mitochondria to be further detoxified by enzymes like gluthathione perioxidase or catalase. Work in animal models has demonstrated that the severity of neurodegeneration due to loss of *Sod2* can be modulated in a dose-dependent manner with antioxidants that prevent oxidative damage (Melov et al., 1998, Melov et al., 2001, Hinerfeld et al., 2004). Dosing of N-acetylcysteine (NAC), a ROS scavenger, *in vivo* or *ex vivo,* could provide insight into the importance of ROS neutralisation across early postnatal developmental. NAC is a derivative of the natural amino acid cysteine, which is a substrate of glutathione (GSH), also known as the "master antioxidant" (Teskey et al., 2018). NAC acts by supporting antioxidant synthesis under conditions where demands increase, such as in conditions of oxidative stress. GSH levels increase with age and in disease states (Teskey et al., 2018, Ballatori et al., 2009), thus we would hypothesise that NAC dosing would increase antioxidant capacity, and exert neuroprotective effects. ROS scavengers have been shown to delay WD and axon pathology associated with neurodegenerative disorders (Wagner et al., 1998, Calixto et al., 2012, Lopez-Erauskin et al., 2011). Resveratrol, a compound thought to have antioxidant effects, has been shown to delay axonal degeneration *in vitro* and following nerve crush *in vivo* (Calliari et al., 2014). Investigating whether administration of antioxidants *in vivo* or *ex vivo* can alter the rate of synaptic degeneration in the context of postnatal development would provide insight into the role of antioxidant mechanisms across this time frame.

Flavoproteins are also critical components of ROS neutralisation, which I have shown increase across development, however the role of flavoproteins remains unclear in the context of peripheral nerve injury. Flavin adenine dinucleotide (FAD) and flavin mononucleotide (FMN) are redox cofactors that are required for the activity of over 100 human enzymes, with inactivity having been linked to neurodegenerative disease (Lienhart et al., 2013). For example, mutations in the flavoprotein D-amino acid oxidase have been linked to familial cases of ALS, with a pathogenic role for D-serine accumulation being postulated to reduce motor neuron survival (Mitchell et al., 2010). Flavoproteins appear capable of influencing neuronal survival in disease, therefore it would be interesting to determine if they can influence rates of synaptic degeneration in other contexts. Considering the importance of ROS neutralisation, this represents an interesting candidate for further work in determining the factors that can regulate synaptic stability.

Chapter 3 : **The role of P53 in morphologically distinct types of degeneration**

1.26 Chapter overview and principle findings

This chapter aimed to examine the role of P53 in synaptic degeneration; specifically, I examined whether reductions in P53 could reduce levels of synaptic loss following injury, during disease, or during developmental synaptic elimination. Applying an *ex vivo* model of peripheral nerve injury to tissue from a mouse model with reduced levels of P53, I examined whether P53 reduction could reduce synaptic loss following injury. In a mouse model of SMA with reduced levels of P53, I then assessed whether P53 reduction could reduce synaptic loss in the context of a die-back. In a mouse model with reduced P53, I investigated whether P53 reductions could delay synaptic elimination during development. In P53-reduced SMA and wild-type mice, I also examined the impact of P53 reduction on the expression of synaptic genes that are thought to be regulated by P53.

Principle Findings

- Cre-LoxP mediated recombination of P53 causes measurable changes in P53-dependant processes
- P53 reduction has no effect on the level of synaptic loss following injury
- P53 reduction has no effect on the level of synaptic loss in a mouse model of SMA
- P53 reduction has no effect on polyinnervation levels in young mice
- The expression of the synaptic genes *Bin1, Mef2c* and *Picalm* are unaffected by reduced levels of SMN or P53

1.27 Introduction

Neuronal dysfunction, and ultimately cell death, is a characteristic of many neurodegenerative diseases. Despite growing appreciation of distinct morphologies of synaptic degeneration in response to various stimuli, the mechanisms of neuronal degeneration remain largely unknown. Understanding factors that can influence the rate of degeneration will provide mechanistic insight which is of critical importance if we are to identify and develop therapies to target neurodegeneration in different contexts. The P53 signalling pathway, due to its role in inducing and regulating apoptotic cell death, is one such factor that has emerged as an intriguing candidate (Fridman and Lowe, 2003, Aubrey et al., 2018).

The *TP53* gene is well-recognised for its role as a tumour suppresser within the body, and mutations have been extensively linked to tumour development in cancers (Eliyahu et al., 1989, Finlay et al., 1989, Aubrey et al., 2018, Vogelstein et al., 2000). In response to a variety of signals, including DNA damage and cell stress, the P53 signalling pathway is activated and plays a key role in cell cycle control, DNA repair and apoptosis (Eizenberg et al., 1996, Vousden, 2000, Elmore, 2007, Li and Yuan, 2008, Williams and Schumacher, 2016). P53 acts to integrate multiple stress signals, and plays a fundamental, and conserved, role in promoting apoptosis (Fridman and Lowe, 2003, Brodsky et al., 2000, Jin et al., 2000, Ollmann et al., 2000). The ability of P53 to promote cell death has led to much interest in whether P53 also plays a role in pro-apoptotic pathways that ultimately result in synaptic and axonal degeneration.

It is widely accepted that P53 acts as a nuclear transcription factor that induces the production of pro-apoptotic proteins in the cell body, however there is also evidence to support that P53 acts locally at the synapse (Gilman et al., 2003, Gilman and Mattson, 2002). Injury models represent intriguing candidates to study the role of P53, as communication between the cell body and distal axon is disrupted. Microarray analysis of expression changes in the distal nerve stump across the first 28 days after sciatic nerve injury in rats have highlighted upregulations in P53 signalling, indicating a local role for P53 in synaptic degeneration (Yao et al., 2013). P53 has been identified

in synaptosomes of cortical neurons *in vivo,* with P53 levels and activity seen to increase following DNA damage (Gilman et al., 2003). Synaptosomes from P53 knockout mice, and those from mice treated with the P53 inhibitor, pifithrin-α, display increased resistance to oxidative and excitotoxic injury, with the mitochondrial membrane potential being preserved and ROS production decreased (Gilman et al., 2003). Mitochondria that have been isolated from synaptosomes of P53 knockout mice also show greater resistance to oxidative and excitotoxic injury in response to pharmacologically-induced DNA damage in hippocampal neuron cultures (Gilman et al., 2003).

The ability of P53 to influence the transcription of pro- and anti-apoptotic transcripts has implicated P53 in regulating compartmental degeneration in neurons, such as during development, where select synapses and axonal branches are 'pruned' or eliminated, whilst the motor neuron persists (Maor-Nof et al., 2016). Trophic deprivation is a well-known model for investigating axonal pruning and the mechanisms of neuronal apoptosis (Maor-Nof and Yaron, 2013, Geden and Deshmukh, 2016). Apoptotic pathways and proteins, including P53, have been strongly implicated in axonal degeneration in response to trophic deprivation (Kaplan and Miller, 2000, Aloyz et al., 1998, Maor-Nof and Yaron, 2013). Trophic factors, such as NGF, are critical regulators of axonal maintenance and survival, with withdrawal of trophic support found to activate pro-apoptotic pathways (Sanes and Lichtman, 1999, Harrington and Ginty, 2013). Increases in P53 phosphorylation have been seen following trophic withdrawal, which has been shown to induce synaptic elimination (Maor-Nof et al., 2016). Phosphorylated and activated P53 act as a transcription factor for a number of pro-apoptotic transcripts including *Bax*, *Bak* and *Pmaip*. These can increase permeability of the mitochondrial membrane, leading to the release of pro-apoptotic factors and the activation of 'executioner' caspases, including caspase-3 (Schuler and Green, 2001). In line with this, *in vivo*, knockout of caspase-3 has been shown to delay developmental pruning in retinocollicular axons, but also leads to severe developmental defects, highlighting a crucial role for apoptotic machinery at synapses during development (Simon et al., 2012, Shan et al., 2018). Previous, *in vitro* work has demonstrated that genetic deletion of caspase-3 is

protective against axon degeneration that is induced by trophic factor withdrawal, however does not protect against injury-induced WD (Simon et al., 2012). Synaptic function may also be influenced by P53, with P53 shown to regulate genes involved with regulating synaptic function including BIN1, MEF2C and PICALM, in a model of Alzheimer's disease, and suggested to play a key role in maintaining synaptic function (Merlo et al., 2014).

P53 is also implicated in synaptic degeneration in disease scenarios. An upregulation of P53-associated transcripts in response to reduced Smn is well-documented in the literature (Murray et al., 2015, Baumer et al., 2009, Jangi et al., 2017, Staropoli et al., 2015, Zhang et al., 2008). Recent transcriptional profiling in SMA mice has identified pre-symptomatic upregulations of transcripts that are associated with P53 signalling (Murray et al., 2015, Simon et al., 2017). In work by Murray et al., 2015, RNAseq analysis and functional clustering in an SMA mouse model identified an upregulation of downstream, P53-targeted transcripts including Fas, CDKN1a and PMAIP1, that preceded NMJ loss and symptom onset (Murray et al., 2015). Gene expression profiling in SMA mice has also highlighted upregulations of P53 transcriptional targets in vulnerable – but not resistant – SMA motor neurons, suggesting that P53 may influence synaptic vulnerability and contribute to selective vulnerability (Murray et al., 2015). Similar upregulations in P53 have been reported in mice in which SMN deficiency is induced postnatally using antisense oligonucleotides (Jangi et al., 2017). Gene expression profiling undertaken Simon et al., agreed with these findings, highlighting specific upregulations of P53 transcriptional targets in vulnerable populations of motor neurons (Simon et al., 2017). Simon et al., also demonstrated that pharmacological or genetic inhibition of the P53 pathway could rescue vulnerable motor neurons from degeneration in a mouse model of SMA (Simon et al., 2017). However, in severe mouse models of SMA, and in ALS mouse models, despite elevations in P53 being reported in both patient post-mortem tissue and experimental models, P53 knockout does not reduce motor neurons loss, indicating P53-independent mechanisms also exist (Simic et al., 2000, Culmsee and Mattson, 2005). More recently, in a paper that I was a co-author on, P53 knockout was shown to reduce NMJ loss in the $Smn^{2B/-}$ mouse model of SMA, suggesting that axonal and synaptic

degeneration in this context is P53-dependent (Courtney et al., 2019) (see co-author paper in Appendix 3 for reference).

Unlike other studies that have focused on P53 and its pro-apoptotic role, studies such as that by Merlo et al., 2014, have investigated the role of P53 as a neuroprotective agent. Rather than promoting cell death, Merlo et al., present evidence in a model of Alzheimer's disease to support that P53 may instead contribute to a protective stress response that is critical to neuronal systems, including synaptic function (Merlo et al., 2014). Merlo et al., identify a group of susceptibility genes that are regulated by P53 that are involved in controlling synaptic function. This group suggest that regulation of synaptic genes can prevent neurodegeneration, with genetic manipulation of P53 target genes shown to be capable of modifying tau neurotoxicity in a *Drosophila* model (Merlo et al., 2014). Taken together, there is much evidence that highlights P53 as a potential target to modify the progress of synaptic degeneration.

Overall, whilst the role of P53 in apoptosis is widely appreciated, the role of P53 at the synapse and in the axon remains unclear. Although P53 has been implicated at early stages of neuronal death, with local actions suggested to contribute to dysfunction and degeneration of synapses, further work is required to understand how P53 is involved in different neurodegenerative contexts. Here, I aimed to investigate the role of P53 in axonal and synaptic degeneration, asking whether reductions in P53 can reduce synaptic loss under conditions of injury, during a die-back or during synapse elimination that occurs as part of normal development. In P53-reduced SMA and wild-type mice, I also sought to examine the impact of P53 reduction on the expression of synaptic genes that are thought to be regulated by P53. Overall, my data indicate a lack of association with P53 in all of the contexts examined, with no reductions in synaptic loss seen in injury or during a die-back, and normal levels of polyinnervation observed during development. In conditions where P53 or SMN protein is reduced, I also report no significant impact on the expression of synaptic genes. Collectively, data presented in this thesis supports that synaptic and axonal degeneration in these scenarios is not impacted by reductions in P53.

1.28 Results

1.28.1 Tamoxifen treatment leads to recombination in P53-floxed mice

To confirm cre-mediated recombination had taken place in P53-floxed mice, PCR reaction was undertaken on genomic DNA to probe for the presence of the recombined allele (Fig. 3.1). The recombined allele was only detected in P53-floxed mice that had been treated with tamoxifen, as demonstrated by the presence of a band at 612bp (Fig. 3.1, B). qPCR was then performed on DNA from treated mice at age of sacrifice to determine the relative quantities of P53, to indicate the extent of P53 reduction.

Following treatment with tamoxifen over two (Fig. 3.1, C) or three (Fig. 3.1, D and E) days, and at different time points, significant reductions in P53 levels were confirmed (Unpaired t-test with Welch correction, $p < 0.018$ in all cases). Postnatal induction of P53 recombination in floxed (Cre^+) mice resulted on average in 2.3 fold reductions in P53 quantity, which is consistent with previous descriptions by our group (Courtney et al., 2019) (Fig. 3.1, C-E). In $Smn^{2B/-}$ mice, this level of reduction can return numbers of activated caspase-3 (AC3) positive cells – indicative of ongoing apoptosis – to baseline levels in heart, muscle, liver and spinal cord (Fig. 3.2). Thus, although postnatal, Cre-LoxP-mediated recombination of P53 does not lead to complete knockout of P53 in this model, it is sufficient to prevent pathology-induced apoptosis.

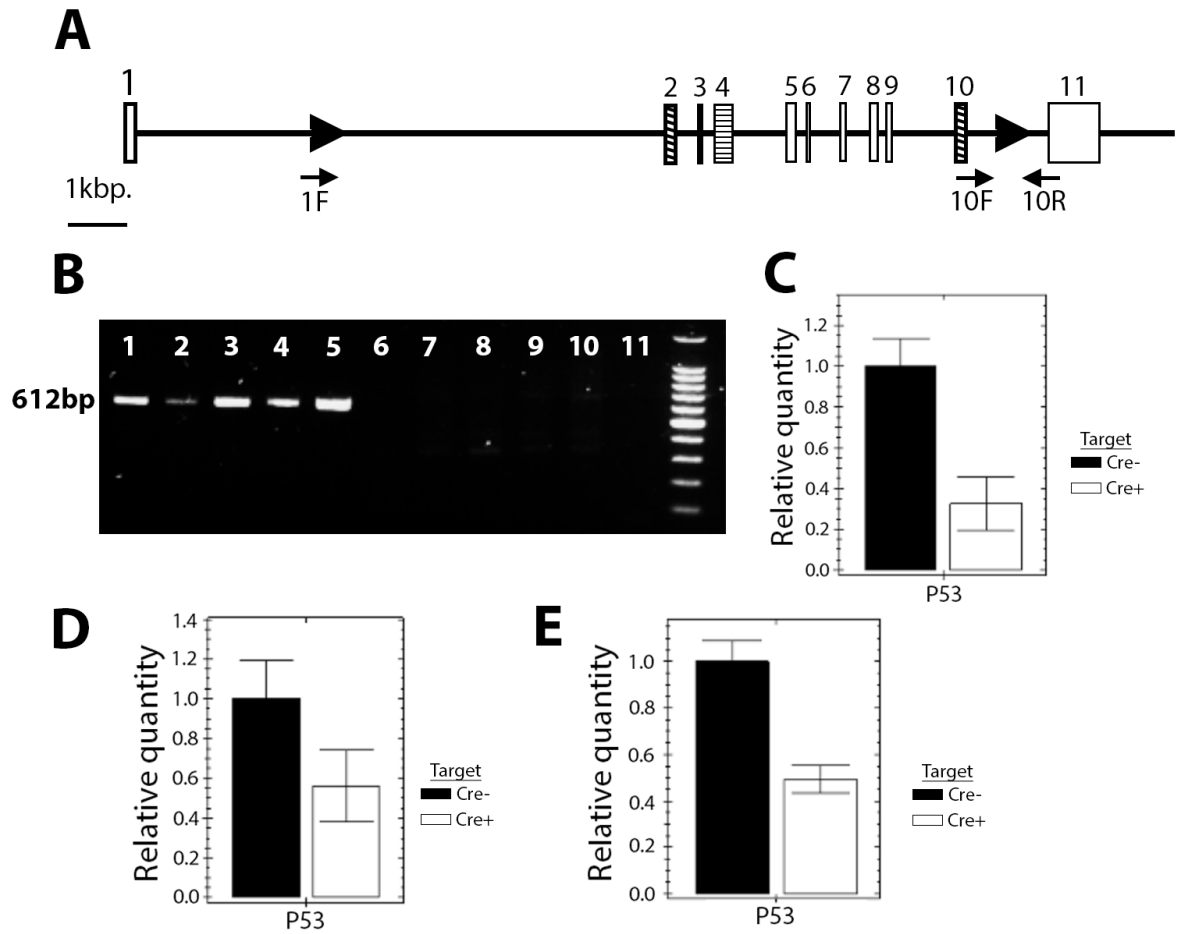
A
1
2 3 4
5 6
7
8 9
10
11
1kbp.
1F
10F
10R
B
612bp
1 2 3 4 5 6 7 8 9 10 11
C
Relative quantity
1.2
1.0
0.8
0.6
0.4
0.2
0.0
P53
Target
Cre-
Cre+
D
Relative quantity
1.4
1.2
1.0
0.8
0.6
0.4
0.2
0.0
P53
Target
Cre-
Cre+
E
Relative quantity
1.0
0.8
0.6
0.4
0.2
0.0
P53
Target
Cre-
Cre+

Figure 3.1: P53 recombination occurs after tamoxifen treatment in P53-floxed mice only. (**A**) Structure of the P53-floxed allele adapted from Marino et al., 2000 (Marino et al., 2000). (**B**) Agarose gel imaged by UV illuminator showing PCR result. After tamoxifen dosing for 2-3 consecutive days, P53 recombination occurs and a band is detected in animals that express the floxed allele ($P53^{fl/fl}$) and have been treated. Lanes 1-5 contain DNA from $P53^{fl/fl}$ animals that have been treated with tamoxifen; Lanes 6-8 contain DNA from littermate controls ($P53^{+/+}$) that do not possess the floxed allele and have been treated with tamoxifen; Lanes 9 and 10 contain DNA from untreated controls with and without the floxed allele respectively, that have not been treated with tamoxifen. Lane 11 was loaded with sample that was devoid of DNA. Lane 12 contains a 100bp DNA ladder. The $P53^{fl/fl}$ allele is identified by a band at 612bp (primers IF and 10R shown in (**A**) by PCR in treated $P53^{fl/fl}$ animals only, referred to here as Cre+, confirming recombination. Note that this band is only detected in animals that both express the floxed allele and have been treated with tamoxifen. (**C-E**) Relative quantities of P53 in *P53*-floxed mice shown relative to control as determined by qPCR. These data show that expression of P53 following tamoxifen treatment is significantly reduced after treatment at either P4 and P5 (**C**), P4, P5 and P6 (**D**) or P1, P2 and P3 (**E**); in all cases, P53 expression is significantly downregulated at the time of sacrifice ($p < 0.001$, $p < 0.01$, and $p < 0.018$ respectively, Unpaired t-test with Welch's correction). Black bars represent $P53^{+/+}$ control treated animals, whilst white bars represent $P53^{fl/fl}$ treated animals. n = 3 biological replicates. Error bars represent mean ± SEM.

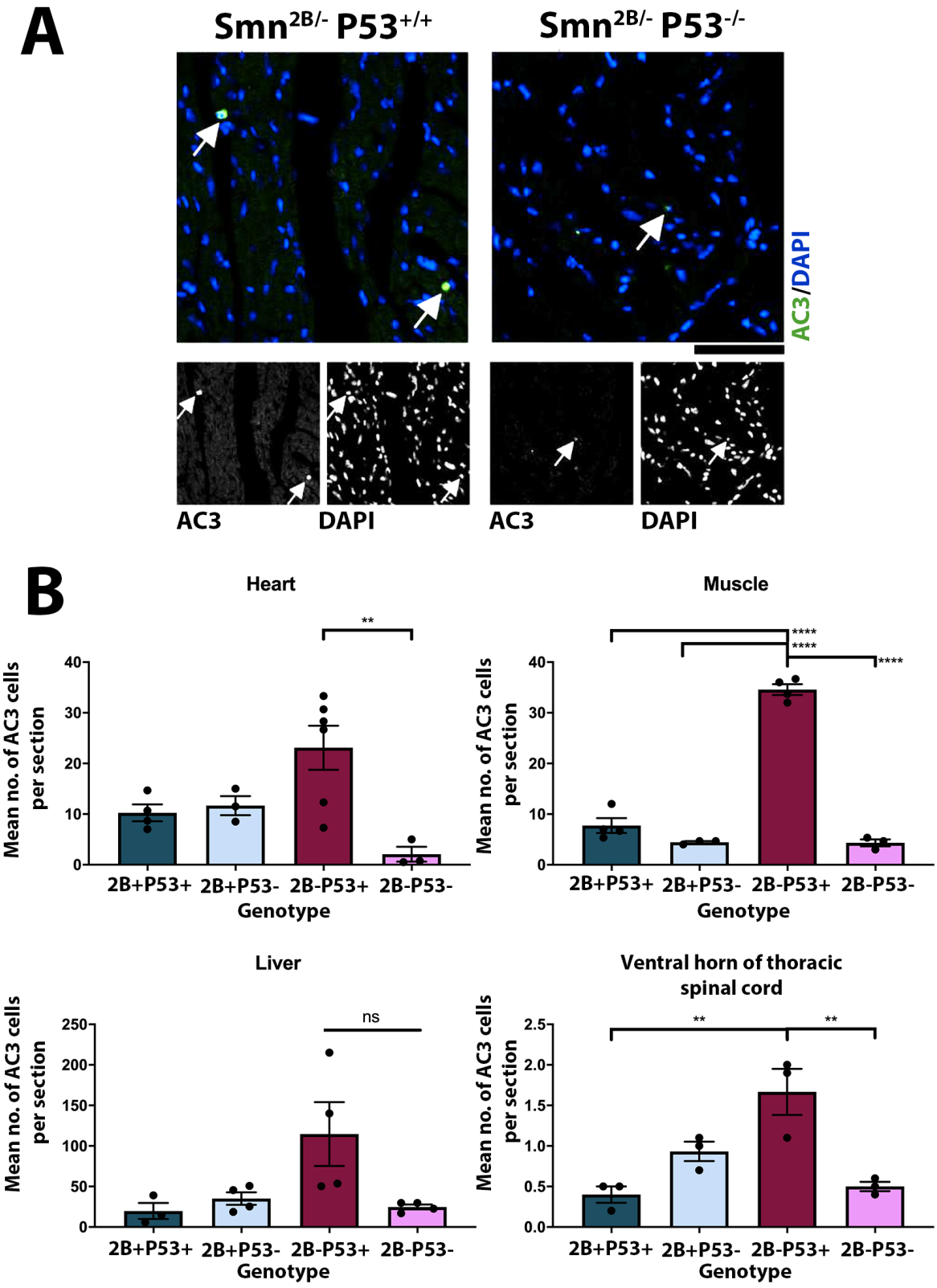
A
Smn2B/- P53+/+
Smn2B/- P53-/-
AC3/DAPI
AC3
DAPI
AC3
DAPI
B
Heart
Muscle
Liver
Ventral horn of thoracic spinal cord
Mean no. of AC3 cells per section
2B+P53+
2B+P53-
2B-P53+
2B-P53-
Genotype
**
****
ns

Figure 3.2: P53 reduction induced by postnatal tamoxifen treatment over two days is sufficient to return levels of activated caspase 3 (AC3) positive cells to baseline values in a number of tissues in P53-floxed $Smn^{2B/-}$ mice. (**A**) Micrographs from P15 $Smn^{2B/-};P53^{+/+}$ and $Smn^{2B/-};P53^{-/-}$ heart sections showing immunostaining of cardiomyocyte nuclei with DAPI (blue) and activated caspase-3 (AC3) (green) to indicate apoptotic cells. Examples of AC3 positive cells are indicated by white arrows. Scale bar: 50μm. (**B**) Comparison of the mean number of AC3 positive stained cells per section in different tissues at P15 in $Smn^{2B/+};P53^{+/+}$, $Smn^{2B/+};P53^{-/-}$, $Smn^{2B/-};P53^{+/+}$, and $Smn^{2B/-};P53^{-/-}$ mice. Note that in heart, tibialis anterior muscle, and in the ventral horn of the thoracic spinal cord, there are significant reductions in the number of AC3 positive cells in $Smn^{2B/-};P53^{-/-}$ mice, indicating that the induced reduction of P53 is sufficient to return apoptotic levels to baseline. This trend is also seen in liver. ns = not significant, p = 0.052; **, p < 0.007; ****, p < 0.0001; One-way ANOVA with Tukey correction. N (heart) = 4,6,3,3; n (muscle) = 4,4,3,3; n (liver) = 3,4,4,4 and n (spinal cord) = 3,3,3,3 for $Smn^{2B/+};P53^{+/+}$, $Smn^{2B/-};P53^{+/+}$, $Smn^{2B/+};P53^{-/-}$, and $Smn^{2B/-};P53^{-/-}$ groups respectively. All comparisons where no statistical result is shown were not significantly different. Error bars represent mean ± SEM. I acknowledge Victoria Zimmel, Mohammad Omar Khan, Dr. Alison Thomson and Dr. Laura Comley for their assistance with this work.

1.28.2 P53 reduction has no effect on levels of NMJ loss following injury

Previous work has indicated that P53 signalling progressively increases in the distal nerve following injury, suggesting that P53 may play a role in synaptic degeneration in WD (Yao et al., 2013). Here, I aimed to investigate the role of P53 in WD using an *ex vivo* model of peripheral nerve injury with reduced P53 levels. It was hypothesised that P53 reduction would reduce synaptic loss following injury, consistent with P53 playing a local role in synaptic degeneration during WD.

To test this, the *ex vivo* model of nerve injury described in Chapter 1 was utilised. Following the induction of *P53* recombination through tamoxifen treatment at P4, 5 and 6, cranial nerve/muscle preparations from *P53*-floxed wild-type mice and

littermate controls were collected. These preparations were maintained in oxygenated physiological saline at 30ºC for 24 hr as described previously (see Chapter 1). This therefore generated a model of peripheral nerve injury with reduced levels of P53. As demonstrated in Chapter 1, rates of WD are age-dependent. At P25, minimal innervation would be expected to remain in any of the cranial muscles following injury in wild-type animals. If P53 signalling is involved in the mechanisms of synaptic degeneration following injury, then P53 reduction would be expected to reduce NMJ loss following injury.

At P25, it was found that P53 reduction had no significant influence on the level of synaptic loss following injury (Two-way ANOVA with Sidak correction, $p > 0.30$). For example, in the LALr, when P53 levels are normal, there is just 8.32 ± 3.14% fully innervated endplates remaining, which is comparable to the 9.77 ± 5.40% remaining when P53 levels were reduced (Fig. 3.3).

It is possible that P53 could only exhibit marginal affects at the synapse, which would be more apparent when synaptic degeneration is slower. I therefore expanded this analysis to assess the impact of P53 loss on the level of innervation remaining at P18. At the younger time point of P18, rates of synaptic loss are lower, with over 34% innervation remaining in the LALr, LALc and AS muscles (see Chapter 1, *Results 1.20.2*). However, at P18, P53 reduction was found to have no significant influence on the level of synaptic loss following injury (Two-way ANOVA with Sidak correction, $p > 0.15$). For example, in the LALr, when P53 levels are normal, there is 34.99 ± 6.73% fully innervated NMJs remaining after injury, which is comparable to P53-reduced conditions, where the percentage of fully innervated endplates is 32.29 ± 11.68% (Fig. 3.3).

Overall, the loss of P53 had no significant effect on the level of synaptic loss at two age points, indicating P53-independence.

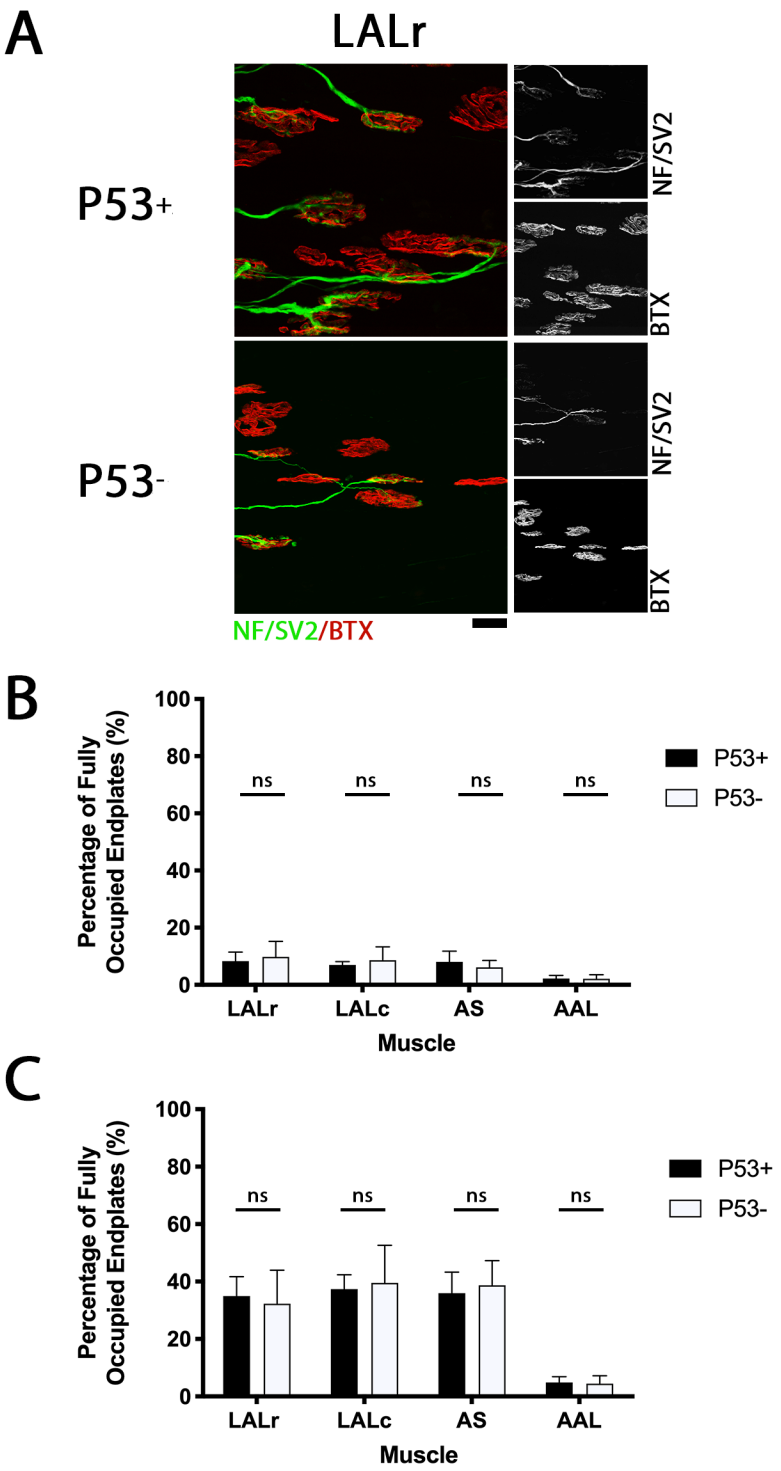
A
LALr
P53+
P53-
NF/SV2
BTX
NF/SV2
BTX
NF/SV2/BTX
B
Percentage of Fully Occupied Endplates (%)
100
80
60
40
20
0
ns
ns
ns
ns
P53+
P53-
LALr
LALc
AS
AAL
Muscle
C
Percentage of Fully Occupied Endplates (%)
100
80
60
40
20
0
ns
ns
ns
ns
P53+
P53-
LALr
LALc
AS
AAL
Muscle

Figure 3.3: Synaptic loss following injury is not affected by reduced P53 levels in the cranial muscles. (**A**) NMJs labelled with antibodies against neurofilament (NF, green) and synaptic vesicle protein 2 (SV2, green), and α-bungarotoxin (BTX, red) from the LALr of control and *P53*-floxed mice at P18 after *ex vivo* maintenance at 30ºC for 24 hr. Scale bar: 20μm. (**B**) Quantification of the percentage of fully occupied endplates in a range of cranial muscles from wild-type animals at P25 under conditions of normal versus reduced P53 (P53+ and P53- respectively). Note that there is no significant difference between these groups. (**C**) Quantification of the percentage of fully occupied endplates in a range of cranial muscles from wild-type animals at P18 under conditions of normal versus reduced P53 (P53+ and P53- respectively). Note that there is no significant difference between these groups. In both (**B**) and (**C**), controls with normal levels of P53 are represented by black bars, whilst those with reduced P53 are represented by white bars. Ns = not significant, $p > 0.99$ in all cases; two-way ANOVA with Sidak correction. Note that at P25, n = 4 and 6 for the P53+ group and P53- group respectively. At P18, n = 6, 5, 6, 6 muscles for the P53+ group and 6, 5, 6, 6 muscles for the P53- group for the LALr, LALc, AS and AAL respectively. Error bars represent mean ± SEM.

1.28.3 P53 reduction has no effect on levels of NMJ loss in an SMA mouse model

Previously, we demonstrated that postnatal reductions in P53 can result in a significant reduction in NMJ loss in the TVA muscle of $Smn^{2B/-}$ mice at P15 (Courtney et al., 2019, see Appendix 3). Here, I aimed to undertake a more comprehensive analysis to assess whether reductions in P53 can promote similar improvements in neuromuscular pathology in other muscles. Firstly, analysis of the TVA muscle from P53-floxed $Smn^{2B/-}$ mice was undertaken to ensure that I could replicate previous findings in this muscle.

Contrasting previous work, however, there was no significant improvement in NMJ retention in the TVA (Fig. 3.4). Since this finding was in contrast to previous results, quantification was performed by 3 independent researchers and all found no difference

in the percentage of fully innervated NMJs remaining at P15 between P53-floxed $Smn^{2B/-}$ mice and $Smn^{2B/-}$ littermate controls. For assistance with this validation, I acknowledge Victoria Zimmel and Dr. Laura Comley. I suggest that this inconsistency could be due to high variability in innervation across this muscle, which could have resulted in inadvertent selection for areas with high innervation. To ensure a fair representation of the muscle and reduce the chance of selection bias for innervated areas, bungarotoxin staining was used to select >100 motor endplates per muscle for analysis, with selected fields of view distributed across the entire muscle (detailed in Materials and Methods, 1.17 *Quantification and Statistical Analyses*).

To provide a comprehensive overview of the effect of P53 reduction on synaptic loss in this model, the percentage of full, partial and vacant endplates were also quantified in the triangularis sterni (TS) and external oblique (EO) muscles at P15 from $Smn^{2B/-}$ mice following cre-mediated *P53* recombination through tamoxifen induction at P4 and 5. Note that consistent with previous work, tamoxifen treatment was initiated prior to P5, as this time point precedes evidence of *P53* pathway activation in the spinal cord (Courtney et al., 2019).

In the TS and EO, the $Smn^{2B/-}$ $P53^{+/+}$ control group, referred to as 2B/- P53+, remained 97.98 ± 0.84% and 93.41 ± 3.41% innervated respectively, and the $Smn^{2B/-}$ $P53^{-/-}$ experimental group, referred to as 2B/- P53-, remained 94.62 ± 3.09% and 91.38 ± 2.76% innervated respectively (Figures 3.5 and 3.6 respectively). Concurrent with findings in the TVA, no significant improvements in neuromuscular innervation were observed in $Smn^{2B/-}$ mice when P53 was reduced in either TS (Fig. 3.5) or EO muscles (Fig. 3.6) (Two-way ANOVA with Sidak correction, $p > 0.23$ in both cases). P53 reduction had no significant effect on the percentage of vacant endplates, which, for ease of visualisation, are also displayed on an extended axis (Fig. 3.5, C and Fig. 3.6, C) (One-way ANOVA with Tukey correction, $p > 0.1$). I did note a trend towards an increase in the percentage of fully occupied endplates in $Smn^{2B/-}P53^{-/-}$ mice when compared to $Smn^{2B/-}P53^{+/+}$ mice, however this was not statistically significant (Two-way ANOVA with Sidak correction, $p > 0.45$ and $p > 0.55$ for TS and EO respectively).

Overall, I conclude that P53 reduction does not significantly reduce levels of NMJ loss in *Smn*$^{2B/-}$ mice.

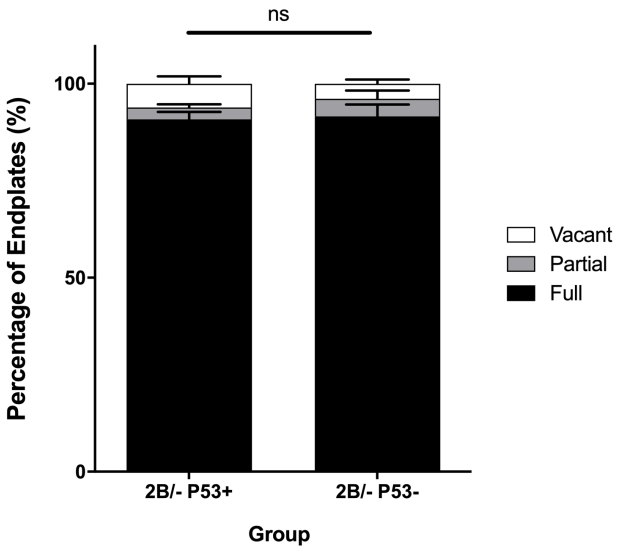

Figure 3.4: P53 reduction has no significant effect on the level of NMJ innervation remaining in transversus abdominis (TVA) muscle from a SMA mouse model. Quantification of the percentage of full, partial and vacant endplates in the TVA muscle at P15 from *Smn*$^{2B/-}$ mice. Note that there is no significant difference between 2B/- P53+ and 2B/- P53- groups. For assistance with validation, I acknowledge Victoria Zimmel and Dr. Laura Comley. Ns = not significant, $p > 0.81$ in all cases; Two-way ANOVA with Sidak correction. N = 8, 4 muscles for the 2B/- P53+ and 2B/- P53- groups respectively. Error bars represent mean ± SEM.

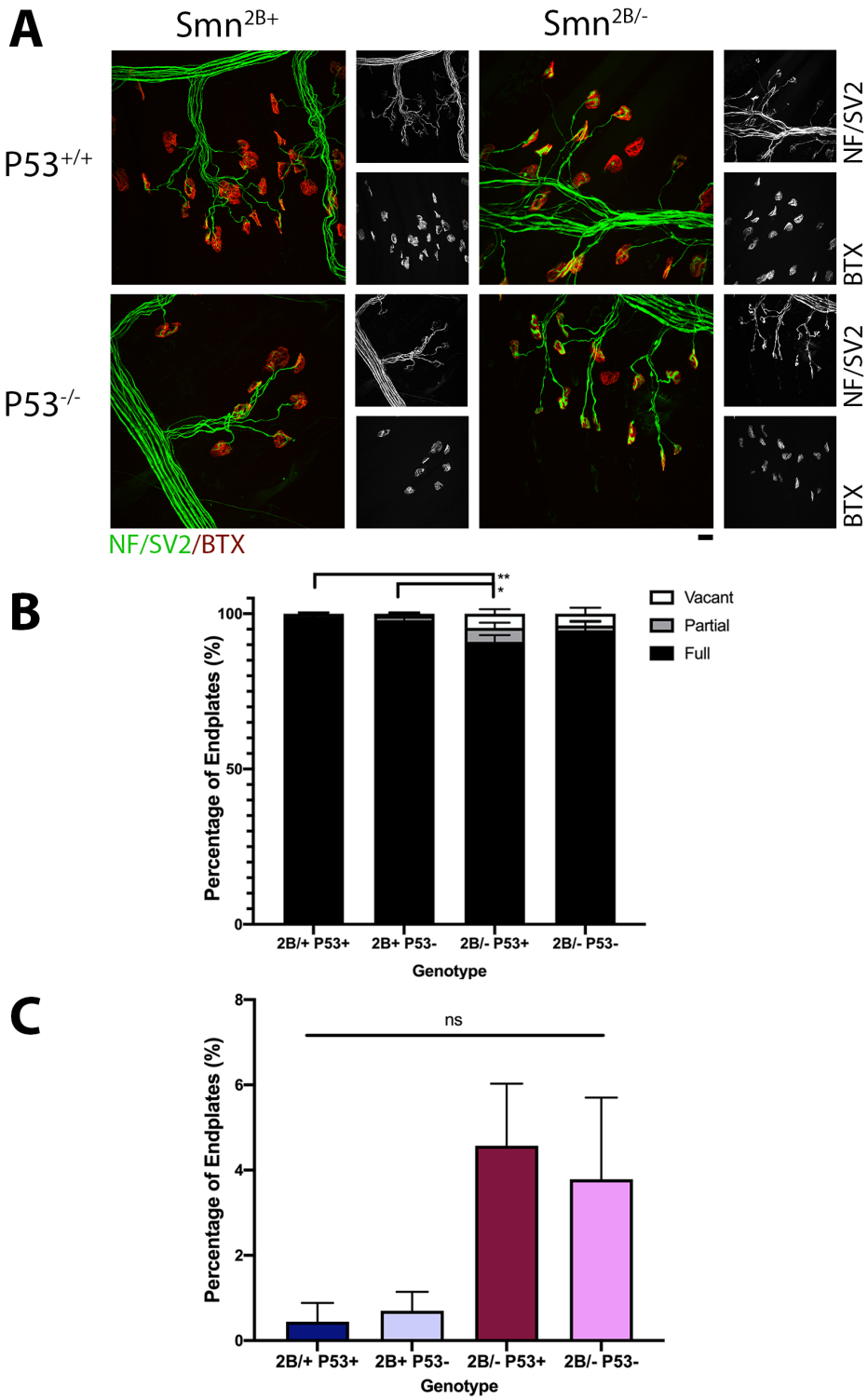
A
Smn2B+
Smn2B/-
P53+/+
P53-/-
NF/SV2
BTX
NF/SV2
BTX
NF/SV2/BTX
B
Vacant
Partial
Full
Percentage of Endplates (%)
100
50
0
**
*
2B/+ P53+
2B+ P53-
2B/- P53+
2B/- P53-
Genotype
C
ns
Percentage of Endplates (%)
8
6
4
2
0
2B/+ P53+
2B+ P53-
2B/- P53+
2B/- P53-
Genotype

Figure 3.5: P53 reduction has no significant effect on the level of NMJ innervation remaining in triangularis sterni (TS) muscle from a SMA mouse model. **(A)** Confocal micrographs showing NMJs labelled with antibodies against neurofilament (NF, green) and synaptic vesicle protein 2 (SV2, green), and α-bungarotoxin (BTX, red) from the TS of *$Smn^{2B/+}$ and $Smn^{2B/-}$* mice with normal and reduced levels of P53 at P15. Scale bar: 20μm. (**B**) Quantification of the percentage of full, partial and vacant endplates in the TS muscle at P15 from *$Smn^{2B/+}$ and $Smn^{2B/-}$* mice with normal and reduced levels of P53. Statistical significance applies to the 'full' category only. * p = 0.012, ** p = 0.0049; Two-way ANOVA with Sidak correction. All comparisons where no statistical result is shown were not significantly different. (**C**) Graph with extended axis to display quantification of the percentage of vacant endplates only in the TS muscle at P15 from *$Smn^{2B/+}$ and $Smn^{2B/-}$* mice with normal and reduced levels of P53. Again, note that P53 reduction had no significant effect on levels of endplate vacancy. Ns, p > 0.1; One-way AVOVA with Tukey correction. N = 4,5,5,5 muscles in 2B/+ P53+, 2B+ P53-, 2B/- P53+ and 2B/- P53- groups respectively. Error bars represent mean ± SEM.

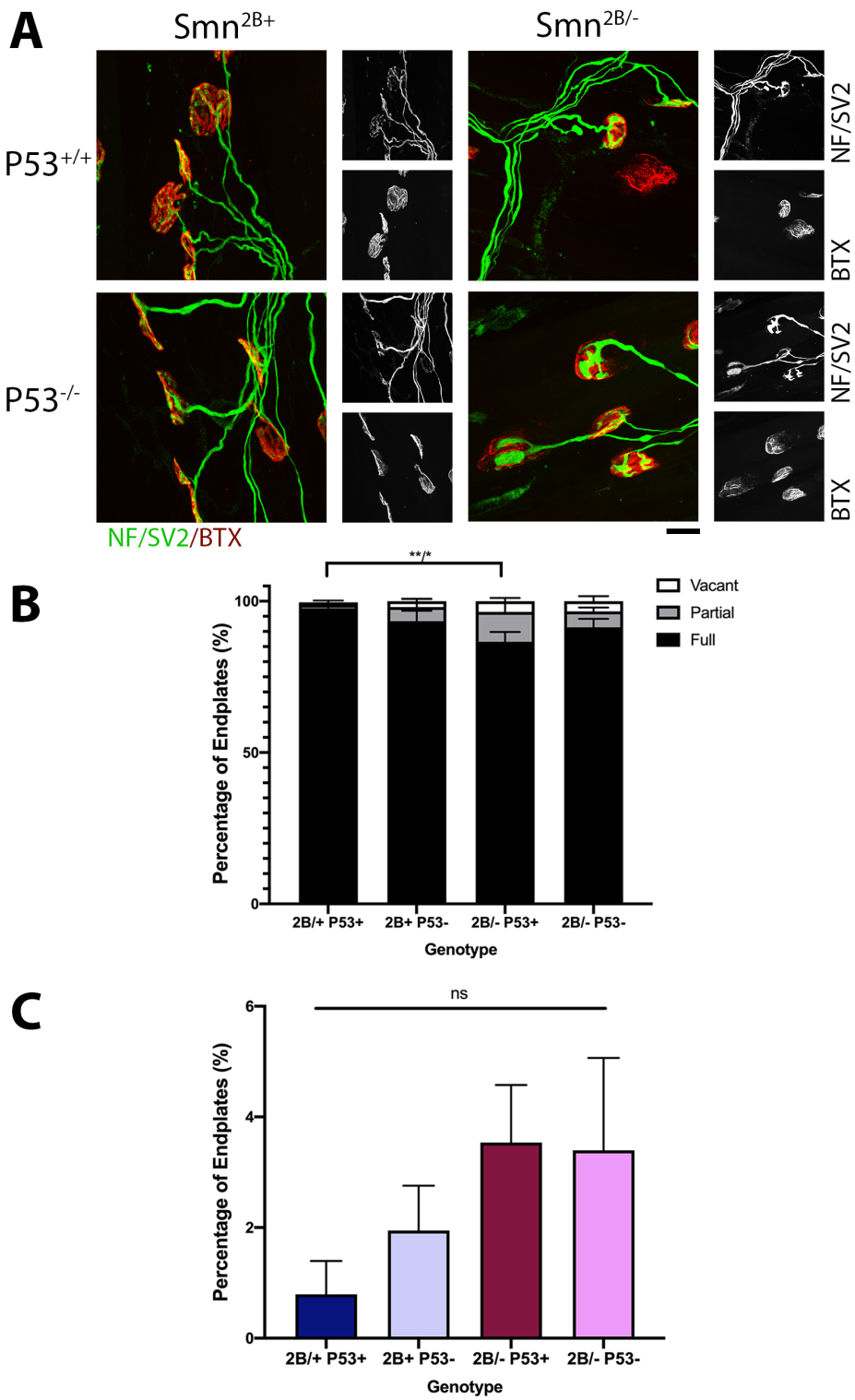
A
Smn2B+
Smn2B/-
P53+/+
P53-/-
NF/SV2
BTX
NF/SV2
BTX
NF/SV2/BTX
B
**/*
Vacant
Partial
Full
Percentage of Endplates (%)
100
50
0
2B/+ P53+
2B+ P53-
2B/- P53+
2B/- P53-
Genotype
C
ns
Percentage of Endplates (%)
6
4
2
0
2B/+ P53+
2B+ P53-
2B/- P53+
2B/- P53-
Genotype

Figure 3.6: P53 reduction has no significant effect on the level of NMJ innervation remaining in external oblique (EO) muscle from a SMA mouse model. **(A)** Confocal micrographs showing NMJs labelled with antibodies against neurofilament (NF, green) and synaptic vesicle protein 2 (SV2, green), and α-bungarotoxin (BTX, red) from the EO of $Smn^{2B/-}$ mice with normal and reduced levels of P53 at P15. Scale bar: 20μm. (**B**) Quantification of the percentage of full, partial and vacant endplates in the EO muscle from $Smn^{2B/+}$ *and* $Smn^{2B/-}$ mice with normal and reduced levels of P53 at P15. **/* represents statistical analyses from full/partial categories respectively. * p = 0.035, ** p = 0.0036. All comparisons where no statistical result is shown were not significantly different. (**C**) Graph with extended axis to display quantification of the percentage of vacant endplates only in the EO muscle at P15 from $Smn^{2B/+}$ *and* $Smn^{2B/-}$ mice with normal and reduced levels of P53. Again, note that P53 reduction had no significant effect on levels of endplate vacancy. Ns, $p > 0.3$; One-way AVOVA with Tukey correction. N = 6 biological replicates in all groups. Error bars represent mean ± SEM.

1.28.4 P53 reduction has no effect on rates of synapse elimination

Thus far, I have established that NMJ degeneration that occurs following injury or during a die-back are not affected by reductions in P53. It is well-known that across first few weeks of development in mice, synapses also degenerate as part of the normal development, in a process known as synapse elimination. Here, I aimed to investigate whether reductions in P53 could alter rates of synapse elimination. To address this, *P53* recombination was induced in *P53*-floxed wild-type mice by treatment with tamoxifen at P1, 2 and 3. I hypothesised that reduced P53 levels would delay synaptic pruning, consistent with P53 playing a role in synaptic remodelling.

To assess whether P53 reduction could delay the withdrawal of synapses, I first analysed the level of monoinnervation remaining in two muscles at P14. By P14, the majority of endplates (over 94% in both muscles) had reached adult maturity, and therefore only exhibited one axonal input. P53 reduction had no significant effect on levels of monoinnervation at P14 in either the LALr or AS (Fig. 3.7) (Two-way

ANOVA with Sidak correction, $p > 0.4$). In the LALr, when P53 levels were normal, 98.16 ± 0.61% of endplates were monoinnervated, which was comparable to 98.94 ± 0.47% monoinnervation when P53 was reduced. At P14, in P53+ mice, the majority of endplates are monoinnervated (>96%), suggesting that at this time point, the developmental period of synapse elimination is almost complete. I therefore also investigated synaptic maturity at a younger timepoint where higher levels of polyinnervation were expected. At P10, in P53+ mice, monoinnervation levels varied across different muscles, but did not exceed 83%.

As discussed in Chapter 1, the temporal profile of synapse elimination varies across different muscles. For example, the TVA is over 82% monoinnervated at P10, whilst AAL is under 50% monoinnervated. To provide a more comprehensive analysis and examine whether intermuscular differences exist in P53 dependency, I examined a range of muscles at P10. It was found that P53 reduction had no significant effect on levels of the percentage of mono- or polyinnervation at P10 (Figures 3.8 and 3.9) (Two-way ANOVA with Sidak correction, $p > 0.7$). For example, in the LALr, 69.82 ± 1.09% of endplates were monoinnervated, which was not significantly altered by P53 reduction, where 75.48 ± 1.63% of endplates were monoinnervated. It was interesting to note that there were significant regional variations in NMJ maturation at P10, which have been discussed in terms of their role in altering synaptic stability in Chapter 1 (Fig. 3.9). Such differences were no longer apparent, nor significant, at P14 (Two-way ANOVA, $p > 0.08$). For the purpose of this chapter, regional differences in the rate of synapse elimination will not be discussed.

Overall, synaptic loss during development is unaffected when P53 levels are reduced. It therefore appears that P53-independence is a common feature of synaptic degeneration in different physiological scenarios.

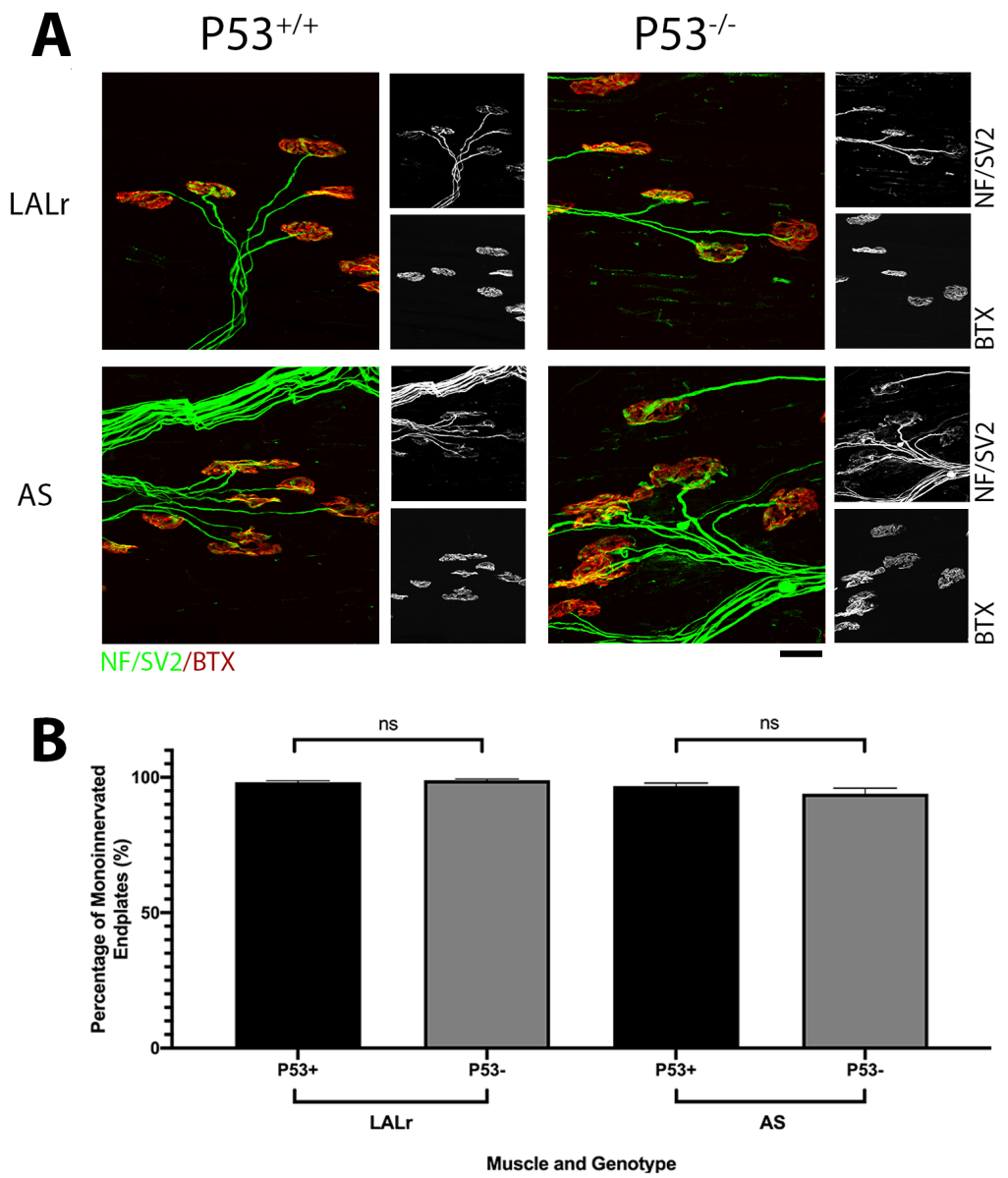

Figure 3.7: Synapse elimination is P53-independent at P14. (**A**) Confocal micrographs showing NMJs labelled with antibodies against neurofilament (NF, green) and synaptic vesicle protein 2 (SV2, green), and α-bungarotoxin (BTX, red) in the LALr and AS of control and *P53*-floxed mice at P14. Scale bar: 20μm. (**B**) Quantification of the percentage of monoinnervated inputs in a range of cranial muscles from wild-type animals at P10 under conditions of normal versus reduced P53 (P53+ (black bars) and P53- (grey bars) respectively). Note that there is no significant difference between these groups in either case. Ns = not significant, $p > 0.4$; two-way ANOVA with Sidak correction. N = 4 and 6 muscles for the P53+ and P53- groups respectively. Error bars represent mean ± SEM.

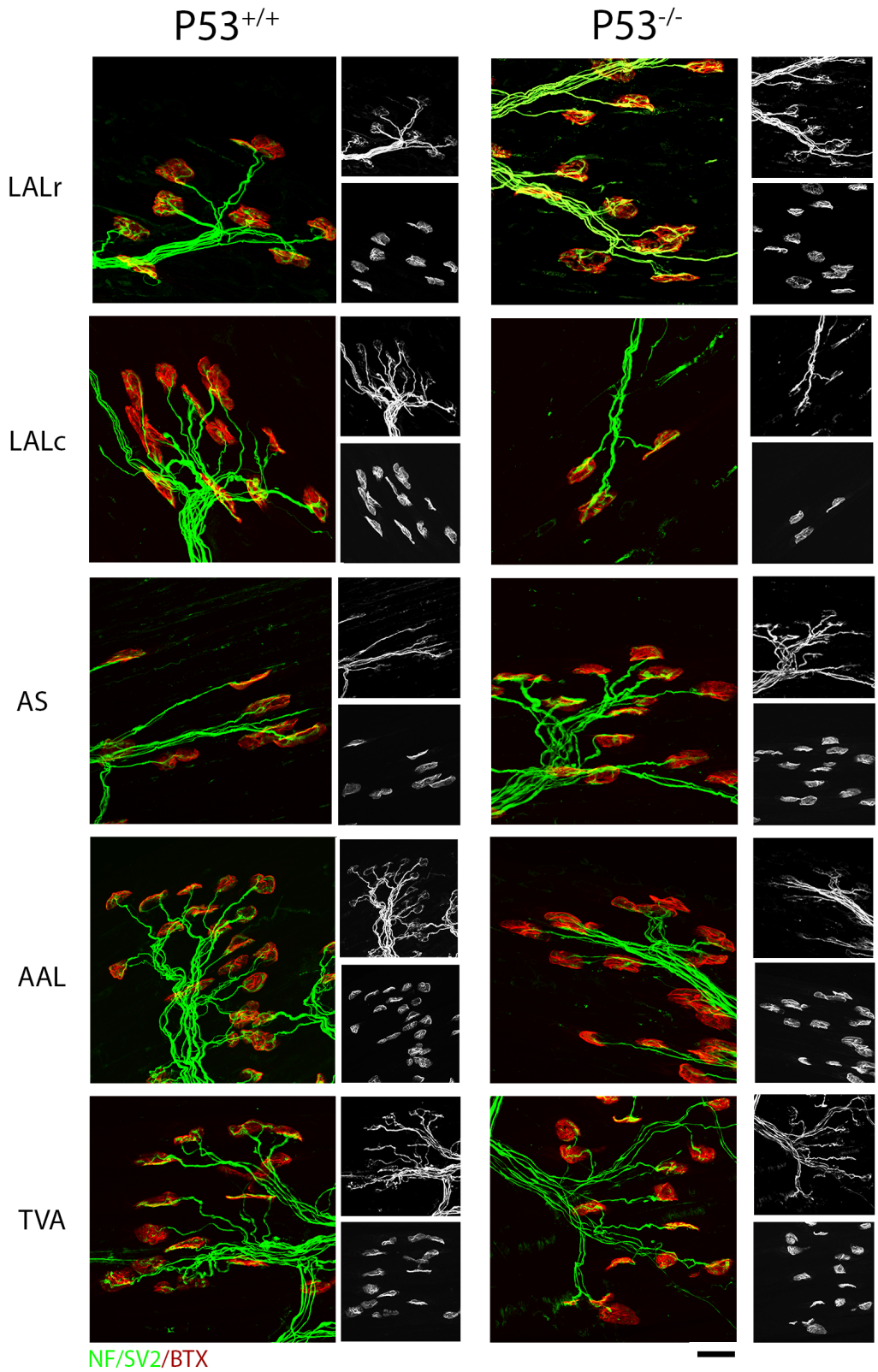
P53+/+
P53-/-
LALr
LALc
AS
AAL
TVA
NF/SV2/BTX

Figure 3.8: Levels of mono- and polyinnervation are unaffected by P53 reduction at P10 in a range of different muscles. Confocal micrographs showing NMJs labelled with antibodies against neurofilament (NF, green) and synaptic vesicle protein 2 (SV2, green), and α-bungarotoxin (BTX, red) in a range of cranial muscles and TVA of control and *P53*-floxed mice at P10. Note that P53 reduction does not appear to affect the rate of synaptic maturation. Scale bar: 20μm.

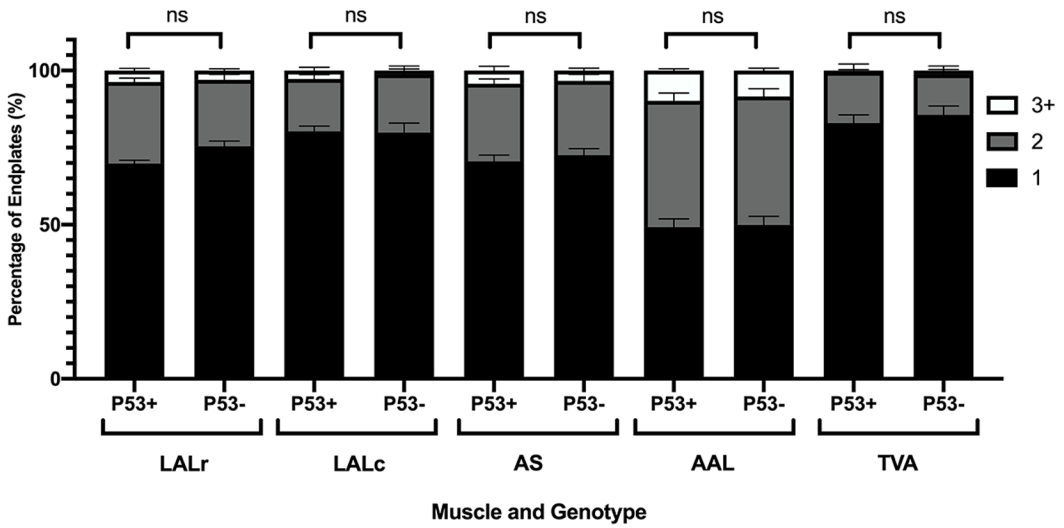

Figure 3.9: The rate of synapse elimination is not affected by P53 reduction at P10 in a range of different muscles. Quantification of the percentage of endplates with 1, 2 or 3+ inputs in a range of cranial muscles from wild-type animals at P10 under conditions of normal versus reduced P53 (P53+ and P53- respectively). Monoinnervated endplates (with 1 input) are represented by black, whilst those with 2 inputs are grey, and those with 3 or more are white. Note that there is no significant difference between these groups in any case. Ns = not significant, $p > 0.7$ in all categories; Two-way ANOVA with Sidak correction. N = 8 muscles in all cases. Error bars represent mean ± SEM.

1.28.5 Analysis of transcripts implicated as being regulated by P53

In previous work by Merlo et al., genes involved in controlling synaptic function emerged as being the top pathway regulated by *P53* (Merlo et al., 2014). Since P53 signalling has been shown to be upregulated in mouse models of SMA (Zhang et al., 2008, Staropoli et al., 2015, Murray et al., 2015, Jangi et al., 2017, Baumer et al., 2009), I aimed to investigate transcript levels of *Bin1, Mef2c* and *Picalm* in the $Smn^{2B/-}$ mouse model of SMA to determine whether these synaptic genes were dysregulated.

In symptomatic $Smn^{2B/-}$ mice (P15), it was found that there were no significant differences in the relative normalised expression of *Bin1, Mef2c* or *Picalm*, suggesting that these genes are not disrupted by SMN loss in this model (two-way ANOVA with Sidak correction, $p > 0.8$) (Fig. 3.10). Despite upregulations of P53 transcripts in this mouse (Murray et al., 2015), expression of these synaptic genes were unaffected; upregulations in P53 therefore do not appear to correlate with alterations to these synaptic genes, suggesting their expression is P53-independent.

I further confirmed P53-independence by examining the levels of *Bin1, Mef2c* and *Picalm* in $Smn^{+/+}$ mice when P53 was reduced through cre-mediated recombination of *P53*. P53 reduction had no effect on the expression levels of these transcripts, suggesting that these synaptic genes are not regulated by P53 (Two-way ANOVA with Sidak correction, $p > 0.2$) (Fig. 3.11).

Overall, it is concluded that transcript levels of *Bin1, Mef2c* and *Picalm* are unaffected by reduced SMN or altered P53 levels, suggesting that their regulation is both SMN- and P53-independent. Further work to confirm this at the protein level would be valuable.

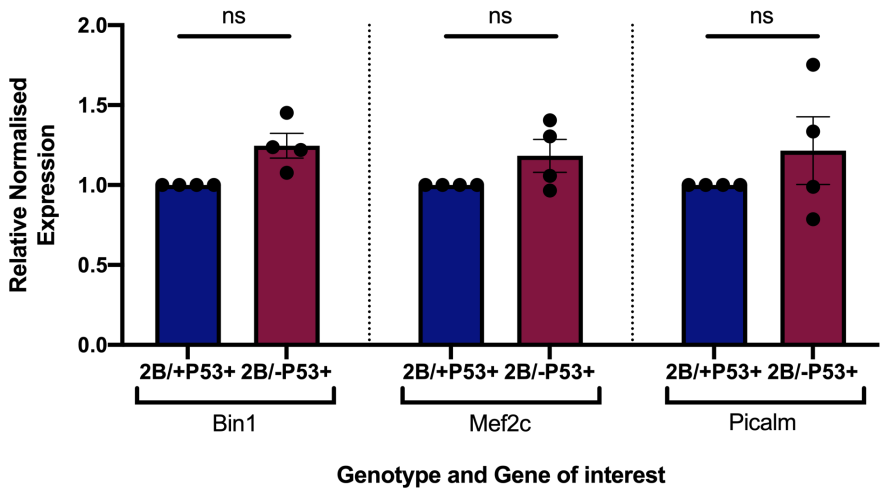

Figure 3.10: Expression of genes involved in synaptic function are unaffected by loss of SMN protein as assessed by RT-qPCR and $2^{-\Delta\Delta CT}$ method in $Smn^{2B/-}$ mice. Using RT-qPCR, the expression levels of *Bin1, Mef2c* and *Picalm* were analysed at P15 in spinal cords of $Smn^{2B/-}$ mice. The disease model is represented by a pink bar, whilst control mice are represented by a blue bar. Note that no significant differences were detected in the expression of these genes. Data is expressed normalised to *Actin*, *Gapdh* and *Ywhaz* and relative to the 2B/+P53+ control group. Ns = not significant, $p > 0.8$; two-way ANOVA with Sidak correction. N = 4 biological replicates. Error bars represent mean ± SEM.

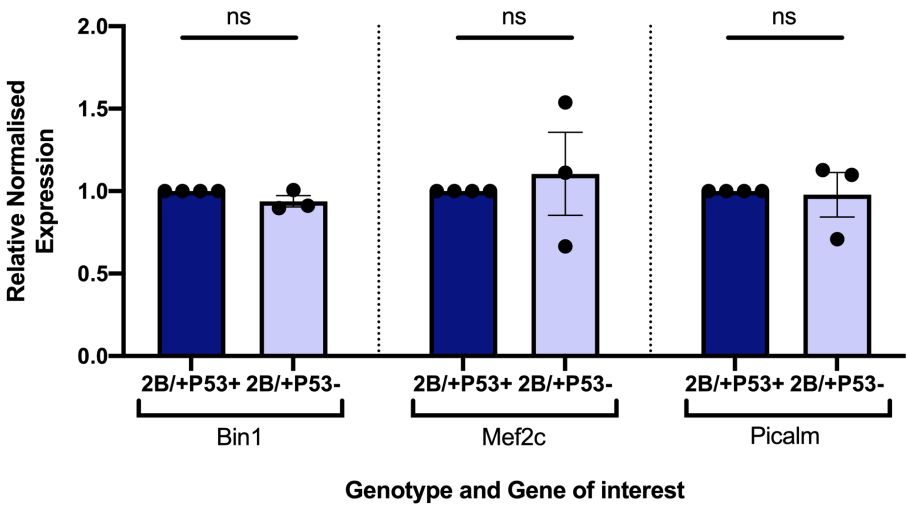

Figure 3.11: Expression of genes involved in synaptic function are not affected by reduced P53 levels as assessed by RT-qPCR and $2^{-\Delta\Delta CT}$ method in P53-floxed mice. Using RT-qPCR, the expression levels of *Bin1, Mef2c* and *Picalm* were analysed at P15 in spinal cords following *P53* recombination. The control group, with normal P53 levels are represented by a dark blue bar, whilst the experimental group with reduced P53 are represented by a paler blue bar. Note that no significant differences were detected in the expression of these genes. Data is expressed normalised to *Actin, Gapdh* and *Ywhaz* and relative to the 2B/+ P53+ control group. Ns = not significant, p > 0.2; two-way ANOVA with Sidak correction. N = 4, 3 biological replicates for control and experimental groups respectively. Error bars represent mean ± SEM.

1.29 Discussion

1.29.1 Overview of Results

In this chapter I investigated the role of P53 in morphologically distinct types of degeneration, including in the contexts of injury, disease and during development. I firstly demonstrated that postnatal Cre-LoxP-mediated recombination could significantly reduce P53 levels and prevent upregulation of apoptotic-associated markers in a range of tissues. I demonstrated that P53 reduction had no effect on levels of synaptic loss across a range of different muscles in a murine *ex vivo* model of peripheral nerve injury. Similarly, P53 reduction had no effect on levels of synaptic loss across different muscles in a mouse model of SMA. P53 reduction also had no effect on levels of polyinnervation across a range of different muscles, suggesting that synapse elimination is also P53-independent. Synaptic genes that are thought to be regulated by P53, including *Bin1*, *Mef2c* and *Picalm*, were not dysregulated in SMA mice, nor were transcript levels altered when P53 was reduced in wild-type mice, suggesting that their regulation is SMN- and P53-independent.

1.29.2 Is the reduction in P53 levels sufficient?

Here, I utilised an inducible, P53-floxed mouse model to investigate the role of P53 in different physiological scenarios. I utilised an inducible mouse model, which I have demonstrated undergoes Cre-LoxP-mediated recombination to express significantly reduced levels of P53 following postnatal treatment with tamoxifen. In this model, P53 expression was reduced by 2.3-fold compared to mice that do not express the floxed allele.

It must therefore be acknowledged that this model does not represent a complete knockout. This raises the question as to whether this level of P53 reduction is sufficient to cause measurable changes in P53-dependent processes? To address this, we examined levels of AC3 positive cells in a mouse model of SMA in a range of tissues. Caspase-3 plays a role in co-ordinating the destruction of cellular structures and is activated in cells that are undergoing apoptotic cell death, thus AC3 is considered a

biomarker of apoptosis (McIlwain et al., 2013). In *Smn*$^{2B/-}$ mice, we see a significant increase in the number of AC3 positive cells in skeletal muscle and spinal cord. In tamoxifen-treated, P53-floxed *Smn*$^{2B/-}$ mice, the number of AC3 positive cells is reduced back to baseline levels, suggesting that P53 reduction is sufficient to prevent upregulations in apoptosis.

There are other models that may have been utilised that could have provided a more complete knockout. Gene targeting in embryonic stem cells is one such approach (Tong et al., 2010). A P53-germline knockout model could have been generated, however, there were several reasons why this was not selected. Firstly, numerous studies have suggested that P53 disruption can lead to developmental anomalies and malignancies, including the development of neural tube defects, and high rates of embryonic lethality (Armstrong et al., 1995, Sah et al., 1995, Kawamata and Ochiya, 2012). P53 has been labelled 'the guardian of the genome', and has also been defined as a 'guardian of embryogenesis,' playing a crucial role in maintaining embryonic stem cell quality and genomic integrity (Kawamata and Ochiya, 2012). P53-null embryonic stem cells exhibit several abnormal features, including blockade of differentiation and severe chromosomal instability (Kawamata and Ochiya, 2012).

It is also possible that knockout of P53 at the germline level could have resulted in embryonic-derived compensatory events to compensate for a lack of P53, which could have masked consequences of P53 reduction. Several studies have demonstrated that there are phenotypic differences between knockout and knockdown models (El-Brolosy and Stainier, 2017). Deleterious mutations in zebrafish have been shown to result in profound phenotypic differences compared to gene knockdown (Rossi et al., 2015). For example, whilst mutant zebrafish with an endothelial gene knocked out appear normal, knockdown of this endothelial gene leads to severe vascular defects (Rossi et al., 2015); proteomic and transcriptomic comparisons between knockout and knockdown zebrafish revealed compensatory gene activation in knockouts that could be responsible for such phenotypic disparity (Rossi et al., 2015). Genetic compensation has also been described in murine knockout models. For example, mutations in the cellular prion protein gene (*Prnp*), should be lethal, however a second

gene – *Sprn* – can compensate. Only when this compensatory gene is also knocked out, is lethality seen (Daude et al., 2012). Overall, it appears that compensatory networks in knockout animals may buffer against deleterious mutations, but less so in knockdown scenarios. In this respect, postnatal induction of P53 loss would reduce the chance of confounding, compensatory events that could mask the effects of P53 reduction. Recently published work has also suggested that germline knockout of P53 fails to prevent motor neuron loss or extend lifespan in an SMA mouse model, providing further support for work presented here (Reedich et al., 2021).

I could also have induced P53 knockout pharmacologically, such as by using the small molecule pifithrin-α, however previous work in our lab, and that of others, has demonstrated that pharmacological inhibition of P53 does not inhibit all aspects of P53 function (Zhu et al., 2020). Overall, although our postnatal P53 knockout is incomplete, data suggest that this is sufficient to prevent upregulations in apoptosis peripherally and centrally, whilst reducing the likelihood of genetic compensation. In future work, validation of P53 reduction at the protein level would be valuable.

1.29.3 The role of P53 in axons and synapses

In a murine *ex vivo* model of peripheral nerve injury, I found that P53 reduction had no effect on the level of synaptic loss after 24 hr when compared to control in a range of different muscles. In a P53-floxed mouse model of SMA, there were also no improvements in the percentage of fully occupied NMJs in a range of different muscles. I also demonstrated that P53 reduction did not prevent synaptic elimination during early postnatal development. A selection of synaptic genes also demonstrated P53-independent expression. My data collectively indicate that reductions in P53 do not reduce levels of synaptic loss in different physiological scenarios. There is evidence that has indicated that local P53 signalling at synapses can induce apoptosis (Mattson, 2000), therefore it is intriguing that P53 reduction does not improve synaptic retention in these contexts. Since P53 reduction does not prevent synaptic loss, what role does P53 play in axons and synapses?

It has been suggested that P53 could play a fundamental role in axonal outgrowth and regeneration following damage. Previous work has demonstrated that P53 is present at the synapse and that P53 signalling is progressively upregulated across in the distal axon following injury (Yao et al., 2013, Gilman et al., 2003). Compared to wild-type controls, P53 knockout mice show reduced levels of spontaneous regeneration following transection, whilst cell survival is unaffected, suggesting that P53 is required for regeneration (Di Giovanni et al., 2006, Tedeschi and Di Giovanni, 2009). P53 is required for neurite outgrowth *in vitro* in primary neurons and *in vivo* in mice. For example, P53 drives the expression of pro-regenerative responses, including through activating actin-binding protein Coronin 1b and the GTPase Rab13, which associate with the cytoskeleton and regulate neurite outgrowth (Di Giovanni et al., 2006). Di Giovanni et al., demonstrate that acetylation of P53 on lysine 320 is a requirement for neurite outgrowth and axonal regeneration (Di Giovanni et al., 2006). Regeneration could be hindered by a lack of removal of damaged cells, therefore P53's role in DNA repair and elimination of damaged cells also appears to be critical to regenerative efforts. To ensure successful outgrowth and regeneration, axon guidance and pathfinding are also essential. The role of P53 in these processes remains unclear, however there is evidence that suggests that P53 can drive the expression of various factors that regulate axon guidance, including semaphorins (Futamura et al., 2007, Ochi et al., 2002, Arakawa, 2005, Barallobre et al., 2005, Harel and Strittmatter, 2006, Pasterkamp and Verhaagen, 2006). Overall, P53 may therefore contribute to and coordinate axonal regenerative efforts.

Interestingly, it has been reported that 80% of mice can develop normally despite P53 knockout, which draws the role of P53 in development into question (Tedeschi and Di Giovanni, 2009). However, it has been proposed that other P53 family members, like P63 or P73, may compensate for the loss of P53. Truncated isoforms of P73 have been shown to protect neurons from cell death following apoptotic stimuli in both the CNS and PNS (Pozniak et al., 2000, Pozniak et al., 2002). It has been proposed that P73 may even counteract the pro-apoptotic functions of P53 in developing neurons, with increased levels of truncated P73 found to rescue neurons from apoptosis induced by trophic withdrawal or P53 overexpression (Pozniak et al., 2000). Studies investigating

P53 and P63 deletion have demonstrated that full-length P63 is required and sufficient to induce cell death following trophic withdrawal, and that absence of P53 does not affect P63-induced apoptosis (Jacobs et al., 2005). In the context of the work presented here, this may suggest that other P53 family members could be influencing, or exhibiting compensatory actions, independently of P53 at the synapse too. Although the role of different members of the P53 family have been investigated in terms of embryonic development and in cancer, their postnatal roles and interaction remain unclear (Van Nostrand et al., 2017). Investigating the role of other P53 family members in synaptic degeneration following different insults will be an important consideration for future work if we are to fully understand its role.

Apoptotic pathways converge on caspases, such as caspase 3 which is described as being an 'executioner of apoptosis' (Elmore, 2007, Simon et al., 2012). Manipulation of executioner caspases could provide greater insight into the role of pro-apoptotic pathways in different contexts. Previous *in vitro* work has demonstrated that caspase-3 knockout is protective against axon degeneration that is induced by trophic factor withdrawal *in vitro*, and can delay axon pruning of exuberant retinocollicular axons during development *in vivo* (Simon et al., 2012). Inhibition of caspase 3, has also been shown to rescue motor neurons cultured from SMA patient-iPSCs (Sareen et al., 2012). However, caspase-3 deletion does not protect against WD following axon transection, indicating that caspase-3 is not involved in WD (Simon et al., 2012). Manipulating caspase-3 may provide further insight into the role of pro-apoptotic pathways in synaptic degeneration under different degenerative scenarios. Overall, the role of P53 is undoubtedly complex, due to its ability to influence pro- and anti-apoptotic pathways. More work is clearly required if we are to fully appreciate the role of P53 in the axon and synapse.

General Discussion

1.30 *Overview of Results*

Work presented within this thesis has explored factors that can influence the rate of degeneration under different degenerative scenarios, including following injury, during disease and during postnatal development.

In Chapter 1, I expanded an *ex vivo* model of peripheral nerve injury which I subsequently applied to a range of different scenarios. I demonstrated that developmental regulation and selective vulnerability are features of WD in the murine cranial muscles, and described a remarkable resistance to degeneration following injury in the thoracoabdominal musculature. Patterns of selective vulnerability in WD were found to be distinct from those described during a die-back in the $Smn^{2B/-}$ mouse model of SMA. Using preparations from the $Smn^{2B/-}$ mouse, I applied the *ex vivo* assay to demonstrate that WD is Smn-independent, and that the presence of a die-back can accelerate synaptic loss following injury. Work presented in this chapter favours the conclusion that there is convergence in degenerative mechanisms in WD and dying-back pathology.

In Chapter 2, I analysed two independent proteomic datasets to demonstrate that there were common and consistent increases in mitochondrial proteins across early postnatal development in the deep lumbrical and tibialis anterior muscles, that coincide with accelerations in the rate of synaptic degeneration following injury across the first few weeks of life in mice. I demonstrated that these proteomic changes could be accounted for by an increase in mitochondrial number in nerve, but not in muscle. I expanded this analysis to assess whether mitochondrial number or protein levels could explain differences in synaptic vulnerability in a range of other nerves and muscles. I found that changes in mitochondrial complex protein levels did not correlate with accelerations in the rate of synaptic degeneration during postnatal development.

Differential rates of synaptic degeneration between muscles did not correlate with changes in mitochondrial number in muscle or nerve. However, differential rates of synaptic degeneration in different muscles did correlate with CI levels in nerve. Overall, data presented in this chapter suggest that although there are global changes in mitochondrial proteins across P15 to 24, these do not correlate with accelerations in the rate of synaptic degeneration following injury across early postnatal development in muscle, although changes in nerve may play a role in conferring selective vulnerability.

In Chapter 3, I used a P53-floxed inducible mouse model to assess the role of P53 under different degenerative scenarios. Application of the *ex vivo* model demonstrated that P53 reductions had no effect on the level of synaptic loss following injury, suggesting that WD is P53-independent. In the $Smn^{2B/-}$ mouse model, I demonstrated that P53 reduction had no effect on the level of NMJ loss in a range of different muscles at a late-symptomatic stage. This suggests that dying-back pathology in SMA is also P53-independent. P53 reduction had no effect on levels of polyinnervation during postnatal development, suggesting that synapse elimination is also P53-independent. Finally, I demonstrated that neither P53 nor SMN reductions had any effect on the expression of a selection of synaptic genes. Overall, data presented within this chapter suggest that P53-independence is a common feature across morphologically distinct types of synaptic and axonal degeneration.

1.31 *A valuable tool for mechanistic insight: ex vivo applications*

In this work, I have expanded an *ex vivo* model and subsequently demonstrated that this can be applied to effectively test various hypotheses. For example, I applied the *ex vivo* assay to test whether the developmental phenomenon of acceleration in synaptic degeneration was present in a range of other muscles. This assay also revealed that selective vulnerability is a feature of WD. Selective vulnerability has not been described in WD before, and future work could exploit intermuscular differences as a tool to investigate the molecular underpinnings of such differences.

Through application of the *ex vivo* model, I have demonstrated that in a muscle with extensive dying-back pathology induced by reduced Smn, injury-induced synaptic loss is accelerated. This demonstrates that the presence of a die-back can accelerate WD, suggesting that mechanistic convergence exists. This supports the hypothesis that there are common mechanisms involved in synaptic degeneration in morphologically distinct types of synaptic degeneration. To further test this, preparations from other models that exhibit a die-back could be tested in the *ex vivo* system. It is hypothesised that similar accelerations in synaptic loss would be seen in other models that exhibit dying-back pathology, such as in the SOD1 mouse model of ALS. This would be consistent with convergent degenerative pathways being responsible for dying-back and WD, and could facilitate the identification of common targets of neurodegeneration which could have efficacy across different diseases where dying-back is a pathological feature.

To address the debate over mechanistic divergence, we could also introduce preparations from mouse models where Wld^S has previously failed to confer protection. For example, we could introduce preparations from the *pmn* mouse (Ferri et al., 2003) or myelin protein zero mouse (Samsam et al., 2003) and assess levels of synaptic loss after injury. If the rate of WD is unaffected, then this would indicate that different pathways are responsible for dying-back, and ultimately motor neuron death, in these scenarios, despite morphological similarities. It would also be interesting to assess the level of synaptic loss in *Wst* mice. In *Wst* mice, loss of *eEF1A2* results in a die-back, and significantly delays synaptic loss induced by axotomy in the DL muscles *in vivo* (Murray et al., 2008b). It would be interesting to assess whether the loss of *eEF1A2* expression, and the consequent presence of a die-back, can similarly delay injury-induced synaptic loss in other muscles. We could test this by introducing *Wst* preparations to the *ex vivo* system. If the rate of WD is delayed, then this would support the hypotheses that opposing mechanisms exist, as the presence of a die-back induced by loss of *eEF1A2* would be sufficient to block WD. Overall, using this *ex vivo* model, we can begin to categorise synaptic degeneration into pathologies which can accelerate or modify the rate of WD, and those which cannot. This mechanism-based

categorisation will help us to identify diseases where common therapeutic approaches could be utilised.

The nature of *ex vivo* experimentation, where preparations are suspended in a physiological solution, facilitates easy manipulation of variables pharmacologically. I have demonstrated that there is a lack of correlation between changes in mitochondrial proteins or number and accelerations in the rate of synaptic loss during early postnatal development. This conclusion could be further supported through *ex vivo* application of pharmacological agents that target oxidative phosphorylation. We have previously demonstrated that *in vitro* application of an inhibitor of CI (rotenone) can reduce axonal loss in DRG cultures (Kline et al., 2019). Based on results presented in Chapter 2, it could be hypothesised that rotenone application would not delay synaptic loss in the cranial or thoracoabdominal musculature in an *ex vivo* injury scenario. In addition, although I have demonstrated that increases in CI cannot account for developmental regulation, I found that CI changes in nerve did correlate with patterns of selective vulnerability following injury. It would therefore be interesting to assess whether rotenone application *ex vivo* could alter levels of synaptic loss following injury across different muscles. If rotenone application can modify the pattern of injury-induced selective vulnerability, then this would be consistent with the hypothesis that increases in CI are responsible for intermuscular differences. Pharmacological intervention *ex vivo* is also clearly not restricted to oxidative phosphorylation, and other factors could be manipulated through the inclusion of pharmacological agents in the suspension buffer. By utilising cranial muscle/facial nerve preparations as described in Chapter 1, we could simultaneously assess the impact of stimulation or inhibition of different targets on selective vulnerability and developmental regulation following injury. Notably, however, there are limitations to pharmacological manipulation, including that inhibition could be incomplete or have off-target effects. Genetic manipulation through the introduction of mutant preparations to the *ex vivo*, following the workflow described in Chapter 3, may therefore provide a more powerful tool to test hypotheses relating to mechanisms of synaptic and axonal degeneration.

1.32 *A workflow for investigating common pathways of synaptic degeneration*

Ex vivo assaying allows us to deliver reproducible injuries that can be performed across various mouse models with different loss- or gain-of-function mutations. I have provided an example of this by applying the *ex vivo* assay to test the hypothesis that P53 reduction can reduce synaptic loss following injury in mice. Although the data from P53 work is negative, this underlines the value of the *ex vivo* model and scope to test other scenarios to elucidate factors that can influence rates of degeneration. Whilst P53 does not appear to be a convergent regulator of synaptic degeneration, the workflow implemented in Chapter 3 has described an approach to investigate morphologically distinct types of degeneration. *Ex vivo* assaying permits reproducible injuries which can be performed across various mouse models with different loss- or gain-of-function mutations. A similar workflow could be implemented to assess the involvement of other pathways in synaptic degeneration.

For example, this could be implemented to investigate the role of ubiquitination pathways which have been implicated in synaptic degeneration (Gillingwater and Wishart, 2013). Ubiquitin-mediated protein degradation, also known as the ubiquitin proteasome system, is an evolutionarily conserved and tightly regulated biochemical pathway (Ding and Shen, 2008, Schlesinger and Goldstein, 1975). Ubiquitination processes are most well-known for their role in targeting proteins for degradation, however it is widely accepted that ubiquitination is a post-translational modification that can influence protein activity and localisation (Kim and Rao, 2006, Pickart and Fushman, 2004). At the synapse, such post-translational changes have been shown to regulate many functions, including endocytosis (Schwarz and Patrick, 2012, d'Azzo et al., 2005), pre- and post-synaptic neurotransmission (Speese et al., 2003, Dreier et al., 2005), and, perhaps most relevant for this discussion, axon pruning and synapse elimination (Zhai et al., 2003, Kuo et al., 2006). Inhibiting the ubiquitin proteasome system through pharmacologic or genetic means has been shown to delay axonal degeneration following nerve transection (Zhai et al., 2003). Increased levels of E1-ubiquitin activating enzyme (Ube1) are also reported in proteomic screens in *Wld*^{S}, suggesting that it plays a role in determining synaptic stability (Wishart et al., 2007).

Mutations in an Ube1 have also been linked to pathogenesis in SMA (Ramser et al., 2008). Mutations in other members of the ubiquitin family have been linked to many other neurodegenerative diseases (Gillingwater and Wishart, 2013).

There is therefore evidence that ubiquitin pathways are involved in the regulation of synaptic stability. If ubiquitin pathways are commonly involved in determining the rate of synaptic degeneration, and since increased levels are reported in Wld^S, then it could be hypothesised that loss of Ube1 would accelerate synaptic loss under different physiological scenarios. This could be tested in a similar way as I have described for P53. For example, we could utilise Ube1 knockout mice to assess how Ube1 knockout can influence the rate of synaptic degeneration in morphologically distinct scenarios. We could introduce Ube1 knockout preparations to the *ex vivo* system to assess how loss of Ube1 impacts synaptic loss in different muscles following injury. We could also cross this knockout mutation into $Smn^{2B/-}$ mice to assess whether Ube1 knockout improves synaptic retention at late-symptomatic time points. Finally, we could assess whether the loss of Ube1 could delay synapse elimination in early postnatal development in different muscles. In this way, the hypothesis that Ube1 is a convergent regulator of synaptic degeneration can be effectively tested. This exemplifies how *ex vivo* assaying can be applied to test another pathway, however ubiquitination pathways are not the only candidate.

Another example could be to test the hypothesis that Rho-kinase (ROCK) signalling pathway inhibition could promote synaptic retention in different contexts. As reviewed by Koch et al., 2018, pathophysiological changes in ROCK signalling have been implicated in a wide range of neurodegenerative diseases, and there is also evidence to support that ROCK activity plays an important role in regulating synaptic function; inhibition of ROCK signalling has been shown to interfere with the induction of apoptotic pathways, and so inhibition of ROCK signalling could have neuroprotective effects (Koch et al., 2018). I have therefore described a workflow which provides the basis to investigate the involvement of other pathways that may influence the rate of synaptic and axonal degeneration.

1.33 *Concluding remarks*

This work has expanded an *ex vivo* model of peripheral nerve injury that provides an invaluable tool with which to investigate mechanisms of axonal and synaptic degeneration. I have demonstrated that this model can be applied to provide novel insight into the mechanistic underpinnings of synaptic and axonal degeneration. Application of this model has allowed me to demonstrate that mechanistic commonality exists between dying-back pathology and WD, which will contribute towards resolving the debate surrounding mechanistic convergence and divergence in morphologically distinct forms of synaptic degeneration. I would like to conclude by reiterating that the importance of understanding mechanisms of synaptic degeneration under different physiological scenarios cannot be understated; by identifying common factors that can alter the rate of synaptic degeneration in different scenarios, we move closer to targeting and preventing neurodegeneration in a range of conditions.

Bibliography

Aloyz RS, Bamji SX, Pozniak CD, et al. (1998) p53 is essential for developmental neuron death as regulated by the TrkA and p75 neurotrophin receptors. *J Cell Biol,* **143,** 1691-703.

Arakawa H (2005) p53, apoptosis and axon-guidance molecules. *Cell Death Differ,* **12,** 1057-65.

Armstrong JF, Kaufman MH, Harrison DJ, Clarke AR (1995) High-frequency developmental abnormalities in p53-deficient mice. *Curr Biol,* **5,** 931-6.

Aubrey BJ, Kelly GL, Janic A, Herold MJ, Strasser A (2018) How does p53 induce apoptosis and how does this relate to p53-mediated tumour suppression? *Cell Death Differ,* **25,** 104-113.

Avery MA, Rooney TM, Pandya JD, et al. (2012) WldS prevents axon degeneration through increased mitochondrial flux and enhanced mitochondrial Ca2+ buffering. *Curr Biol,* **22,** 596-600.

Avery MA, Sheehan AE, Kerr KS, Wang J, Freeman MR (2009) Wld S requires Nmnat1 enzymatic activity and N16-VCP interactions to suppress Wallerian degeneration. *J Cell Biol,* **184,** 501-13.

Babetto E, Beirowski B, Janeckova L, et al. (2010) Targeting NMNAT1 to axons and synapses transforms its neuroprotective potency in vivo. *J Neurosci,* **30,** 13291-304.

Ballatori N, Krance SM, Notenboom S, Shi S, Tieu K, Hammond CL (2009) Glutathione dysregulation and the etiology and progression of human diseases. *Biol Chem,* **390,** 191-214.

Bandmann O, Burton EA (2010) Genetic zebrafish models of neurodegenerative diseases. *Neurobiol Dis,* **40,** 58-65.

Barallobre MJ, Pascual M, Del Rio JA, Soriano E (2005) The Netrin family of guidance factors: emphasis on Netrin-1 signalling. *Brain Res Brain Res Rev,* **49,** 22-47.

Barkeeva LE, Chentsov YS, Skulachev, VP (1981) Ontogenesis of mitochondrial reticulum in rat diaphragm muscle. *Eur J Cell Biol*, **25**, 175-81.

Barrientos SA, Martinez NW, Yoo S, et al. (2011) Axonal degeneration is mediated by the mitochondrial permeability transition pore. *J Neurosci,* **31,** 966-78.

Battaglia G, Princivalle A, Forti F, Lizier C, Zeviani M (1997) Expression of the SMN gene, the spinal muscular atrophy determining gene, in the mammalian central nervous system. *Hum Mol Genet,* **6,** 1961-71.

Baumer D, Lee S, Nicholson G, et al. (2009) Alternative splicing events are a late feature of pathology in a mouse model of spinal muscular atrophy. *PLoS Genet,* **5,** e1000773.

Beal MF (2002) Oxidatively modified proteins in aging and disease. *Free Radic Biol Med,* **32,** 797-803.

Bear MF, Connor BW, Paradiso MA (2007) *Neuroscience: Exploring the Brain,* Lippincott Williams & Wilkins.

Bebee TW, Dominguez CE, Chandler DS (2012) Mouse models of SMA: tools for disease characterization and therapeutic development. *Hum Genet,* **131,** 1277-93.

Becker TS, Rinkwitz S (2012) Zebrafish as a genomics model for human neurological and polygenic disorders. *Dev Neurobiol,* **72,** 415-28.

Bede P, Pradat PF (2019) Editorial: Biomarkers and Clinical Indicators in Motor Neuron Disease. *Front Neurol,* **10,** 1318.

Beirowski B, Adalbert R, Wagner D, et al. (2005) The progressive nature of Wallerian degeneration in wild-type and slow Wallerian degeneration (WldS) nerves. *BMC Neurosci,* **6,** 6.

Beirowski B, Babetto E, Gilley J, et al. (2009) Non-nuclear Wld(S) determines its neuroprotective efficacy for axons and synapses in vivo. *J Neurosci,* **29,** 653-68.

Beirowski B, Berek L, Adalbert R, et al. (2004) Quantitative and qualitative analysis of Wallerian degeneration using restricted axonal labelling in YFP-H mice. *J Neurosci Methods,* **134,** 23-35.

Benard G. Bellance N, Jose C, Rossignol R (2011) Relationships between mitochondrial dynamics and bioenergetics. In *Mitochondrial Dynamics and Neurodegeneration*, Lu B, Ed; Springer Science + Business Media B.V: Dordrecht, Netherlans, 47-68.

Bendszus M, Stoll G (2003) Caught in the act: in vivo mapping of macrophage infiltration in nerve injury by magnetic resonance imaging. *J Neurosci,* **23,** 10892-6.

Billger M, Wallin M, Karlsson JO (1988) Proteolysis of tubulin and microtubule-associated proteins 1 and 2 by calpain I and II. Difference in sensitivity of assembled and disassembled microtubules. *Cell Calcium,* **9,** 33-44.

Birben E, Sahiner UM, Sackesen C, Erzurum S, Kalayci O (2012) Oxidative stress and antioxidant defense. *World Allergy Organ J,* **5,** 9-19.

Bishop DL, Misgeld T, Walsh MK, Gan WB, Lichtman JW (2004) Axon branch removal at developing synapses by axosome shedding. *Neuron,* **44,** 651-61.

Bowerman M, Murray LM, Beauvais A, Pinheiro B, Kothary R (2012) A critical smn threshold in mice dictates onset of an intermediate spinal muscular atrophy phenotype associated with a distinct neuromuscular junction pathology. *Neuromuscul Disord,* **22,** 263-76.

Boyd PJ, Tu WY, Shorrock HK, et al. (2017) Bioenergetic status modulates motor neuron vulnerability and pathogenesis in a zebrafish model of spinal muscular atrophy. *PLoS Genet,* **13,** e1006744.

Brand MD (2010) The sites and topology of mitochondrial superoxide production. *Exp Gerontol,* **45,** 466-72.

Brockington A, Ning K, Heath PR, et al. (2013) Unravelling the enigma of selective vulnerability in neurodegeneration: motor neurons resistant to degeneration in ALS show distinct gene expression characteristics and decreased susceptibility to excitotoxicity. *Acta Neuropathol,* **125,** 95-109.

Brodsky MH, Nordstrom W, Tsang G, Kwan E, Rubin GM, Abrams JM (2000) Drosophila p53 binds a damage response element at the reaper locus. *Cell,* **101,** 103-13.

Brown R, Hynes-Allen A, Swan AJ, Dissanayake KN, Gillingwater TH, Ribchester RR (2015) Activity-dependent degeneration of axotomized neuromuscular synapses in Wld S mice. *Neuroscience,* **290,** 300-20.

Caillaud M, Richard L, Vallat JM, Desmouliere A, Billet F (2019) Peripheral nerve regeneration and intraneural revascularization. *Neural Regen Res,* **14,** 24-33.

Calixto A, Jara JS, Court FA (2012) Diapause formation and downregulation of insulin-like signaling via DAF-16/FOXO delays axonal degeneration and neuronal loss. *PLoS Genet,* **8,** e1003141.

Calliari A, Bobba N, Escande C, Chini EN (2014) Resveratrol delays Wallerian degeneration in a NAD(+) and DBC1 dependent manner. *Exp Neurol,* **251,** 91-100.

Calucho M, Bernal S, Alias L, et al. (2018) Correlation between SMA type and SMN2 copy number revisited: An analysis of 625 unrelated Spanish patients and a compilation of 2834 reported cases. *Neuromuscul Disord,* **28,** 208-215.

Casanova B, Martinez-Bisbal MC, Valero C, et al. (2003) Evidence of Wallerian degeneration in normal appearing white matter in the early stages of relapsing-remitting multiple sclerosis: a HMRS study. *J Neurol,* **250,** 22-8.

Cavanagh JB (1964) The significance of the "dying back" process in experimental and human neurological disease. *Int Rev Exp Pathol,* **3,** 219-67.

Chaytow H, Huang YT, Gillingwater TH, Faller KME (2018) The role of survival motor neuron protein (SMN) in protein homeostasis. *Cell Mol Life Sci,* **75,** 3877-3894.

Chen X, Gays D, Santoro MM (2016) Transgenic Zebrafish. *Methods Mol Biol,* **1464,** 107-114.

Chhabra A, Ahlawat S, Belzberg A, Andreseik G (2014) Peripheral nerve injury grading simplified on MR neurography: As referenced to Seddon and Sunderland classifications. *Indian J Radiol Imaging,* **24,** 217-24.

Chio A, Logroscino G, Hardiman O, et al. (2009) Prognostic factors in ALS: A critical review. *Amyotroph Lateral Scler,* **10,** 310-23.

Ciccarelli O, Werring DJ, Barker GJ, et al. (2003) A study of the mechanisms of normal-appearing white matter damage in multiple sclerosis using diffusion tensor imaging--evidence of Wallerian degeneration. *J Neurol,* **250,** 287-92.

Coady TH, Lorson CL (2011) SMN in spinal muscular atrophy and snRNP biogenesis. *Wiley Interdiscip Rev RNA,* **2,** 546-64.

Coleman M (2005) Axon degeneration mechanisms: commonality amid diversity. *Nat Rev Neurosci,* **6,** 889-98.

Coleman MP, Conforti L, Buckmaster EA, et al. (1998) An 85-kb tandem triplication in the slow Wallerian degeneration (Wlds) mouse. *Proc Natl Acad Sci U S A,* **95,** 9985-90.

Coleman MP, Freeman MR (2010) Wallerian degeneration, wld(s), and nmnat. *Annu Rev Neurosci,* **33,** 245-67.

Comley L, Allodi I, Nichterwitz S, et al. (2015) Motor neurons with differential vulnerability to degeneration show distinct protein signatures in health and ALS. *Neuroscience,* **291,** 216-29.
Comley LH, Nijssen J, Frost-Nylen J, Hedlund E (2016) Cross-disease comparison of amyotrophic lateral sclerosis and spinal muscular atrophy reveals conservation of selective vulnerability but differential neuromuscular junction pathology. *J Comp Neurol,* **524,** 1424-42.
Conforti L, Gilley J, Coleman MP (2014) Wallerian degeneration: an emerging axon death pathway linking injury and disease. *Nat Rev Neurosci,* **15,** 394-409.
Conforti L, Wilbrey A, Morreale G, et al. (2009) Wld S protein requires Nmnat activity and a short N-terminal sequence to protect axons in mice. *J Cell Biol,* **184,** 491-500.
Costanzo EM, Barry JA, Ribchester RR (2000) Competition at silent synapses in reinnervated skeletal muscle. *Nat Neurosci,* **3,** 694-700.
Courtney NL, Mole AJ, Thomson AK, Murray LM (2019) Reduced P53 levels ameliorate neuromuscular junction loss without affecting motor neuron pathology in a mouse model of spinal muscular atrophy. *Cell Death Dis,* **10,** 515.
Crawford TO, Hsieh ST, Schryer BL, Glass JD (1995) Prolonged axonal survival in transected nerves of C57BL/Ola mice is independent of age. *J Neurocytol,* **24,** 333-40.
Cross CE, Halliwell B, Borish ET, et al. (1987) Oxygen radicals and human disease. *Ann Intern Med,* **107,** 526-45.
Culmsee C, Mattson MP (2005) p53 in neuronal apoptosis. *Biochem Biophys Res Commun,* **331,** 761-77.
d'Azzo A, Bongiovanni A, Nastasi T (2005) E3 ubiquitin ligases as regulators of membrane protein trafficking and degradation. *Traffic,* **6,** 429-41.
Daude N, Wohlgemuth S, Brown R, et al. (2012) Knockout of the prion protein (PrP)-like Sprn gene does not produce embryonic lethality in combination with PrP(C)-deficiency. *Proc Natl Acad Sci U S A,* **109,** 9035-40.
David S, Ousman SS (2002) Recruiting the immune response to promote axon regeneration in the injured spinal cord. *Neuroscientist,* **8,** 33-41.
Di Giovanni S, Knights CD, Rao M, et al. (2006) The tumor suppressor protein p53 is required for neurite outgrowth and axon regeneration. *EMBO J,* **25,** 4084-96.
Di Stefano M, Nascimento-Ferreira I, Orsomando G, et al. (2015) A rise in NAD precursor nicotinamide mononucleotide (NMN) after injury promotes axon degeneration. *Cell Death Differ,* **22,** 731-42.
DiDonato CJ, Lorson CL, De Repentigny Y, et al. (2001) Regulation of murine survival motor neuron (Smn) protein levels by modifying Smn exon 7 splicing. *Hum Mol Genet,* **10,** 2727-36.
Ding M, Shen K (2008) The role of the ubiquitin proteasome system in synapse remodeling and neurodegenerative diseases. *Bioessays,* **30,** 1075-83.
Dreier L, Burbea M, Kaplan JM (2005) LIN-23-mediated degradation of beta-catenin regulates the abundance of GLR-1 glutamate receptors in the ventral nerve cord of C. elegans. *Neuron,* **46,** 51-64.

Du H, Guo L, Yan S, Sosunov AA, McKhann GM, Yan SS (2010) Early deficits in synaptic mitochondria in an Alzheimer's disease mouse model. *Proc Natl Acad Sci U S A,* **107,** 18670-5.
Ducker GS, Rabinowitz JD (2017) One-Carbon Metabolism in Health and Disease. *Cell Metab,* **25,** 27-42.
Eizenberg O, Faber-Elman A, Gottlieb E, Oren M, Rotter V, Schwartz M (1996) p53 plays a regulatory role in differentiation and apoptosis of central nervous system-associated cells. *Mol Cell Biol,* **16,** 5178-85.
El-Brolosy MA, Stainier DYR (2017) Genetic compensation: A phenomenon in search of mechanisms. *PLoS Genet,* **13,** e1006780.
Eliyahu D, Michalovitz D, Eliyahu S, Pinhasi-Kimhi O, Oren M (1989) Wild-type p53 can inhibit oncogene-mediated focus formation. *Proc Natl Acad Sci U S A,* **86,** 8763-7.
Elmore S (2007) Apoptosis: a review of programmed cell death. *Toxicol Pathol,* **35,** 495-516.
Elsheikh B, Prior T, Zhang X, et al. (2009) An analysis of disease severity based on SMN2 copy number in adults with spinal muscular atrophy. *Muscle Nerve,* **40,** 652-6.
Essuman K, Summers DW, Sasaki Y, Mao X, DiAntonio A, Milbrandt J (2017) The SARM1 Toll/Interleukin-1 Receptor Domain Possesses Intrinsic NAD(+) Cleavage Activity that Promotes Pathological Axonal Degeneration. *Neuron,* **93,** 1334-1343 e5.
Ferrer I, Lopez-Gonzalez I, Carmona M, Dalfo E, Pujol A, Martinez A (2012) Neurochemistry and the non-motor aspects of PD. *Neurobiol Dis,* **46,** 508-26.
Ferri A, Sanes JR, Coleman MP, Cunningham JM, Kato AC (2003) Inhibiting axon degeneration and synapse loss attenuates apoptosis and disease progression in a mouse model of motoneuron disease. *Curr Biol,* **13,** 669-73.
Finlay CA, Hinds PW, Levine AJ (1989) The p53 proto-oncogene can act as a suppressor of transformation. *Cell,* **57,** 1083-93.
Fischer LR, Culver DG, Davis AA, et al. (2005) The WldS gene modestly prolongs survival in the SOD1G93A fALS mouse. *Neurobiol Dis,* **19,** 293-300.
Fridman JS, Lowe SW (2003) Control of apoptosis by p53. *Oncogene,* **22,** 9030-40.
Futamura M, Kamino H, Miyamoto Y, et al. (2007) Possible role of semaphorin 3F, a candidate tumor suppressor gene at 3p21.3, in p53-regulated tumor angiogenesis suppression. *Cancer Res,* **67,** 1451-60.
Geden MJ, Deshmukh M (2016) Axon degeneration: context defines distinct pathways. *Curr Opin Neurobiol,* **39,** 108-15.
George EB, Glass JD, Griffin JW (1995) Axotomy-induced axonal degeneration is mediated by calcium influx through ion-specific channels. *J Neurosci,* **15,** 6445-52.
Giachin G, Bouverot R, Acajjaoui S, Pantalone S, Soler-Lopez M (2016) Dynamics of Human Mitochondrial Complex I Assembly: Implications for Neurodegenerative Diseases. *Front Mol Biosci,* **3,** 43.

Giavazzi A, Setola V, Simonati A, Battaglia G (2006) Neuronal-specific roles of the survival motor neuron protein: evidence from survival motor neuron expression patterns in the developing human central nervous system. *J Neuropathol Exp Neurol,* **65,** 267-77.

Gilley J, Adalbert R, Yu G, Coleman MP (2013) Rescue of peripheral and CNS axon defects in mice lacking NMNAT2. *J Neurosci,* **33,** 13410-24.

Gilley J, Coleman MP (2010) Endogenous Nmnat2 is an essential survival factor for maintenance of healthy axons. *PLoS Biol,* **8,** e1000300.

Gilley J, Orsomando G, Nascimento-Ferreira I, Coleman MP (2015) Absence of SARM1 rescues development and survival of NMNAT2-deficient axons. *Cell Rep,* **10,** 1974-81.

Gillingwater TH, Haley JE, Ribchester RR, Horsburgh K (2004) Neuroprotection after transient global cerebral ischemia in Wld(s) mutant mice. *J Cereb Blood Flow Metab,* **24,** 62-6.

Gillingwater TH, Ingham CA, Coleman MP, Ribchester RR (2003) Ultrastructural correlates of synapse withdrawal at axotomized neuromuscular junctions in mutant and transgenic mice expressing the Wld gene. *J Anat,* **203,** 265-76.

Gillingwater TH, Ingham CA, Parry KE, et al. (2006) Delayed synaptic degeneration in the CNS of Wlds mice after cortical lesion. *Brain,* **129,** 1546-56.

Gillingwater TH, Ribchester RR (2001) Compartmental neurodegeneration and synaptic plasticity in the Wld(s) mutant mouse. *J Physiol,* **534,** 627-39.

Gillingwater TH, Ribchester RR (2003) The relationship of neuromuscular synapse elimination to synaptic degeneration and pathology: insights from WldS and other mutant mice. *J Neurocytol,* **32,** 863-81.

Gillingwater TH, Thomson D, Mack TG, et al. (2002) Age-dependent synapse withdrawal at axotomised neuromuscular junctions in Wld(s) mutant and Ube4b/Nmnat transgenic mice. *J Physiol,* **543,** 739-55.

Gillingwater TH, Wishart TM (2013) Mechanisms underlying synaptic vulnerability and degeneration in neurodegenerative disease. *Neuropathol Appl Neurobiol,* **39,** 320-34.

Gilman CP, Chan SL, Guo Z, Zhu X, Greig N, Mattson MP (2003) p53 is present in synapses where it mediates mitochondrial dysfunction and synaptic degeneration in response to DNA damage, and oxidative and excitotoxic insults. *Neuromolecular Med,* **3,** 159-72.

Gilman CP, Mattson MP (2002) Do apoptotic mechanisms regulate synaptic plasticity and growth-cone motility? *Neuromolecular Med,* **2,** 197-214.

Glancy B, Hartnell LM, Malide D, Yu Z, Combs CA, Connelly PS, Subramaniam S, Balaban RS (2015) Mitochondrial reticulum for cellular energy distribution in muscle. *Nature*, **523**, 617-20.

Glass JD, Schryer BL, Griffin JW (1994) Calcium-mediated degeneration of the axonal cytoskeleton in the Ola mouse. *J Neurochem,* **62,** 2472-5.

Goda Y, Davis GW (2003) Mechanisms of synapse assembly and disassembly. *Neuron,* **40,** 243-64.

Golubitzky A, Dan P, Weissman S, Link G, Wikstrom JD, Saada A (2011) Screening for active small molecules in mitochondrial complex I

deficient patient's fibroblasts, reveals AICAR as the most beneficial compound. *PLoS One,* **6,** e26883.

Goulet BB, Kothary R, Parks RJ (2013) At the "junction" of spinal muscular atrophy pathogenesis: the role of neuromuscular junction dysfunction in SMA disease progression. *Curr Mol Med,* **13,** 1160-74.

Graham LC, Eaton SL, Brunton PJ, et al. (2017) Proteomic profiling of neuronal mitochondria reveals modulators of synaptic architecture. *Mol Neurodegener,* **12,** 77.

Griffin JW, George EB, Hsieh ST, Glass JD (1995) Axonal degeneration and disorders of the axonal cytoskeleton. In *The Axon: Structure, Function and Pathophysiology* (eds Waxman SG, Kocsis JD, Stys PK), pp. 375-390. NY: Oxford University Press.

Hagenacker T, Wurster CD, Gunther R, et al. (2020) Nusinersen in adults with 5q spinal muscular atrophy: a non-interventional, multicentre, observational cohort study. *Lancet Neurol,* **19,** 317-325.

Hahnen E, Forkert R, Marke C, et al. (1995) Molecular analysis of candidate genes on chromosome 5q13 in autosomal recessive spinal muscular atrophy: evidence of homozygous deletions of the SMN gene in unaffected individuals. *Hum Mol Genet,* **4,** 1927-33.

Hamilton G, Gillingwater TH (2013) Spinal muscular atrophy: going beyond the motor neuron. *Trends Mol Med,* **19,** 40-50.

Hammond SM, Gogliotti RG, Rao V, Beauvais A, Kothary R, DiDonato CJ (2010) Mouse survival motor neuron alleles that mimic SMN2 splicing and are inducible rescue embryonic lethality early in development but not late. *PLoS One,* **5,** e15887.

Han C, Jan LY, Jan YN (2011) Enhancer-driven membrane markers for analysis of nonautonomous mechanisms reveal neuron-glia interactions in Drosophila. *Proc Natl Acad Sci U S A,* **108,** 9673-8.

Harel NY, Strittmatter SM (2006) Can regenerating axons recapitulate developmental guidance during recovery from spinal cord injury? *Nat Rev Neurosci,* **7,** 603-16.

Harrington AW, Ginty DD (2013) Long-distance retrograde neurotrophic factor signalling in neurons. *Nat Rev Neurosci,* **14,** 177-87.

Hedlund E, Karlsson M, Osborn T, Ludwig W, Isacson O (2010) Global gene expression profiling of somatic motor neuron populations with different vulnerability identify molecules and pathways of degeneration and protection. *Brain,* **133,** 2313-30.

Hinerfeld D, Traini MD, Weinberger RP, et al. (2004) Endogenous mitochondrial oxidative stress: neurodegeneration, proteomic analysis, specific respiratory chain defects, and efficacious antioxidant therapy in superoxide dismutase 2 null mice. *J Neurochem,* **88,** 657-67.

Hirsch NP (2007) Neuromuscular junction in health and disease. *Br J Anaesth,* **99,** 132-8.

Horner PJ, Gage FH (2000) Regenerating the damaged central nervous system. *Nature,* **407,** 963-70.

Hsieh-Li HM, Chang JG, Jong YJ, et al. (2000) A mouse model for spinal muscular atrophy. *Nat Genet,* **24,** 66-70.

Huang da W, Sherman BT, Lempicki RA (2009) Systematic and integrative analysis of large gene lists using DAVID bioinformatics resources. *Nat Protoc,* **4,** 44-57.
Huang EJ, Reichardt LF (2001) Neurotrophins: roles in neuronal development and function. *Annu Rev Neurosci,* **24,** 677-736.
Huang YT, van der Hoorn D, Ledahawsky LM, et al. (2019) Robust Comparison of Protein Levels Across Tissues and Throughout Development Using Standardized Quantitative Western Blotting. *J Vis Exp*.
Hussain G, Wang J, Rasul A, et al. (2020) Current Status of Therapeutic Approaches against Peripheral Nerve Injuries: A Detailed Story from Injury to Recovery. *Int J Biol Sci,* **16,** 116-134.
Jacobs WB, Govoni G, Ho D, et al. (2005) p63 is an essential proapoptotic protein during neural development. *Neuron,* **48,** 743-56.
Jager S, Handschin C, St-Pierre J, Spiegelman BM (2007) AMP-activated protein kinase (AMPK) action in skeletal muscle via direct phosphorylation of PGC-1alpha. *Proc Natl Acad Sci U S A,* **104,** 12017-22.
Jangi M, Fleet C, Cullen P, et al. (2017) SMN deficiency in severe models of spinal muscular atrophy causes widespread intron retention and DNA damage. *Proc Natl Acad Sci U S A,* **114,** E2347-E2356.
Jedrzejowska M, Borkowska J, Zimowski J, et al. (2008) Unaffected patients with a homozygous absence of the SMN1 gene. *Eur J Hum Genet,* **16,** 930-4.
Jin S, Martinek S, Joo WS, et al. (2000) Identification and characterization of a p53 homologue in Drosophila melanogaster. *Proc Natl Acad Sci U S A,* **97,** 7301-6.
Johnson GV, Litersky JM, Jope RS (1991) Degradation of microtubule-associated protein 2 and brain spectrin by calpain: a comparative study. *J Neurochem,* **56,** 1630-8.
Kampfl A, Posmantur R, Nixon R, et al. (1996) mu-calpain activation and calpain-mediated cytoskeletal proteolysis following traumatic brain injury. *J Neurochem,* **67,** 1575-83.
Kaplan A, Spiller KJ, Towne C, et al. (2014) Neuronal matrix metalloproteinase-9 is a determinant of selective neurodegeneration. *Neuron,* **81,** 333-48.
Kaplan DR, Miller FD (2000) Neurotrophin signal transduction in the nervous system. *Curr Opin Neurobiol,* **10,** 381-91.
Kariya S, Mauricio R, Dai Y, Monani UR (2009) The neuroprotective factor Wld(s) fails to mitigate distal axonal and neuromuscular junction (NMJ) defects in mouse models of spinal muscular atrophy. *Neurosci Lett,* **449,** 246-51.
Kariya S, Park GH, Maeno-Hikichi Y, et al. (2008) Reduced SMN protein impairs maturation of the neuromuscular junctions in mouse models of spinal muscular atrophy. *Hum Mol Genet,* **17,** 2552-69.
Kawamata M, Ochiya T (2012) Two distinct knockout approaches highlight a critical role for p53 in rat development. *Sci Rep,* **2,** 945.

Kerschensteiner M, Schwab ME, Lichtman JW, Misgeld T (2005) In vivo imaging of axonal degeneration and regeneration in the injured spinal cord. *Nat Med,* **11,** 572-7.
Kim I, Rao H (2006) What's Ub chain linkage got to do with it? *Sci STKE,* **2006,** pe18.
Kim Y, Yang DS, Katti P, Glancy B (2019) Protein composition of the muscle mitochondrial reticulum during postnatal development. *J Physiol,* **597,** 2707-2727.
Kline RA, Dissanayake KN, Hurtado ML, et al. (2019) Altered mitochondrial bioenergetics are responsible for the delay in Wallerian degeneration observed in neonatal mice. *Neurobiol Dis,* **130,** 104496.
Kline RA, Kaifer KA, Osman EY, et al. (2017) Comparison of independent screens on differentially vulnerable motor neurons reveals alpha-synuclein as a common modifier in motor neuron diseases. *PLoS Genet,* **13,** e1006680.
Knoferle J, Koch JC, Ostendorf T, et al. (2010) Mechanisms of acute axonal degeneration in the optic nerve in vivo. *Proc Natl Acad Sci U S A,* **107,** 6064-9.
Koch JC, Tatenhorst L, Roser AE, Saal KA, Tonges L, Lingor P (2018) ROCK inhibition in models of neurodegeneration and its potential for clinical translation. *Pharmacol Ther,* **189,** 1-21.
Kolb SJ, Kissel JT (2015) Spinal Muscular Atrophy. *Neurol Clin,* **33,** 831-46.
Kowaltowski AJ, de Souza-Pinto NC, Castilho RF, Vercesi AE (2009) Mitochondria and reactive oxygen species. *Free Radic Biol Med,* **47,** 333-43.
Kuo CT, Zhu S, Younger S, Jan LY, Jan YN (2006) Identification of E2/E3 ubiquitinating enzymes and caspase activity regulating Drosophila sensory neuron dendrite pruning. *Neuron,* **51,** 283-90.
Lanuza MA, Tomas J, Garcia N, Cilleros V, Borras L, Tomas M (2018) Axonal competition and synapse elimination during neuromuscular junction development. *Curr Opin in Physiology,* **4,** 25-31.
Larsen S, Nielsen J, Hansen CN, et al. (2012) Biomarkers of mitochondrial content in skeletal muscle of healthy young human subjects. *J Physiol,* **590,** 3349-60.
Le TT, Pham LT, Butchbach ME, et al. (2005) SMNDelta7, the major product of the centromeric survival motor neuron (SMN2) gene, extends survival in mice with spinal muscular atrophy and associates with full-length SMN. *Hum Mol Genet,* **14,** 845-57.
Lee SH, Kim KR, Ryu SY, et al. (2012) Impaired short-term plasticity in mossy fiber synapses caused by mitochondrial dysfunction of dentate granule cells is the earliest synaptic deficit in a mouse model of Alzheimer's disease. *J Neurosci,* **32,** 5953-63.
Lee YI (2020) Developmental neuromuscular synapse elimination: Activity-dependence and potential downstream effector mechanisms. *Neurosci Lett,* **718,** 134724.
Lefebvre S, Burglen L, Reboullet S, et al. (1995) Identification and characterization of a spinal muscular atrophy-determining gene. *Cell,* **80,** 155-65.

Li J, Yuan J (2008) Caspases in apoptosis and beyond. *Oncogene,* **27,** 6194-206.
Li R, Liu Z, Pan Y, Chen L, Zhang Z, Lu L (2014) Peripheral nerve injuries treatment: a systematic review. *Cell Biochem Biophys,* **68,** 449-54.
Li Y, Park JS, Deng JH, Bai Y (2006) Cytochrome c oxidase subunit IV is essential for assembly and respiratory function of the enzyme complex. *J Bioenerg Biomembr,* **38,** 283-91.
Lichtman JW, Colman H (2000) Synapse elimination and indelible memory. *Neuron,* **25,** 269-78.
Lienhart WD, Gudipati V, Macheroux P (2013) The human flavoproteome. *Arch Biochem Biophys,* **535,** 150-62.
Liu P, Peng J, Han GH, et al. (2019) Role of macrophages in peripheral nerve injury and repair. *Neural Regen Res,* **14,** 1335-1342.
Llavero Hurtado M, Fuller HR, Wong AMS, et al. (2017) Proteomic mapping of differentially vulnerable pre-synaptic populations identifies regulators of neuronal stability in vivo. *Sci Rep,* **7,** 12412.
Llobet Rosell A, Neukomm LJ (2019) Axon death signalling in Wallerian degeneration among species and in disease. *Open Biol,* **9,** 190118.
Lopez-Erauskin J, Fourcade S, Galino J, et al. (2011) Antioxidants halt axonal degeneration in a mouse model of X-adrenoleukodystrophy. *Ann Neurol,* **70,** 84-92.
Loreto A, Hill CS, Hewitt VL, et al. (2020) Mitochondrial impairment activates the Wallerian pathway through depletion of NMNAT2 leading to SARM1-dependent axon degeneration. *Neurobiol Dis,* **134,** 104678.
Luiro K, Kopra O, Blom T, et al. (2006) Batten disease (JNCL) is linked to disturbances in mitochondrial, cytoskeletal, and synaptic compartments. *J Neurosci Res,* **84,** 1124-38.
Lunn ER, Perry VH, Brown MC, Rosen H, Gordon S (1989) Absence of Wallerian Degeneration does not Hinder Regeneration in Peripheral Nerve. *Eur J Neurosci,* **1,** 27-33.
Lunn MR, Wang CH (2008) Spinal muscular atrophy. *Lancet,* **371,** 2120-33.
Luo L, O'Leary DD (2005) Axon retraction and degeneration in development and disease. *Annu Rev Neurosci,* **28,** 127-56.
Mack TG, Reiner M, Beirowski B, et al. (2001) Wallerian degeneration of injured axons and synapses is delayed by a Ube4b/Nmnat chimeric gene. *Nat Neurosci,* **4,** 1199-206.
Malek MH, Huttemann M, Lee I (2018) Mitochondrial Structure, Function, and Dynamics: The Common Thread across Organs, Disease, and Aging. *Oxid Med Cell Longev,* **2018,** 1863414.
Malik AN, Czajka A (2013) Is mitochondrial DNA content a potential biomarker of mitochondrial dysfunction? *Mitochondrion,* **13,** 481-92.
Maor-Nof M, Romi E, Sar Shalom H, et al. (2016) Axonal Degeneration Is Regulated by a Transcriptional Program that Coordinates Expression of Pro- and Anti-degenerative Factors. *Neuron,* **92,** 991-1006.
Maor-Nof M, Yaron A (2013) Neurite pruning and neuronal cell death: spatial regulation of shared destruction programs. *Curr Opin Neurobiol,* **23,** 990-6.

Marino S, Vooijs M, van Der Gulden H, Jonkers J, Berns A (2000) Induction of medulloblastomas in p53-null mutant mice by somatic inactivation of Rb in the external granular layer cells of the cerebellum. *Genes Dev,* **14,** 994-1004.

Martin LJ, Liu Z, Chen K, et al. (2007) Motor neuron degeneration in amyotrophic lateral sclerosis mutant superoxide dismutase-1 transgenic mice: mechanisms of mitochondriopathy and cell death. *J Comp Neurol,* **500,** 20-46.

Martineau E, Di Polo A, Vande Velde C, Robitaille R (2018) Dynamic neuromuscular remodeling precedes motor-unit loss in a mouse model of ALS. *Elife,* **7**.

Martinez-Hernandez R, Bernal S, Also-Rallo E, et al. (2013) Synaptic defects in type I spinal muscular atrophy in human development. *J Pathol,* **229,** 49-61.

Mattson MP (2000) Apoptotic and anti-apoptotic synaptic signaling mechanisms. *Brain Pathol,* **10,** 300-12.

McGurk L, Berson A, Bonini NM (2015) Drosophila as an In Vivo Model for Human Neurodegenerative Disease. *Genetics,* **201,** 377-402.

McIlwain DR, Berger T, Mak TW (2013) Caspase functions in cell death and disease. *Cold Spring Harb Perspect Biol,* **5,** a008656.

McWhorter ML, Monani UR, Burghes AH, Beattie CE (2003) Knockdown of the survival motor neuron (Smn) protein in zebrafish causes defects in motor axon outgrowth and pathfinding. *J Cell Biol,* **162,** 919-31.

Melov S, Doctrow SR, Schneider JA, et al. (2001) Lifespan extension and rescue of spongiform encephalopathy in superoxide dismutase 2 nullizygous mice treated with superoxide dismutase-catalase mimetics. *J Neurosci,* **21,** 8348-53.

Melov S, Schneider JA, Day BJ, et al. (1998) A novel neurological phenotype in mice lacking mitochondrial manganese superoxide dismutase. *Nat Genet,* **18,** 159-63.

Mendell JR, Al-Zaidy S, Shell R, et al. (2017a) AVXS-101 phase 1 gene therapy clinical trial in SMA Type 1: end-of-Study event free survival and achievement of developmental milestones. *Neuromuscul Disord,* **27,** S208.

Mendell JR, Al-Zaidy S, Shell R, et al. (2017b) Single-Dose Gene-Replacement Therapy for Spinal Muscular Atrophy. *N Engl J Med,* **377,** 1713-1722.

Menorca RM, Fussell TS, Elfar JC (2013) Nerve physiology: mechanisms of injury and recovery. *Hand Clin,* **29,** 317-30.

Menzies FM, Ince PG, Shaw PJ (2002) Mitochondrial involvement in amyotrophic lateral sclerosis. *Neurochem Int,* **40,** 543-51.

Mercuri E, Finkel RS, Kirschner J, et al. (2017) Efficacy and safety of nusinersen in children with later-onset spinal muscular atrophy (SMA): end of study results from the phase 3 CHERISH study. *Neuromuscul Disord,* **27,** S210.

Merlo P, Frost B, Peng S, Yang YJ, Park PJ, Feany M (2014) p53 prevents neurodegeneration by regulating synaptic genes. *Proc Natl Acad Sci U S A,* **111,** 18055-60.

Mi W, Beirowski B, Gillingwater TH, et al. (2005) The slow Wallerian degeneration gene, WldS, inhibits axonal spheroid pathology in gracile axonal dystrophy mice. *Brain,* **128,** 405-16.
Milde S, Gilley J, Coleman MP (2013) Subcellular localization determines the stability and axon protective capacity of axon survival factor Nmnat2. *PLoS Biol,* **11,** e1001539.
Miledi R, Slater CR (1968) Electrophysiology and electron-microscopy of rat neuromuscular junctions after nerve degeneration. *Proc R Soc Lond B Biol Sci,* **169,** 289-306.
Miledi R, Slater CR (1970) On the degeneration of rat neuromuscular junctions after nerve section. *J Physiol,* **207,** 507-28.
Miller BR, Press C, Daniels RW, Sasaki Y, Milbrandt J, DiAntonio A (2009) A dual leucine kinase-dependent axon self-destruction program promotes Wallerian degeneration. *Nat Neurosci,* **12,** 387-9.
Miller N, Shi H, Zelikovich AS, Ma YC (2016) Motor neuron mitochondrial dysfunction in spinal muscular atrophy. *Hum Mol Genet,* **25,** 3395-3406.
Mitchell J, Paul P, Chen HJ, et al. (2010) Familial amyotrophic lateral sclerosis is associated with a mutation in D-amino acid oxidase. *Proc Natl Acad Sci U S A,* **107,** 7556-61.
Moldovan M, Alvarez S, Krarup C (2009) Motor axon excitability during Wallerian degeneration. *Brain,* **132,** 511-23.
Mole AJ, Bell S, Thomson AK, Dissanayake KN, Ribchester RR, Murray LM (2020) Synaptic withdrawal following nerve injury is influenced by postnatal maturity, muscle-specific properties, and the presence of underlying pathology in mice. *J Anat*.
Monani UR (2005) Spinal muscular atrophy: a deficiency in a ubiquitous protein; a motor neuron-specific disease. *Neuron,* **48,** 885-96.
Monani UR, De Vivo DC (2014) Neurodegeneration in spinal muscular atrophy: from disease phenotype and animal models to therapeutic strategies and beyond. *Future Neurol,* **9,** 49-65.
Monani UR, Sendtner M, Coovert DD, et al. (2000) The human centromeric survival motor neuron gene (SMN2) rescues embryonic lethality in Smn(-/-) mice and results in a mouse with spinal muscular atrophy. *Hum Mol Genet,* **9,** 333-9.
Murray L, Gillingwater TH, Kothary R (2014) Dissection of the transversus abdominis muscle for whole-mount neuromuscular junction analysis. *J Vis Exp***,** e51162.
Murray LM, Beauvais A, Bhanot K, Kothary R (2013) Defects in neuromuscular junction remodelling in the Smn(2B/-) mouse model of spinal muscular atrophy. *Neurobiol Dis,* **49,** 57-67.
Murray LM, Beauvais A, Gibeault S, Courtney NL, Kothary R (2015) Transcriptional profiling of differentially vulnerable motor neurons at pre-symptomatic stage in the Smn (2b/-) mouse model of spinal muscular atrophy. *Acta Neuropathol Commun,* **3,** 55.
Murray LM, Comley LH, Gillingwater TH, Parson SH (2011) The response of neuromuscular junctions to injury is developmentally regulated. *FASEB J,* **25,** 1306-13.

Murray LM, Comley LH, Thomson D, Parkinson N, Talbot K, Gillingwater TH (2008a) Selective vulnerability of motor neurons and dissociation of pre- and post-synaptic pathology at the neuromuscular junction in mouse models of spinal muscular atrophy. *Hum Mol Genet,* **17,** 949-62.

Murray LM, Gillingwater TH, Parson SH (2010) Using mouse cranial muscles to investigate neuromuscular pathology in vivo. *Neuromuscul Disord,* **20,** 740-3.

Murray LM, Thomson D, Conklin A, Wishart TM, Gillingwater TH (2008b) Loss of translation elongation factor (eEF1A2) expression in vivo differentiates between Wallerian degeneration and dying-back neuronal pathology. *J Anat,* **213,** 633-45.

Neary MT, Ng KE, Ludtmann MH, et al. (2014) Hypoxia signaling controls postnatal changes in cardiac mitochondrial morphology and function. *J Mol Cell Cardiol,* **74,** 340-52.

Neve A, Trub J, Saxena S, Schumperli D (2016) Central and peripheral defects in motor units of the diaphragm of spinal muscular atrophy mice. *Mol Cell Neurosci,* **70,** 30-41.

Newbery HJ, Gillingwater TH, Dharmasaroja P, et al. (2005) Progressive loss of motor neuron function in wasted mice: effects of a spontaneous null mutation in the gene for the eEF1 A2 translation factor. *J Neuropathol Exp Neurol,* **64,** 295-303.

Nikolaev A, McLaughlin T, O'Leary DD, Tessier-Lavigne M (2009) APP binds DR6 to trigger axon pruning and neuron death via distinct caspases. *Nature,* **457,** 981-9.

O'Donnell KC, Vargas ME, Sagasti A (2013) WldS and PGC-1alpha regulate mitochondrial transport and oxidation state after axonal injury. *J Neurosci,* **33,** 14778-90.

Ochi K, Mori T, Toyama Y, Nakamura Y, Arakawa H (2002) Identification of semaphorin3B as a direct target of p53. *Neoplasia,* **4,** 82-7.

Ollmann M, Young LM, Di Como CJ, et al. (2000) Drosophila p53 is a structural and functional homolog of the tumor suppressor p53. *Cell,* **101,** 91-101.

Oprea GE, Krober S, McWhorter ML, et al. (2008) Plastin 3 is a protective modifier of autosomal recessive spinal muscular atrophy. *Science,* **320,** 524-7.

Osman EY, Rietz A, Kline RA, et al. (2019) Intraperitoneal delivery of a novel drug-like compound improves disease severity in severe and intermediate mouse models of Spinal Muscular Atrophy. *Sci Rep,* **9,** 1633.

Osterloh JM, Yang J, Rooney TM, et al. (2012) dSarm/Sarm1 is required for activation of an injury-induced axon death pathway. *Science,* **337,** 481-4.

Oyebode OR, Hartley R, Singhota J, Thomson D, Ribchester RR (2012) Differential protection of neuromuscular sensory and motor axons and their endings in Wld(S) mutant mice. *Neuroscience,* **200,** 142-58.

Park JY, Jang SY, Shin YK, et al. (2013) Mitochondrial swelling and microtubule depolymerization are associated with energy depletion in axon degeneration. *Neuroscience,* **238,** 258-69.

Parson SH, Mackintosh CL, Ribchester RR (1997) Elimination of motor nerve terminals in neonatal mice expressing a gene for slow wallerian degeneration (C57Bl/Wlds). *Eur J Neurosci,* **9,** 1586-92.
Pasterkamp RJ, Verhaagen J (2006) Semaphorins in axon regeneration: developmental guidance molecules gone wrong? *Philos Trans R Soc Lond B Biol Sci,* **361,** 1499-511.
Perry VH, Brown MC, Tsao JW (1992) The Effectiveness of the Gene Which Slows the Rate of Wallerian Degeneration in C57BL/Ola Mice Declines With Age. *Eur J Neurosci,* **4,** 1000-2.
Personius KE, Slusher BS, Udin SB (2016) Neuromuscular NMDA Receptors Modulate Developmental Synapse Elimination. *J Neurosci,* **36,** 8783-9.
Picard M, Hepple RT, Burelle Y (2012) Mitochondrial functional specialization in glycolytic and oxidative muscle fibers: tailoring the organelle for optimal function. *Am J Physiol Cell Physiol,* **302,** C629-41.
Pickart CM, Fushman D (2004) Polyubiquitin chains: polymeric protein signals. *Curr Opin Chem Biol,* **8,** 610-6.
Portera-Cailliau C, Weimer RM, De Paola V, Caroni P, Svoboda K (2005) Diverse modes of axon elaboration in the developing neocortex. *PLoS Biol,* **3,** e272.
Pozniak CD, Barnabe-Heider F, Rymar VV, Lee AF, Sadikot AF, Miller FD (2002) p73 is required for survival and maintenance of CNS neurons. *J Neurosci,* **22,** 9800-9.
Pozniak CD, Radinovic S, Yang A, McKeon F, Kaplan DR, Miller FD (2000) An anti-apoptotic role for the p53 family member, p73, during developmental neuron death. *Science,* **289,** 304-6.
Press C, Milbrandt J (2008) Nmnat delays axonal degeneration caused by mitochondrial and oxidative stress. *J Neurosci,* **28,** 4861-71.
Prior TW, Krainer AR, Hua Y, et al. (2009) A positive modifier of spinal muscular atrophy in the SMN2 gene. *Am J Hum Genet,* **85,** 408-13.
Puente BN, Kimura W, Muralidhar SA, et al. (2014) The oxygen-rich postnatal environment induces cardiomyocyte cell-cycle arrest through DNA damage response. *Cell,* **157,** 565-79.
Quiros PM, Goyal A, Jha P, Auwerx J (2017) Analysis of mtDNA/nDNA Ratio in Mice. *Curr Protoc Mouse Biol,* **7,** 47-54.
Raff MC, Whitmore AV, Finn JT (2002) Axonal self-destruction and neurodegeneration. *Science,* **296,** 868-71.
Ramser J, Ahearn ME, Lenski C, et al. (2008) Rare missense and synonymous variants in UBE1 are associated with X-linked infantile spinal muscular atrophy. *Am J Hum Genet,* **82,** 188-93.
Ratni H, Ebeling M, Baird J, et al. (2018) Discovery of Risdiplam, a Selective Survival of Motor Neuron-2 (SMN2) Gene Splicing Modifier for the Treatment of Spinal Muscular Atrophy (SMA). *J Med Chem,* **61,** 6501-6517.
Redfern PA (1970) Neuromuscular transmission in new-born rats. *J Physiol,* **209,** 701-9.
Reedich EJ, Kalski M, Armijo N, Cox GA, DiDonato C (2021) Spinal motor neuron loss occurs through a p53-and-p21-independent mechanism in

the Smn2B/- mouse model of spinal muscular atrophy. *Experimental Neurology*, **337,** 113587.

Ribchester RR, Tsao JW, Barry JA, Asgari-Jirhandeh N, Perry VH, Brown MC (1995) Persistence of neuromuscular junctions after axotomy in mice with slow Wallerian degeneration (C57BL/WldS). *Eur J Neurosci,* **7,** 1641-50.

Rochette CF, Gilbert N, Simard LR (2001) SMN gene duplication and the emergence of the SMN2 gene occurred in distinct hominids: SMN2 is unique to Homo sapiens. *Hum Genet,* **108,** 255-66.

Rodrigues NR, Owen N, Talbot K, Ignatius J, Dubowitz V, Davies KE (1995) Deletions in the survival motor neuron gene on 5q13 in autosomal recessive spinal muscular atrophy. *Hum Mol Genet,* **4,** 631-4.

Rose FF, Jr., Meehan PW, Coady TH, Garcia VB, Garcia ML, Lorson CL (2008) The Wallerian degeneration slow (Wld(s)) gene does not attenuate disease in a mouse model of spinal muscular atrophy. *Biochem Biophys Res Commun,* **375,** 119-23.

Rosenthal JL, Taraskevich PS (1977) Reduction of multiaxonal innervation at the neuromuscular junction of the rat during development. *J Physiol,* **270,** 299-310.

Rossi A, Kontarakis Z, Gerri C, et al. (2015) Genetic compensation induced by deleterious mutations but not gene knockdowns. *Nature,* **524,** 230-3.

Sah VP, Attardi LD, Mulligan GJ, Williams BO, Bronson RT, Jacks T (1995) A subset of p53-deficient embryos exhibit exencephaly. *Nat Genet,* **10,** 175-80.

Sajadi A, Schneider BL, Aebischer P (2004) Wlds-mediated protection of dopaminergic fibers in an animal model of Parkinson disease. *Curr Biol,* **14,** 326-30.

Samsam M, Mi W, Wessig C, et al. (2003) The Wlds mutation delays robust loss of motor and sensory axons in a genetic model for myelin-related axonopathy. *J Neurosci,* **23,** 2833-9.

Sanes JR, Lichtman JW (1999) Development of the vertebrate neuromuscular junction. *Annu Rev Neurosci,* **22,** 389-442.

Sanes JR, Lichtman JW (2001) Induction, assembly, maturation and maintenance of a postsynaptic apparatus. *Nat Rev Neurosci,* **2,** 791-805.

Sareen D, Ebert AD, Heins BM, McGivern JV, Ornelas L, Svendsen CN (2012) Inhibition of apoptosis blocks human motor neuron cell death in a stem cell model of spinal muscular atrophy. *PLoS One,* **7,** e39113.

Sasaki Y, Nakagawa T, Mao X, DiAntonio A, Milbrandt J (2016) NMNAT1 inhibits axon degeneration via blockade of SARM1-mediated NAD(+) depletion. *Elife,* **5**.

Saxena S, Caroni P (2007) Mechanisms of axon degeneration: from development to disease. *Prog Neurobiol,* **83,** 174-91.

Schlaepfer WW, Bunge RP (1973) Effects of calcium ion concentration on the degeneration of amputated axons in tissue culture. *J Cell Biol,* **59,** 456-70.

Schlesinger DH, Goldstein G (1975) Molecular conservation of 74 amino acid sequence of ubiquitin between cattle and man. *Nature,* **255,** 423-4.

Schrank B, Gotz R, Gunnersen JM, et al. (1997) Inactivation of the survival motor neuron gene, a candidate gene for human spinal muscular atrophy, leads to massive cell death in early mouse embryos. *Proc Natl Acad Sci U S A,* **94,** 9920-5.

Schuler M, Green DR (2001) Mechanisms of p53-dependent apoptosis. *Biochem Soc Trans,* **29,** 684-8.

Schwarz LA, Patrick GN (2012) Ubiquitin-dependent endocytosis, trafficking and turnover of neuronal membrane proteins. *Mol Cell Neurosci,* **49,** 387-93.

Seddon HJ (1943) Peripheral Nerve Injuries. *Glasgow Med J,* **139,** 61-75.

Seddon HJ (1948) A review of work on peripheral nerve injuries in Great Britain during World War II. *J Nerv Ment Dis,* **108,** 160-8.

Seddon HJ, Medawar PB, Smith H (1943) Rate of regeneration of peripheral nerves in man. *J Physiol,* **102,** 191-215.

Sena LA, Chandel NS (2012) Physiological roles of mitochondrial reactive oxygen species. *Mol Cell,* **48,** 158-67.

Shababi M, Lorson CL, Rudnik-Schoneborn SS (2014) Spinal muscular atrophy: a motor neuron disorder or a multi-organ disease? *J Anat,* **224,** 15-28.

Shan B, Pan H, Najafov A, Yuan J (2018) Necroptosis in development and diseases. *Genes Dev,* **32,** 327-340.

Sherer TB, Betarbet R, Testa CM, et al. (2003) Mechanism of toxicity in rotenone models of Parkinson's disease. *J Neurosci,* **23,** 10756-64.

Shi L, Fu AK, Ip NY (2012) Molecular mechanisms underlying maturation and maintenance of the vertebrate neuromuscular junction. *Trends Neurosci,* **35,** 441-53.

Shultz LD, Sweet HO, Davisson MT, Coman DR (1982) 'Wasted', a new mutant of the mouse with abnormalities characteristic to ataxia telangiectasia. *Nature,* **297,** 402-4.

Simic G, Seso-Simic D, Lucassen PJ, et al. (2000) Ultrastructural analysis and TUNEL demonstrate motor neuron apoptosis in Werdnig-Hoffmann disease. *J Neuropathol Exp Neurol,* **59,** 398-407.

Simon CM, Dai Y, Van Alstyne M, et al. (2017) Converging Mechanisms of p53 Activation Drive Motor Neuron Degeneration in Spinal Muscular Atrophy. *Cell Rep,* **21,** 3767-3780.

Simon DJ, Weimer RM, McLaughlin T, et al. (2012) A caspase cascade regulating developmental axon degeneration. *J Neurosci,* **32,** 17540-53.

Simon HU, Haj-Yehia A, Levi-Schaffer F (2000a) Role of reactive oxygen species (ROS) in apoptosis induction. *Apoptosis,* **5,** 415-8.

Simon JH, Kinkel RP, Jacobs L, Bub L, Simonian N (2000b) A Wallerian degeneration pattern in patients at risk for MS. *Neurology,* **54,** 1155-60.

Sine SM (2012) End-plate acetylcholine receptor: structure, mechanism, pharmacology, and disease. *Physiol Rev,* **92,** 1189-234.

Singh RN, Singh NN (2018) Mechanism of Splicing Regulation of Spinal Muscular Atrophy Genes. *Adv Neurobiol,* **20,** 31-61.

Sleigh JN, Burgess RW, Gillingwater TH, Cader MZ (2014a) Morphological analysis of neuromuscular junction development and degeneration in rodent lumbrical muscles. *J Neurosci Methods,* **227,** 159-65.

Sleigh JN, Grice SJ, Burgess RW, Talbot K, Cader MZ (2014b) Neuromuscular junction maturation defects precede impaired lower motor neuron connectivity in Charcot-Marie-Tooth type 2D mice. *Hum Mol Genet,* **23,** 2639-50.

Smith RS, Bisby MA (1993) Persistence of axonal transport in isolated axons of the mouse. *Eur J Neurosci,* **5,** 1127-35.

Speese SD, Trotta N, Rodesch CK, Aravamudan B, Broadie K (2003) The ubiquitin proteasome system acutely regulates presynaptic protein turnover and synaptic efficacy. *Curr Biol,* **13,** 899-910.

Spira ME, Oren R, Dormann A, Gitler D (2003) Critical calpain-dependent ultrastructural alterations underlie the transformation of an axonal segment into a growth cone after axotomy of cultured Aplysia neurons. *J Comp Neurol,* **457,** 293-312.

Spring AM, Raimer AC, Hamilton CD, Schillinger MJ, Matera AG (2019) Comprehensive Modeling of Spinal Muscular Atrophy in Drosophila melanogaster. *Front Mol Neurosci,* **12,** 113.

Staropoli JF, Li H, Chun SJ, et al. (2015) Rescue of gene-expression changes in an induced mouse model of spinal muscular atrophy by an antisense oligonucleotide that promotes inclusion of SMN2 exon 7. *Genomics,* **105,** 220-8.

Sunderland S (1951) A classification of peripheral nerve injuries producing loss of function. *Brain,* **74,** 491-516.

Tapia JC, Wylie JD, Kasthuri N, et al. (2012) Pervasive synaptic branch removal in the mammalian neuromuscular system at birth. *Neuron,* **74,** 816-29.

Tedeschi A, Di Giovanni S (2009) The non-apoptotic role of p53 in neuronal biology: enlightening the dark side of the moon. *EMBO Rep,* **10,** 576-83.

Telford JE, Kilbride SM, Davey GP (2009) Complex I is rate-limiting for oxygen consumption in the nerve terminal. *J Biol Chem,* **284,** 9109-14.

Tello JF (1907) Degeneration et regeneration des plagues motrices. *Trav Lab Rech Biol Univ Madrit,* **5,** 117-149.

Teskey G, Abrahem R, Cao R, et al. (2018) Glutathione as a Marker for Human Disease. *Adv Clin Chem,* **87,** 141-159.

Testa CM, Sherer TB, Greenamyre JT (2005) Rotenone induces oxidative stress and dopaminergic neuron damage in organotypic substantia nigra cultures. *Brain Res Mol Brain Res,* **134,** 109-18.

Thomson SR, Nahon JE, Mutsaers CA, et al. (2012) Morphological characteristics of motor neurons do not determine their relative susceptibility to degeneration in a mouse model of severe spinal muscular atrophy. *PLoS One,* **7,** e52605.

Tisdale S, Pellizzoni L (2015) Disease mechanisms and therapeutic approaches in spinal muscular atrophy. *J Neurosci,* **35,** 8691-700.

Tomas J, Garcia N, Lanuza MA, et al. (2017) Presynaptic Membrane Receptors Modulate ACh Release, Axonal Competition and Synapse

Elimination during Neuromuscular Junction Development. *Front Mol Neurosci,* **10,** 132.
Tong C, Li P, Wu NL, Yan Y, Ying QL (2010) Production of p53 gene knockout rats by homologous recombination in embryonic stem cells. *Nature,* **467,** 211-3.
Tsao JW, Brown MC, Carden MJ, McLean WG, Perry VH (1994) Loss of the compound action potential: an electrophysiological, biochemical and morphological study of early events in axonal degeneration in the C57BL/Ola mouse. *Eur J Neurosci,* **6,** 516-24.
Tsao JW, George EB, Griffin JW (1999) Temperature modulation reveals three distinct stages of Wallerian degeneration. *J Neurosci,* **19,** 4718-26.
Turner BJ, Alfazema N, Sheean RK, et al. (2014) Overexpression of survival motor neuron improves neuromuscular function and motor neuron survival in mutant SOD1 mice. *Neurobiol Aging,* **35,** 906-15.
Turner BJ, Parkinson NJ, Davies KE, Talbot K (2009) Survival motor neuron deficiency enhances progression in an amyotrophic lateral sclerosis mouse model. *Neurobiol Dis,* **34,** 511-7.
Van Nostrand JL, Bowen ME, Vogel H, Barna M, Attardi LD (2017) The p53 family members have distinct roles during mammalian embryonic development. *Cell Death Differ,* **24,** 575-579.
Vande Velde C, Garcia ML, Yin X, Trapp BD, Cleveland DW (2004) The neuroprotective factor Wlds does not attenuate mutant SOD1-mediated motor neuron disease. *Neuromolecular Med,* **5,** 193-203.
Vendemiale G, Grattagliano I, Altomare E (1999) An update on the role of free radicals and antioxidant defense in human disease. *Int J Clin Lab Res,* **29,** 49-55.
Verhaart IEC, Robertson A, Leary R, et al. (2017) A multi-source approach to determine SMA incidence and research ready population. *J Neurol,* **264,** 1465-1473.
Villegas R, Martinez NW, Lillo J, et al. (2014) Calcium release from intra-axonal endoplasmic reticulum leads to axon degeneration through mitochondrial dysfunction. *J Neurosci,* **34,** 7179-89.
Vogelstein B, Lane D, Levine AJ (2000) Surfing the p53 network. *Nature,* **408,** 307-10.
Vousden KH (2000) p53: death star. *Cell,* **103,** 691-4.
Wadman RI, Vrancken AF, van den Berg LH, van der Pol WL (2012) Dysfunction of the neuromuscular junction in spinal muscular atrophy types 2 and 3. *Neurology,* **79,** 2050-5.
Wagner R, Heckman HM, Myers RR (1998) Wallerian degeneration and hyperalgesia after peripheral nerve injury are glutathione-dependent. *Pain,* **77,** 173-9.
Waller A (1851) Experiments on the Section of the Glosso-Pharyngeal and Hypoglossal Nerves of the Frog, and Observations of the Alterations Produced Thereby in the Structure of Their Primitive Fibres. *Edinb Med Surg J,* **76,** 369-376.
Wang JT, Medress ZA, Barres BA (2012) Axon degeneration: molecular mechanisms of a self-destruction pathway. *J Cell Biol,* **196,** 7-18.

Wang MS, Fang G, Culver DG, Davis AA, Rich MM, Glass JD (2001) The WldS protein protects against axonal degeneration: a model of gene therapy for peripheral neuropathy. *Ann Neurol,* **50,** 773-9.

Wang MS, Wu Y, Culver DG, Glass JD (2000) Pathogenesis of axonal degeneration: parallels between Wallerian degeneration and vincristine neuropathy. *J Neuropathol Exp Neurol,* **59,** 599-606.

Watts RJ, Hoopfer ED, Luo L (2003) Axon pruning during Drosophila metamorphosis: evidence for local degeneration and requirement of the ubiquitin-proteasome system. *Neuron,* **38,** 871-85.

Watts RJ, Schuldiner O, Perrino J, Larsen C, Luo L (2004) Glia engulf degenerating axons during developmental axon pruning. *Curr Biol,* **14,** 678-84.

Williams AB, Schumacher B (2016) p53 in the DNA-Damage-Repair Process. *Cold Spring Harb Perspect Med,* **6**.

Williams DW, Kondo S, Krzyzanowska A, Hiromi Y, Truman JW (2006) Local caspase activity directs engulfment of dendrites during pruning. *Nat Neurosci,* **9,** 1234-6.

Williams DW, Truman JW (2005) Cellular mechanisms of dendrite pruning in Drosophila: insights from in vivo time-lapse of remodeling dendritic arborizing sensory neurons. *Development,* **132,** 3631-42.

Winlow W, Usherwood PN (1975) Ultrastructural studies of normal and degenerating mouse neuromuscular junctions. *J Neurocytol,* **4,** 377-94.

Wirth B, Brichta L, Hahnen E (2006a) Spinal muscular atrophy and therapeutic prospects. *Prog Mol Subcell Biol,* **44,** 109-32.

Wirth B, Brichta L, Hahnen E (2006b) Spinal muscular atrophy: from gene to therapy. *Semin Pediatr Neurol,* **13,** 121-31.

Wirth B, Brichta L, Schrank B, et al. (2006c) Mildly affected patients with spinal muscular atrophy are partially protected by an increased SMN2 copy number. *Hum Genet,* **119,** 422-8.

Wishart TM, Parson SH, Gillingwater TH (2006) Synaptic vulnerability in neurodegenerative disease. *J Neuropathol Exp Neurol,* **65,** 733-9.

Wishart TM, Paterson JM, Short DM, et al. (2007) Differential proteomics analysis of synaptic proteins identifies potential cellular targets and protein mediators of synaptic neuroprotection conferred by the slow Wallerian degeneration (Wlds) gene. *Mol Cell Proteomics,* **6,** 1318-30.

Wong F, Fan L, Wells S, et al. (2009) Axonal and neuromuscular synaptic phenotypes in Wld(S), SOD1(G93A) and ostes mutant mice identified by fiber-optic confocal microendoscopy. *Mol Cell Neurosci,* **42,** 296-307.

Workman E, Kolb SJ, Battle DJ (2012) Spliceosomal small nuclear ribonucleoprotein biogenesis defects and motor neuron selectivity in spinal muscular atrophy. *Brain Res,* **1462,** 93-9.

Wyatt RM, Balice-Gordon RJ (2003) Activity-dependent elimination of neuromuscular synapses. *J Neurocytol,* **32,** 777-94.

Xi Y, Noble S, Ekker M (2011) Modeling neurodegeneration in zebrafish. *Curr Neurol Neurosci Rep,* **11,** 274-82.

Yan T, Feng Y, Zheng J, et al. (2010) Nmnat2 delays axon degeneration in superior cervical ganglia dependent on its NAD synthesis activity. *Neurochem Int,* **56,** 101-6.

Yao D, Li M, Shen D, et al. (2013) Expression changes and bioinformatic analysis of Wallerian degeneration after sciatic nerve injury in rat. *Neurosci Bull,* **29,** 321-32.

Yaron A, Schuldiner O (2016) Common and Divergent Mechanisms in Developmental Neuronal Remodeling and Dying Back Neurodegeneration. *Curr Biol,* **26,** R628-R639.

Zerres K, Rudnik-Schoneborn S (1995) Natural history in proximal spinal muscular atrophy. Clinical analysis of 445 patients and suggestions for a modification of existing classifications. *Arch Neurol,* **52,** 518-23.

Zhai Q, Wang J, Kim A, et al. (2003) Involvement of the ubiquitin-proteasome system in the early stages of wallerian degeneration. *Neuron,* **39,** 217-25.

Zhang Z, Lotti F, Dittmar K, et al. (2008) SMN deficiency causes tissue-specific perturbations in the repertoire of snRNAs and widespread defects in splicing. *Cell,* **133,** 585-600.

Zhang Z, Pinto AM, Wan L, et al. (2013) Dysregulation of synaptogenesis genes antecedes motor neuron pathology in spinal muscular atrophy. *Proc Natl Acad Sci U S A,* **110,** 19348-53.

Zhao RZ, Jiang S, Zhang L, Yu ZB (2019) Mitochondrial electron transport chain, ROS generation and uncoupling (Review). *Int J Mol Med,* **44,** 3-15.

Zheleznyakova GY, Kiselev AV, Vakharlovsky VG, et al. (2011) Genetic and expression studies of SMN2 gene in Russian patients with spinal muscular atrophy type II and III. *BMC Med Genet,* **12,** 96.

Zhu J, Singh M, Selivanova G, Peuget S (2020) Pifithrin-alpha alters p53 post-translational modifications pattern and differentially inhibits p53 target genes. *Sci Rep,* **10,** 1049.

Appendices

1.34 *Appendix 1: Journal of Anatomy Paper – first author*

Received: 15 October 2019 | Revised: 30 January 2020 | Accepted: 2 March 2020

DOI: 10.1111/joa.13187

ORIGINAL ARTICLE

ANATOMICAL SOCIETY Journal of Anatomy WILEY

Synaptic withdrawal following nerve injury is influenced by postnatal maturity, muscle-specific properties, and the presence of underlying pathology in mice

Alannah J. Mole[1,2] | Sarah Bell[1,2] | Alison K. Thomson[1,2] | Kosala N. Dissanayake[1,2] | Richard R. Ribchester[1,2] | Lyndsay M. Murray[1,2]

[1]Centre for Discovery Brain Sciences, University of Edinburgh, Edinburgh, UK

[2]The Euan MacDonald Centre for Motor Neurone Disease Research, Edinburgh, UK

Correspondence
Lyndsay M. Murray, Centre for Discovery Brain Sciences, University of Edinburgh, Edinburgh, UK.
Email: Lyndsay.Murray@ed.ac.uk

Funding information
Muscular Dystrophy Association, Grant/Award Number: 417757; Institute Stategic Support Fund/Wellcome Trust, Grant/Award Number: IS3-R2.23; Anatomical Society, Grant/Award Number: 011216; Motor Neurone Disease Association, Grant/Award Number: 838-791

Abstract

Axonal and synaptic degeneration occur following nerve injury and during disease. Traumatic nerve injury results in rapid fragmentation of the distal axon and loss of synaptic terminals, in a process known as Wallerian degeneration (WD). Identifying and understanding factors that influence the rate of WD is of significant biological and clinical importance, as it will facilitate understanding of the mechanisms of neurodegeneration and identification of novel therapeutic targets. Here, we investigate levels of synaptic loss following nerve injury under a range of conditions, including during postnatal development, in a range of anatomically distinct muscles and in a mouse model of motor neuron disease. By utilising an ex vivo model of nerve injury, we show that synaptic withdrawal is slower during early postnatal development. Significantly more neuromuscular junctions remained fully innervated in the cranial nerve/muscle preparations analysed at P15 than at P25. Furthermore, we demonstrate variability in the level of synaptic withdrawal in response to injury in different muscles, with retraction being slower in abdominal preparations than in cranial muscles across all time points analysed. Importantly, differences between the cranial and thoracoabdominal musculature seen here are not consistent with differences in muscle vulnerability that have been previously reported in mouse models of the childhood motor neuron disease, spinal muscular atrophy (SMA), caused by depletion of survival motor neuron protein (Smn). To further investigate the relationship between synaptic degeneration in SMA and WD, we induced WD in preparations from the $Smn^{2B/-}$ mouse model of SMA. In a disease-resistant muscle (rostral band of levator auris longus), where there is minimal denervation, there was no change in the level of synaptic loss, which suggests that the process of synaptic withdrawal following injury is Smn-independent. However, in a muscle with ongoing degeneration (transvs. abdominis), the level of synaptic loss significantly increased, with the percentage of denervated endplates increasing by 33% following injury, compared to disease alone. We therefore conclude that the presence of a die-back can accelerate synaptic loss after injury in $Smn^{2B/-}$ mice.

KEYWORDS
axotomy, developmental regulation, die-back, differential vulnerability, ex vivo, motor neuron disease, mouse model, neuromuscular disease, neuromuscular junction, peripheral neuropathy, postnatal development, spinal muscular atrophy, synaptic degeneration, Wallerian degeneration

1 | INTRODUCTION

Motor neurons are vulnerable to degeneration following physical or chemical injury and in a range of neurodegenerative diseases. Damaged axons and synapses degenerate in morphologically distinct ways depending on the nature of the original trauma. Following injury, spontaneous and rapid fragmentation occurs along the length of the injured axon in a characteristic process known as Wallerian degeneration (WD; Waller, 1851; Beirowski *et al.*, 2004, 2005; Conforti *et al.*, 2014). In WD, the cytoskeleton is disassembled and granular degeneration proceeds distal to the injury site (for review see Wang *et al.*, 2012). This is morphologically distinct from degeneration that occurs during peripheral neuropathies, such as amyotrophic lateral sclerosis (ALS) and spinal muscular atrophy (SMA). In some forms of motor neuron disease, axons retrogradely retract away from the synaptic region and are described as 'dying-back' (Cavanagh, 1964). An example of dying-back pathology can be seen in the childhood motor neuron disease, SMA, where a lack of survival motor neuron (SMN) protein leads to the progressive loss of lower motor neurons (Lefebvre *et al.*, 1995; Rodrigues *et al.*, 1995). Despite morphological distinctions between WD and dying-back pathology, their mechanistic differences or commonalities remain unclear. Understanding whether different morphologies also relate to different mechanisms would provide a powerful tool to better categorise different types of, neurodegeneration and potentially it will facilitate the identification of novel therapeutic targets.

Recent work has revealed that rates of axonal and synaptic degeneration are influenced by postnatal age. Significant differences in the response of neonatal vs. adult mice to peripheral nerve injury and hypoxic insult have been reported (Murray *et al.*, 2011). In young adult mice (P25), tibial nerve lesion results in a loss of motor nerve terminals within the deep lumbrical (DL) muscles, with just 3% of motor endplates remaining innervated after 24 hr (Murray et al., 2011). Contrastingly, in mice aged less than 2 weeks of age, the rate of degeneration is much slower, with 86% of endplates remaining innervated after 24 hr (Murray et al., 2011). Synaptic loss in response to injury therefore appears to be developmentally regulated in the DL muscles. Neonatal, murine neuromuscular junctions (NMJs) also remain structurally intact following exposure to an ex vivo model of hypoxia reperfusion injury, with over 99% of endplates remaining fully occupied in P2 murine transvs. abdominis (TVA), compared with just 4% in adult mice (Murray *et al.*, 2011).

Differential rates of degeneration have been reported between different motor neurons pools in humans and in mouse models of motor neuron disease (Bowerman *et al.*, 2012). Transcriptional profiling of differentially vulnerable motor neurons has identified transcripts and pathways which can modify the rate of degeneration (Hedlund *et al.*, 2010; Brockington *et al.*, 2013; Kaplan *et al.*, 2014; Comley *et al.*, 2015; Murray *et al.*, 2015; Kline *et al.*, 2017; Boyd *et al.*, 2017). Properties that are intrinsic to the motor neuron may therefore regulate the rate of axon degeneration. Understanding the properties of different groups of motor neurons should better inform us of the mechanisms of axon degeneration. Due to the limited numbers of muscle that have been studied in detail, it remains unclear whether there is any variability in the rate of synaptic loss that occurs following injury in different muscles. Determining how different pools of motor neurons respond to injury would provide a useful tool to investigate the factors that regulate WD, and how this relates to other types of axonal and synaptic degeneration.

It remains unclear whether developmental resistance to injury is unique to DL preparations. To investigate this, here we measured synaptic degeneration in cranial and thoracoabdominal musculature following nerve injury. This was achieved by using an ex vivo model of axon injury, where the nerve is transected, and the distal portion along with the musculature it innervates is removed and maintained in oxygenated solutions for 24 hr (Brown *et al.*, 2015; Kline *et al.*, 2019). We have applied this model system to cranial muscle/facial nerve and abdominal muscle/intercostal nerve preparation at different postnatal time points. We show that there is a developmental delay in synaptic withdrawal following injury in all cranial muscles. Interestingly, some muscles (such as adductor auris longus; AAL) showing significantly greater loss than other muscles of the same age (such as levator auris longus; LAL). Furthermore, synaptic degeneration was consistently reduced in the thoracoabdominal muscles compared to the cranial muscles. Together these data suggest that factors intrinsic to the muscle/motor neuron affect the degree of synaptic degeneration following injury. Comparison of the degree of synaptic loss following injury with the degree of synaptic loss in a mouse model of SMA, revealed strikingly different patterns. This suggests that the factors which affect the rate of synaptic degeneration following injury are not the same as those which affect the vulnerability of motor neurons to SMA. Finally, by exposing muscles from the mouse model of SMA to the ex vivo model of nerve injury, we show that the presence of SMA-induced synaptic pathology significantly increases synaptic loss following injury.

2 | METHODS

2.1 | Mouse maintenance

All animal procedures were performed in accordance with the UK Home Office and institutional guidelines. *C57BL/6J MCos1*, *C57BL/6 Smn*$^{2B/2B}$ and *Smn*$^{+/-}$ mice were maintained as groups of less than four (or with parents/littermates) in individually ventilated cages under pathogen-free conditions, with ad libitum access to food and water, on a 12:12 light/dark cycle within animal facilities at the University of Edinburgh. MCos1 mice were sacrificed between P15-P25 and *Smn*$^{2B/-}$ mice were sacrificed at P18 (disease end-stage) by an inhalational overdose of anaesthetic (isofluorane). Death was confirmed by exsanguination of the carotid artery. The *Smn*$^{2B/-}$ mouse is a mouse model of the childhood motor neuron disease, spinal muscular atrophy that exhibits dying-back pathology. The *Smn2B* allele consists of a three-nucleotide substitution in the exon enhancer region within exon 7 of the murine *Survival motor neuron* (*Smn*) gene. The resultant mouse has reduced levels of full-length, endogenous SMN protein which leads to progressive loss of lower motor neurons (DiDonato *et al.*, 2001; Hammond *et al.*, 2010; Bowerman *et al.*, 2012). Onset of disease signs occurs at around P10, and, in our colonies, this model has a lifespan of around 21 days.

2.2 | Ex vivo model of nerve injury

Cranial and abdominal nerve/muscle explants were dissected as described previously (Murray *et al.*, 2010a, 2014) in Hepes-buffered saline composed of NaCl (137 mM), KCl (5 mM), $CaCl_2{\cdot}2H_2O$ (2 mM), $MgCl_2{\cdot}6H_2O$ (1 mM), glucose (5.6 mM) and Hepes (5 mM) with pH corrected to 7.4. Nerves (facial or intercostal) were severed at a consistent point, and distal nerve portions with attached musculature were pinned to dental wax and suspended in oxygenated mammalian physiological saline containing: NaCl (120 mM), KCl (5 mM), $CaCl_2{\cdot}2H_2O$ (2 mM), $MgCl_2{\cdot}6H_2O$ (1 mM), $NaH_2PO_4{\cdot}2H_2O$ (0.4 mM), $NaHCO_3$ (23.8 mM), glucose (5.6 mM), gentamicin (50 mg/ml, Thermo Fisher) and kanamycin (100 mg/ml, Thermo Fisher) in a 30-ml bijou tube. The bijou lid was modified, with two 0.8-mm needles, one needle clipped short, above the buffer level, to act as a pressure valve. A length of 0.50 mm tubing (VWR) sufficient to reach the bottom of the receptacle was attached to the other needle to provide a constant supply of 95/5% O_2/CO_2 to equilibrate the saline, at a perfusion rate of approximately 5 ml/min. The bathing solution was equilibrated for approximately 30 min before adding the sample. The receptacle containing the nerve/muscle explant was then incubated in a 30°C water bath for 24 hr. Temperature was monitored during this period using a digital thermometer (Fisher Traceable Digital Thermometer with stainless steel probe).

2.3 | Immunohistochemistry

After 24 hr incubation, preparations were fixed immediately in 4% paraformaldehyde (EMS) for 15 min. Muscles of interest were microdissected and permeabilised in 2% Triton-X-100-PBS (Sigma; PBT) for 30 min on a rocking platform at room temperature. Blocking solution (4% bovine serum albumin [BSA]/1% PBT) was applied for 60 min followed by primary antibodies (SV2, 1:100; 2H3, 1:50, both from Developmental Studies Hybridoma Bank) in blocking solution, and left to incubate at 4°C on a rocking platform for 24 hr. Preparations were then washed three times for 5 min with PBS. Secondary antibody (anti-mouse, Alexa Fluor 488, Stratech, 1:250 in 1×PBS) was added to each well and incubated in the dark at room temperature for a minimum of 4 hr. Muscles were washed three times in 1 × PBS for 5 min, and incubated with tetramethylrhodamine-conjugated α-bungarotoxin (TRITC-BTX; Thermo Fisher, 1:250, 20 min). Muscles were washed and whole-mounted on glass slides with Mowiol® (Calbiochem) and cover-slipped. Slides were stored in the dark at 4°C.

2.4 | Quantification and statistical analyses

Quantification of NMJ occupancy was undertaken by fluorescent microscopy at ×40 magnification. The investigator was blinded to the age, genotype and treatment of the muscle. A minimum of two to three fields of view (depending on muscle size and NMJ distribution) and 50 NMJs were sampled per muscle (average of 118 motor endplates per muscle). Fields of view were chosen at random from across the entire muscle using bungarotoxin staining only, to ensure a fair representation of the entire muscle and to reduce the chance of bias for innervated areas. A set of previously optimised and standardly used protocols for NMJ quantification were applied to quantify the percentage of fully occupied endplates (Murray *et al.*, 2008a, 2011, 2013, 2015; Thomson *et al.*, 2012; Sleigh *et al.*, 2014a, 2014b; Brown *et al.*, 2015; Comley *et al.*, 2016; Kline *et al.*, 2017; Courtney *et al.*, 2019; Osman *et al.*, 2019). In brief, fully occupied endplates were defined as complete apposition between the pre-synaptic terminal and the motor endplate (see Figure 1a for example). This has been expressed as a percentage of the total number of endplates quantified for each muscle, with the remainder of endplates displaying synaptic withdrawal, appearing either only partially innervated (where only part of the AChR cluster is covered by a pre-synaptic terminal) or vacant (where no pre-synaptic staining is evident at the AChR cluster).

All morphological analyses were collated into Microsoft Excel before exporting to GraphPad Prism 8 software for statistical analysis with *n* numbers referring to the number of muscles analysed. Statistical tests are detailed in the legend of the relevant graphs to which they refer. Data were tested for normality using a Shapiro–Wilk test. Data that were normally distributed were tested using one-way analysis of variance (ANOVA) with post-hoc Tukey correction. In groups that were not normally distributed, Kruskal–Wallis tests with Dunn's post-hoc analysis were applied. All data are presented as mean values ± standard error of the mean (SEM). Differences were considered significant when $p < .05$.

Micrographs are projections of Z-image stacks collected on a Nikon A1R FLIM confocal microscope and were adjusted for overall

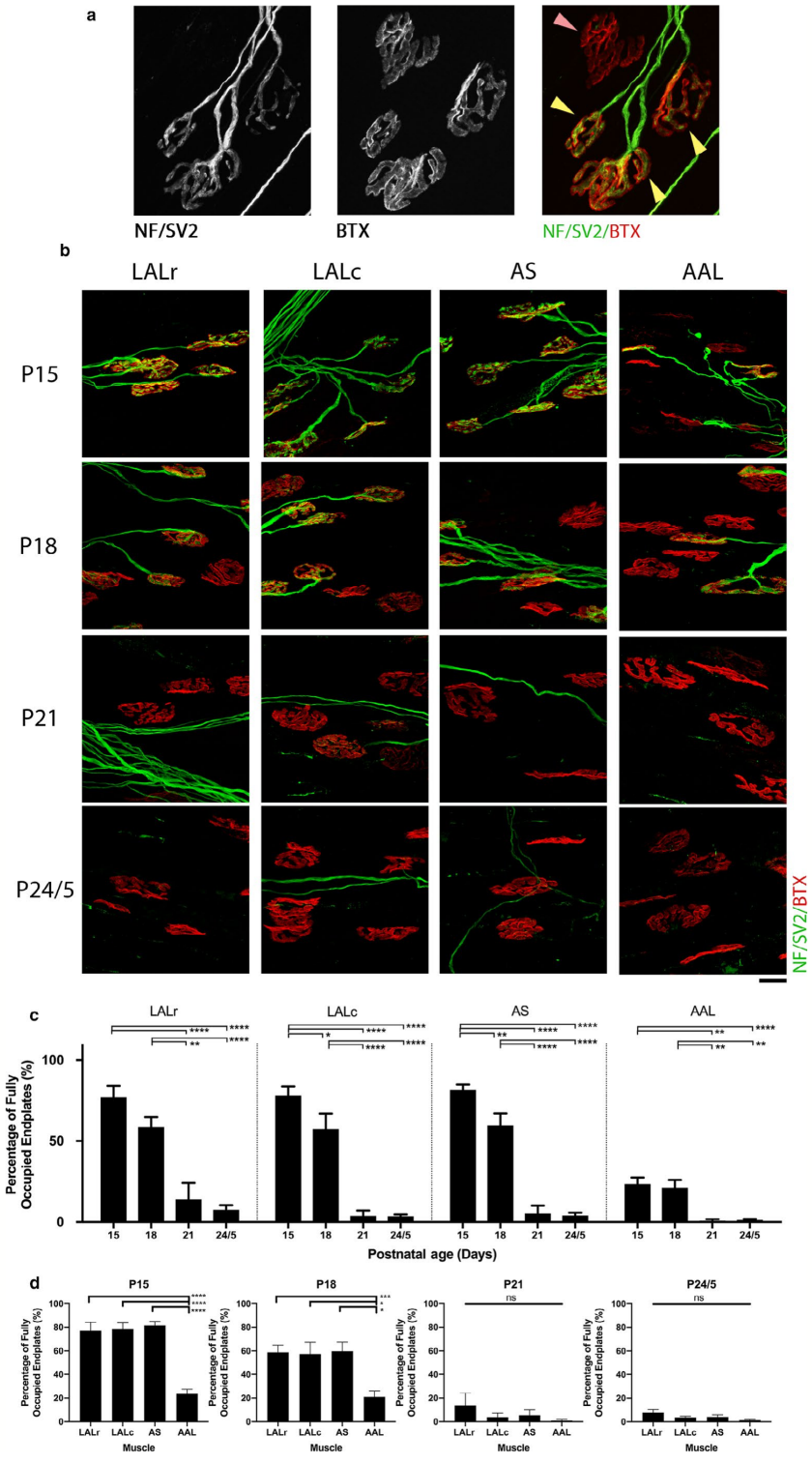
a
NF/SV2
BTX
NF/SV2/BTX
b
LALr
LALc
AS
AAL
P15
P18
P21
P24/5
NF/SV2/BTX
c
LALr
LALc
AS
AAL
Percentage of Fully Occupied Endplates (%)
100
50
0
15
18
21
24/5
Postnatal age (Days)
d
P15
P18
P21
P24/5
ns
Percentage of Fully Occupied Endplates (%)
LALr
LALc
AS
AAL
Muscle

FIGURE 1 Synaptic stability following injury is developmentally regulated and non-uniform in cranial muscles of the mouse. (a) Representative confocal micrographs showing example NMJs to exemplify criteria for occupancy quantification. NMJs are labelled with antibodies against neurofilament (NF, green) and synaptic vesicle protein 2 (SV2, green), and α-bungarotoxin (BTX, red). The yellow arrowheads highlight endplates that would be quantified as 'full', whereas the pink arrowhead indicates a vacant endplate, where apposition between the pre-synaptic terminal and the motor endplate has been lost (see Methods for further detail). (b) Representative confocal micrographs showing NMJs labelled with antibodies against NF (green) and SV2 (green), and BTX (red) from cranial muscles (levator auris longus rostral/caudal band [LALr/c], abductor auris longus [AAL], auricularis superior [AS]) that have been maintained ex vivo at 30°C for 24 hr. Postnatal age refers to the age of the animal at the time of dissection. Scale bar: 20 μm. (c) Bar charts showing quantification of the percentage of fully innervated motor endplates in cranial muscle bands between P15 and P24/5. Note that the percentage of fully occupied endplates decreases as postnatal age increases, supporting the finding that the response to injury is developmentally regulated. (d) Bar charts showing the percentage of fully occupied endplates in cranial muscles grouped by postnatal age at the time of ex vivo nerve injury. Note that there is a significant reduction in the percentage of fully occupied endplates in the AAL at both P15 and P18 time points in comparison with all other muscles. *p < .05, **p < .01, ***p < .001, ****p < .0001; one-way ANOVA with Tukey's correction. n = 10 at P15 and P24/5; n = 18/6 for the LALr/all other muscles at P18; and n = 4/5 at P21 for the AAL/all other muscles. Error bars represent mean ± SEM

image brightness and contrast only using ImageJ (downloadable from https://imagej.nih.gov/ij/) and Adobe Photoshop CS6 software (licence purchased from https://www.adobe.com/uk/products/).

3 | RESULTS

3.1 | Synaptic loss following injury is developmentally regulated and non-uniform in cranial muscles of the mouse

It is unclear whether developmental regulation of synaptic loss in response to injury is unique to the DL muscles or whether developmentally regulated delays in synaptic withdrawal also occurs in other muscle preparations. We therefore examined rates of synaptic withdrawal following injury during the critical time window of P15–P25, using an ex vivo model of nerve injury (see Section 2 for details). Nerve-muscle preparations comprising facial nerve (CN VII) branches innervating the cranial musculature (comprising rostral and caudal bands of levator auris longus [LALr/LALc, respectively], abductor auris longus [AAL] and auricularis superior [AS]) were isolated and maintained in oxygenated physiological solution at 30°C for 24 hr. We hypothesised that synapse loss would be slower in younger mice and that the level of synaptic loss would differ between different muscles. We tested this by analysing levels of muscle innervation following 24-hr exposure to the ex vivo model of nerve injury at different postnatal ages.

The percentage of fully innervated or 'occupied' endplates remaining in immunostained muscles from P15–P25 mice, 24 hr after ex vivo nerve injury were quantified (Figure 1a–d). Note that all ages refer to the age at dissection. The data show that postnatal age affected the degree of synapse loss in all preparations analysed (Figure 1c). For example, at P15, the LALr remained highly innervated, with 77.05 ± 7.05% (mean ± SEM) of endplates covered by motor nerve terminals. As expected, levels of innervation 24 hr after injury declined with age to 58.75 ± 6.06% innervation in preparations from mice aged P18, to 13.81 ± 10.4% aged P21, and 7.53 ± 2.84% aged P24/5. The LALc and AS muscles followed similar patterns. However, we found significantly more denervated endplates in AAL from the outset, with only 23.56 ± 3.85% innervation remaining at P15. This declined with mouse age to 21.02 ± 4.96% at P18, whereas less than 1.3% innervation remained at P21 and P24/5 (Figure 1d). As both AAL and LAL are homogeneously fast twitch muscles, these differences cannot be attributed to fibre type. This data suggests that there are other intrinsic properties of nerve or muscle that influence the rate of synaptic degeneration during postnatal development.

3.2 | Levels of synaptic loss are uniformly reduced in thoracoabdominal muscles of the mouse

Data thus far suggest that developmental delays are present in a range of muscles. However, differences between the rates of synaptic withdrawal observed in the AAL at different time points, led us to ask whether there would be similar differences within thoracoabdominal musculature. To investigate the response to injury in these muscles, we examined the TVA and TS muscles 24 hr after ex vivo nerve injury using the same protocol as for cranial muscles. In contrast to cranial preparations, both the TVA and TS showed high levels of NMJ innervation across all time points analysed (Figure 2). There was no significant difference in the percentage of fully occupied endplates at any time point; in all cases, the muscle remained over 77% innervated (one-way ANOVA with Tukey correction, $p \geq .09$).

Taken together, the data indicate that there are properties intrinsic to the muscle.., and/or motor neuron, that can influence the extent of synaptic withdrawal in response to injury during the postnatal period.

3.3 | Patterns of differential syanptic stability following injury contrast with patterns of selective vulnerability in a mouse model of SMA

Variability in the levels of synaptic degeneration, in a given muscle, has previously been reported in mouse models of motor neuron disease. For instance, in the *Smn*$^{2B/-}$ mouse model of SMA, the TVA muscle is highly vulnerable and displays high levels of synaptic loss, whereas the LALr and AAL muscles are relatively spared, with little

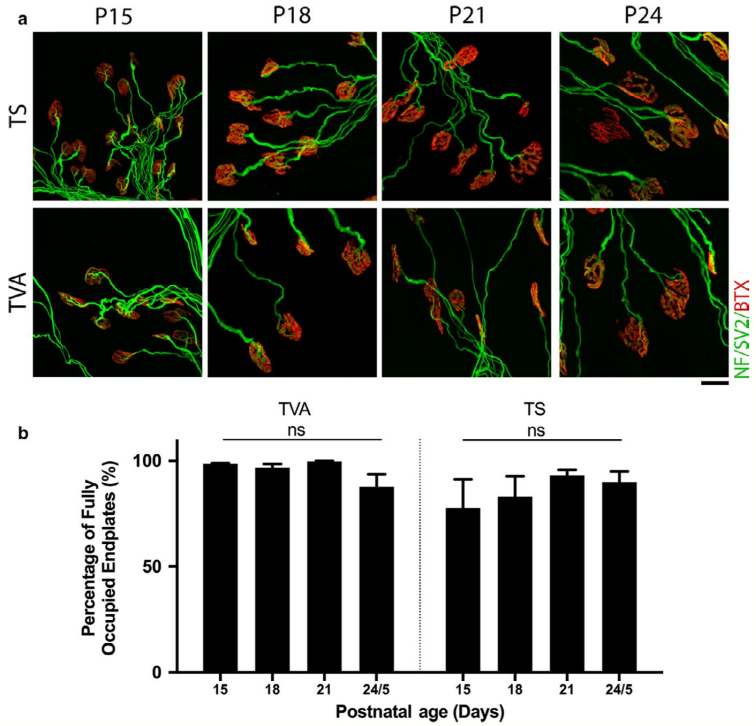

FIGURE 2 Minimal synaptic loss is observed following injury across all time points analysed in thoracoabdominal musculature. (a) Representative confocal micrographs showing NMJs labelled with antibodies against neurofilament (NF, green) and synaptic vesicle protein 2 (SV2, green), and α-bungarotoxin (BTX, red) from transvs. abdominis [TVA] and triangularis sterni (TS) muscles which have been maintained ex vivo at 30°C for 24 hr. Postnatal age refers to the age of the animal at the time of dissection. Note that the majority of endplates remain fully occupied at all ages examined. Scale bar: 20 μm. (b) Bar charts showing quantification of the percentage of fully innervated motor endplates after ex vivo nerve injury in the TVA and TS at P15, P18, P21, and P24/5. The percentage of fully occupied endplates remains high across all time points and there is no significant difference within muscles at any time point. ns = not significant, $p \geq .09$; one-way ANOVA with Tukey's correction. TVA, $n = 6$, 18, 4, and 6 muscles, at P15, 18, 21, and 24/5, respectively, and $n = 6$, 6, 6, and 4 in the TS at P15, 18, 21, and 24/5, respectively. Error bars represent mean ± SEM

synaptic loss 'even at late stages of disease' (Murray *et al.*, 2015). To investigate how synaptic stability differs between disease and injury, we compared levels of innervation remaining in muscles from end-stage (P18) $Smn^{2B/-}$ mice in vivo with levels of innervation remaining in homologous muscles from wild-type animals after ex vivo nerve injury. This provided insight into how synaptic responses differ following these distinct insults.

In line with previous work undertaken by Murray *et al.* (2015), here the LALr and AAL of $Smn^{2B/-}$ mice were largely spared from dying-back neuropathy in vivo, with over 98% of motor endplates remaining fully innervated at P18 (Figure 3). Contrasting this, 24 hr after ex vivo nerve injury in P18 wild-type mice, the LALr was 47.23 ± 2.58% innervated and the AAL only 21.02 ± 4.96% innervated (Figure 3). These cranial muscles therefore appear to exhibit more extensive synaptic loss following injury than in an SMA mouse model (Mann–Whitney *U*-test, $p \leq .0007$). Also in line with descriptions by Murray et al. (2015), in the $Smn^{2B/-}$ model, the TVA is vulnerable to dying-back pathology in vivo, with 62.11 ± 3.78% innervation remaining at P18, compared with 99.54 ± 0.29% innervated in wild-type age-matched mice 24 hr after ex vivo nerve injury (Figure 3). This suggests that the TVA exhibits less extensive synaptic loss following injury than in an SMA mouse model (Mann-Whitney *U* test, $p = .0002$). Thus, the factors responsible for determining relative synaptic stability following both nerve injury and SMA, appear to be distinct.

3.4 | Reduced Smn levels do not influence the incidence of synaptic loss following injury in the LALr cranial muscle of the mouse

We next asked whether a reduction in Smn levels affects synaptic stability after injury. To address this, we isolated and maintained cranial nerve/muscle preparations from wild-type mice and from $Smn^{2B/-}$ mice. In $Smn^{2B/-}$ mice, cranial muscles are classified as selectively resistant, in that even at end-stage of disease, there is no synapse loss evident (cf. Figure 3). Therefore, these muscles have reduced Smn levels but no resultant synaptic loss (Murray *et al.*,

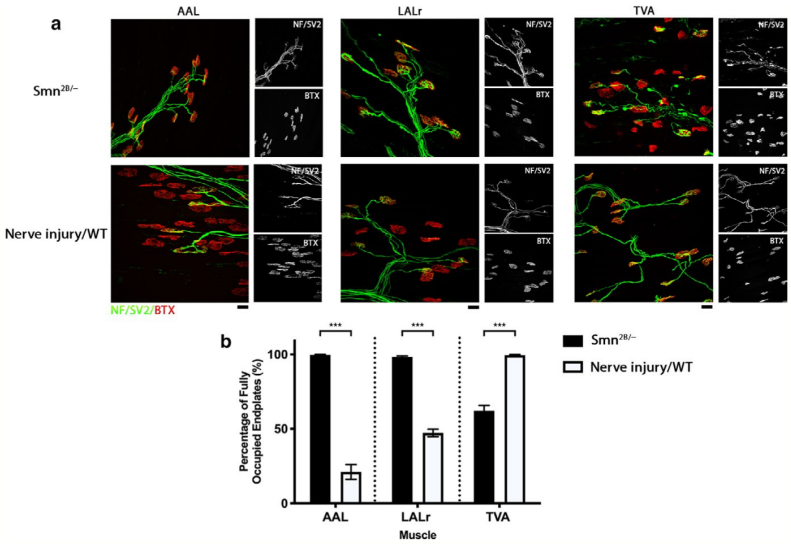

FIGURE 3 Synaptic stability is different in response to disease or injury conditions. (a) Representative confocal micrographs showing NMJs labelled with antibodies against neurofilament (NF, green) and synaptic vesicle protein 2 (SV2, green), and α-bungarotoxin (BTX, red) showing innervation of abductor auris longus (AAL), levator auris longus rostral band (LALr), and transvs. abdominis (TVA) under disease conditions from *Smn*$^{2B/-}$ mice at P18 and following ex vivo nerve injury in wild-type animals at P18. Nerve/muscle explants from the 'nerve injury' group were maintained ex vivo at 30°C for 24 hr. Scale bar: 20 μm. (b) Bar chart showing quantification of the percentage of fully innervated motor endplates in the AAL, LALr, and TVA after ex vivo nerve injury in WT vs. *Smn*$^{2B/-}$ mice. In the *Smn*$^{2B/-}$ mouse, the LALr and AAL cranial muscles are spared from degeneration in comparison with the TVA muscle. Following ex vivo *nerve* injury, LALr and AAL show high levels of synapse loss, whereas the TVA appears preserved. ns = not significant, ***$p < .001$; Mann–Whitney *U*-test. Note that for the AAL, $n = 9, 6$; for the LALr, $n = 8, 6$; and for the TVA, $n = 10, 6$ muscles for *Smn*$^{2B/-}$ and nerve injury/WT groups, respectively. Error bars represent mean ± SEM

2015). We compared levels of denervation in the LALr under three conditions: LALr from wild type after ex vivo nerve injury; LALr from *Smn*$^{2B/-}$; and LALr from *Smn*$^{2B/-}$ after ex vivo nerve injury.

In this disease-resistant muscle, consistent with previous work by Murray *et al.* (2015), minimal denervation was found in vivo in *Smn*$^{2B/-}$ mice, with over 93% of endplates remaining fully occupied. In wild-type mice, ex vivo nerve injury-induced extensive denervation, with 47.12 ± 4.08% of endplates remaining fully occupied. In muscles from *Smn*$^{2B/-}$ mice subject to ex vivo nerve injury, we found that the level of synaptic loss was comparable to wild-type levels, where 58.55 ± 3.528% of endplates remaining fully occupied (Unpaired *t*-test with Welch's correction, $p = .087$; Figure 4). We conclude that in the LALr, where synapse loss due to Smn deficiency is minimal, the synaptic loss caused by nerve injury is not altered. As Smn levels are reduced in this model, despite the lack of NMJ pathology, we conclude that synaptic withdrawal following ex vivo nerve injury is Smn-independent.

3.5 | The presence of dying-back pathology increases the level of synaptic loss following injury in the TVA muscle of the mouse

To investigate the relationship between synaptic loss that occurs in injury vs. disease, we also investigated whether there was any alteration in the level of synaptic loss following injury in the presence of dying-back pathology. Unlike the LALr, the TVA muscle of the *Smn*$^{2B/-}$ mouse model exhibits high levels of synaptic pathology, including denervation, pre-synaptic swelling, and post-synaptic shrinkage at end-stages of disease (P18). We compared levels of denervation in the TVA under three conditions at P18: TVA from wild type after ex vivo nerve injury; TVA from *Smn*$^{2B/-}$; and TVA from *Smn*$^{2B/-}$ after ex vivo nerve injury.

Ex vivo nerve injury of the TVA muscle from *Smn*$^{2B/-}$ mice resulted in a significant reduction in the percentage of fully occupied endplates, to just 8.05 ± 6.23% in comparison with wild-type TVA with ex vivo nerve injury (98.53 ± 0.29% of endplates fully innervated, Kruskal–Wallis with Dunn's correction, $p < .0001$) and to *Smn*$^{2B/-}$ in vivo (41.11 ± 3.98% of endplates fully innervated, Unpaired *t*-test with Welch's correction, $p = .0018$) in isolation (Figure 5). Overall, as we have already established that SMN reduction alone is not sufficient to increase levels of synaptic loss, it follows that the increase in synapse loss observed here is induced by the presence of disease-induced synaptic pathology.

4 | DISCUSSION

In this study, we have applied an ex vivo assay to investigate the effect of traumatic nerve injury in a range of muscles that have not

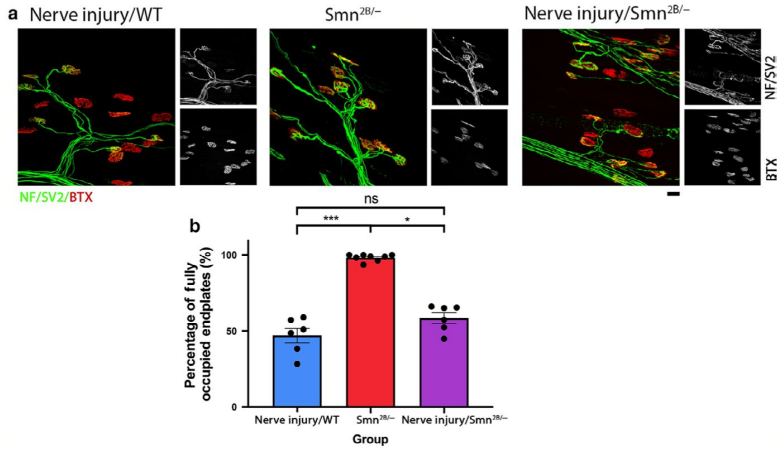

FIGURE 4 Reduced Smn levels have no effect on the level of synaptic degeneration following injury in the LALr cranial muscle of the mouse. (a) Representative confocal micrographs showing NMJs labelled with antibodies against neurofilament (NF, green) and synaptic vesicle protein 2 (SV2, green), and α-bungarotoxin (BTX, red) from levator auris longus rostral band (LALr) in wild-type animals after ex vivo nerve injury (nerve injury/WT), in $Smn^{2B/-}$ mice and in $Smn^{2B/-}$ mice after ex vivo nerve injury (nerve injury/$Smn^{2B/-}$). In nerve injury/WT and nerve injury/$Smn^{2B/-}$ conditions, LALr muscles were maintained ex vivo at 30°C for 24 hr. Scale bar: 20 μm. (b) Bar charts showing quantification of the percentage of fully occupied endplates in LALr in nerve injury/WT, $Smn^{2B/-}$, and nerve injury/$Smn^{2B/-}$ conditions. The percentage of fully occupied endplates after nerve injury in $Smn^{2B/-}$ mice is not significantly different than after nerve injury in wild-type animals. *p < .05, ***p < .001, ns = not significant. For all comparisons with the $Smn^{2B/-}$ group, Kruskal–Wallis with Dunn's correction was used to account for non-normally distributed data; otherwise a one-way ANOVA with Tukey's correction was used. Note that n = 6, 8, 6 for the nerve injury/WT, $Smn^{2B/-}$ and nerve injury/$Smn^{2B/-}$ groups, respectively. Error bars: mean ± SEM

been examined in this context previously. We have demonstrated that postnatal maturity influences the synaptic stability following injury in the cranial muscles. We have also shown that levels of synaptic loss are non-uniform in these muscles, with a significant increase in the rate of synaptic withdrawal in response to injury in the AAL at younger ages when compared with other cranial muscles. We also found that high levels of innervation persisted in the thoracoabdominal muscles after injury across P15–P25. This suggests that muscle and/or motor neuron intrinsic properties affect synaptic stability following injury. Comparison of the patterns of relative synaptic stability following injury to the patterns of synaptic vulnerability in a mouse model of SMA further suggests that the factors which affect synaptic stability following injury are distinct from those in peripheral neuropathies such as SMA. By exposing a muscle from a mouse model of SMA that is resistant to dying-back pathology with the ex vivo nerve injury assay, we have shown that synaptic loss in response to injury is SMN-independent. Furthermore, exposure of a muscle with ongoing dying-back pathology to the ex vivo nerve injury assay has demonstrated that the presence of dying-back pathology accelerates the rate of synaptic loss in response to injury.

4.1 | Synaptic stability following injury is governed by properties intrinsic to the muscle and/or motor neuron

We have shown that synaptic withdrawal in response to injury can be influenced by developmental age. Across all four cranial muscles analysed, we observed an increase in the incidence of denervated endplates with increasing postnatal age. These findings are in line with previous work that has shown that following either peripheral nerve injury or hypoxic insult, resistance is gradually lost across the first few weeks of life as the muscle transitions to adult levels of vulnerability (Murray *et al.*, 2011). Furthermore, some muscles, like the AAL, reach adult levels of degeneration at an earlier time point, whereas others, such as the TVA, remain comparatively stable following injury, even at P25 (Murray *et al.*, 2011). This suggests that postnatal maturity as well as properties specific to the muscle and/or motor neuron, are capable of regulating synaptic degeneration following insult. Discerning these mechanisms would be of great value and would contribute significantly to our understanding of the mechanisms regulating synaptic stability and vulnerability to injury and disease.

Indeed, various genetic mutations have been shown to alter the rate of WD in animal models, and have massively increased our understanding of the mechanisms of WD. This includes Wld^S and Sterile Alpha and TIR motif-containing 1 (SARM1) knockout (Lunn *et al.*, 1989; Ribchester *et al.*, 1995; Mack *et al.*, 2001; Wang *et al.*, 2001; Gillingwater *et al.*, 2002, 2004, 2006; Coleman, 2005; Coleman and Freeman, 2010; Gilley and Coleman, 2010; Osterloh *et al.*, 2012; Di Stefano *et al.*, 2015; Gilley *et al.*, 2015). Furthermore, differences in synaptic vulnerability in motor neuron disease have been exploited to investigate the underlying factors that may be responsible making motor neurons vulnerable in motor neuron disease. Transcriptional profiling of differentially vulnerable motor neurons has helped identify transcripts and pathways which can modify the rate of degeneration (Hedlund *et al.*, 2010; Brockington *et al.*, 2013; Kaplan *et al.*, 2014;

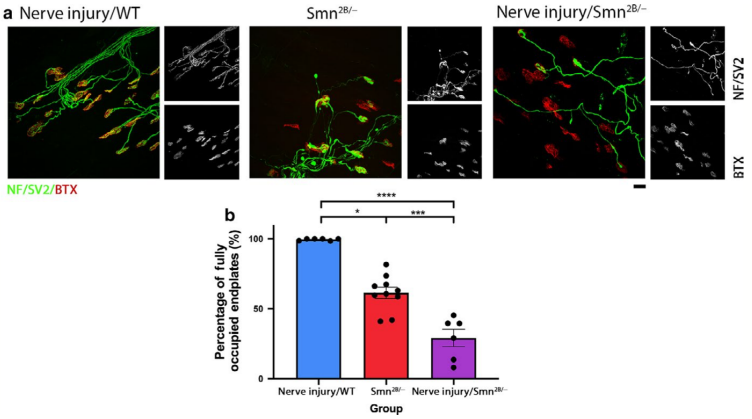

FIGURE 5 Presence of synaptic pathology in the *Smn*$^{2B/-}$ mouse significantly amplifies the level of synaptic loss induced by injury in the TVA muscle. (a) Representative confocal micrographs showing NMJs labelled with antibodies against neurofilament (NF, green) and synaptic vesicle protein 2 (SV2, green), and α-bungarotoxin (BTX, red) from transvs. abdominis (TVA) at P18 in wild-type animals after ex vivo nerve injury (nerve injury/WT), in the *Smn*$^{2B/-}$ mice, and in *Smn*$^{2B/-}$ after ex vivo nerve injury (nerve injury/*Smn*$^{2B/}$) conditions, respectively. In ex vivo conditions, TVA muscles were maintained ex vivo at 30°C for 24 hr. P18 refers to the postnatal age of the animal at the time of dissection. Scale bar: 20 μm. (b) Bar charts showing quantification of the percentage of fully occupied endplates in the TVA in nerve injury/WT, *Smn*$^{2B/-}$, and nerve injury/*Smn*$^{2B/-}$ conditions. The percentage of fully occupied endplates following injury in *Smn*$^{2B/-}$ mice was significantly increased in comparison with either wild-type injury or *Smn*$^{2B/-}$ conditions in isolation. **p* < .05, ***p* < .01, *****p* < .0001. For all comparisons with the nerve injury/WT group, Kruskal–Wallis with Dunn's correction was used to account for non-normally distributed data, otherwise a one-way ANOVA with Tukey's correction was used. Note that *n* = 6, 10, 6 muscles for the nerve injury/WT, *Smn*$^{2B/-}$, and nerve injury/*Smn*$^{2B/-}$ groups, respectively. Error bars: mean ± SEM

Comley *et al.*, 2015; Murray *et al.*, 2015; Boyd *et al.*, 2017; Kline *et al.*, 2017). We have recently used this approach to identify alpha-synuclein and stathmin 1 as phenotypic modifiers of pathology in motor neuron diseases. Importantly, when levels of alpha-synuclein or stathmin 1 were increased, disease severity was reduced and NMJ pathology ameliorated (Kline *et al.*, 2017; Villalon *et al.*, 2019). Identification of motor neurons that are differentially affected during axon degeneration therefore serves as a useful tool to identify factors that can modify axon degeneration in both disease and injury.

Here we have shown that muscle and/or motor neuron-specific properties are another factor that can influence the rate of synaptic loss, with responses varying between muscles. This is unlikely to be attributed to muscle fibre type. For example, both LAL and AAL are predominantly fast twitch muscles, but they display a marked difference in synaptic stability following injury (Erzen *et al.*, 2000; Murray *et al.*, 2008a, 2010a, 2010b). In wild-type rats and in Wld^{S} mice, the rate of synaptic loss has also been shown to be dependent on nerve stump length, with failure of neuromuscular transmission occurring more rapidly when nerve stump length is shorter (Slater, 1966; Ribchester *et al.*, 1995). However, the differences we have reported here cannot be attributed to differences in nerve stump length, as stump length is the same for all of the cranial muscles.

A promising avenue which may explain the differing synaptic stability following injury in different muscles at different postnatal ages, is differences in mitochondrial bioenergetics. In a recent study, we have profiled the nerve and muscle proteome in tibial nerve/lumbrical muscles between P12 and P24, and report a consistent up-regulation in proteins involved with mitochondrial bioenergetics in both muscle and nerve. Interestingly, this same profile has been observed in the tibialis anterior muscle, and during postnatal development of the heart (Puente *et al.*, 2014; Kim *et al.*, 2019). Importantly, we further showed that inhibition of complex I of the mitochondrial respiratory chain could slow axon degeneration, whereas pharmacological activation of oxidative phosphorylation accelerated synaptic degeneration (Kline *et al.*, 2019). It will now be important to investigate mitochondrial bioenergetics in the range of ages and muscles investigated in this study, to determine whether this can explain the differences in synaptic stability observed. This will help identify factors responsible for conferring rate differences and will provide insight into the mechanisms of synaptic degeneration, and aid in the identification of targets to manipulate the rate of degeneration.

4.2 | Mechanisms of synaptic loss following injury vs. dying-back neuropathy

Following traumatic injury in the *Smn*$^{2B/-}$ mouse model of SMA, we assessed the influence on the level of synaptic loss. Differential vulnerability is a known feature in this disease model, therefore we investigated both a die-back-resistant (LALr) and die-back-vulnerable (TVA) muscle (Murray *et al.*, 2015). As synaptic withdrawal after injury was amplified in the presence of a die-back, we conclude that the presence of dying-back pathology can increase synaptic loss in following injury.

Our results are perhaps initially surprising based on previous work where the presence of dying-back pathology reduced synaptic loss and axon fragmentation following nerve injury. In *Wasted* mice, which display a dying-back neuromuscular phenotype, translation elongation factor eEF1A2 expression is required to prevent dying-back pathology at the NMJ, whereas loss of this factor inhibits the initiation and progression of WD (Murray *et al.*, 2008b). Although differing requirements for eEF1A2 expression may represent a mechanistic distinction between injury-induced degeneration and dying-back pathology, this does not exclude the possible occurrence of convergence in degenerative pathways further downstream.

Commonalities between WD and dying-back neuropathies have been reported in animal models of motor neuron disease. For example, Wld^S has been found to be protective in some motor neuron disease and peripheral neuropathy models, suggesting that there may be some convergence between degenerative mechanisms. Similarly, in mice with progressive motor neuronopathy, Wld^S expression also delays dying-back pathology (Ferri *et al.*, 2003). Delays have also been reported in animal models of Parkinson's and demyelinating diseases (Conforti *et al.*, 2014). Several similarities have also been highlighted at the cellular level between WD and dying-back pathology, including poor axonal transport, mitochondrial dysfunction, and an increase in intra-axonal calcium (for review see Coleman, 2005; Conforti *et al.*, 2014). Our recent proteomic work in mice has identified alterations in mitochondrial bioenergetics that coincide with delays in the change in level of synaptic loss in response to injury during postnatal development in the hindlimb (Kline *et al.*, 2019). Targeting bioenergetic pathways by enhancing mitochondrial bioenergetics has also been found to rescue motor axon defects in a model of SMA (Boyd *et al.*, 2017). Alterations in mitochondrial dynamics may therefore represent a promising, and perhaps uniting factor in WD and dying-back neuropathy. Overall, the identification of common factors capable of influencing the rate of neurodegeneration under different physiological conditions could aid in the identification of targets that are common across multiple diseases.

ACKNOWLEDGEMENTS

This work was funded by grants from the Muscular Dystrophy Association (MDA) to L.M.M. (grant number 417757), the Motor Neuron Disease Association (MNDA) to R.R.R. (Ref. 838-791), and the Institute Strategic Support Fund (ISSF3) from the University of Edinburgh supported by the Wellcome Trust (IS3-R2.23) to L.M.M. A.J.M. is a recipient of a studentship from the Anatomical Society.

CONFLICT OF INTEREST

The authors have no conflicts of interest to declare.

AUTHOR CONTRIBUTIONS

A. J. Mole: Design of experiments in Figures 1–5, acquisition, analysis, and interpretation of data for Figures 1–5; drafting of manuscript. S. Bell: Acquisition and processing of data for Figures 4 and 5, approval of manuscript. A .K. Thomson: Design of experiments for Figures 1 and 2, optimisation of experimental systems, critical reading and approval of manuscript. K. N. Dissanayake: Concept and design of Figures 1 and 2, approval of manuscript. R. R. Ribchester: Concept and design, critical reading and approval of manuscript. L. M. Murray: Concept and design of study, critical revision of the manuscript and approval of the manuscript.

DATA AVAILABILITY STATEMENT

The raw data that support the findings of this study are available from the corresponding author (L.M.M.) upon reasonable request.

ORCID

Lyndsay M. Murray https://orcid.org/0000-0001-6841-702X

REFERENCES

Beirowski, B., Berek, L., Adalbert, R., Wagner, D., Grumme, D.S., Addicks, K., et al. (2004) Quantitative and qualitative analysis of Wallerian degeneration using restricted axonal labelling in YFP-H mice. *Journal of Neuroscience Methods*, 134, 23–35.

Beirowski, B., Adalbert, R., Wagner, D., Grumme, D.S., Addicks, K., Ribchester, R.R., et al. (2005) The progressive nature of Wallerian degeneration in wild-type and slow Wallerian degeneration (WldS) nerves. *BMC Neuroscience*, 6, 6.

Bowerman, M., Murray, L.M., Beauvais, A., Pinheiro, B. and Kothary, R. (2012) A critical Smn threshold in mice dictates onset of an intermediate spinal muscular atrophy phenotype associated with a distinct neuromuscular junction pathology. *Neuromuscular Disorders*, 22, 263–276.

Boyd, P.J., Tu, W.Y., Shorrock, H.K., Groen, E.J.N., Carter, R.N., Powis, R.A., et al. (2017) Bioenergetic status modulates motor neuron vulnerability and pathogenesis in a zebrafish model of spinal muscular atrophy. *PLoS Genetics*, 13, e1006744.

Brockington, A., Ning, K., Heath, P.R., Wood, E., Kirby, J., Fusi, N., et al. (2013) Unravelling the enigma of selective vulnerability in neurodegeneration: Motor neurons resistant to degeneration in ALS show distinct gene expression characteristics and decreased susceptibility to excitotoxicity. *Acta Neuropathologica*, 125, 95–109.

Brown, R., Hynes-Allen, A., Swan, A.J., Dissanayake, K.N., Gillingwater, T.H. and Ribchester, R.R. (2015) Activity-dependent degeneration of axotomized neuromuscular synapses in Wld S mice. *Neuroscience*, 290, 300–320.

Cavanagh, J.B. (1964) The significance of the 'dying back' process in experimental and human neurological disease. *International Review of Experimental Pathology*, 3, 219–267.

Coleman, M. (2005) Axon degeneration mechanisms: commonality amid diversity. *Nature Reviews Neuroscience*, 6, 889–898.

Coleman, M.P. and Freeman, M.R. (2010) Wallerian degeneration, Wld(s), and Nmnat. *Annual Review of Neuroscience*, 33, 245–267.

Comley, L., Allodi, I., Nichterwitz, S., Nizzardo, M., Simone, C., Corti, S., et al. (2015) Motor neurons with differential vulnerability to degeneration show distinct protein signatures in health and ALS. *Neuroscience*, 291, 216–229.

Comley, L.H., Nijssen, J., Frost-Nylen, J. and Hedlund, E. (2016) Cross-disease comparison of amyotrophic lateral sclerosis and spinal muscular atrophy reveals conservation of selective vulnerability but differential neuromuscular junction pathology. *Journal of Comparative Neurology*, 524, 1424–1442.

Conforti, L., Gilley, J. and Coleman, M.P. (2014) Wallerian degeneration: An emerging axon death pathway linking injury and disease. *Nature Reviews Neuroscience*, 15, 394–409.

Courtney, N.L., Mole, A.J., Thomson, A.K. and Murray, L.M. (2019) Reduced P53 levels ameliorate neuromuscular junction loss without affecting motor neuron pathology in a mouse model of spinal muscular atrophy. *Cell Death & Disease*, 10, 515.

Di Stefano, M., Nascimento-Ferreira, I., Orsomando, G., Mori, V., Gilley, J., Brown, R., et al. (2015) A rise in NAD precursor nicotinamide mononucleotide (NMN) after injury promotes axon degeneration. *Cell Death and Differentiation*, 22, 731–742.

DiDonato, C.J., Lorson, C.L., De Repentigny, Y., Simard, L., Chartrand, C., Androphy, E.J., et al. (2001) Regulation of murine survival motor neuron (Smn) protein levels by modifying Smn exon 7 splicing. *Human Molecular Genetics*, 10, 2727–2736.

Erzen, I., Cvetko, E., Obreza, S. and Angaut-Petit, D. (2000) Fiber types in the mouse levator auris longus muscle: a convenient preparation to study muscle and nerve plasticity. *Journal of Neuroscience Research*, 59, 692–697.

Ferri, A., Sanes, J.R., Coleman, M.P., Cunningham, J.M. and Kato, A.C. (2003) Inhibiting axon degeneration and synapse loss attenuates apoptosis and disease progression in a mouse model of motoneuron disease. *Current Biology*, 13, 669–673.

Gilley, J. and Coleman, M.P. (2010) Endogenous Nmnat2 is an essential survival factor for maintenance of healthy axons. *PLoS Biology*, 8, e1000300.

Gilley, J., Orsomando, G., Nascimento-Ferreira, I. and Coleman, M.P. (2015) Absence of SARM1 rescues development and survival of NMNAT2-deficient axons. *Cell Reports*, 10, 1974–1981.

Gillingwater, T.H., Haley, J.E., Ribchester, R.R. and Horsburgh, K. (2004) Neuroprotection after transient global cerebral ischemia in Wld(s) mutant mice. *Journal of Cerebral Blood Flow and Metabolism*, 24, 62–66.

Gillingwater, T.H., Ingham, C.A., Parry, K.E., Wright, A.K., Haley, J.E., Wishart, T.M., et al. (2006) Delayed synaptic degeneration in the CNS of Wlds mice after cortical lesion. *Brain*, 129, 1546–1556.

Gillingwater, T.H., Thomson, D., Mack, T.G., Soffin, E.M., Mattison, R.J., Coleman, M.P.,, et al. (2002) Age-dependent synapse withdrawal at axotomised neuromuscular junctions in Wld(s) mutant and Ube4b/Nmnat transgenic mice. *Journal of Physiology*, 543, 739–755.

Hammond, S.M., Gogliotti, R.G., Rao, V., Beauvais, A., Kothary, R. and DiDonato, C.J. (2010) Mouse survival motor neuron alleles that mimic SMN2 splicing and are inducible rescue embryonic lethality early in development but not late. *PLoS ONE*, 5, e15887.

Hedlund, E., Karlsson, M., Osborn, T., Ludwig, W. and Isacson, O. (2010) Global gene expression profiling of somatic motor neuron populations with different vulnerability identify molecules and pathways of degeneration and protection. *Brain*, 133, 2313–2330.

Kaplan, A., Spiller, K.J., Towne, C., Kanning, K.C., Choe, G.T., Geber, A., et al. (2014) Neuronal matrix metalloproteinase-9 is a determinant of selective neurodegeneration. *Neuron*, 81, 333–348.

Kim, Y., Yang, D.S., Katti, P. and Glancy, B. (2019) Protein composition of the muscle mitochondrial reticulum during postnatal development. *Journal of Physiology*, 597, 2707–2727.

Kline, R.A., Dissanayake, K.N., Hurtado, M.L., Martínez, N.W., Ahl, A., Mole, A.J., et al. (2019) Altered mitochondrial bioenergetics are responsible for the delay in Wallerian degeneration observed in neonatal mice. *Neurobiology of Diseases*, 130, 104496.

Kline, R.A., Kaifer, K.A., Osman, E.Y., Carella, F., Tiberi, A., Ross, J., et al. (2017) Comparison of independent screens on differentially vulnerable motor neurons reveals alpha-synuclein as a common modifier in motor neuron diseases. *PLoS Genetics*, 13, e1006680.

Lefebvre, S., Burglen, L., Reboullet, S., Clermont, O., Burlet, P., Viollet, L., et al. (1995) Identification and characterization of a spinal muscular atrophy-determining gene. *Cell*, 80, 155–165.

Lunn, E.R., Perry, V.H., Brown, M.C., Rosen, H. and Gordon, S. (1989) Absence of Wallerian degeneration does not hinder regeneration in peripheral nerve. *European Journal of Neuroscience*, 1, 27–33.

Mack, T.G., Reiner, M., Beirowski, B., Mi, W., Emanuelli, M., Wagner, D., et al. (2001) Wallerian degeneration of injured axons and synapses is delayed by a Ube4b/Nmnat chimeric gene. *Nature Neuroscience*, 4, 1199–1206.

Murray, L.M., Comley, L.H., Thomson, D., Parkinson, N., Talbot, K. and Gillingwater, T.H. (2008a) Selective vulnerability of motor neurons and dissociation of pre- and post-synaptic pathology at the neuromuscular junction in mouse models of spinal muscular atrophy. *Human Molecular Genetics*, 17, 949–962.

Murray, L.M., Thomson, D., Conklin, A., Wishart, T.M. and Gillingwater, T.H. (2008b) Loss of translation elongation factor (eEF1A2) expression in vivo differentiates between Wallerian degeneration and dying-back neuronal pathology. *Journal of Anatomy*, 213, 633–645.

Murray, L.M., Gillingwater, T.H. and Parson, S.H. (2010a) Using mouse cranial muscles to investigate neuromuscular pathology in vivo. *Neuromuscular Disorders*, 20, 740–743.

Murray, L.M., Lee, S., Baumer, D., Parson, S.H., Talbot, K. and Gillingwater, T.H. (2010b) Pre-symptomatic development of lower motor neuron connectivity in a mouse model of severe spinal muscular atrophy. *Human Molecular Genetics*, 19, 420–433.

Murray, L.M., Comley, L.H., Gillingwater, T.H. and Parson, S.H. (2011) The response of neuromuscular junctions to injury is developmentally regulated. *FASEB Journal*, 25, 1306–1313.

Murray, L.M., Beauvais, A., Bhanot, K. and Kothary, R. (2013) Defects in neuromuscular junction remodelling in the Smn(2B/-) mouse model of spinal muscular atrophy. *Neurobiology of Diseases*, 49, 57–67.

Murray, L., Gillingwater, T.H. and Kothary, R. (2014) Dissection of the transvs. abdominis muscle for whole-mount neuromuscular junction analysis. *Journal of Visualized Experiments*, 83, e51162.

Murray, L.M., Beauvais, A., Gibeault, S., Courtney, N.L. and Kothary, R. (2015) Transcriptional profiling of differentially vulnerable motor neurons at pre-symptomatic stage in the Smn (2b/-) mouse model of spinal muscular atrophy. *Acta Neuropathologica Communications*, 3, 55.

Osman, E.Y., Rietz, A., Kline, R.A., Cherry, J.J., Hodgetts, K.J., Lorson, C.l., et al. (2019) Intraperitoneal delivery of a novel drug-like compound improves disease severity in severe and intermediate mouse models of Spinal Muscular Atrophy. *Scientific Reports*, 9, 1633.

Osterloh, J.M., Yang, J., Rooney, T.M., Fox, A.N., Adalbert, R., Powell, E.H., et al. (2012) dSarm/Sarm1 is required for activation of an injury-induced axon death pathway. *Science*, 337, 481–484.

Puente, B.N., Kimura, W., Muralidhar, S.A., Moon, J., Amatruda, J.F., Phelps, K.L., et al. (2014) The oxygen-rich postnatal environment induces cardiomyocyte cell-cycle arrest through DNA damage response. *Cell*, 157, 565–579.

Ribchester, R.R., Tsao, J.W., Barry, J.A., Asgari-Jirhandeh, N., Perry, V.H. and Brown, M.C. (1995) Persistence of neuromuscular junctions after axotomy in mice with slow Wallerian degeneration (C57BL/WldS). *European Journal of Neuroscience*, 7, 1641–1650.

Rodrigues, N.R., Owen, N., Talbot, K., Ignatius, J., Dubowitz, V. and Davies, K.E. (1995) Deletions in the survival motor neuron gene on 5q13 in autosomal recessive spinal muscular atrophy. *Human Molecular Genetics*, 4, 631–634.

Slater, C.R. (1966) Time course of failure of neuromuscular transmission after motor nerve section. *Nature*, 209, 305–306.

Sleigh, J.N., Burgess, R.W., Gillingwater, T.H. and Cader, M.Z. (2014a) Morphological analysis of neuromuscular junction development and degeneration in rodent lumbrical muscles. *Journal of Neuroscience Methods*, 227, 159–165.

Sleigh, J.N., Grice, S.J., Burgess, R.W., Talbot, K. and Cader, M.Z. (2014b) Neuromuscular junction maturation defects precede impaired lower motor neuron connectivity in Charcot-Marie-Tooth type 2D mice. *Human Molecular Genetics*, 23, 2639–2650.

Thomson, S.R., Nahon, J.E., Mutsaers, C.A., Thomson, D., Hamilton, G., Parson, S.H., et al. (2012) Morphological characteristics of motor

neurons do not determine their relative susceptibility to degeneration in a mouse model of severe spinal muscular atrophy. *PLoS ONE*, 7, e52605.

Villalon, E., Kline, R.A., Smith, C.E., Lorson, Z.C., Osman, E.Y., O'Day, S., et al. (2019) AAV9-Stathmin1 gene delivery improves disease phenotype in an intermediate mouse model of Spinal Muscular Atrophy. *Human Molecular Genetics*, 28(22), 3742–3754.

Waller, A. (1851) Experiments on the section of the glosso-pharyngeal and hypoglossal nerves of the frog, and observations of the alterations produced thereby in the structure of their primitive fibres. *Edinburgh Medical and Surgical Journal*, 76, 369–376.

Wang, M.S., Fang, G., Culver, D.G., Davis, A.A., Rich, M.M. and Glass, J.D. (2001) The WldS protein protects against axonal degeneration: A model of gene therapy for peripheral neuropathy. *Annals of Neurology*, 50, 773–779.

Wang, J.T., Medress, Z.A. and Barres, B.A. (2012) Axon degeneration: Molecular mechanisms of a self-destruction pathway. *Journal of Cell Biology*, 196, 7–18.

How to cite this article: Mole AJ, Bell S, Thomson AK, Dissanayake KN, Ribchester RR, Murray LM. Synaptic withdrawal following nerve injury is influenced by postnatal maturity, muscle-specific properties, and the presence of underlying pathology in mice. *J. Anat.* 2020;00:1–12. https://doi.org/10.1111/joa.13187

1.35 *Appendix 2: Journal of Neurobiology of Disease paper – co-author*

Neurobiology of Disease 130 (2019) 104496

Contents lists available at ScienceDirect

Neurobiology of Disease

journal homepage: www.elsevier.com/locate/ynbdi

Altered mitochondrial bioenergetics are responsible for the delay in Wallerian degeneration observed in neonatal mice

Rachel A. Kline[a,b,d,1], Kosala N. Dissanayake[b,c,1], Maica Llavero Hurtado[b,d], Nicolás W. Martínez[e], Alexander Ahl[a], Alannah J. Mole[a,b], Douglas J. Lamont[f], Felipe A. Court[e,g,h], Richard R. Ribchester[b,c], Thomas M. Wishart[b,d], Lyndsay M. Murray[a,b,*]

[a] Centre for Discovery Brain Science, University of Edinburgh, Hugh Robson Building, Edinburgh EH8 9XD, UK
[b] Euan MacDonald Centre for Motor Neuron Disease Research, University of Edinburgh, UK
[c] Centre for Cognitive and Neural Systems, University of Edinburgh, 1 George Square, Edinburgh EH8 9JZ, UK
[d] The Roslin Institute and Royal (Dick) School of Veterinary Studies, University of Edinburgh, Easter Bush, EH25 9RG, UK
[e] Center for Integrative Biology, Faculty of Sciences, Universidad Mayor, Santiago, Chile
[f] Fingerprints Proteomics Facility, Dundee University, Dundee DD1 4HN, United Kingdom
[g] Geroscience Center for Brain Health and Metabolism, Santiago, Chile
[h] The Buck Institute for Research on Aging, Novato, CA, United States

ARTICLE INFO

Keywords:
Neurodegeneration
Wallerian
Neonate
Axon degeneration
Neuromuscular junction
NMJ
Proteomics
Mitochondria

ABSTRACT

Neurodegenerative and neuromuscular disorders can manifest throughout the lifespan of an individual, from infant to elderly individuals. Axonal and synaptic degeneration are early and critical elements of nearly all human neurodegenerative diseases and neural injury, however the molecular mechanisms which regulate this process are yet to be fully elucidated. Furthermore, how the molecular mechanisms governing degeneration are impacted by the age of the individual is poorly understood. Interestingly, in mice which are under 3 weeks of age, the degeneration of axons and synapses following hypoxic or traumatic injury is significantly slower. This process, known as Wallerian degeneration (WD), is a molecularly and morphologically distinct subtype of neurodegeneration by which axons and synapses undergo distinct fragmentation and death following a range of stimuli. In this study, we first use an *ex-vivo* model of axon injury to confirm the significant delay in WD in neonatal mice. We apply tandem mass-tagging quantitative proteomics to profile both nerve and muscle between P12 and P24 inclusive. Application of unbiased *in silico* workflows to relevant protein identifications highlights a steady elevation in oxidative phosphorylation cascades corresponding to the accelerated degeneration rate. We demonstrate that inhibition of Complex I prevents the axotomy-induced rise in reactive oxygen species and protects axons following injury. Furthermore, we reveal that pharmacological activation of oxidative phosphorylation significantly accelerates degeneration at the neuromuscular junction in neonatal mice. In summary, we reveal dramatic changes in the neuromuscular proteome during post-natal maturation of the neuromuscular system, and demonstrate that endogenous dynamics in mitochondrial bioenergetics during this time window have a functional impact upon regulating the stability of the neuromuscular system.

1. Introduction

Throughout the lifespan of an individual, neurons are susceptible to degeneration in heritable and spontaneous disease, and following a wide variety of insults, including chemical damage and physical trauma. Neurodegenerative disorders are a primary cause of death in adult and elderly populations, and although specific neurodegenerative disorders in children are considered rare, collectively they have been

Abbreviations: 2H3, Neurofilament; AMPK, Adenosine Monophosphate Kinase; DHE, Dihydroethidium; DRG, Dorsal Root Ganglion; ELISA, Enzyme Link Immuno; ETC, Electron Transport Chain; IPA, Ingenuity Pathway Analysis; MPS, Mammalian Physiological Saline; NMJ, Neuromuscular Junction; OXPHOS, Oxidative Phosphorylation; P, Post Natal Day; QFWB, Quantitative Fluorescent Western Blotting; ROS, Reaction Oxygen Species; SV2, Synaptic Vesicle Protein 2; TEAB, Tetraethylammonium Bromide; TMT-QMS, Tandem-Mass Tagging Quantitative Mass Spectrometry; TMT, Tandem Mass Tagging; WD, Wallerian Degeneration

* Corresponding author at: College of Medicine & Veterinary Medicine, University of Edinburgh, Old Medical School, Teviot Place, Edinburgh EH8 9XD, UK.
E-mail address: Lyndsay.Murray@ed.ac.uk (L.M. Murray).

[1] The authors wish it to be known that the authors indicated by a (1) contributed equally to this work.

https://doi.org/10.1016/j.nbd.2019.104496
Received 10 January 2019; Received in revised form 26 April 2019; Accepted 5 June 2019
Available online 06 June 2019

estimated to account for 28% of admissions to pediatric neurology wards(de Pedro-Cuesta et al., 2015; Dyken and Krawiecki, 1983). Neurodegeneration caused by both pathological and traumatic insult are united by a common vulnerability of the axonal and synaptic compartments of the cell. Although axonal and synaptic degeneration appears to be mechanistically distinct from somatic degeneration, the molecular mechanisms which regulate the vulnerability of the axonal and synaptic compartments of the neuron, and the process by which they degenerate are yet to be fully elucidated. Furthermore, how the molecular mechanisms governing degeneration are impacted by the age of the individual is poorly understood.

Axon and synapses can degenerate in a range of mechanistically distinct manners(Yaron and Schuldiner, 2016). Wallerian degeneration (WD) refers to one of these processes, during which axons and their presynaptic terminals undergo rapid fragmentation, degradation and clearance by scavenging macrophages and Schwann Cells (Saxena and Caroni, 2007; Catenaccio et al., 2017). This pattern of degeneration is also observed following trauma to the axon or in diseases that include multiple sclerosis or stroke (Kawachi and Lassmann, 2017; Stoll and Muller, 1999; Wang et al., 2012). We have recently described that the rate of WD following axotomy is significantly slower in neonatal mice compared to adults (Murray et al., 2011). An *ex-vivo* model of hypoxia-reperfusion injury using tissue from adult (P28) mice induced degeneration of 95% of neuromuscular junctions (NMJs) within 24 h. However, the same injury in nerve-muscle preparations from neonatal (P2) mice resulted in loss of motor nerve terminals from only 5% of NMJs. A similar delay in WD following traumatic nerve injury from axotomy was observed in mice aged up to P20. Further investigation into this phenomenon revealed that the delay in the rate of injury-induced NMJ degeneration was progressively lost between P12 and P25. Interestingly, a preconditioning lesion to generate immature NMJs in adult mice (*cf.* (Gillingwater et al., 2002)) failed to mitigate this rapid degeneration response post axotomy in adult mice (Murray et al., 2011). It therefore appears that the regulatory elements responsible for this dramatic increase in the rate of WD at the NMJ arise from the surrounding environment, namely the nerve or muscle, rather than the NMJ itself. Consequently, factors which contribute to the stability and degeneration axonal and synaptic compartments of the cell are developmentally regulated. In order to gain insight into the mechanisms which underlie neurodegeneration, and how they evolve and adapt during the lifespan of an individual, it is important to understand the mechanisms which regulate the delay in axon degeneration in neonatal mice.

While the definitive mechanisms underpinning WD remain unresolved, a number of specific mutations have been shown to profoundly influence its rate, and thus serve as compelling tools to study perturbed WD profiles: Perhaps the best known of these mutations (indeed named for its effect on the process), – Wallerian Degeneration Slow (Wld^S) - in mice delays axonal degeneration by a factor of ten (Brown et al., 1994; Lyon et al., 1993; Oyebode et al., 2012). This mutation incorporates an in-frame fusion between genes encoding nicotinamide nucleotide adenylyltransferase 1 (Nmnat1) and the N-terminus of ubiquitination factor E4B (Ube4b) (Coleman et al., 1998; Conforti et al., 2000; Wishart et al., 2007). Transgenic expression of the chimeric protein delays axon degeneration following nerve injury in mice, rats, *Drosophila* and zebrafish (Adalbert et al., 2005; Hoopfer et al., 2006; Mack et al., 2001; O'Donnell et al., 2014; Wang et al., 2001a; Wishart et al., 2012). Axonal protection by Wld^S protein is also observed following a range of traumatic, chemical and pathological insults, in both the central and peripheral nervous systems (Beirowski et al., 2008; Beirowski et al., 2010; Ferri et al., 2003; Gillingwater et al., 2004; Howell et al., 2007; Meyer zu Hoeste et al., 2011; Mi et al., 2005; Sajadi et al., 2004; Samsam et al., 2003; Wang et al., 2001b, 2002; Zhu et al., 2014).

Recently, Sterile Alpha and TIR motif-containing 1 (*Sarm1*) was identified as a critical component of the Wallerian Degeneration pathway. Knockout of *Sarm1* in both *Drosophila* and mice phenocopies Wld^S gene expression and protects axons from WD for weeks post axotomy (Osterloh et al., 2012). Studies of Wld^S and Sarm1, and the mechanisms by which they exert their protective influence have not only enabled the discovery of key molecular players involved in the degenerative process, but also have cast light upon other factors that may modulate axonal and synaptic protection. Indeed, work on both Wld^S and Sarm1 suggest mitochondria have an important role in the progression of WD. This was first suggested as a possibility ten years ago following early proteomic investigations into altered synaptic stability using Wld^S (Wishart et al., 2007). Subsequently, Barrientos et al., demonstrated that inhibition of the mitochondrial permeability transition pore (MPTP) could phenocopy the axon protection observed with Wld^S (Barrientos et al., 2011). More recently Avery et al. demonstrated that Wld^S is indeed likely acting through altered mitochondrial processes such as activity, dynamics and buffering capacity (Avery et al., 2012). Although mitochondria have been strongly implicated in the process of WD (Court and Coleman, 2012), their importance in the process of WD has also been questioned. Specifically, the protective effects of Wld^S were still present in axon depleted of mitochondria (Kitay et al., 2013) and while over expression of Nmnat2 was protective to the axon, it does not appear to colocalise with the mitochondria (Milde et al., 2013). Although changes in energy status and ATP production have been implicated in WD, it has been suggested that this is due to changes in glycolysis, rather than mitochondrial respiration (Godzik and Coleman, 2015). Furthermore, although *Sarm1* knockout or an increase in Nmn levels can protect axons from degeneration, they do no prevent changes in mitochondrial motility or depolarisation (Loreto et al., 2015). The precise involvement of mitochondria in the process of WD remains somewhat controversial, and further work is required to define their involvement and importance in regulating axon degeneration.

In this present study, we hypothesized that the observed acceleration in the rate of synaptic and axonal WD is attributed to dynamic changes in the postnatal nerve and muscle proteome. We utilized an *ex-vivo* model of nerve injury to re-examine the age-dependent observations we reported previously (Murray et al., 2011). This confirmed that delayed NMJ degeneration was progressively lost between ages of P10 to P26. To address the mechanisms, we utilized tandem-mass tagging quantitative mass spectrometry (TMT-QMS) to profile the proteome of both the nerve and muscle at 5 time points between P12 and P24. This resulted in the identification of 7440 and 6079 proteins in nerve and muscle respectively. Following a bioinformatics-based refinement of the data, we employed pathway analysis of the most biologically relevant protein alterations to reveal an up-regulation in molecular networks implicated in oxidative phosphorylation (OXPHOS) and related mitochondrial functions. Finally, we demonstrated that pharmacological up-regulation of basal OXPHOS activity levels accelerated synaptic degeneration, whilst exposure to the Complex I inhibitor rotenone was strongly axoprotective. In summary, this study details postnatal changes in the nerve muscle proteome, and identifies protein changes which can account for the delay in axon degeneration observed in neonatal mice.

2. Materials and methods

2.1. Animal handling and husbandry

All procedures were performed in adherence with the guidelines set out by the UK Home Office. MCos1 C56BL6/J mice were maintained under Specific and Opportunistic Pathogen-Free conditions in breeding facilities at the University of Edinburgh. All mice were sacrificed by an overdose of anesthetic and cervical dislocation.

2.2. Ex-vivo model of nerve injury

Mice ranging from P12 to P24 were sacrificed and immediately dissected to minimize any post-mortem molecular changes. Hind legs were removed and legs were microdissected in mammalian physiological saline (MPS) of following ionic composition (mM): Na^+ (158.4); K^+ (5); Ca^{2+} (2); Mg^{2+} (1); Cl^- (145); HCO_3^- (24), $H_2PO_4^-$ (0.4), glucose (5); equilibrated by bubbling in 95%O_2/5% CO_2 to pH 7.2–7.4. The deep lumbrical muscles with overlying FDB tendon and muscle attached were dissected, along with the distal nerve stump of the sciatic nerve, including all the nerve branches which innervate the lumbrical muscles. This preparation therefore represented the muscles with attached innervation, wherein the axons have been severed from the cell body. This system therefore reflects an *ex-vivo* model of axon injury. This preparation was pinned to dental wax and incubated for 24 h at 28 °C in oxygenated MPS bubbled continuously with 95/5% O_2/CO_2. When specified, 2 mM AICAR (Sigma) was added to oxygenated ringer solution.

2.3. Immunocytochemical staining of nerve-muscle explants

Following 24 h incubation *ex-vivo*, nerve-muscle preparations were incubated at room temperature with TRITC-conjugated α-bungarotoxin at a concentration of 5 μg/ml in phosphate buffered saline to label AChR at motor endplates. Preparations were fixed at room temperature for 15 min in 4% paraformaldehyde in PBS, then incubated for 72 h at 4 °C with primary antibodies against synaptic vesicle protein (SV2), and neurofilament (2H3) at a concentration of 1:100 and 1:50 respectively (Developmental Studies Hybridoma Bank, Iowa) then for 24 h at 4 °C in FITC-conjugated IgG anti-mouse secondary antibody (Jackson).

2.4. Imaging and analysis

Endplate occupancy was quantified using a Leica DMi8 inverted epifluorescent microscope (10×, 20× and 40× objectives; 0.53, 0.55 and 0.9NA; Leica DMi9 microscope, Leica DFC7000-T camera). Quantification of endplate occupancy was performed blind, and incorporated a minimum of 50 NMJs from at least three distinct fields of view per muscle per mouse (n = number of muscles, N = number of mice), using the following criteria: fully occupied, *i.e.* complete coverage of the post-synaptic endplate by the branches of the nerve terminal; partially occupied, or vacant, ie. complete withdrawal of the pre-synaptic terminal from the post-synaptic endplate.

Individual statistical tests and *n* numbers used are noted in figure legends. Statistical significance was considered to be $p \leq 0.05$.

Confocal microscopy was performed using a Nikon A1R$^+$ Resonant Scanning System (Nikon) (10× and 40× objectives; 0.3 and 1.3 oil NA; Nikon A1R$^+$ microscope; simultaneous image acquisition). 488 and 543 nm laser lines were used for excitation. The resultant confocal *Z*-series produced in NIS Elements 2D Analysis software were exported and merged using public domain Fiji ImageJ software downloadable from https://fiji.sc/.

Figures were created using GNU Image Manipulation Program (GIMP) for Windows.

2.5. Sample preparation for LC-MS/MS

Tandem mass tagging and fractionation of extracted samples was performed by the FingerPrints Proteomics facilities at the University of Dundee, to the following protocol:

Protein samples were thawed, trypsinised and desalted at room temperature. 100 μg of desalted tryptic peptides per sample were dissolved in 100 μl of 100 mM tetraethylammonium bromide (TEAB). The 10 different tandem mass tag (TMT) labels comprising the TMT10plex™ kit (Thermo Fisher Scientific) were dissolved in 41 μl anhydrous acetonitrile. Each dissolved label was added to a different sample; see Fig. 2 for the specificities of which label corresponded to which sample. The sample-label mixture was incubated for 1 h at room temperature. Labelling reaction was stopped by adding 8 μl of 5% hydroxylamine per sample.

Following labelling with TMT, samples were mixed, desalted, and dried in a speed-vac at 30 °C. Samples were re-dissolved in 200 μl ammonium formate (NH_4HCO_3) (10 mM, pH 10) and peptides were fractionated using an Ultimate 3000 RP-High pH High Performance Liquid Chroenatography column (Thermo-Scientific) containing an XBridge C18 column (XBridge peptide BEH, 130 Å, 3.5 μm, 2.1 × 150 mm) (Waters, Ireland) with an XBridge guard column (XBridge, C18, 3.5 μm, 2.1X10mm) (Waters, Ireland). Buffers A and B used for fractionation consist, respectively, of (A) 10 mM ammonium formate in milliQ water and (B) 10 mM ammonium formate with 90% acetonitrile. Before use, both buffers were adjusted to pH 10 with ammonia. Fractions were collected using a WPS-3000FC auto-sampler (Thermo-Scientific) at 1 min intervals. Column and guard column were equilibrated with 2% Buffer B for twenty minutes at a constant flow rate of 0.2 ml/min. 175 μl per sample was loaded onto the column at a rate of 0.2 ml/min, and the separation gradient was started 1 min after sample was loaded onto the column. Peptides were eluted from the column with a gradient of 2% Buffer B to 5% Buffer B in 6 min, and then from 5% Buffer B to 60% Buffer B in 50 min. Column was washed for 16 min in 100% Buffer B and equilibrated at 2% Buffer B for 20 min as mentioned previously. The fraction collection started 1 min after injection and stopped after 80 min (total 80 fractions, 200 μl each). The total number of fractions concatenated was set to 15 and the content of the fractions was dried and suspended in 50 μl of 1% formic acid prior to analysis with LC-MS.

2.6. LC-MS/MS analysis

Liquid chromatography- tandem mass spectrometry was performed by FingerPrints Proteomics Facilities at the University of Dundee, to the following protocol: Analysis of peptide readout was performed on a Q Exactive™ HF Hybrid Quadrupole-Orbitrap™ Mass Spectrometer (Thermo Scientific) coupled with a Dionex Ultimate 3000 RS (Thermo Scientific). LC buffers were made up to the following: Buffer A (2% acetonitrile and 0.1% formic acid in Milli-Q water (v/v)) and Buffer B (80% acetonitrile and 0.08% formic acid in Milli-Q water (v/v). Aliquots of 15 μl per sample were loaded at a rate of 5 μl/min onto a trap column (100 μm × 2 cm, PepMap nanoViper C18 column, 5 μm, 100 Å, Thermo Scientific) which was equilibrated with 98% Buffer A. The trap column was washed for 6 min at the same flow rate and then the trap column was switched in-line with a resolving C18 column (Thermo Scientific) (75 μm × 50 cm, PepMap RSLC C18 column, 2 μm, 100 Å). Peptides were eluted from the column at a constant flow rate of 300 nl/min with a linear gradient from 95% Buffer A to 40% Buffer B in 122 min, and then to 98% Buffer B by 132 min. The resolving column was then washed with 95% Buffer B for 15 min and re-equilibrated in 98% Buffer A for 32 min. Q Exactive™ HF was used in data dependent mode. A scan cycle was comprised of a MS1 scan (*m/z* range from 335 to 1800, with a maximum ion injection time of 50 ms, a resolution of 120,000 and automatic gain control (AGC) value of 3 × 106) followed by 15 sequential-dependent MS2 scans (with an isolation window set to 0.4 Da, resolution at 60000, maximum ion injection time at 200 ms and AGC 1 × 105. To ensure mass accuracy, the mass spectrometer was calibrated on the first day that the runs were performed.

2.7. Database search and protein identifications

Raw MS data from the 15 fractions were searched against mouse (*Mus musculus*) protein sequences from UniProtKB/Swiss-Prot using the MASCOT search engine (Matrix Science, Version 2.2) through Proteome Discoverer™ software (Version 1.4, Thermo Fisher). Parameters for database search were as follows: MS1 Tolerance: 10 ppm; MS2 Tolerance: 0.06da; fixed modification: Carbamidomethyl (C) Variable

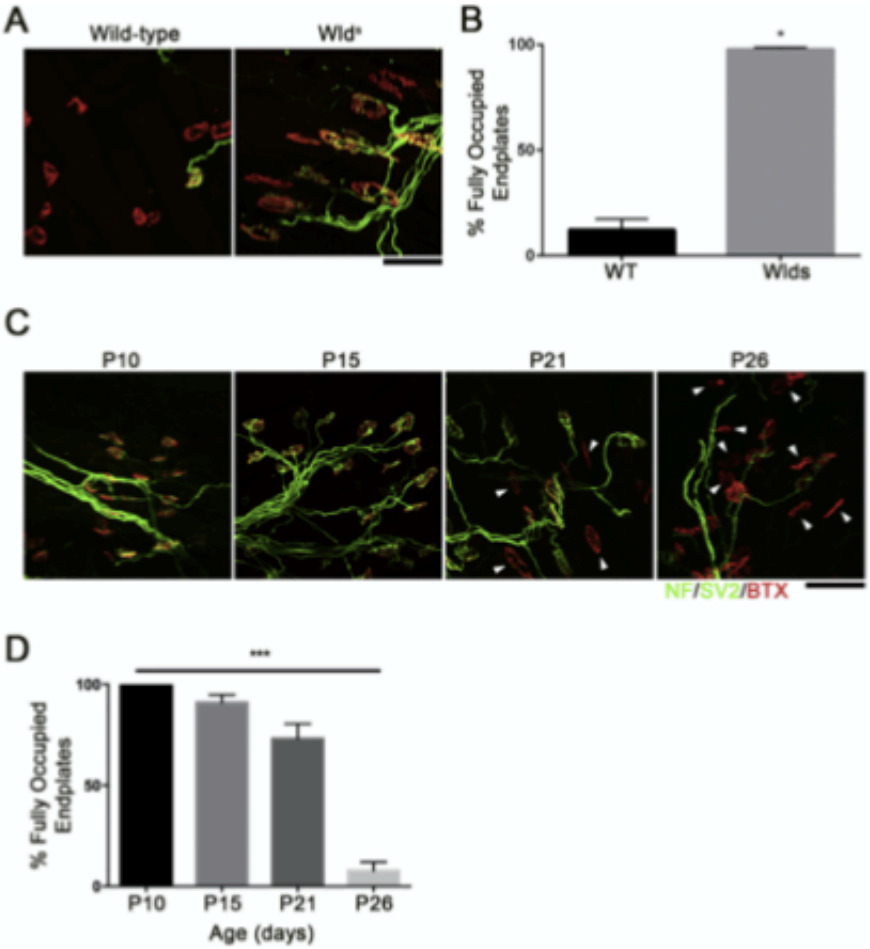

Fig. 1. An *ex-vivo* system confirms decreased rate of axon degeneration in *Wld*^{s} and neonatal mice. (A) Representative confocal micrographs of NMJs from age-matched adult C57BL/6 *J* wildtype and *Wld*^{s} mouse lumbrical muscles after 24 h incubation *ex-vivo* at 28 °C in oxygenated ringer solution. Note the retention of NMJ integrity in the *Wld*^{s} model compared to the marked loss of pre-synaptic inputs in the wildtype muscle. Scale bar = 25 μm (B) Bar chart (Mean ± SEM) showing the percentage of fully occupied endplates 24 h post-axotomy reveals an increased in the percentage of fully occupied endplates in *Wld*^{s} mice compared to wildtype C57BL/6 *J* mice. (*$p < 0.05$ by Mann-Whitney *U* test; $n = 3$ preparations per group, data are Mean ± SEM). (C) Representative confocal micrographs of NMJs from the deep lumbrical muscles from P10, P15, P21 and P26 mice after 24 h incubation *ex-vivo* at 28 °C in oxygenated mammalian physiological saline. Note the increase in vacant endplates (denoted by arrowhead) at P21 and P26 compared to P12 and P15. Scale bar = 25 μm (D) Bar chart (Mean ± SEM) of the percentage of fully occupied endplates in the deep lumbrical muscles from P12, P15, P21 and P26 mice confirms an age-associated decrease in the percentage of fully occupied endplates. (***$p < 0.001$, by Kruskall-Wallis test; $n = 3$ preparations per group.

Modification: Oxidation (M), Dioxidation (M), Acetyl (N-term), Gln- > pyro-Glu (N-term Q), TMT 10(N-term and K); maximum missed cleavage: 2; and target FDR 0.01.

All identifications were quantified as relative ratios of expression compared to the first time point (P12) through Proteome Discoverer™ software (Thermo Fisher, Version 1.4). Relative ratios along with UnitProtKB/Swiss-Prot identifications were exported into Microsoft Excel as a raw data file containing ID, ratio of change in expression at each time point (P15, P18, P21, P24) compared to P12 = 1.

2.8. Selection of relevant expression clusters from filtered data in BioLayout Express3D

Filtering raw proteomic data by an expression change of > 20% at P24 than at P12 in produced a separate filtered list of proteins in nerve and muscle. These lists were imported separately into BioLayout

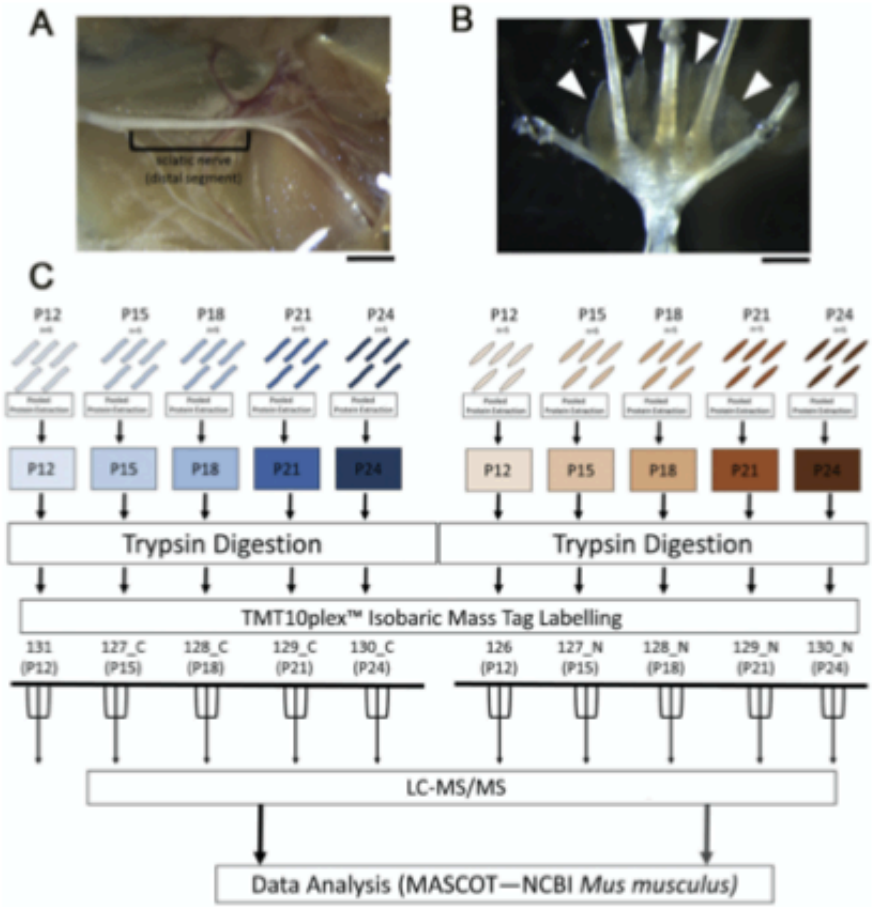

Fig. 2. Schematic of sample preparation, TMT 10plex™ Tandem Mass Tag labelling, and quantitative LC-MS/MS workflow. (A, B) Images showing region of sciatic nerve (A) or lumbrical muscles (B) which were isolated for proteomics (C) Schematic of sample preparation workflow for TMT 10plex™ labelling and subsequent LC-MS/MS. Sciatic nerves (n = 5 mice, 10 nerves) and lumbrical muscles (5 mice, 20 muscles per timepoint) were pooled for a single extraction in label-free buffer per timepoint. Pooled samples were labelled using all 10 isobaric mass tags from a TMT 10plex™ kit (Thermo Fisher). Labelled samples were prepared for LC-MS/MS and run in technical triplicate. Scale bars = 2 mm.

Express3D (Theocharidis et al., 2009) and clustered based on relative expression profile from P12 to P24. Algorithms in BioLayout Express3D generate a visual network to represent each data set, utilizing special proximity to represent the similarity in expression profile of individual proteins over time. The resultant visual networks were utilized to distinguish expression clusters that followed either a general upward or downward trend in expression from P12 to P24. These "upregulated" and "downregulated" clusters in nerve and muscle respectively were analyzed on an individual basis to exclude clusters that did not follow an experimentally relevant expression profile from P12 to P24. For example, clusters containing proteins that exhibited a consistent increase or decrease in expression were selected, while clusters consisting of proteins that exhibited an overall upregulation or downregulation but oscillated in expression during middle time points were excluded.

2.9. DAVID analysis

Proteins exhibiting a consistent up-regulation or down-regulation in nerve or muscle from P12 through all four subsequent time points to P24, regardless of magnitude of change, were submitted as a gene list and converted into DAVID IDs against the DAVID 6.7 *Mus musculus* database(Huang et al., 2009). Four separate analyses were performed from the following lists of proteins, grouped as: (1) Consistent upregulated expression in nerve, (2) Consistent downregulated expression in nerve, (3) Consistent upregulated expression in muscle, and (4) Consistent downregulated expression in muscle. These lists were analyzed using the Functional Annotation Clustering tool in DAVID Bioinformatics Resources (Version 6.7) to produce a list of functional annotations. Functional annotations are ranked by a DAVID enrichment score.

An enrichment score > 1.3 in DAVID is equivalent to $p < 0.05$, and considered to be statistically significant.

2.10. In silico protein pathway analysis

The Ingenuity Pathway Analysis (IPA) application (Ingenuity Systems, Silicon Valley, CA) was used to visualize and explore the cellular and molecular pathways that may have been altered as a result of expression changes over time. IPA generates networks of gene and protein interactions and disease associations, amongst other results, based on *in silico* predicted or experimentally reported interactions stored within the "hand-curated" Ingenuity Knowledge database (Wishart et al., 2012; Savli et al., 2008). The majority (90%) of data comprising the Ingenuity Knowledge database are derived from peer-reviewed publications; the remaining 10% of stored interactions have been identified by other *in silico* techniques. Networks generated using IPA were set to a maximum of 35 member molecules, and were ranked according to a score calculated by a right-tailed Fisher's exact test, which considers total protein input and size of the produced network. Network scores represent the relevance of the particular network to the overall analysis (i.e. proteomic alterations in nerve or muscle between P12 and P24). In this study, networks generated using IPA were limited to those producing the top 25 scores. For more information on the computational methodology underpinning IPA, please refer to http://www.ingenuity.com/.

Separate pathway analyses were performed on the filtered nerve and muscle data sets, which produced 25 predictive molecular networks each. A third, combined analysis, which consolidated nerve and muscle results, enabled the identification of molecular overlap within networks generated from nerve and muscle data. Extrapolation of this overlap through the Pathway Designer function generated a combined network in which molecular interactions conserved between both nerve and muscle data sets were explored.

2.11. Complex I activity assay

Mitochondrial OXPHOS Complex I activity was determined by immunocapture ELISA kit following the manufacturer's instructions (ab109721). Nerve (sciatic, brachial plexus, intercostal nerves) and muscle (deep lumbrical muscle) were isolated from recently sacrificed mice and snap-frozen on dry ice prior to assay. Thawed tissue was homogenized in ice-cold PBS with Dounce homogenizer and protein extracted with detergent solution at a concentration of 1:10. 250 µg of protein was incubated to the wells of microplate pre-coated with Complex I capture antibody for 3 h at room temperature. Activity of immunocaptured Complex I enzyme (NADH dehydrogenase) was determined by measuring the oxidation of NADH to NAD+ and simultaneous reduction of a dye which leads to increased absorbance at 450 nm. Each reaction was performed in duplicate. Activity was expressed as a change in absorbance per minute per quantity of protein per reaction, and values are expressed normalized to P12.

2.12. Quantitative fluorescent western blotting

Levels of Complex I protein were determined by quantitative fluorescent western blot (QFWB). Gastrocnemius muscles were isolated from recently sacrificed mice and snap-frozen on dry ice prior to immunoblotting. Thawed tissue was homogenized in ice-cold PBS with Dounce homogenizer and extracted in RIPA buffer (Fisher Scientific) with 1% Halt protease inhibitor cocktail (Sigma Aldrich). Concentration of protein was determined by micro-BCA assay (Pierce Biosystems). Samples were prepared to load 25 µg of protein in 10 µl deionised water and 5 µl of NuPage® LDS Sample buffer 4× (Invitrogen, UK) and run on a NuPAGE™ Novex™ 4–12%Bis-Tris protein gel (Invitrogen, UK) before transfer to a PVDF membrane using the i-Blot2® transfer system (Invitrogen, UK).

To determine total protein concentration for a loading control, membranes were incubated in 5 ml of Ponceau S solution; 0.1% Ponceau S (Sigma-Aldrich), 0.5% acetic acid (Sigma-Aldrich) in ddH2O at room temperature for 30 min before washing in ddH2O until bands were visible. Total protein image was scanned in greyscale using a CanoScan LiDE220 digital scanner (Canon) and saved as a TIFF image for total protein analysis.

For QFWB, membranes were blocked in 5 ml Odyssey® Blocking Buffer (Li-COR Biosciences) at room temperature for 30 min and incubated in primary antibody solution containing primary antibodies at the following concentration (SIRT2 1:500, Abcam; Igf2 1:1000, Abcam; Total OXPHOS 1:1000, Abcam) with 1% tween-20 (Sigma) in 5 ml Odyssey® Blocking Buffer (Li-COR Biosystems) at 4 °C overnight. Antibody to SIRT2 was generously provided by members of the Gillingwater laboratory. Membranes were incubated in secondary antibody solution containing either IRDye® 680RD donkey anti-mouse IgG (H + L) or IRDye® 680RD donkey antirabbit IgG (H + L) antibodies (Li-COR Biosciences) at a concentration of 1:5000 (0.02%) in a solution of 1% tween-20 (Sigma) in 5 ml Odyssey® Blocking Buffer (Li-.

COR Biosciences for 90 min at room temperature before drying and storage at 4 °C prior to imaging and analysis. For measurement and analysis, TIFF images of Ponceau-stained blots were imported into Odyssey® ImageStudio Lite software (Version 5.2). ImageStudio Lite (Version 5.2) was used to analyze the intensity of identical sections of total protein banding against background. Readouts of the intensity of total protein banding relative to background were imported into Microsoft Excel (Windows 2013) to calculate loading consistency and normalization factors. Western blots were imaged on the 700 nm channel using the Odyssey® Infrared Imaging System at a resolution of 169 µm. All quantification was performed on the 700 nm channel, with the intensity of bands normalized using the factors generated from total protein analysis. All statistical analysis and generation of graphs was performed in GraphPad Prism7 (Windows). Individual statistical tests used are noted in figure legends. Statistical significance was considered to be $p \leq 0.05$.

2.13. Dorsal root ganglion cultures

Briefly, E16 rat embryos were decapitated, and the limbs and organs were removed. The spinal cord with dorsal root ganglia (DRGs) was dissected and placed in a Petri dish containing cold L-15 medium (Gibco, 11,415–064). For DRG explants, complete DRGs were cultured in 24-well dishes containing 400 µl of Neurobasal medium, 2% B27, 0.3% L-glutamine, 1% streptomycin/penicillin, 4 µM aphidicolin (Sigma, A0781), 7.5 µg/ml 5-fluoro-2- deoxyuridine (Sigma, F0503), and 50 ng/ml nerve growth factor (NGF) (Invitrogen, 13,257–019). The mixture of aphidicolin and fluoro-2-deoxyuridine inhibits proliferation of Schwann cells by inhibition of DNA polymerase (Spadari et al., 1985; Wallace and Johnson Jr., 1989), thus constituting a highly pure sensory neuron culture (Heermann et al., 2012). DRGs were cultured for 7–11 days at 37 °C and 5% CO_2. Axotomy of DRG explants was made using a micropipette tip to separate all the axons from their somas.

2.14. Axonal degeneration index

Number of axons per area of nerve tissue was assessed in confocal images of neurofilament-immunostained explant sections (matched for laser power, photomultiplier tube gain/offset, and post processing) using the particle analysis macro of ImageJ. Relative neurite integrity was based on the ratio of the areas of fragmented axons *versus* total axonal area (Villegas et al., 2014). Degenerated axon fragments were detected using the particle analyzer algorithm of ImageJ (NIH, USA) and the total fragmented axon area *versus* total axonal area was used to estimate a degeneration index.

2.15. DHE assay

Superoxide levels were measured using dihydroethidium (DHE) fluorescence 6 h after DRG axotomy in an epifluorescence microscope. After axotomy, neurites were incubated in the last 30 min with 5 M DHE under culture conditions. DHE fluorescence was obtained under a Cy5 emission filter. Superoxide levels on neurites were determined using NIH ImageJ colocalization highlighter plugin. Oxidative stress levels were calculated as the ratio of DHE fluorescent signal area in neurites. Briefly, DHE signal and phase-contrast colocalization were used to obtain DHE area and neurite length. Photoshop (Adobe Systems) and NIH ImageJ were used to perform this analysis.

3. Results

Previous work has demonstrated that axotomised NMJs from neonatal mice showed a reduced rate of WD compared to NMJs from adult mice under otherwise identical experimental conditions (Murray et al., 2011). Between postnatal day 12 (P12) and P24 the rate of axotomy induced degeneration accelerates until the adult response of rapid synaptic degeneration is established. We first sought to determine whether age-dependent regulation of synaptic degeneration could be replicated using an "*ex-vivo*" assay of synaptic degeneration (Brown et al., 2015). Nerve-muscle preparations, comprising the tibial nerve and all branches innervating the attached deep lumbrical muscles were swiftly isolated from euthanized mice, and maintained in oxygenated physiological solution, then assayed for innervation 24 h later. This protocol mimics axotomy *in vivo* (Brown et al., 2015). Comparison of endplate occupancy at immunostained NMJs from the deep lumbrical muscles from adult *Wld*^{S} mice revealed that, as expected, the percentage of fully occupied NMJs was significantly greater than that of NMJs from age-matched wild-type C57BL/6 adults (Fig. 1A, B). Thus, this assay is sufficiently sensitive to reveal factors that influence the rate of WD. Equivalent preparations were isolated from mice aged P10 to P26. Analysis of NMJs from the lumbrical muscles revealed a significant decrease in the percentage of fully occupied endplates between P10 and P26 (Fig. 1C,D). Together, the data suggest that an *ex-vivo* model of traumatic injury can be used to detect differences in the rate of axon degeneration and confirms the age-associated decrease in the rate of axon degeneration in mice aged between P10 and P26.

3.1. Tandem mass tagging (TMT) quantitative proteomics produces a robust and comprehensive coverage of the nerve and muscle proteome

The combination of published work and the data presented above clearly demonstrate a marked increase in the rate of WD during the neonatal time period. We therefore reasoned that whatever regulates this progressive increase in the rate of WD, may also be changing progressively over the time period between P12 and P24. Given that the process of WD occurs after the axonal and synaptic compartments of the cell are severed from the cell body, and the overall speed of WD, we reasoned that the molecular regulators of this process would be most likely evidenced at the protein level, as opposed to at the level of transcription. We therefore performed a comprehensive proteomic analysis of muscle and nerve between P12 and P24, with the goal of identifying proteins and cellular processes which demonstrated a steady alteration correlating with the change in the rate of axon degeneration.

For this analysis, we employed tandem mass tagging (TMT) based proteomics using a 10plex (TM) labelling kit to allow comparative protein profiling across ten different sample groups. For this analysis we collected deep lumbrical muscle and sciatic nerve samples from mice aged P12, P15, P18, P21 and P24 and performed TMT proteomic analysis (Fig. 2). Consolidation of raw peptide outputs across all five time points within sciatic nerve and muscle samples respectively were translated into protein identifications by searching against murine protein sequences using the MASCOT protein database (Matrix Science, Version 2.2) and quantified expression as relative ratios compared to the first time point (P12) in each tissue type. This produced a list of protein identifications and ratios of expression/detection throughout the time course for muscle and nerve (see Methods for more information). Both nerve and muscle analyses are traditionally faced with the problem of detection saturation due to particularly abundant protein groups *i.e.* myelin related proteins in nerve or myosin groups in muscle (Comley et al., 2011; Mutsaers et al., 2013, 2011). The application of TMT combined with developments in sample handling workflows (smaller sample requirements, reduced processing losses, greater fractionation control) and recent technological advances in mass spectrometry sensitivity, has resulted in an unexpectedly high number of reliable protein identifications in all sample groups.

Within the sciatic nerve, 7440 total proteins were identified, of which 5625 were identified by 2 or more unique peptides (Supplementary Table 1). Within the lumbrical muscles, 6079 total proteins were identified, of which 4414 were identifiable by > 2 unique peptides (Supplementary Table 2).

Having identified so many proteins in both nerve and muscle, we applied a filtering protocol in order to identify protein alterations which are likely to be biologically relevant to the phenomenon of early age dependent neuronal stability. Thus, we began by further filtering the proteomic output to exclude any proteins with altered expression < 20% in either direction at P24 compared to P12. Previous studies in neural tissue and skeletal muscle have demonstrated that the 20% cut-off threshold produces a reliable list of candidate molecules (Comley et al., 2011; Mutsaers et al., 2013, 2011; Aghamaleky Sarvestany et al., 2014; Fuller et al., 2014).

In order to identify proteins whose expression are likely to correlate with the differential vulnerability described above, we used the network-based software BioLayout *Express*^{3D}. This software uses complex pattern recognition algorithms to cluster data by user-defined dimensions, while generating visual networks that utilize spatial proximity to represent relatedness. By clustering our refined protein list based on protein expression profile over the 5 time points, it was possible to visualize and isolate clusters of proteins exhibiting similar expression profiles over the time-course. We were therefore able to further filter the nerve and muscle data sets to include only those candidates which exhibited a desirable expression profile over the experimental P12-P24 period (Fig. 3). Specifically, clusters which exhibited a relatively consistent up-regulation or down-regulation in expression from P12 to P24 were selected for further analysis. Conversely, clusters containing proteins which showed a discontinuous expression profile, for example, those oscillating between an increase and decrease over the experimental period, were excluded. Through this filtering process, we produced a consolidated data set containing only proteins exhibiting a relative change in expression > 20% at P24 relative to P12 and an experimentally relevant expression profile (Supplementary Tables 3 and 4).

To validate the proteomic data, we performed quantitative fluorescent western blotting on protein candidates selected from the raw LC-MS/MS output. Candidates were selected on the basis of their magnitude of change over the experimental period, implication in injury-induced or disease-related neuronal degeneration, and availability of quality antibodies suitable for fluorescent-based western blotting. For example, the NAD-dependent deacetylase sirtuin-2 (SIRT2) exhibited an increase in the proteomic data (1.330 P24/P12 ratio in nerve) and has been demonstrated to be up-regulated across a number of neurodegenerative disease and injury models (Allodi et al., 2016; Amorim et al., 2015; Graham et al., 2017; Hedlund et al., 2010; Murray et al., 2015; Zhang et al., 2013). Quantitative florescent western blot analysis confirmed a consistent increase in protein levels observed between P12 and P24 (1.44 ± 0.06, P24/P12 ratio of Mean ± SEM; Fig. 4A,B). Additionally, the neurotrophic factor insulin-like growth factor 2 (IGF2) exhibited a decrease in the proteomic data (0.410 P24/P12 ratio in muscle) and has been implicated in in a mouse models of motor neuron

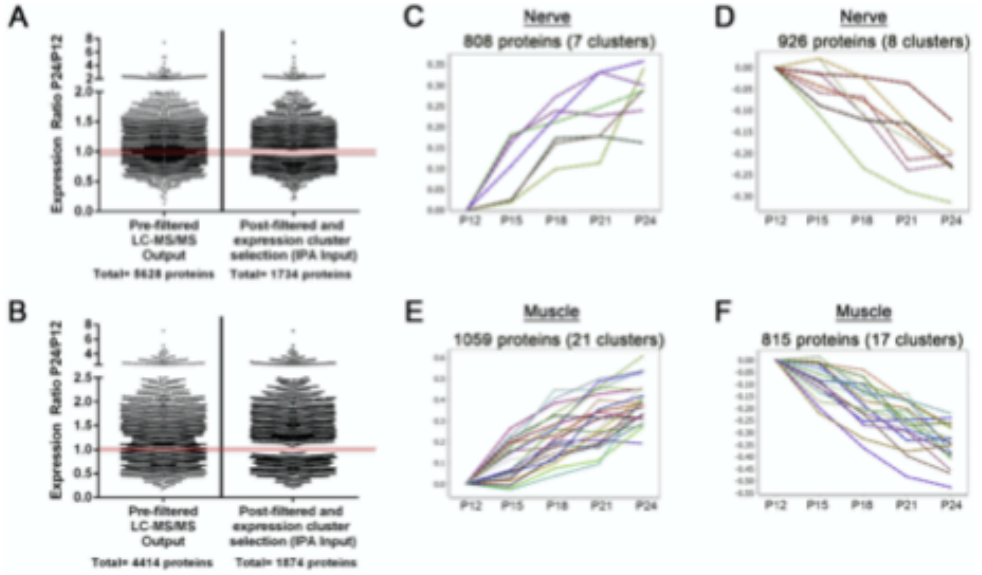

Fig. 3. Filtering of raw proteomic data produces an analysis-ready dataset of experimentally relevant proteins. (A,B) Scatter plot depicting the filtering process undertaken on raw proteomics nerve data (LC-MS/MS output identified by 2 more unique peptides) through manual selection of relevant expression clusters to generate a final list of 1734 proteins exhibiting consistent increases or decreases in expression in the murine sciatic nerve (A) or lumbrical muscle(B). Data are presented as expression ratios (P12/P24) and each data points represents an individual protein. (C-F) Graphs displays the relative change in protein levels relative to P12 of protein clusters, clustered on the basis of a similar trend, which display a desirable profile of continuous increase (C,E) or continuous decrease (D,F) in levels in either sciatic nerve (C,D) or lumbrical muscle (E,F). Cluster generated in BioLayout *Express*^{3D} from the filtered nerve dataset (exhibiting a > 20% change in relative expression at P24 from P12). Proteins within these clusters feature a steady relative increase or decrease in levels over the P12-P24 time period, and were therefore selected for future analysis.

disease (Allodi et al., 2016; Hedlund et al., 2010; Murray et al., 2015; Zhang et al., 2013). Quantitative fluorescent western blot analysis on protein extracted from lumbrical muscle (IGF2) confirmed a consistent decrease in protein levels observed between P12 and P24 (0.402 ± 0.044, P24/P12 ratio of Mean ± SEM; Fig. 4A,C). Thus, these results confirm the direction and magnitude of expression change reported in our proteomic profiling.

3.2. Functional annotation analysis of filtered nerve and muscle data reveals a conserved enrichment for proteins related to oxidative phosphorylation and mitochondrial bioenergetics

The refined nerve and muscle data sets were sorted into four lists: (1) consistent up-regulated expression in nerve, (2) consistent down-regulated expression in nerve, (3) consistent up-regulated expression in muscle and (4) consistent down-regulated expression in muscle. These lists were analyzed using the Functional Annotation Clustering tool in DAVID Bioinformatics Resources (Version 6.7) to determine if the proteins whose expressions trend together share functional annotations. Interestingly, consistently up-regulated protein groups within the sciatic nerve revealed a marked enrichment for processes implicated in oxidative phosphorylation and mitochondrial respiration (Table 1). The most significantly enriched group was comprised of proteins involved in NAD-dependent "redox" processes. Analysis of proteins consistently down-regulated within the sciatic nerve was dominated by the presence of biological groups involved in mRNA processing and binding, as well as RNA-editing machinery such as the RNP complex and spliceosome (Table 1). Other top groups contained proteins pertaining to endoplasmic reticulum activity.

In the muscle, analysis of proteins consistently up-regulated also revealed an enrichment of processes relating to mitochondria, specifically (as with nerve) oxidative phosphorylation (Table 2). Indeed, all "top-5" biological groups produced by this analysis were clusters involved in electron transport chain activity or broader mitochondrial functions. Analysis of proteins consistently down-regulated within the lumbrical muscles identified endoplasmic reticulum (similar to nerve), protein transport, membrane-bound vesicles, and actin-binding (Table 2). Thus, the functional clustering analysis suggest a general shared consistent increase in proteins pertaining to mitochondria, oxidation reduction and the electron transport chain in muscle and nerve.

3.3. In silico pathway analysis reveals conserved direct interactions between components of the oxidative phosphorylation pathway in both muscle and nerve

Given the enrichment for proteins associated with mitochondrial functions within our refined candidate lists, we next employed IPA software to our cluster-derived lists in order to contextualize these protein changes into specific cellular cascades with the aim of identifying potential intervention points, as performed previously (Catenaccio et al., 2017; Graham et al., 2017; Llavero Hurtado et al., 2017). Unlike other network-based approaches, IPA generates molecular networks based on interactions reported in its "hand-curated" database, with the option for restricting analyses to only experimentally

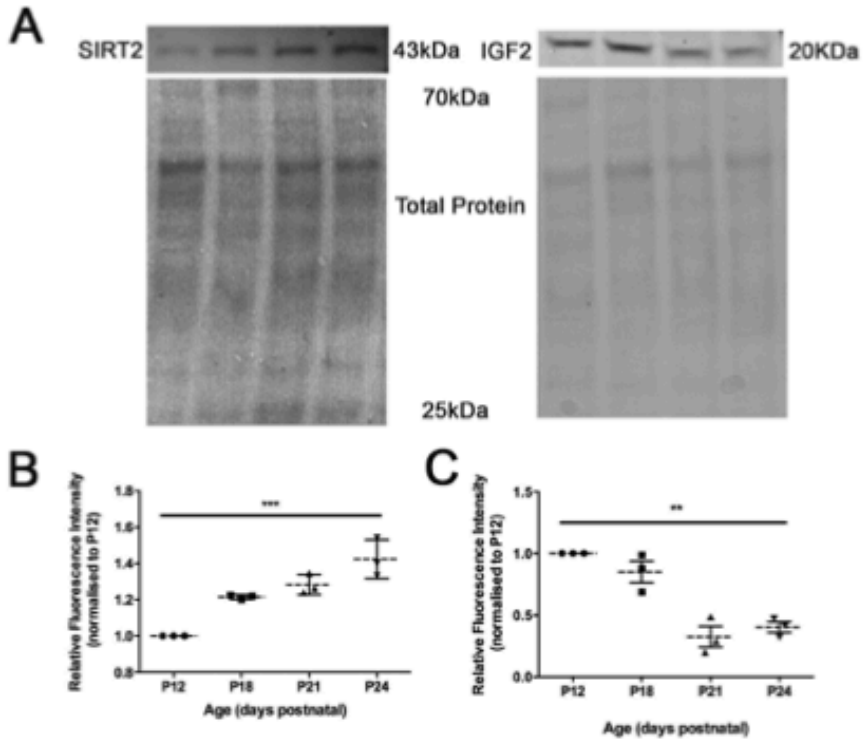

Fig. 4. Candidate validation of proteomic data by quantitative fluorescent Western blotting. (A) Representative western blots for NAD-dependent deacetylase sirtuin-2 (Sirt2) in nerve and insulin-like growth factor 2 (Igf2) in muscle. All candidate blots were normalized to total protein load (Ponceau S stain) (B,C) Scatter plots (individual data points; Mean ± SEM) of relative expression of Sirt2 (B) and Igf2 (C) relative to P12. Note direction and magnitude of change is consistent with TMT data. (n = 3 pairs of nerves (SIRT2) or 8 lumbrical muscles (IGF2) per time point; $^{**}p < 0.01$, $^{***}P < 0.001$ by Kruskall-Wallis test).

reported interactions. Initially, this analysis was performed on nerve and muscle data sets independently. This analysis of nerve and muscle included all mappable proteins from both nerve and muscle data sets (1713 and 1862 respectively) and were analyzed in parallel, with interactions restricted to only those reported experimentally (as opposed to *in silico* predictions). The filtered list of proteins from nerve and muscle were imported into IPA and of these, > 98% were mappable by the software and therefore suitable for data mining of the published literature to generate interaction networks. As expected, this revealed molecular networks dominated by proteins pertaining to mitochondrial respiratory components, specifically, components of the electron transport chain—and redox sensitivity in both muscle and nerve (Supplementary Figs. 1 and 2).

We next utilized the Path Designer function in IPA to identify a molecular overlap between the predicted networks generated from the previous independent nerve and muscle analyses. Extrapolation of this convergence into a visual network, organized by cellular location, revealed the conservation of multiple direct interactions between components of the electron transport chain in both nerve and muscle data sets, with a specific enrichment for factors involved with Complex I and IV (Fig. 5). In accordance with the previous functional annotation analyses of nerve and muscle data sets, these results demonstrated an

Table 1
Top 5 most significantly enriched functional clusters in sciatic nerve.

Up from P12-P24		Down from P12-P24	
Cluster name	Enrichment score	Cluster name	Enrichment score
Mitochondrial oxidation reduction; NAD-dependent	8.44	mRNA processing/Spliceosome	25.24
Cell fraction	4.61	RNP complex/ribosome	23.19
Cytoskeletal actin binding	4.53	RNA binding	16.1
Membrane lipoproteins	4.26	Intracellular organelle lumen	12.54
Magnesium binding	4.06	Endoplasmic reticulum	11.87

Table 2
Top 5 most significantly enriched functional clusters between P12 and P24 in the lumbrical muscles.

Up from P12-P24		Down from P12-P24	
Cluster name	Enrichment score	Cluster name	Enrichment score
Mitochondria	134.15	Endoplasmic reticulum	12.26
Mitochondrial membrane	82.63	Protein transport	10.38
Oxidation reduction/electron transport chain (ETC)	43.65	Membrane-bound vesicle	9.81
Electron transport/oxidoreductase/NADH dehydrogenase activity	25.4	Actin binding/actin cytoskeleton	8.89
Cellular respiration/electron transport chain	22.5	Actin cytoskeleton organization	8.52

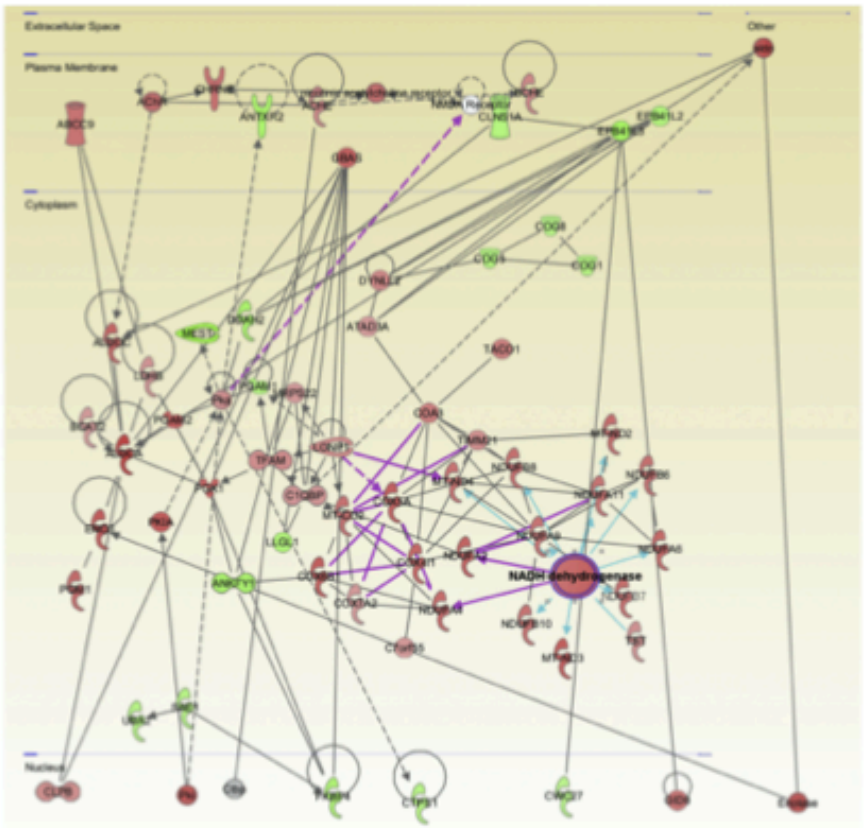

Fig. 5. Combined analysis in nerve and muscle reveals conserved escalation in mitochondrial oxidative phosphorylation related proteins. Use of the Path Designer function in IPA software, to reveal combined interaction network, reveals an overlap in molecular interactions pertaining to the mitochondrial oxidative phosphorylation process. Specifically, candidates identified as components of mitochondrial Complex I (NADH dehydrogenase) and Complex IV (cytochrome *c* oxidase) exhibit conserved expression changes in both nerve and muscle data sets. Proteins within this network reflect those which up-regulated (red) and down-regulated (green) during the P12-P24 time-course in either nerve or muscle; intensity of colour corresponds with magnitude of expression change. White represents a molecule that is absent from both datasets but an important component of the network. Grey represents a molecule that is present in the datasets but the change in levels is below the 20% cut-off. Solid connecting lines represent a direct interaction, while dashed connecting lines indicate an indirect interaction. Interactions conserved between nerve and muscle data sets are highlighted as purple connecting lines. Blue connecting lines represent the highlighted interactions of NADH dehydrogenase. All suggested indirect interactions were confirmed manually using the IPA software to identify publications indicating an experimentally reported interaction between the two components. (For interpretation of the references to colour in this figure legend, the reader is referred to the web version of this article.)

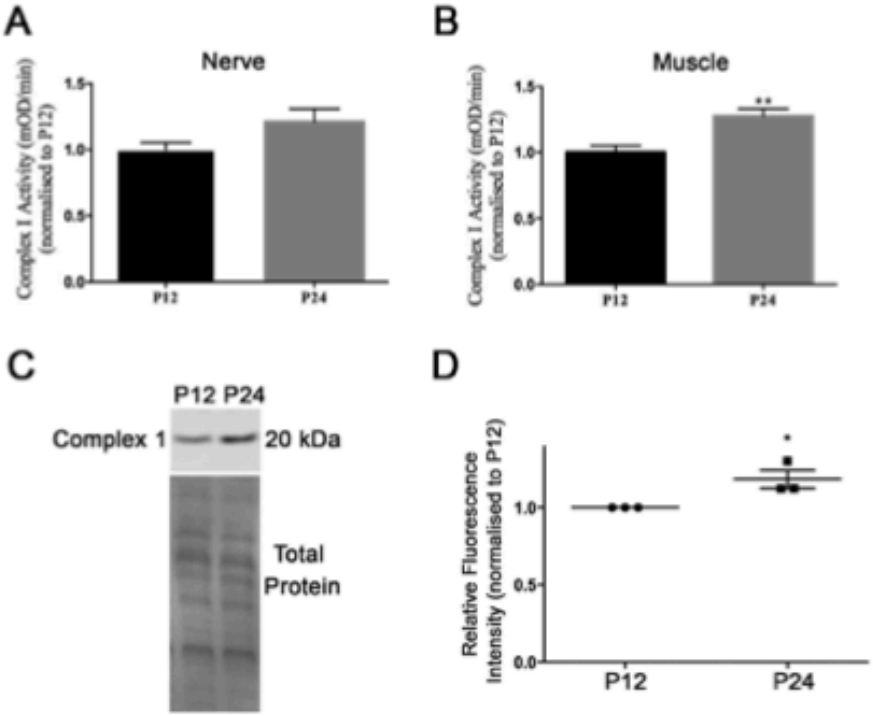

Fig. 6. Complex I activity and levels are up-regulated between P12 and P24 in muscle and nerve. (A, B) Bar chart (Mean ± SEM) showing Complex I (NADH dehydrogenase) activity in P12 and P24 sciatic nerve (A) and lumbrical muscle (B). NADH dehydrogenase activity was measured kinetically over 60 min and the rate was determined as change in optical density over time, and expressed normalized to P12 ($n = 3$ biological replicates, 5 mice per group; ** $P < 0.05$ by Mann Whitney *U* test). (C) Image showing example western blot using antibodies against Complex I subunit on muscle from P12 and P24 mice, with Ponceau S staining showing total protein as a loading control. (D) Bar chart (Mean ± SEM) showing quantification of western blot against Complex I. Data expressed normalized to loading control and relative to levels at P12. ($N = 3$ biological replicates, 5 mice per time point, * $P < 0.05$ by Mann Whitney U test).

increased expression in proteins involved in the mitochondrial electron transport chain over the P12-P24 period. This suggests that differences in mitochondrial electron transport chain component expression and/or activity may serve as a key hub for the regulation of the molecular processes being mapped out through this temporal profiling of progressive vulnerability.

We next performed enzyme-linked immunosorbance assays (ELISA) of Complex I NADH dehydrogenase activity in order to determine whether our *in silico*-derived suggestion of an increase in Complex I expression was accompanied by a functional increase of Complex I activity. Analysis of these results suggested a consistent increase of Complex I activity in both the nerve and skeletal muscle of P24 compared to P12 mice, which reached statistical significance in muscle (Fig. 6A,B). We also aimed to assess the expression of Complex I by quantitative fluorescent western blotting, and confirmed an increase in Complex I expression levels in the skeletal muscle of P24 mice compared to P12 mice as predicted (Fig. 6C,D). This therefore confirms the validity of the data filtering strategy employed and the identified molecular cascades being represented in the subsequent *in silico* analysis.

3.4. Inhibition of Complex I prevents the rise in reactive oxygen species and protects axons following injury

The above data indicate that an increase in Complex I of the mitochondrial respiratory chain correlates with the acceleration in the rate of axon degeneration in response to injury. We therefore aimed to determine whether inhibition of Complex I could delay axon degeneration. For these experiments, we employed the Complex I inhibitor, rotenone and used an established murine dorsal root ganglion primary culture model (Lopez-Leal et al., 2018). This model has the benefit of allowing us to assess axon intrinsic factors regulating axon degeneration. 12 h after axotomy (induced by severing cell bodies from their axons), robust degeneration was observed in control cultures, as evidence by widespread fragmentation of neurofilament labelled axons (Fig. 7A). However, in cultures exposed to 10 μM rotenone, axonal fragmentation was visibly reduced. Quantitation of the degree of axon degeneration revealed a significant decrease in cultures treated with rotenone, to levels similar to those of non-injured controls (Fig. 7B), demonstrating that inhibition of Complex I can indeed be protective to the axonal compartment of neurons.

Reactive oxygen species (ROS) have previously been implicated in axon degeneration (Barrientos et al., 2011; Villegas et al., 2014; O'Donnell et al., 2013; Park et al., 2013; Calixto et al., 2012). As

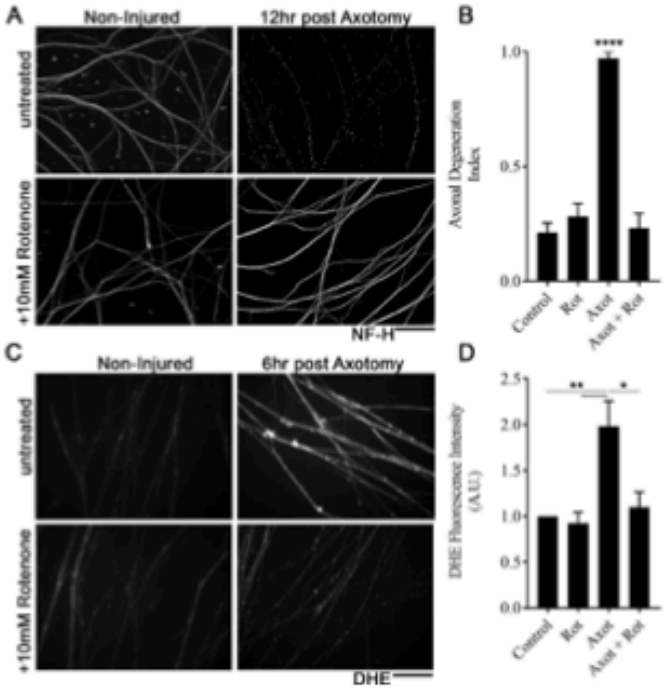

Fig. 7. Rotenone protects axons and ameliorates rise in ROS in a DRG model of axon injury. A) Fluorescent images show axons from dorsal root ganglion primary cultures labelled with antibodies against neurofilament heavy chain (NF-H) which are either non-injured or 12 h post axotomy. Note widespread axon fragmentation following axotomy which is prevented by treatment with 10 μM rotenone. Scale bar = 20 μM B) Bar chart (Mean ± SEM) shown axon degeneration index in non-injured (Control/Rot) on injured (Axot/Axot + Rot) cultures which were either untreated (Control/Axot) or exposed to 10 μM Rotenone (Rot/Axot + Rot). **** $P < 0.0001$ Axot compared to all other groups, ANOVA with Tukeys multiple comparison test. C) Fluorescent images show axons from dorsal root ganglion primary cultures labelled with DHE which are either non-injured or 6 h post axotomy. Note increase in fluorescence following axotomy which is not observed following treatment with 10 μM rotenone. Scale bar = 20 μM D Bar chart (Mean ± SEM) shown DHE fluorescence in non-injured (Control/Rot) on injured (Axot/Axot + Rot) cultures which were either untreated (Control/Axot) or exposed to 10 μM Rotenone (Rot/Axot + Rot). **$P < 0.01$; *$P < 0.05$; ANOVA with Tukeys multiple comparison test.

Complex I is a major source of reactive ROS, we hypothesized that the protection following Complex I inhibition may be linked to a decrease in ROS. Dihydroethidium (DHE; a Redox sensitive fluorescent probe) was applied to DRG cultures. 6 h following axon injury, a significant increase in DHE fluorescence was observed compared to non-injured controls (Fig. 7C,D). However, in cultures treated with rotenone, DHE fluorescence remained similar to non-injured controls, and was significantly reduced compared to untreated cultures. Together, these data suggest that inhibition of Complex I *via* rotenone can inhibit the axotomy related rise in ROS and prevent axon degeneration.

3.5. Up-regulating basal OXPHOS at P15 accelerates degeneration of NMJs

The data thus far reveal an up-regulation in oxidative phosphorylation between P12 and P24, which coincides with the acceleration of WD with postnatal age. This data support the hypothesis that a decrease in Complex I activity results in the neuroprotective phenotype observed in neonatal mice. We therefore asked whether experimentally upregulating basal OXPHOS levels would abolish the delayed WD phenotype in neonatal mice. Adenosine monophosphate kinase (AMPK) is capable of sensing AMP levels and impacts upon downstream pathways, most markedly those acting upon the energy status of the cell. Activation of AMPK *via* the AMPK agonist AICAR results in up-regulation of oxidative metabolism (Golubitzky et al., 2011; Jager et al., 2007; Pacelli et al., 2015). In order to determine whether stimulation of mitochondrial activity could accelerate axon degeneration, we used an *ex-vivo* assay of nerve-muscle preparations from P15 mice in either the presence of absence of AICAR. Addition of 2 mM AICAR significantly enhanced the rate of NMJ degeneration after 24 h *ex-vivo* (Fig. 8). This suggest that increasing the amount of proteins related to (and thus overall activity of) oxidative phosphorylation between P12 and P24, could account for the acceleration of WD *in vivo*. Together with the findings above, these data support the notion that the changes in mitochondrial proteins observed between P12 and P24 could account for the acceleration in the rate of WD in this same time window.

4. Discussion

In this study we applied a tandem mass tagging method to quantitatively profile the proteome of the nerve and muscle over a critical period of postnatal development when the rate of WD following axonal injury is increasing. The data suggest that elevation in proteins associated with mitochondria and oxidative phosphorylation closely accompanies the acceleration in WD of the distal compartments of the motor neuron following axotomy. Specifically, there was a shared increase in protein expression associated with Complex I and IV of the OXPHOS pathways in both muscle and nerve. An increase in both the activity and levels of Complex I was confirmed in muscle. We also demonstrate that inhibition of Complex I prevents the axotomy related rise in ROS and protects the axon from degeneration. Finally, using the *ex-vivo* model of neuronal injury, we demonstrate that up-regulating basal OXPHOS levels ablates the delay in WD observed in neonatal mice. These findings imply a regulatory role for mitochondria in synaptic maintenance and degeneration. The data also provide evidence for a dynamically evolving postnatal proteome, including altered levels of mitochondrial proteins that can influence sensitivity to triggers of synaptic and axonal degeneration.

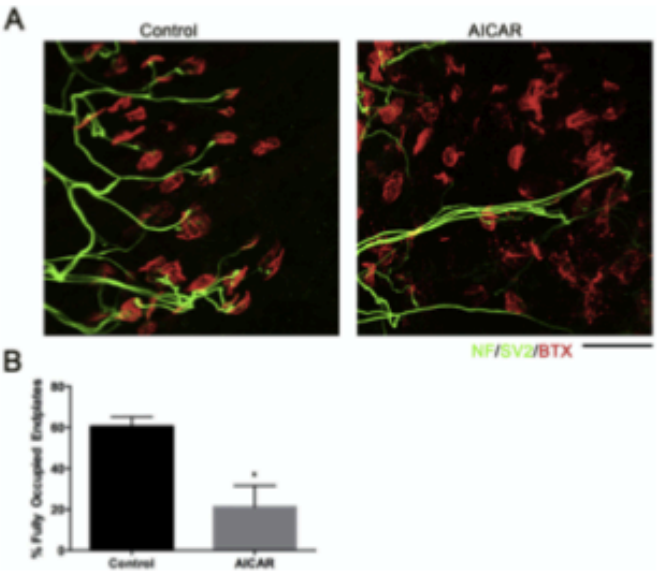

Fig. 8. The AMP-kinase agonist AICAR accelerates NMJ loss in P15 mice in an *ex-vivo* model of axonal injury. (A) Representative confocal micrographs of NMJs from deep lumbrical muscles isolated from P15 C57BL/6 J wildtype mice, after 24 h incubation *ex-vivo* at 28 °C in either standard MPS CO_2 ringer solution or MPS CO_2 ringer solution +2 mM AICAR. NMJs labelled with antibodies against neurofilament (NF; green) and synaptic vesicle protein 2 (SV2; green) and alpha-bungarotoxin (BTX; red). Note increase in the number of vacant endplates following AICAR treatment. Scale bar = 50 μm (B) Bar chart (Mean ± SEM) confirms significant decrease in the percentage of fully occupied NMJs in AICAR-incubated muscles compared to control. ($n = 4$ muscles/4 mice per group; $^*p < 0.05$ by Mann-Whitney *U* test). (For interpretation of the references to colour in this figure legend, the reader is referred to the web version of this article.)

4.1. Implications of the evolving postnatal proteome for neuromuscular disease

The findings we present in this study demonstrate that a broad range of molecular pathways evolve steadily and dynamically over postnatal development. It is therefore likely that a broad array of molecular pathways, including those potentially impacting upon pathogenic cascades, could be markedly influenced by the age of the individual. This immediately invites consideration into the family of neuromuscular diseases arising in early childhood, including: spinal muscular atrophy, Duchenne's muscular dystrophy, Charcot-Marie-Tooth disease and spinal bulbar muscular atrophy. There are clearly important implications both for the use of animal models to research these diseases, and for the prognosis and treatment of patients.

Mouse models of a variety of neuromuscular disorders tend to manifest during the first post-natal month. The is certainly true of those models mimicking pediatric neuromuscular disorders (Bowerman et al., 2012; Le et al., 2005), but is also evident in spontaneous mutants with peripheral neuropathies (Hedlund et al., 2010; Brown et al., 1995) and models mimicking adult onset disorders (Schmalbruch et al., 1991; Xu et al., 1993). Such models are commonly used to understand the molecular and structural events which occur during the disease time course. Whilst this is clearly of great importance, it is also important to consider how the evolving proteome impact upon the pathological processes. Some pertinent examples of this arise from the SMA research field. This includes a marked difference in the severity in pathology when *Smn*, the disease gene, is turned off in adulthood compared to in neonates (Kariya et al., 2014) and a change in the severity and pattern of selective vulnerability between SMA mouse models which manifest at different ages (Bowerman et al., 2012; Le et al., 2005; Murray et al., 2008). The data we present here suggest that the differences in the manifestation of neuromuscular pathology observed between these mouse models is due to the evolving proteome occurring during the time period. Indeed, several proteins which are known to impact upon the pathological mechanisms implicated in neuromuscular pathology in SMA and other motor neuron diseases were found to be altered during the postnatal period. This includes proteins such as IGF2 which has been shown to be an important modifier in motor neuron disease (Allodi et al., 2016; Hedlund et al., 2010).

It becomes increasing apparent that it will be of great importance to understand how the timing of murine postnatal development relates to human postnatal development. Mice clearly have a different lifespan, and are born with considerably different motor abilities, and potentially at a different stage of neuromuscular maturity. The morphological events occurring in the first postnatal month in the mouse have been extensively characterized, but the lack of available tissue makes it very difficult to know if and when these morphological changes occur into humans. In mice, axons of the ventral ramus appear to grow out from the spinal cord at around E12.5, reach the dorsal and ventral muscle masses at around E13.5, and initial nerve muscle contacts are formed at around E14.5 (Hurren et al., 2015). Acetylcholine receptor clusters are not observed until around E14, becoming numerous at around E15 (Hurren et al., 2015). This suggests formation of neuromuscular contacts occurs at around 60 to 70% of the way through gestation. Detail on the equivalent process in human is inevitably more sparse, but clusters of acetylcholine receptors and axon bundles have been observed at around 10 gestational weeks, with plaque like endplate structure visible at 14 gestational weeks (Martinez-Hernandez et al., 2013). It has also been suggested that mono-innervated endplates could be observed at 14 gestational weeks (Martinez-Hernandez et al., 2013). Human NMJ formation therefore likely occurs at around 30% of the way through gestation. Based on these figures, it would appear that the initial formation of NMJs occurs at a comparably earlier time point in humans than it does in mice. It is therefore tempting to assume that humans are born with a comparatively more mature neuromuscular system although clearly the details of human neuromuscular maturation requires further investigation. However, the current profiling of molecular events in mice will be of fundamental importance for future comparison with human data.

4.2. The role of mitochondria in WD

Functional annotation analysis of proteins exhibiting a steady up-regulation over the P12-P24 period revealed a striking enrichment for the processes of OXPHOS and associated mitochondrial functions, in both the nerve and muscle. Strikingly, pathway analysis of proteomic alterations occurring in both the nerve and the muscle further suggested a conserved escalation in mitochondrial OXPHOS activity and redox sensitivity pathways. Taken together, these findings invite consideration of both how this might relate to the progressive acceleration in the rate of WD, and how this information may impact upon our understanding of the mechanisms of synaptic and axonal degeneration.

The implication of mitochondria in the process of WD is certainly not novel, although there is controversy as to the extent to which they are required for the process of WD. Mitochondrial swelling during WD has been noted in early ultra-structural studies of degenerating nerves (Vial, 1958). It has been shown that over-expression of the mitochondrially localized form of Nicotinamide mononucleotide adenylyltransferase, Nmnat3, can protect axons from injury in both mouse and drosophila models (Avery et al., 2012; Berger et al., 2005; Yahata et al., 2009). The specifics of the involvement of mitochondria in WD remain highly debated. It is clear that axon injury results in a reduction in mitochondrial motility, and that this sudden reduction in mitochondrial motility observed in wildtype axons following axotomy, is markedly suppressed in Wld^{s} axons (Avery et al., 2012). However it has also been shown that there is also reduced mitochondrial motility in axons from *Sarm1* deficient mice, in which the axons show a similar Wld^{s} like protection from axon degeneration (Summers et al., 2014). This suggests that a reduction in mitochondrial motility is not necessary for axon degeneration. A number of other cellular events which are closely linked with mitochondria have been shown to have an important effect upon axon degeneration. This includes energy depletion, as evidenced by a reduction in NAD and ATP levels, a rise in calcium levels and increased production of reactive oxygen species (Park et al., 2013). Indeed it has been suggested that a key event in axon degeneration is the opening of the mitochondrial permeability transitioning pore, which results in the observed swelling of the mitochondria and the release of ROS and increase in calcium levels (Barrientos et al., 2011; Villegas et al., 2014; Calixto et al., 2012). The specifics of the relationships between the individual factors which have been shown to influence axon degeneration remain to be defined. However, from this work, an important role for mitochondria is evident. For this reason, our observed increase in mitochondrial protein expression is highly likely to be associated with the acceleration in the rate of WD.

How then may the progressive increase in mitochondrial proteins observed in neonatal mice lead to the progressive increase in the rate of WD? The proteomic analysis points to a specific enrichment for proteins pertaining to Complex I of the electron transport chain. Complex I has been shown to be the rate limiting step in energy production at the nerve terminal, a major source of protons for ATP synthesis and therefore a major source of ROS production (Giachin et al., 2016; Telford et al., 2009). ROS levels rise rapidly after axon injury and inhibition of ROS can delay axon degeneration (O'Donnell et al., 2013). Indeed, here we show that the rise in ROS following injury in prevented by application of a Complex I inhibitor, and this correlated with protection of the axon. This rise is ROS levels is not observed in Wld^{s} mice, thus presenting a possible mechanism of action (O'Donnell et al., 2013). Furthermore, although the rise in ROS is still observed in $Sarm1^{-/-}$ axons, they appear to be somehow resistant to oxidative damage caused by ROS. This suggests that Sarm1 may mediate the damage caused by ROS, and loss of Sarm1 leads to a delayed axon degeneration as the cell is protected from damage caused by ROS (Summers et al., 2014). Given that Complex I is a major source of ROS production (Giachin et al., 2016; Telford et al., 2009), and inhibition of Complex I is protective to axons, it seems reasonable to speculate that the increase in Complex I activity between P12 and P24 can account for the acceleration in the rate of WD over this same time period. Similarly, the lower level of Complex I activity in neonatal nerve, results in a slower production of ROS after nerve injury, and therefore a slower rate of WD. Previous work has also shown that the opening of the MPTP induces a conformational change in Complex I, which leads to a rapid increase in ROS production and release (Batandier et al., 2004). It is therefore possible that the progressive increase in Complex I levels between P12 and P24 lead to increased ROS production following MPTP opening during WD. In future work, it would be interesting to address the basal and induced levels of ROS during axon degeneration in neonatal nerve.

5. Conclusions

Quantitative analysis revealed that the neuromuscular proteome changes between the ages of P12 and P24, dynamically altering the state of a broad range of molecular networks, most significantly in those involved in mitochondrial bioenergetics. Based on these findings, we determined that pharmacologically up-regulating basal OXPHOS activity at P12, an age characterized both *in vivo* and *ex-vivo* by a delay in the rate of synaptic degeneration, results in significantly increased sensitivity of NMJ to axotomy. This suggests that basal levels of mitochondrial OXPHOS activity may pre-condition the motor neuron to degenerate more rapidly in the event of traumatic injury, perhaps thereby facilitating axonal regeneration. We show than inhibition of Complex I can prevent the axotomy related increase in ROS and that this correlates with axon protection. Elucidating the mechanism by which mitochondrial bioenergetics contributes to the injury-induced molecular response should enhance understanding of motor neuron degeneration. In a broader context, alterations in protein expression across early postnatal development may influence the particular vulnerability of the motor neuron and skeletal muscle in neuromuscular diseases of early childhood.

Supplementary data to this article can be found online at https://doi.org/10.1016/j.nbd.2019.104496.

Acknowledgements

The proteomic analysis was performed by FingerPrints Proteomics Facilities at the University of Dundee (Mr. Dougie Lamont). Antibodies to SIRT2 were generously provided by the Gillingwater Laboratory, University of Edinburgh, UK. The authors would like to thank Miss Samantha Eaton (Roslin Institute) and Dr. Abdel Atrih (FingerPrints Proteomics Facility) for their expertise and assistance in the preparation of samples for protein analysis and mass spectrometry experiments. We would also like to thank Dr. Paul Skehel for critical reading of the manuscript.

Funding

This work was funded by grants from Fight SMA (www.fightsma.org) to LMM; Muscular Dystrophy Association (www.mda.org) development grant to LMM (MDA294433); Tenovus (http://www.tenovus-scotland.org.uk) grant to LMM (E15/4); Newlife foundation for disabled children (http://www.newlifecharity.co.uk) start up grant to LMM (SG/14-15/08); Gwendolyn Strong Foundation (http://thegsf.org) Masters Scholarship to RAK; Medical Research Council Grant to RRR [https://mrc.ukri.org; Ref MR/M024075/1], Motor Neuron Disease Association grant to RRR [https://www.mndassociation.org; Ref 838-791], TMW is supported by Institute Strategic Programme Grant Funding from the BBSRC (TMW; https://bbsrc.ukri.org) and The Darwin Trust of Edinburgh (MLH). RK is funded by a PhD studentship from the Euan McDonald Centre for Motor Neuron Disease Research. FC is funded by Geroscience Center for Brain Health and Metabolism (FONDAP-15150012) and Fondo Nacional de Desarrollo Científico y Tecnológico (http://www.conicyt.cl/fondecyt/; FONDECYT, No. 1150766).

The funding bodies had no input in the study design, collection, analysis or interpretation of data or writing the manuscript.

References

Adalbert, R., Gillingwater, T.H., Haley, J.E., Bridge, K., Beirowski, B., Berek, L., Wagner, D., Grumme, D., Thomson, D., Celik, A., et al., 2005. A rat model of slow Wallerian degeneration (WldS) with improved preservation of neuromuscular synapses. Eur. J. Neurosci. 21 (1), 271–277.

Aghamaleky Sarvestany, A., Hunter, G., Tavendale, A., Lamont, D.J., Llavero Hurtado, M., Graham, L.C., Wishart, T.M., Gillingwater, T.H., 2014. Label-free quantitative proteomic profiling identifies disruption of ubiquitin homeostasis as a key driver of Schwann cell defects in spinal muscular atrophy. J. Proteome Res. 13 (11), 4546–4557.

Allodi, I., Comley, L., Nichterwitz, S., Nizzardo, M., Simone, C., Benitez, J.A., Cao, M., Corti, S., Hedlund, E., 2016. Differential neuronal vulnerability identifies IGF-2 as a protective factor in ALS. Sci. Rep. 6, 25960.

Amorim, I.S., Mitchell, N.L., Palmer, D.N., Sawiak, S.J., Mason, R., Wishart, T.M., Gillingwater, T.H., 2015. Molecular neuropathology of the synapse in sheep with CLN5 batten disease. Brain Behav. 5 (11), e00401.

Avery, M.A., Rooney, T.M., Pandya, J.D., Wishart, T.M., Gillingwater, T.H., Geddes, J.W., Sullivan, P.G., Freeman, M.R., 2012. WldS prevents axon degeneration through increased mitochondrial flux and enhanced mitochondrial Ca2+ buffering. Curr. Biol. 22 (7), 596–600.

Barrientos, S.A., Martinez, N.W., Yoo, S., Jara, J.S., Zamorano, S., Hetz, C., Twiss, J.L., Alvarez, J., Court, F.A., 2011. Axonal degeneration is mediated by the mitochondrial permeability transition pore. J. Neurosci. 31 (3), 966–978.

Batandier, C., Leverve, X., Fontaine, E., 2004. Opening of the mitochondrial permeability transition pore induces reactive oxygen species production at the level of the respiratory chain complex I. J. Biol. Chem. 279 (17), 17197–17204.

Beirowski, B., Babetto, E., Coleman, M.P., Martin, K.R., 2008. The WldS gene delays axonal but not somatic degeneration in a rat glaucoma model. Eur. J. Neurosci. 28 (6), 1166–1179.

Beirowski, B., Morreale, G., Conforti, L., Mazzola, F., Di Stefano, M., Wilbrey, A., Babetto, E., Janeckova, L., Magni, G., Coleman, M.P., 2010. WldS can delay Wallerian degeneration in mice when interaction with valosin-containing protein is weakened. Neuroscience 166 (1), 201–211.

Berger, F., Lau, C., Dahlmann, M., Ziegler, M., 2005. Subcellular compartmentation and differential catalytic properties of the three human nicotinamide mononucleotide adenylyltransferase isoforms. J. Biol. Chem. 280 (43), 36334–36341.

Bowerman, M., Murray, L.M., Beauvais, A., Pinheiro, B., Kothary, R., 2012. A critical smn threshold in mice dictates onset of an intermediate spinal muscular atrophy phenotype associated with a distinct neuromuscular junction pathology. Neuromuscul. Disord. 22 (3), 263–276.

Brown, M.C., Perry, V.H., Hunt, S.P., Lapper, S.R., 1994. Further studies on motor and sensory nerve regeneration in mice with delayed Wallerian degeneration. Eur. J. Neurosci. 6 (3), 420–428.

Brown, A., Bernier, G., Mathieu, M., Rossant, J., Kothary, R., 1995. The mouse dystonia musculorum gene is a neural isoform of bullous pemphigoid antigen 1. Nat. Genet. 10 (3), 301–306.

Brown, R., Hynes-Allen, A., Swan, A.J., Dissanayake, K.N., Gillingwater, T.H., Ribchester, R.R., 2015. Activity-dependent degeneration of axotomized neuromuscular synapses in Wld S mice. Neuroscience 290, 300–320.

Calixto, A., Jara, J.S., Court, F.A., 2012. Diapause formation and downregulation of insulin-like signaling via DAF-16/FOXO delays axonal degeneration and neuronal loss. PLoS Genet. 8 (12), e1003141.

Catanzaro, A., Llavero Hurtado, M., Diaz, P., Lamont, D.J., Wishart, T.M., Court, F.A., 2017. Molecular analysis of axonal-intrinsic and glial-associated co-regulation of axon degeneration. Cell Death Dis. 8 (11), e3166.

Coleman, M.P., Conforti, L., Buckmaster, E.A., Tarlton, A., Ewing, R.M., Brown, M.C., Lyon, M.F., Perry, V.H., 1998. An 85-kb tandem triplication in the slow Wallerian degeneration (Wlds) mouse. Proc. Natl. Acad. Sci. U. S. A. 95 (17), 9985–9990.

Comley, L.H., Fuller, H.R., Wishart, T.M., Mutsaers, C.A., Thomson, D., Wright, A.K., Ribchester, R.R., Morris, G.E., Parson, S.H., Horsburgh, K., et al., 2011. ApoE isoform-specific regulation of regeneration in the peripheral nervous system. Hum. Mol. Genet. 20 (12), 2406–2421.

Conforti, L., Tarlton, A., Mack, T.G., Mi, W., Buckmaster, E.A., Wagner, D., Perry, V.H., Coleman, M.P., 2000. A Ufd2/D4Cole1e chimeric protein and overexpression of Rbp7 in the slow Wallerian degeneration (WldS) mouse. Proc. Natl. Acad. Sci. U. S. A. 97 (21), 11377–11382.

Court, F.A., Coleman, M.P., 2012. Mitochondria as a central sensor for axonal degenerative stimuli. Trends Neurosci. 35 (6), 364–372.

de Pedro-Cuesta, J., Rabano, A., Martinez-Martin, P., Ruiz-Tovar, M., Alcalde-Cabero, E., Almazan-Isla, J., Avellanal, F., Calero, M., 2015. Comparative incidence of conformational, neurodegenerative disorders. PLoS ONE 10 (9), e0137342.

Dyken, P., Krawiecki, N., 1983. Neurodegenerative diseases of infancy and childhood. Ann. Neurol. 13 (4), 351–364.

Ferri, A., Sanes, J.R., Coleman, M.P., Cunningham, J.M., Kato, A.C., 2003. Inhibiting axon degeneration and synapse loss attenuates apoptosis and disease progression in a mouse model of motoneuron disease. Curr. Biol. 13 (8), 669–673.

Fuller, H.R., Hurtado, M.L., Wishart, T.M., Gates, M.A., 2014. The rat striatum responds to nigro-striatal degeneration via the increased expression of proteins associated with growth and regeneration of neuronal circuitry. Proteome Sci. 12, 20.

Giachin, G., Bouveret, R., Acajjaoui, S., Pantalone, S., Soler-Lopez, M., 2016. Dynamics of human mitochondrial complex I assembly: implications for neurodegenerative diseases. Front. Mol. Biosci. 3, 43.

Gillingwater, T.H., Thomson, D., Mack, T.G., Soffin, E.M., Mattiesen, R.J., Coleman, M.P., Ribchester, R.R., 2002. Age-dependent synapse withdrawal at axotomised neuromuscular junctions in Wld(s) mutant and Ube4b/Nmnat transgenic mice. J. Physiol. 543, 739–755 Pt 3.

Gillingwater, T.H., Haley, J.E., Ribchester, R.R., Horsburgh, K., 2004. Neuroprotection after transient global cerebral ischemia in Wld(s) mutant mice. J. Cereb. Blood Flow Metab. 24 (1), 62–66.

Godzik, K., Coleman, M.P., 2015. The axon-protective WLD(S) protein partially rescues mitochondrial respiration and glycolysis after axonal injury. J. Mol. Neurosci. 55 (4), 865–871.

Golubitzky, A., Dan, P., Weissman, S., Link, G., Wikstrom, J.D., Saada, A., 2011. Screening for active small molecules in mitochondrial complex I deficient patient's fibroblasts, reveals AICAR as the most beneficial compound. PLoS ONE 6 (10), e26883.

Graham, L.C., Eaton, S.L., Brunton, P.J., Atrih, A., Smith, C., Lamont, D.J., Gillingwater, T.H., Pennetta, G., Skehel, P., Wishart, T.M., 2017. Proteomic profiling of neuronal mitochondria reveals modulators of synaptic architecture. Mol. Neurodegener. 12 (1), 77.

Hedlund, E., Karlsson, M., Osborn, T., Ludwig, W., Isacson, O., 2010. Global gene expression profiling of somatic motor neuron populations with different vulnerability identify molecules and pathways of degeneration and protection. Brain 133 (Pt 8), 2313–2330.

Heermann, S., Spittau, B., Zajzon, K., Schwab, M.H., Krieglstein, K., 2012. Schwann cells migrate along axons in the absence of GDNF signaling. BMC Neurosci. 13, 92.

Hoopfer, E.D., McLaughlin, T., Watts, R.J., Schuldiner, O., O'Leary, D.D., Luo, L., 2006. Wlds protection distinguishes axon degeneration following injury from naturally occurring developmental pruning. Neuron 50 (6), 883–895.

Howell, G.R., Libby, R.T., Jakobs, T.C., Smith, R.S., Phalan, F.C., Barter, J.W., Barbay, J.M., Marchant, J.K., Mahesh, N., Porciatti, V., et al., 2007. Axons of retinal ganglion cells are insulted in the optic nerve early in DBA/2J glaucoma. J. Cell Biol. 179 (7), 1523–1537.

Huang, da W., Sherman, B.T., Lempicki, R.A., 2009. Systematic and integrative analysis of large gene lists using DAVID bioinformatics resources. Nat. Protoc. 4 (1), 44–57.

Hurren, B., Collins, J.J., Duxson, M.J., Deries, M., 2015. First neuromuscular contact correlates with onset of primary myogenesis in rat and mouse limb muscles. PLoS ONE 10 (7), e0133811.

Jager, S., Handschin, C., St-Pierre, J., Spiegelman, B.M., 2007. AMP-activated protein kinase (AMPK) action in skeletal muscle via direct phosphorylation of PGC-1alpha. Proc. Natl. Acad. Sci. U. S. A. 104 (29), 12017–12022.

Kariya, S., Obis, T., Garone, C., Akay, T., Sera, F., Iwata, S., Homma, S., Monani, U.R., 2014. Requirement of enhanced survival Motoneuron protein imposed during neuromuscular junction maturation. J. Clin. Invest. 124 (2), 785–800.

Kawachi, I., Lassmann, H., 2017. Neurodegeneration in multiple sclerosis and neuromyelitis optica. J. Neurol. Neurosurg. Psychiatry 88 (2), 137–145.

Kitay, B.M., McCormack, R., Wang, Y., Tsoulfas, P., Zhai, R.G., 2013. Mislocalization of neuronal mitochondria reveals regulation of Wallerian degeneration and NMNAT/WLD(S)-mediated axon protection independent of axonal mitochondria. Hum. Mol. Genet. 22 (8), 1601–1614.

Le, T.T., Pham, L.T., Butchbach, M.E., Zhang, H.L., Monani, U.R., Coovert, D.D., Gavrilina, T.O., Xing, L., Bassell, G.J., Burghes, A.H., 2005. SMNDelta7, the major product of the centromeric survival motor neuron (SMN2) gene, extends survival in mice with spinal muscular atrophy and associates with full-length SMN. Hum. Mol. Genet. 14 (6), 845–857.

Llavero Hurtado, M., Fuller, H.R., Wong, A.M.S., Eaton, S.L., Gillingwater, T.H., Pennetta, G., Cooper, J.D., Wishart, T.M., 2017. Proteomic mapping of differentially vulnerable pre-synaptic populations identifies regulators of neuronal stability in vivo. Sci. Rep. 7 (1), 12412.

Lopez-Leal, R., Diaz, P., Court, F.A., 2018. In vitro analysis of the role of Schwann cells on axonal degeneration and regeneration using sensory neurons from dorsal root ganglia. Methods Mol. Biol. 1739, 255–267.

Loreto, A., Di Stefano, M., Gering, M., Conforti, L., 2015. Wallerian degeneration is executed by an NMN-SARM1-dependent late Ca(2+) influx but only modestly influenced by mitochondria. Cell Rep. 13 (11), 2539–2552.

Lyon, M.F., Ogunkolade, B.W., Brown, M.C., Atherton, D.J., Perry, V.H., 1993. A gene affecting Wallerian nerve degeneration maps distally on mouse chromosome 4. Proc. Natl. Acad. Sci. U. S. A. 90 (20), 9717–9720.

Mack, T.G., Reiner, M., Beirowski, B., Mi, W., Emanuelli, M., Wagner, D., Thomson, D., Gillingwater, T., Court, F., Conforti, L., et al., 2001. Wallerian degeneration of injured axons and synapses is delayed by a Ube4b/Nmnat chimeric gene. Nat. Neurosci. 4 (12), 1199–1206.

Martinez-Hernandez, R., Bernal, S., Also-Rallo, E., Alias, L., Barceló, M.J., Hereu, M., Esquerda, J.E., Tizzano, E.F., 2013. Synaptic defects in type I spinal muscular atrophy in human development. J. Pathol. 229 (1), 49–61.

Meyer zu Horste, G., Misbach, T.A., Muller, J.I., Fledrich, R., Stassart, R.M., Kieseier, B.C., Coleman, M.P., Sereda, M.W., 2011. The Wlds transgene reduces axon loss in a Charcot-Marie-Tooth disease 1A rat model and nicotinamide delays post-traumatic axonal degeneration. Neurobiol. Dis. 42 (1), 1–8.

Mi, W., Beirowski, B., Gillingwater, T.H., Adalbert, R., Wagner, D., Grumme, D., Osaka, H., Conforti, L., Arnhold, S., Addicks, K., et al., 2005. The slow Wallerian degeneration gene, WldS, inhibits axonal spheroid pathology in gracile axonal dystrophy mice. Brain 128, 405–416 Pt 2.

Milde, S., Gilley, J., Coleman, M.P., 2013. Subcellular localization determines the stability and axon protective capacity of axon survival factor Nmnat2. PLoS Biol. 11 (4), e1001539.

Murray, L.M., Comley, L.H., Thomson, D., Parkinson, N., Talbot, K., Gillingwater, T.H., 2008. Selective vulnerability of motor neurons and dissociation of pre- and post-synaptic pathology at the neuromuscular junction in mouse models of spinal muscular atrophy. Hum. Mol. Genet. 17 (7), 949–962.
Murray, L.M., Comley, L.H., Gillingwater, T.H., Parson, S.H., 2011. The response of neuromuscular junctions to injury is developmentally regulated. FASEB J. 25 (4), 1306–1313.
Murray, L.M., Beauvais, A., Gibeault, S., Courtney, N.L., Kothary, R., 2015. Transcriptional profiling of differentially vulnerable motor neurons at pre-symptomatic stage in the Smn (2b/−) mouse model of spinal muscular atrophy. Acta Neuropathol. Commun. 3, 55.
Mutsaers, C.A., Wishart, T.M., Lamont, D.J., Riessland, M., Schreml, J., Comley, L.H., Murray, L.M., Parson, S.H., Lochmüller, H., Wirth, B., et al., 2011. Reversible molecular pathology of skeletal muscle in spinal muscular atrophy. Hum. Mol. Genet. 20 (22), 4334–4344.
Mutsaers, C.A., Lamont, D.J., Hunter, G., Wishart, T.M., Gillingwater, T.H., 2013. Label-free proteomics identifies Calreticulin and GRP75/Mortalin as peripherally accessible protein biomarkers for spinal muscular atrophy. Genome Med. 5 (10), 95.
O'Donnell, K.C., Vargas, M.E., Sagasti, A., 2013. Wld(S) and PGC-1alpha regulate mitochondrial transport and oxidation state after axonal injury. J. Neurosci. 33 (37), 14778–14790.
O'Donnell, K.C., Lulla, A., Stahl, M.C., Wheat, N.D., Bronstein, J.M., Sagasti, A., 2014. Axon degeneration and PGC-1alpha-mediated protection in a zebrafish model of alpha-synuclein toxicity. Dis. Model. Mech. 7 (5), 571–582.
Osterloh, J.M., Yang, J., Rooney, T.M., Fox, A.N., Adalbert, R., Powell, E.H., Sheehan, A.E., Avery, M.A., Hackett, R., Logan, M.A., et al., 2012. dSarm/Sarm1 is required for activation of an injury-induced axon death pathway. Science 337 (6093), 481–484.
Oyebode, O.R., Hartley, R., Singhota, J., Thomson, D., Ribchester, R.R., 2012. Differential protection of neuromuscular sensory and motor axons and their endings in Wld(S) mutant mice. Neuroscience 200, 142–158.
Pacelli, C., Giguere, N., Bourque, M.J., Levesque, M., Slack, R.S., Trudeau, L.E., 2015. Elevated mitochondrial bioenergetics and axonal arborization size are key contributors to the vulnerability of dopamine neurons. Curr. Biol. 25 (18), 2349–2360.
Park, J.Y., Jang, S.Y., Shin, Y.K., Koh, H., Suh, D.J., Shinji, T., Araki, T., Park, H.T., 2013. Mitochondrial swelling and microtubule depolymerization are associated with energy depletion in axon degeneration. Neuroscience 238, 258–269.
Sajadi, A., Schneider, B.L., Aebischer, P., 2004. Wlds-mediated protection of dopaminergic fibers in an animal model of Parkinson disease. Curr. Biol. 14 (4), 326–330.
Samsam, M., Mi, W., Wessig, C., Zielasek, J., Toyka, K.V., Coleman, M.P., Martini, R., 2003. The Wlds mutation delays robust loss of motor and sensory axons in a genetic model for myelin-related axonopathy. J. Neurosci. 23 (7), 2833–2839.
Savli, H., Szendroi, A., Romics, I., Nagy, B., 2008. Gene network and canonical pathway analysis in prostate cancer: a microarray study. Exp. Mol. Med. 40 (2), 176–185.
Saxena, S., Caroni, P., 2007. Mechanisms of axon degeneration: from development to disease. Prog. Neurobiol. 83 (3), 174–191.
Schmalbruch, H., Jensen, H.J., Bjaerg, M., Kamieniecka, Z., Kurland, L., 1991. A new mouse mutant with progressive motor neuronopathy. J. Neuropathol. Exp. Neurol. 50 (3), 192–206.
Spadari, S., Focher, F., Kuenzle, C., Corey, E.J., Myers, A.G., Hardt, N., Rebuzzini, A., Ciarrocchi, G., Pedrali-Noy, G., 1985. In vivo distribution and activity of aphidicolin on dividing and quiescent cells. Antivir. Res. 5 (2), 93–101.
Stoll, G., Muller, H.W., 1999. Nerve injury, axonal degeneration and neural regeneration: basic insights. Brain Pathol. 9 (2), 313–325.
Summers, D.W., DiAntonio, A., Milbrandt, J., 2014. Mitochondrial dysfunction induces Sarm1-dependent cell death in sensory neurons. J. Neurosci. 34 (28), 9338–9350.
Telford, J.E., Kilbride, S.M., Davey, G.P., 2009. Complex I is rate-limiting for oxygen consumption in the nerve terminal. J. Biol. Chem. 284 (14), 9109–9114.
Theocharidis, A., van Dongen, S., Enright, A.J., Freeman, T.C., 2009. Network visualization and analysis of gene expression data using BioLayout Express(3D). Nat. Protoc. 4 (10), 1535–1550.
Vial, J.D., 1958. The early changes in the axoplasm during wallerian degeneration. J. Biophys. Biochem. Cytol. 4 (5), 551–555.
Villegas, R., Martinez, N.W., Lillo, J., Pihan, P., Hernandez, D., Twiss, J.L., Court, F.A., 2014. Calcium release from intra-axonal endoplasmic reticulum leads to axon degeneration through mitochondrial dysfunction. J. Neurosci. 34 (21), 7179–7189.
Wallace, T.L., Johnson Jr., E.M., 1989. Cytosine arabinoside kills postmitotic neurons: evidence that deoxycytidine may have a role in neuronal survival that is independent of DNA synthesis. J. Neurosci. 9 (1), 115–124.
Wang, M.S., Fang, G., Culver, D.G., Davis, A.A., Kich, M.M., Glass, J.D., 2001a. The WldS protein protects against axonal degeneration: a model of gene therapy for peripheral neuropathy. Ann. Neurol. 50 (6), 773–779.
Wang, M., Wu, Y., Culver, D.G., Glass, J.D., 2001b. The gene for slow Wallerian degeneration (Wld(s)) is also protective against vincristine neuropathy. Neurobiol. Dis. 8 (1), 155–161.
Wang, M.S., Davis, A.A., Culver, D.G., Glass, J.D., 2002. WldS mice are resistant to paclitaxel (taxol) neuropathy. Ann. Neurol. 52 (4), 442–447.
Wang, J.T., Medress, Z.A., Barres, B.A., 2012. Axon degeneration: molecular mechanisms of a self-destruction pathway. J. Cell Biol. 196 (1), 7–18.
Wishart, T.M., Macdonald, S.H., Chen, P.E., Shipston, M.J., Coleman, M.P., Gillingwater, T.H., Ribchester, R.R., 2007. Design of a novel quantitative PCR (QPCR)-based protocol for genotyping mice carrying the neuroprotective Wallerian degeneration slow (Wlds) gene. Mol. Neurodegener. 2, 21.
Wishart, T.M., Rooney, T.M., Lamont, D.J., Wright, A.K., Morton, A.J., Jackson, M., Freeman, M.R., Gillingwater, T.H., 2012. Combining comparative proteomics and molecular genetics uncovers regulators of synaptic and axonal stability and degeneration in vivo. PLoS Genet. 8 (8), e1002936.
Xu, Z., Cork, L.C., Griffin, J.W., Cleveland, D.W., 1993. Increased expression of neurofilament subunit NF-L produces morphological alterations that resemble the pathology of human motor neuron disease. Cell 73 (1), 23–33.
Yahata, N., Yuasa, S., Araki, T., 2009. Nicotinamide mononucleotide adenylyltransferase expression in mitochondrial matrix delays Wallerian degeneration. J. Neurosci. 29 (19), 6276–6284.
Yaron, A., Schuldiner, O., 2016. Common and divergent mechanisms in developmental neuronal remodeling and dying back neurodegeneration. Curr. Biol. 26 (13), R628–R639.
Zhang, Z., Pinto, A.M., Wan, L., Wang, W., Berg, M.G., Oliva, I., Singh, L.N., Dengler, C., Wei, Z., Dreyfuss, G., 2013. Dysregulation of synaptogenesis genes antecedes motor neuron pathology in spinal muscular atrophy. Proc. Natl. Acad. Sci. U. S. A. 110 (48), 19348–19353.
Zhu, S., Yang, Y., Hu, J., Qian, L., Jiang, Y., Li, X., Yang, Q., Bai, H., Chen, Q., 2014. Wld (S) ameliorates renal injury in a type 1 diabetic mouse model. Am. J. Physiol. Ren. Physiol. 306 (11), F1348–F1356.

Courtney et al. *Cell Death and Disease* (2019)10:515
https://doi.org/10.1038/s41419-019-1727-6

Cell Death & Disease

ARTICLE Open Access

Reduced P53 levels ameliorate neuromuscular junction loss without affecting motor neuron pathology in a mouse model of spinal muscular atrophy

Natalie L. Courtney[1,2], Alannah J. Mole[1,2], Alison K. Thomson[1,2] and Lyndsay M. Murray[1,2]

Abstract

Spinal Muscular Atrophy (SMA) is a childhood motor neuron disease caused by mutations or deletions within the *SMN1* gene. At endstages of disease there is profound loss of motor neurons, loss of axons within ventral roots and defects at the neuromuscular junctions (NMJ), as evidenced by pathological features such as pre-synaptic loss and swelling and post-synaptic shrinkage. Although these motor unit defects have been widely described, the time course and interdependancy of these aspects of motor unit degeneration are unclear. Recent reports have also revealed an early upregulation of transcripts associated with the P53 signalling pathway. The relationship between the upregulation of these transcripts and pathology within the motor unit is also unclear. In this study, we exploit the prolonged disease timecourse and defined pre-symptomatic period in the $Smn^{2B/-}$ mouse model to perform a temporal analysis of the different elements of motor unit pathology. We demonstrate that NMJ loss occurs prior to cell body loss, and coincides with the onset of symptoms. The onset of NMJ pathology also coincides with an increase in P53-related transcripts at the cell body. Finally, using a tamoxifen inducible P53 knockout, we demonstrate that post-natal reduction in P53 levels can reduce NMJ loss, but does not affect other aspects of NMJ pathology, motor neuron loss or the phenotype of the $Smn^{2B/-}$ mouse model. Together this work provides a detailed temporal description of pathology within motor units of an SMA mouse model, and demonstrates that NMJ loss is a P53-dependant process. This work supports the role for P53 as an effector of synaptic and axonal degeneration in a die-back neuropathy.

Introduction

Spinal Muscular Atrophy (SMA) is a childhood form of motor neuron disease that is caused by homozygous loss of the *SMN1* gene[1,2]. The most common form of this disease has an onset of less than 6 months of age and a life expectancy of under 2 years without significant respiratory support.

The classic morphological features of motor unit pathology in SMA have been extensively characterised and widely used to assess outcome in pre-clinical testing[3]. They include a loss and cytoplasmic shrinkage of motor neuron cell bodies, loss of axons in the ventral roots and pathology at the neuromuscular junctions (NMJ), including denervation, pre-synaptic accumulation of neurofilaments, endplate abnormalities, and muscle fibre atrophy[4,5]. Such defects have been consistently observed in both patients and animal models of SMA at symptomatic stages of disease. How these pathologies throughout the motor unit are temporally related to each other, and to the onset of symptoms, is currently less clear.

Correspondence: Lyndsay M. Murray (Lyndsay.Murray@ed.ac.uk)
[1]Centre for Discovery Brain Sciences, Edinburgh Medical School: Biomedical Sciences, Edinburgh, UK
[2]Euan MacDonald Centre for Motor Neurone Disease Research, University of Edinburgh, Edinburgh, Scotland EH8 9XD, UK
Edited by C. Parish

Official journal of the Cell Death Differentiation Association

It is thought that motor neurons degenerate in a 'die-back' manner, as the pre-synaptic terminal appears to withdraw from the post-synaptic endplate, leaving partially occupied endplates[6]. Furthermore, ventral root axon loss appears to be more severe than motor neuron cell body loss, which is indicative of distal to proximal degeneration of the motor neuron[7]. NMJ defects occur prior to symptom onset in mouse models of SMA suggesting that the NMJ is an 'early pathological target' in SMA[6,8]. However, the temporal and causative relationship of NMJ degeneration to the loss of motor neuron cell bodies is unknown.

It may be suggested that the observed defects at the NMJ in SMA mosue models are reflective of a requirement for Smn in the axon or synapse. However it is currently unclear whether synaptic pathology is a cause or effect of motor neuron death, and it remains possible that synaptic and axonal pathology observed are morphlogical evidence of cell death, as the motor neuron retracts its most distal processes. This idea is supported by the osbervation that there is an increase in transcripts associated with the P53 signalling pathway in motor neuron cell bodies at pre-symptomatic time points in SMA mouse models[4]. As this upregulation is more prominent in selectively vulnerable motor neurons, P53 may play a role in the breakdown of the motor unit[8,9].

P53 plays a crucial role in co-ordinating the cellular response to stress. Initially characterised as a transcription factor, more recent work indicates it can also act as a translational regulator and interact with regulatory RNAs[10–12]. P53 is activated in response to a variety of cues including cell stress and DNA damage, and directs cellular responses, including senescence, DNA repair and apoptosis[13]. Although best characterised as a tumour suppressor, P53 has also been strongly implicated in a range of neurodegenerative disorders, including the adult onset motor neuron disease amyotrophic lateral sclerosis (ALS)[14–19]. An increase in P53 has been reported in postmortem patient spinal cord[20] and an increase in transcripts associated with the P53 signalling pathway have been widely reported in motor neurons and spinal cord tissue from SMA model mice[8,21–24].

The cause and consequence of P53 upregulation in SMA motor neurons is currently unclear. Given its well-established involvement in pro-apoptotic pathways, it is tempting to speculate that this upregulation is reflective of the onset of cell death pathways at the motor neuron. However, a direct interaction between Smn and P53 has also been observed, which was suggestive of an anti-apoptotic role for Smn[25]. The increase in the P53 signalling pathway may therefore be reflective of a primary defect caused by reduced Smn levels. However, since P53 activity appears restricted to selectively vulnerable motor neurons, it is also possible that P53 acts downstream of Smn, in mediating the breakdown of selectively vulnerable motor neuron pools. P53 has also been shown to localise to the synapse where it plays a role in mitochondrial dysfunction and oxidative stress following DNA damage[26]. P53 has also been shown to regulate a range of synaptic genes and that synaptic activity can regulate P53 levels[27,28]. It is therefore unclear what, if any, role P53 has in the onset and progression of motor unit pathology in SMA.

Here, we use the $Smn^{2B/-}$ mouse model of SMA to demonstrate that the onset of NMJ degeneration precedes motor neuron cell body loss, thus confirming that motor neurons degenerate in a distal to proximal manner. We demonstrate that the first evidence of pre-synaptic swelling at the NMJ coincides with an increase in P53 associated transcripts in the spinal cord. In order to investigate the causal effects of P53 pathway activation, we have crossed the $Smn^{2B/-}$ mouse model with a mouse carrying a tamoxifen inducible P53 knockout. Postnatal knockout of P53 led to a reduction in NMJ loss, with no benefit observed upon any other features of NMJ pathology, motor neuron loss or mouse phenotype. In summary, we show that NMJ loss is a consequence of P53 pathway activation, and that partially preserving the structure of the NMJ confers no benefit to the overall health of the motor neuron or mouse. P53 therefore appears to play a role in the breakdown and degeneration of synaptic connections, but does not appear to be central to the motor unit pathology caused by depleted Smn levels.

Results

NMJ pathology precedes motor neuron cell body loss in the $Smn^{2B/-}$ mouse model

To investigate the correlation between NMJ and cell body pathology, we have performed a detailed temporal analysis of the NMJ and motor neuron cell body throughout disease in the $Smn^{2B/-}$ mouse model of SMA[29]. The aim of this work was to give insight into the causal relationship between pathology in these distinct parts of the motor neuron.

In our hands, the $Smn^{2B/-}$ mouse model displays a significant reduction in body weight from around P10, and motor deficits (as evidenced by an increase in the time taken to self right) which are evident at around P9 (Supplementary Fig. 1). It has a life expectancy of around 20 days.

NMJ pathology was assessed in the transversus abdominis muscle (TVA), a muscle which has demonstrated significant defects across all mouse models of SMA which have been studied to date[6,29,30]. Consistent with previous reports[29], analysis of the TVA muscle at P15 revealed significant pre-synaptic pathology, as evidenced by a decrease in the percentage of fully occupied endplates and

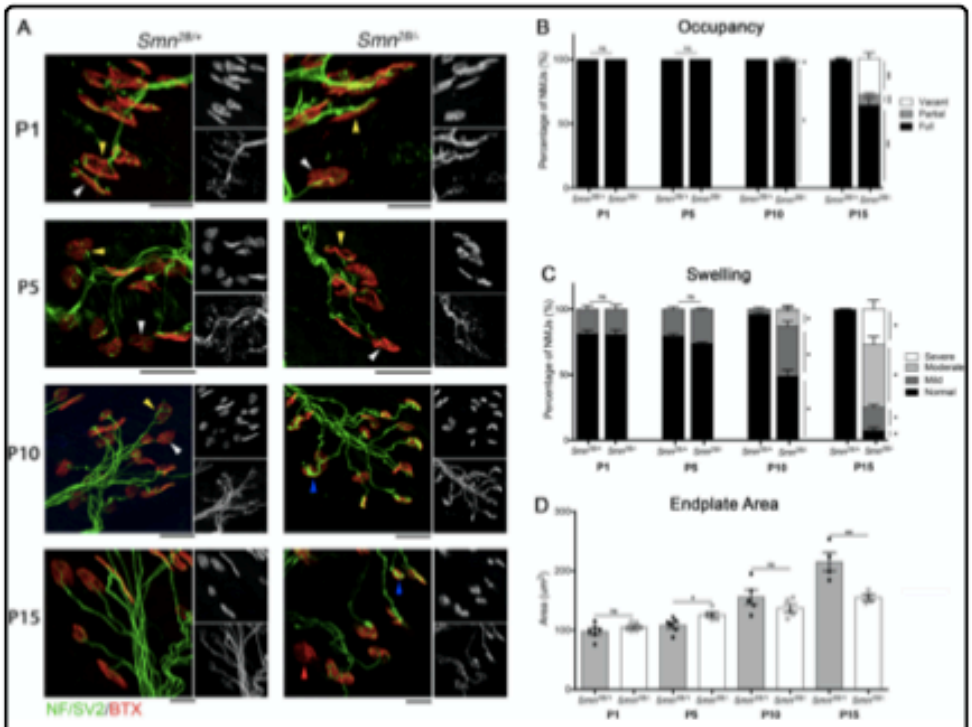

Fig. 1 The onset of NMJ pathology is between P5 and P10 in the *Smn*$^{2B/-}$ mouse model of SMA. a Representative confocal images showing maximum intensity projection of confocal z-stack of NMJs in the TVA of *Smn*$^{2B/-}$ and *Smn*$^{2B/+}$ mice at P1, P5, P10 and P15. Note that white arrowheads show no pre-synaptic swelling, yellow arrowheads show mild pre-synaptic swelling while blue arrowheads show moderate pre-synaptic swelling. Vacant endplates (red arrowhead) are seen at P15 in the *Smn*$^{2B/-}$ mouse model of SMA. The grayscale images show, from top to bottom, BTX and NF/SV2. Scale bar = 20 µm. **b** Bar chart (mean ± SEM) compares the percentage of full, partial and vacant endplates in *Smn*$^{2B/-}$ mice compared to *Smn*$^{2B/+}$ controls. At P1 and P5, 100% of endplates in *Smn*$^{2B/-}$ and *Smn*$^{2B/+}$ mice were fully occupied by the pre-synaptic terminal. At P10, there is significant increase in the percentage of partially occupied endplates and at P15, there is a significant increase in the percentage of both vacant and partially occupied endplates in *Smn*$^{2B/-}$ compared to *Smn*$^{2B/+}$ mice (by Mann–Whitney-U test, *$p < 0.05$, **$p < 0.01$; $n = 4$ mice per genotype). **c** Bar chart (mean ± SEM) compares the stages of pre-synaptic swelling in *Smn*$^{2B/-}$ and *Smn*$^{2B/+}$ mice. There is no significant difference in the level of swelling in *Smn*$^{2B/-}$ mice compared to controls at P1 and P5. At P10, there is a significant increase in the percentage of NMJs with stage 2 and stage 3 swelling in *Smn*$^{2B/-}$ mice. At P15, there is a significant increase in the percentage of pre-synaptic terminals with stage 2, 3 and 4 swelling in *Smn*$^{2B/-}$ mice compared to *Smn*$^{2B/+}$ controls (by Mann–Whitney-U test, *$p < 0.05$; $n = 4$ mice per genotype). **d** The graph (mean ± SEM) compares the average size of endplates in the TVA of *Smn*$^{2B/-}$ mice compared to controls. At P1 and P10 there is no significant difference in the area of post synaptic endplates in *Smn*$^{2B/-}$ mice compared to *Smn*$^{2B/+}$ controls. At P5, there is a small but significant increase in endplate area in *Smn*$^{2B/-}$ mice. At P15 there is a significant decrease in the size of endplates in *Smn*$^{2B/-}$ mice compared to controls (unpaired t-test, *$p < 0.05$, **$p < 0.01$; $n = 4$ mice per genotype)

significant increase the percentage of NMJs displaying mild, moderate or severe swelling (Fig. 1a–c). A time-course analysis of these markers of pre-synaptic pathology revealed that the earliest time point at which they could be detected was at P10. This was the first time point at which denervation could be detected, as evidenced by a small but significant increase in the percentage of partially occupied endplates. There was also a significant increase in the percentage of NMJs with mild or moderate pre-synaptic swelling. There was a trend towards a decrease in endplate size at P10, which was statistically significant by P15 (Fig. 1a–d). Overall, this data suggests that the onset of NMJ pathology occurs after P5 but is present by P10.

As hindlimb weakness is a prominent feature of this mouse model, we also analysed the tibialis anterior muscle. At P10, there was no evidence of denervation

(Supplementary Fig. 2). This confirms that, although there is evidence of NMJ swelling in the P10, it is not more affected than the TVA muscle.

To investigate how pre-synaptic pathology is associated with a loss of motor neuron cell bodies, we quantified the number of motor neurons in the thoracic spinal cord. The first decrease in motor neuron cell body number could be detected at P15, where a 48.4% decrease in motor neuron number was observed (Fig. 2b). Prior to this time point, there was no decrease in the number of motor neurons and indeed, an intriguing trend towards an increase in the number of motor neurons at P5, in the $Smn^{2B/-}$ model compared to controls. There was also a significant decrease in motor neuron cell body area at P15, with no observable difference at P10 or younger (Fig. 2c).

Together with the data above, this demonstrates that NMJ pathology, which was first observed at P10, precedes motor neuron cell body shrinkage and loss, which was first observed at P15. This would suggest that motor neuron pathology does indeed progress in a distal to proximal manner, with NMJ loss preceding motor neuron cell body loss.

NMJ pathology coincides with an increase in P53 related transcripts at the cell body

The data above indicate that NMJ pathology starts between P5 and P10. Previous work has shown that in this mouse model, at P10 there is an increase in transcripts associated with the P53 signalling pathway, including *Fas*, *Pmaip* and *Cdkn1a*[8]. Given the known links between the P53 signalling pathway and the onset of apoptosis, we have previously hypothesised that the increase in these transcripts was associated with the onset of motor neuron cell death. As we have now also observed that NMJ pathology first appears around the same time, it is possible that NMJ pathology is a consequence of P53 pathway activation at the cell body. We were therefore keen to explore the temporal relationship between an increase in transcripts associated with the P53 signalling pathway, and the onset of NMJ pathology.

We first aimed to further narrow down the time point at which NMJ pathology could be first seen. We therefore analysed NMJs in the TVA muscle from P7 mice (Fig. 3a–c). This revealed no evidence of denervation, but a significant increase in NMJs with mild pre-synaptic swelling. From this, we conclude denervation starts between P7 and P10 and is preceded by pre-synaptic swelling, which starts between P5 and P7.

Previous work has shown the transcripts *Fas*, *Pmaip* and *Cdkn1a* are significantly increased at P10 in this mouse model[8]. We therefore analysed spinal cords at P5 and P7. This revealed no increase in transcripts at P5, but a significant increase in *Fas* and *Pmaip* at P7 (Fig. 3d, e). Together this data shows a remarkable temporal correlation between the onset of NMJ swelling and the increase in transcripts associated with the P53 signalling pathway.

Inhibition of the P53 signalling pathway reduces NMJ loss without affecting phenotype of the $Smn^{2B/-}$ mouse model

Thus far we show that NMJ pathology precedes cell body loss, but coincides with the increase in transcripts associated with the P53 signalling pathway. To investigate the relationship between P53 pathway activation and NMJ pathology, we aimed to inhibit the P53 signalling pathway by generating an inducible P53 knockout mouse on an SMA model background. We generated this model by introducing a P53 gene flanked by loxP sites ($P53^{fl/fl}$) as well as cre-recombinase under the control of the oestrogen receptor promoter (CAG-Cre) onto the $Smn^{2B/-}$ background. The resultant $Smn^{2B/-}$; $P53^{fl/fl}$; *CAG-Cre* mice are equivalent to the original $Smn^{2B/-}$ mouse model, however upon the administration of tamoxifen, the Cre-recombinase causes the recombination of the P53 gene to render it non-functional.

For these experiments we have four genotypes of mice: $Smn^{2B/+}$ control mice who have the $P53^{fl/fl}$ gene but do not carry CAG-Cre ($Smn^{2B/+}$; $P53^{+/+}$); $Smn^{2B/-}$ mice who have the $P53^{fl/fl}$ gene but do not carry CAG-Cre ($Smn^{2B/-}$; $P53^{+/+}$); $Smn^{2B/+}$ control mice who have the $P53^{fl/fl}$ gene and CAG-Cre ($Smn^{2B/+}$; $P53^{-/-}$); and $Smn^{2B/-}$ mice who have the $P53^{fl/fl}$ gene and CAG-Cre ($Smn^{2B/-}$; $P53^{-/-}$) (Fig. 4a). Upon administration of tamoxifen, the P53 gene in only the latter two groups of mice will undergo recombination and essentially be 'knocked out'. Tamoxifen (75 mg/kg) was administered at P4 and P5. This time point was selected as it was prior to any evidence of P53 pathway activation in the spinal cord. Quantitative PCR results on cDNA from spinal cord from P15 mice revealed P53 levels were reduced by around 50% in both $Smn^{2B/+}$; $P53^{-/-}$ and $Smn^{2B/-}$; $P53^{-/-}$ mice compared to their respective controls (Fig. 4b).

To determine the effect of P53 knockout on the phenotype of the $Smn^{2B/-}$ mouse, weight and motor performance were assessed daily following administration of tamoxifen at P4 and P5. Knockout of P53 did not improve the phenotype of $Smn^{2B/-}$ mice (Fig. 4c–e). Indeed, both groups with reduced P53 levels displayed a small but significant decrease in body weight. There was a trend towards poorer performance in the time to right test for both $Smn^{2B/-}$ groups at P8, but there was no significant difference between $Smn^{2B/-}$; $P53^{+/+}$ and $Smn^{2B/-}$; $P53^{-/-}$ at either P8 or P10. Furthermore, in the 'turn around' test, although $Smn^{2B/-}$;$P53^{-/-}$ mice performed significantly worse at P13, 14 and 15 compared to $Smn^{2B/+}$; $P53^{-/-}$ controls, there was no significant difference between $Smn^{2B/-}$; $P53^{+/+}$ and $Smn^{2B/-}$; $P53^{-/-}$ mice. This data demonstrate that reduction of P53 confers no benefit

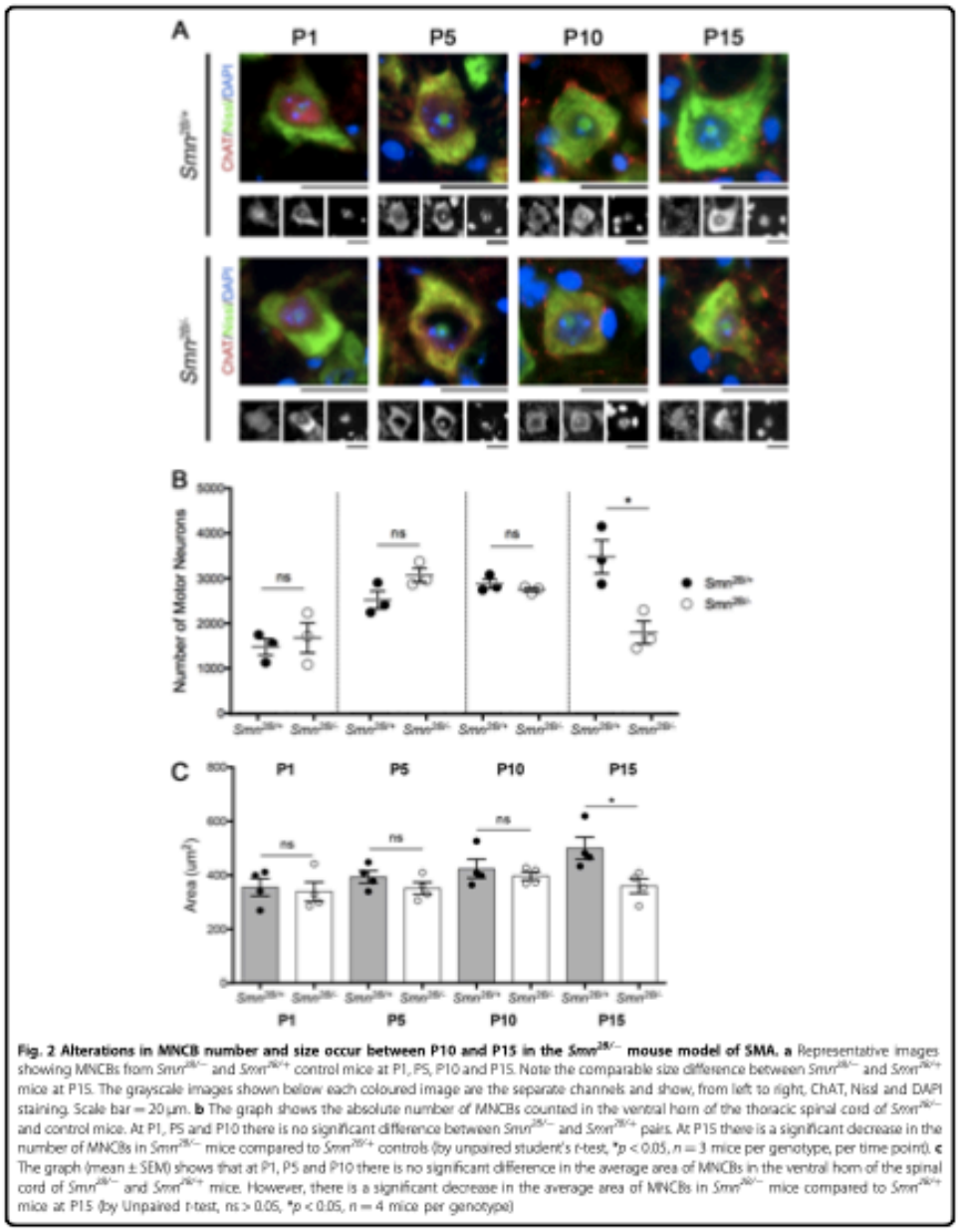

Fig. 2 Alterations in MNCB number and size occur between P10 and P15 in the *Smn*$^{2B/-}$ mouse model of SMA. a Representative images showing MNCBs from *Smn*$^{2B/-}$ and *Smn*$^{2B/+}$ control mice at P1, P5, P10 and P15. Note the comparable size difference between *Smn*$^{2B/-}$ and *Smn*$^{2B/+}$ mice at P15. The grayscale images shown below each coloured image are the separate channels and show, from left to right, ChAT, Nissl and DAPI staining. Scale bar = 20 µm. **b** The graph shows the absolute number of MNCBs counted in the ventral horn of the thoracic spinal cord of *Smn*$^{2B/-}$ and control mice. At P1, P5 and P10 there is no significant difference between *Smn*$^{2B/-}$ and *Smn*$^{2B/+}$ pairs. At P15 there is a significant decrease in the number of MNCBs in *Smn*$^{2B/-}$ mice compared to *Smn*$^{2B/+}$ controls (by unpaired student's *t*-test, *$p < 0.05$, $n = 3$ mice per genotype, per time point). **c** The graph (mean ± SEM) shows that at P1, P5 and P10 there is no significant difference in the average area of MNCBs in the ventral horn of the spinal cord of *Smn*$^{2B/-}$ and *Smn*$^{2B/+}$ mice. However, there is a significant decrease in the average area of MNCBs in *Smn*$^{2B/-}$ mice compared to *Smn*$^{2B/+}$ mice at P15 (by Unpaired *t*-test, ns > 0.05, *$p < 0.05$, $n = 4$ mice per genotype)

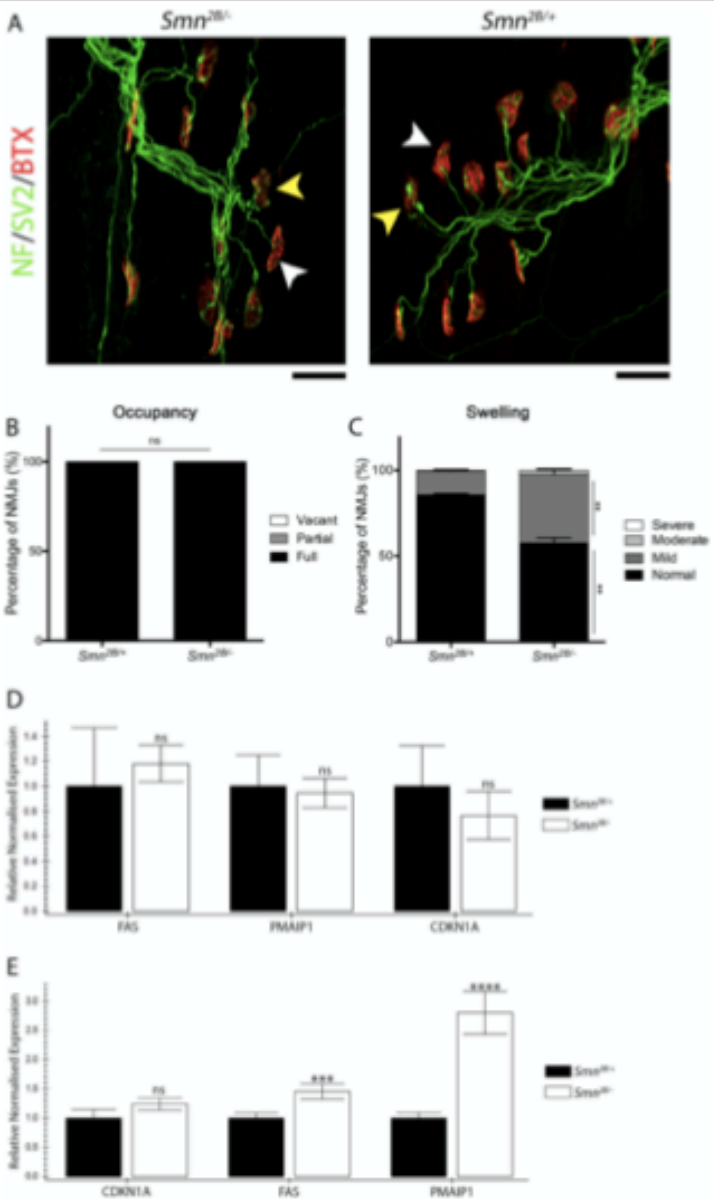

Fig. 3 (See legend on next page.)

(see figure on previous page)

Fig. 3 Activation of the P53 signalling pathway coincides with the onset of NMJ pathology. a Representative images of NMJs in the TVA of P7 $Smn^{2B/-}$ and $Smn^{2B/+}$ mice. White arrowheads show stage 1 swelling and yellow arrowheads show stage 2 pre-synaptic swelling. Scale bar = 20 µm. **b** Bar chart (mean ± SEM) shows that at P7, 100% of endplates in the TVA of $Smn^{2B/-}$ and $Smn^{2B/+}$ mice were fully occupied by the pre-synaptic terminal of an axon. (Mann–Whitney-U test, ns > 0.05; n = 4 mice per genotype). **c** Bar chart (mean ± SEM) compares the stages of pre-synaptic swelling in $Smn^{2B/-}$ mice compared to $Smn^{2B/+}$ controls. There is a significant decrease in the percentage of pre-synaptic terminals with stage 1 swelling and increase in stage 2 swelling in the TVA of $Smn^{2B/-}$ mice compared to $Smn^{2B/+}$ controls at P7. (Mann Whitney-U test, **p < 0.01; n = 4 mice per genotype). **d** The bar chart (mean ± SEM) shows that there is no significant difference in the expression of transcripts involved in the P53 signalling pathway in the thoracic spinal cord of $Smn^{2B/-}$ mice compared to $Smn^{2B/+}$ mice at P5 (by Mann–Whitney-U test; ns > 0.05; n = 4 per genotype). **e** The bar chart (mean ± SEM) shows that there is a significant increase in the expression of transcripts involved in the P53 signalling pathway, specifically in Cdkn1A and Pmaip1, in the thoracic spinal cord of $Smn^{2B/-}$ mice compared to $Smn^{2B/+}$ mice at P7 (by Mann–Whitney-U test; ns > 0.05; *n* = 4 per genotype)

to the motor performance of $Smn^{2B/-}$ mice, and if anything, makes it worse.

We next assessed the impact of reduced P53 levels on motor neuron cell body loss. Reduced P53 levels did not affect motor neuron cell body loss or shrinkage. Quantification of the number of motor neurons in the T4–T8 segments of the spinal cord at P15 revealed a loss of 55.2 ± 9.6% and 52.0 ± 1.7% in $Smn^{2B/-}$; $P53^{+/+}$ and $Smn^{2B/-}$; $P53^{-/-}$ compared to their respective controls (Fig. 5b). There was no significant difference between $Smn^{2B/-}$; $P53^{+/+}$and $Smn^{2B/-}$; $P53^{-/-}$ mice. There was a trend for motor neurons from $Smn^{2B/-}$; $P53^{+/+}$ and $Smn^{2B/-}$; $P53^{-/-}$ mice to be smaller compared to their respective controls but again there was no significant difference between $Smn^{2B/-}$; $P53^{+/+}$ and $Smn^{2B/-}$; $P53^{-/-}$ mice (Fig. 5c). Overall, in the $Smn^{2B/-}$ mouse model, reduced P53 levels do not appear to reduce motor neuron cell body loss or shrinkage.

Finally, we assessed the effect of reduced P53 levels of NMJ pathology. This revealed that reduced P53 levels decreased NMJ loss (Fig. 6). Quantification of the percentage of fully occupied endplates at P15 in $Smn^{2B/-}$; $P53^{-/-}$ mice revealed a significant increase (Fig. 6b). This was accompanied by a significant decrease in the percentage of vacant endplates (Fig. 6c). Interestingly, examination of pre-synaptic swelling, endplate maturation and endplate area revealed no improvement in $Smn^{2B/-}$; $P53^{-/-}$ compared to $Smn^{2B/-}$; $P53^{+/+}$ (Fig. 6d–f). Together this data suggest that NMJ loss is a consequence of P53 pathway activation, and dissociates NMJ loss from other markers of pathology at the NMJ, which are P53 independent.

Discussion

Here we have shown that pathology at the NMJ precedes loss or shrinkage of motor neurons at the level of the cell body. A loss of NMJs was first observed at P10, whereas motor neuron loss was not observed until P15. This first evidence of NMJ swelling appears to coincide with an increase in transcripts associated with the P53 signalling pathway in the spinal cord. Importantly, post-natal 'knockout' of P53 led to a reduction in NMJ loss, without affecting other aspects of NMJ pathology, motor neuron loss or affecting the phenotype of the mouse. Together the work provides a detailed temporal description of pathology within the motor units of an SMA mouse model, and demonstrates that NMJ loss is a P53-dependent process. This work supports the role for P53 as an effector of synaptic and axonal degeneration in a die-back neuropathy.

Temporal and mechanistic dissociation of motor unit pathology in SMA

The protracted lifespan of the $Smn^{2B/-}$ mouse, compared to the majority of other commonly used mouse models, has allowed us to examine the evolution of different aspects of motor unit pathology, and revealed a temporal dissociation between them. Motor neuron loss and shrinkage is one of the last detectable morphological abnormalities and evident only after symptom onset. Swelling of the pre-synaptic terminal preceded NMJ loss and post-synaptic changes, and also preceded the emergence of symptoms. This is in agreement with studies on the $SOD1^{G93A}$ mouse model of adult onset motor neuron disease in which pre-synaptic defects were shown to coincide with symptom onset, and motor neuron cell body loss was observed as a late event[31]. Swelling appeared to coincide with the earliest time point that increased levels of *Fas*, and *Pmaip* can be detected. Given the known links of these transcripts with the P53 signalling pathway, this suggests that there is a correlation between the onset of NMJ abnormalities and P53 pathway activation. Together this data suggest that, with regards to motor unit pathology, the first detectable abnormality is swelling of NMJs, which coincides with transcriptional changes at the cell body. This is then followed by denervation, then by post-synaptic shrinkage and loss and shrinkage of the motor neuron cell body.

The reduction in P53 levels allows us to more carefully dissect the interdependency of these early events. Reduced P53 levels had no effect on swelling, but did reduce denervation. This shows that pre-synaptic swelling is a

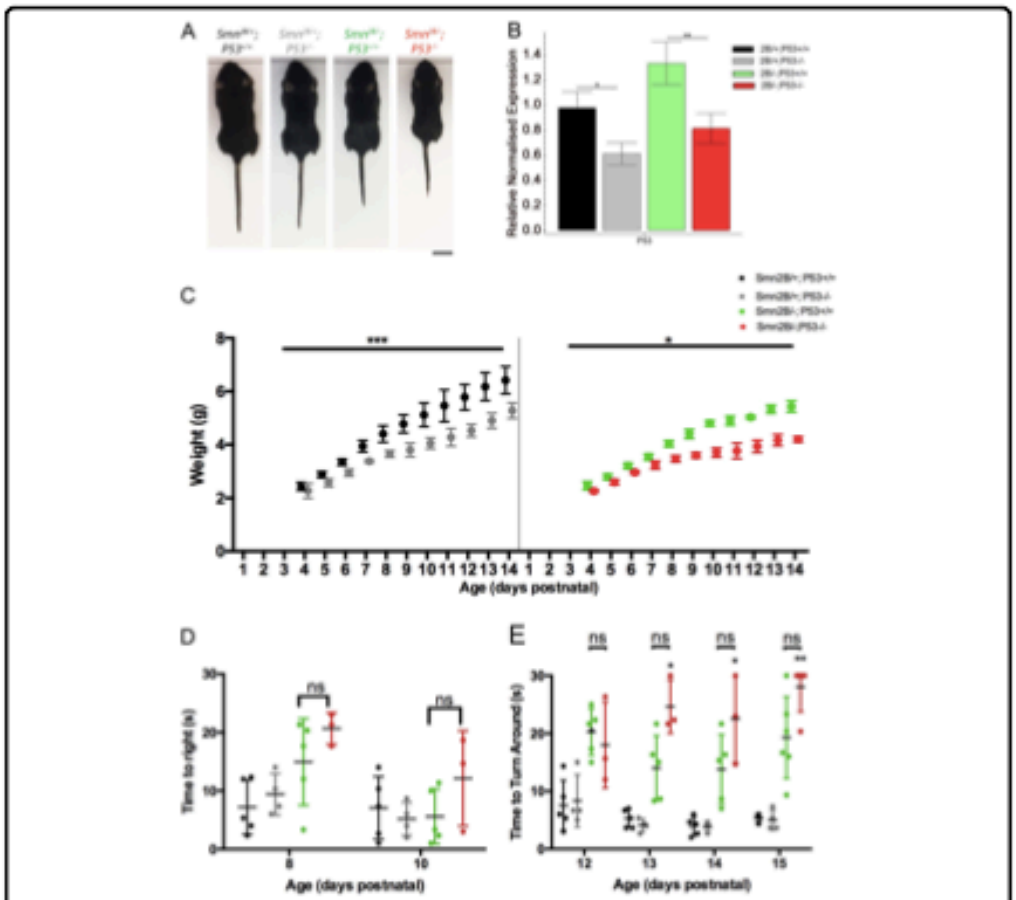

Fig. 4 Reduction in P53 levels does not ameliorate the phenotype of the $Smn^{2B/-}$ mouse model. a Representative images of mice with the various genotypes within experimental litters at P15. Scale bar = 1 cm. **b** Bar chart (mean ± SEM) shows that there is a significant decrease in P53 at the transcript level in the spinal cord of $Smn^{2B/+}$; $P53^{-/-}$ mice compared to $Smn^{2B/+}$; $P53^{+/+}$ mice and in $Smn^{2B/-}$; $P53^{-/-}$ mice compared to $Smn^{2B/-}$; $P53^{+/+}$ mice (by Mann–Whitney-U test, *p < 0.05, **p < 0.001; n = 3 for $Smn^{2B/-}$; $P53^{+/+}$, n = 4 for all other genotypes). **c** The graph (mean ± SEM) shows body weight in $Smn^{2B/+}$; $P53^{+/+}$ and $Smn^{2B/+}$; $P53^{-/-}$ on the left and $Smn^{2B/-}$; $P53^{+/+}$ and $Smn^{2B/-}$; $P53^{-/-}$ on the right. There is a significant reduction of weight in mice that are $P53^{-/-}$ in both $Smn^{2B/+}$ and $Smn^{2B/-}$ groups, compared to $P53^{+/+}$ mice. Two-way ANOVA with multiple comparison *P < 0.05; *P < 0.001 (**d**, **e**) Graphs (mean ± SEM, with individual data points showing mean of three trials for individual animals) shows performance in the time to right test (**d**) and the time to turn around test (**e**) for $Smn^{2B/+}$; $P53^{+/+}$, $Smn^{2B/-}$; $P53^{+/+}$, $Smn^{2B/+}$; $P53^{-/-}$ and $Smn^{2B/-}$; $P53^{-/-}$ at P8 and P10 (**d**) and between P12 and P15 (**e**). In both tests, at all-time points, there is no significant difference in motor performance between $Smn^{2B/-}$; $P53^{-/-}$ and $Smn^{2B/-}$; $P53^{+/+}$ mice. At P13, 14 and 15, $Smn^{2B/-}$; $P53^{-/-}$ displayed a significantly longer time to turn around than $Smn^{2B/+}$; $P53^{-/-}$ controls. (Kruskal Wallis with Dunn's multiple comparison test; ns > 0.05, *p < 0.05, **p < 0.01, n = 5 for $Smn^{2B/+}$; $P53^{+/+}$ and $Smn^{2B/-}$; $P53^{+/+}$; n = 4 for $Smn^{2B/+}$; $P53^{-/-}$; n = 3 for $Smn^{2B/-}$; $P53^{-/-}$ for all time points except P15 where *n* = 4 for $Smn^{2B/+}$; $P53^{+/+}$ and $Smn^{2B/+}$; $P53^{-/-}$; n = 6 for $Smn^{2B/-}$; $P53^{+/+}$ and *n* = 5 for $Smn^{2B/-}$; $P53^{-/-}$

P53-independent event, whilst denervation is a P53-dependant event. Thereby, whilst the pathology present at the NMJ is not dependent upon the P53 pathway, the actual process of pre-synaptic withdrawal is.

A role for P53 in mediating synaptic and axonal degeneration

The data presented here demonstrate that knockout of P53 can reduce NMJ loss, and therefore suggest that axon

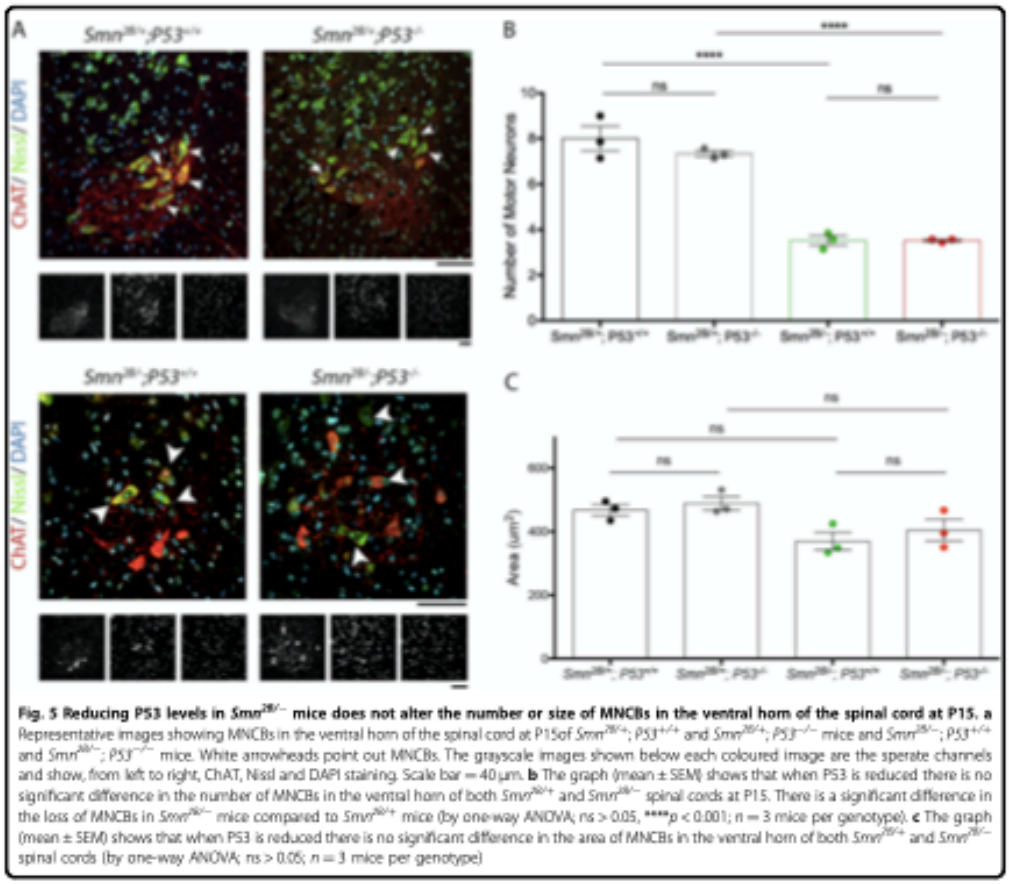

Fig. 5 Reducing P53 levels in *Smn*$^{2B/-}$ mice does not alter the number or size of MNCBs in the ventral horn of the spinal cord at P15. a Representative images showing MNCBs in the ventral horn of the spinal cord at P15of *Smn*$^{2B/+}$; *P53*$^{+/+}$ and *Smn*$^{2B/+}$; *P53*$^{-/-}$ mice and *Smn*$^{2B/-}$; *P53*$^{+/+}$ and *Smn*$^{2B/-}$; *P53*$^{-/-}$ mice. White arrowheads point out MNCBs. The grayscale images shown below each coloured image are the sperate channels and show, from left to right, ChAT, Nissl and DAPI staining. Scale bar = 40 µm. **b** The graph (mean ± SEM) shows that when P53 is reduced there is no significant difference in the number of MNCBs in the ventral horn of both *Smn*$^{2B/+}$ and *Smn*$^{2B/-}$ spinal cords at P15. There is a significant difference in the loss of MNCBs in *Smn*$^{2B/-}$ mice compared to *Smn*$^{2B/+}$ mice (by one-way ANOVA; ns > 0.05, ****$p < 0.001$; $n = 3$ mice per genotype). **c** The graph (mean ± SEM) shows that when P53 is reduced there is no significant difference in the area of MNCBs in the ventral horn of both *Smn*$^{2B/+}$ and *Smn*$^{2B/-}$ spinal cords (by one-way ANOVA; ns > 0.05; $n = 3$ mice per genotype)

and synaptic degeneration in SMA is a P53-dependant process. P53 has been identified in synaptosomes of cortical neurons[26]. Synaptosomes from P53 knockout mice displayed reduced levels of reactive oxygen species and preserved mitochondrial membrane potential following exposure to the topoisomerase-II inhibitor etoposide[26]. Furthermore, mitochondria in isolated synaptosomes from P53 knockout mice showed greater resistance to excitotoxic or oxidative insults, and inhibition of P53 decreased synapse loss in hippocampal neuron cultures following treatment with etoposide. This clearly shows that P53 can have a local role in mediating synapse loss and mitochondrial dysfunction. An increase in P53 phosphorylation has also been observed following trophic withdrawal, a stimulus known to result in axon pruning[32]. How then, might P53 mediate the removal of axonal and synaptic compartments of the cell? A significant body of work has implicated pro-apoptotic proteins and pathways in the process of axon degeneration[33]. Interestingly, this includes developmental axon pruning, which demonstrates that the activation of apoptotic cascades can be compartment specific and that mediating removal of axonal and synaptic parts of the neuron allow the motor neuron to persist. Indeed, it has been suggested that as P53 has the ability to regulate both pro- and anti-apoptotic transcripts, it can serve as a key regulator for compartmental degeneration in neurons[32,34]. Further work is clearly required to identify the molecular effectors of P53-dependant synaptic degeneration in SMA, and determine whether P53 is an important mediator of axonal and synaptic degeneration in other neurodegenerative contexts.

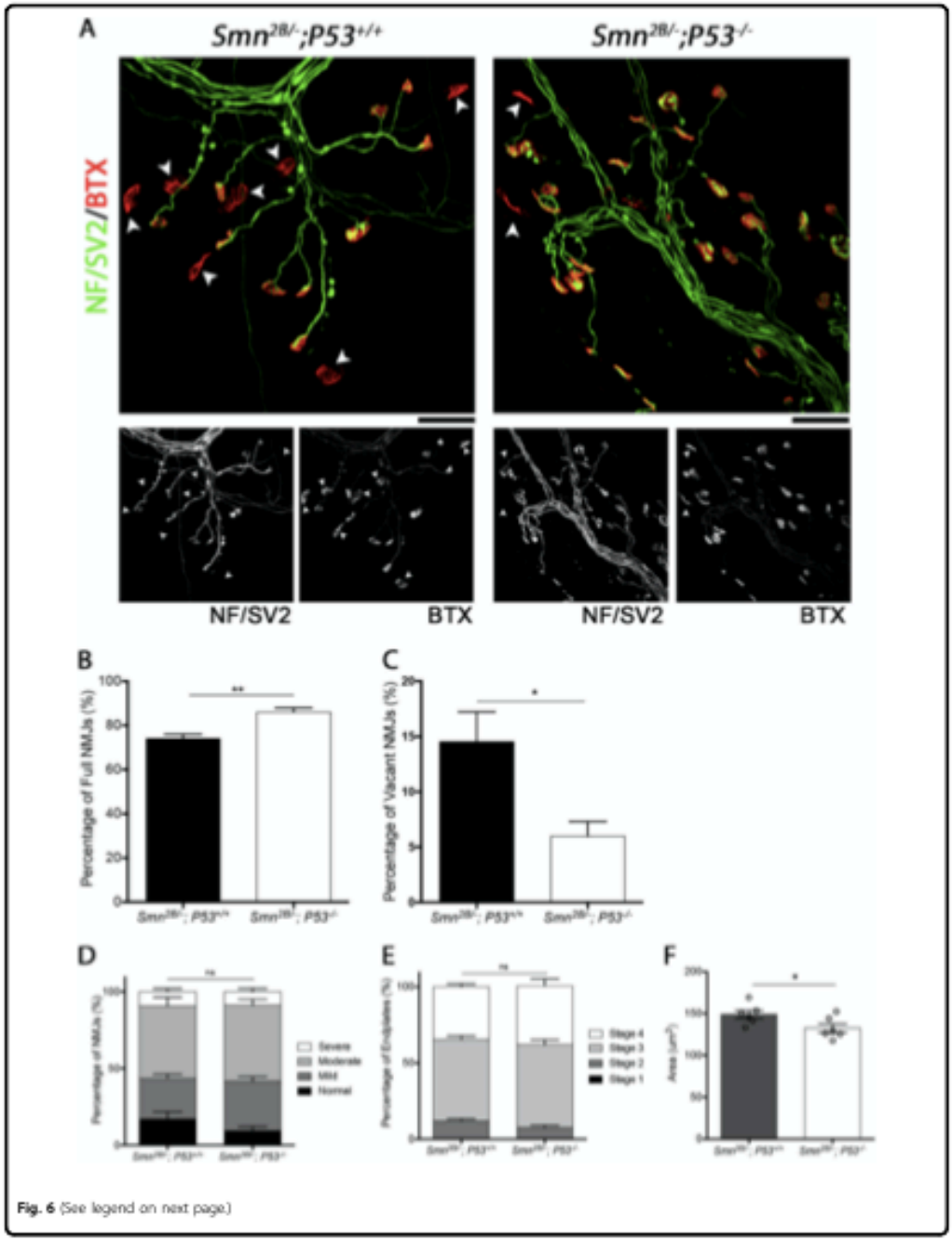

Fig. 6 (See legend on next page.)

(see figure on previous page)
Fig. 6 Reduction in P53 reduces NMJ loss but does not affect other morphological signs of degeneration. a Representative images showing NMJs from the TVA of $Smn^{2B/-}$; $P53^{+/+}$ and $Smn^{2B/-}$; $P53^{-/-}$ mice. Note that the white arrowheads point out vacant endplates. Scale bar = 40 µm. **b** The graph (mean ± SEM) shows that a reduction in P53 decreases denervation in the TVA muscle, with $Smn^{2B/-}$; $P53^{-/-}$ mice showing a significant increase in the percentage of fully occupied endplates compared to $Smn^{2B/-}$; $P53^{+/+}$ mice (by Mann–Whitney-U test; **p < 0.01; n = 6 muscles per genotype). **c** In addition, this graph (mean ± SEM) shows a significant decrease in the percentage of vacant endplates in $Smn^{2B/-}$; $P53^{-/-}$ mice compared to $Smn^{2B/-}$; $P53^{+/+}$ mice (by Mann–Whitney-U test; *p < 0.05; n = 6 muscles per genotype). **d** The graph (mean ± SEM) shows that there is no significant difference in the level of pre-synaptic swelling in the TVA of $Smn^{2B/-}$; $P53^{+/+}$ and $Smn^{2B/-}$; $P53^{-/-}$ mice (by Mann–Whitney-U test; ns > 0.05; n = 6 muscles per genotype). **e** The graph (mean ± SEM) shows that there is no significant difference in the maturity of endplates in the TVA of $Smn^{2B/-}$; $P53^{+/+}$ and $Smn^{2B/-}$; $P53^{-/-}$ mice (by Mann–Whitney-U test; ns > 0.05; n = 6 muscles per genotype). **f** The graph (mean ± SEM) shows that there is a small but significant decrease in the area of endplates in the TVA of $Smn^{2B/-}$; $P53^{+/+}$ and $Smn^{2B/-}$; $P53^{-/-}$ mice (by Unpaired T-test; *p < 0.05; n = 6 muscles per genotype)

P53 independent motor neuron loss in SMA

An upregulation of transcripts associated with the P53 signalling pathway has been consistently observed in response to reduced Smn levels[8,21–24]. Due to the well-established links between P53 and caspase mediated apoptosis, this has led to the suggestion that motor neurons in SMA are dying by a P53 mediated form of apoptosis. In this canonical pathway, an increase in cell stress, brought about by a variety of triggers, causes the phosphorylation and activation of P53, which in turn act as a transcription factor for a number of pro-apoptotic transcripts including *Bax*, *Bak* and *Pmaip*. These factors cause an increase in the permeability of the mitochondrial membrane, resulting in a release of pro-apoptotic factors, leading to the activation of effector caspases. This includes caspase 3, which mediates the cleavage of cellular components and is essential for the chromatin condensation and DNA fragmentation, all of which are morphological hallmarks of apoptosis. The data presented here demonstrate that inhibition of P53 does not reduce motor neuron loss, suggesting that motor neuron loss in this mouse model is P53 independent. Although this is in contrast to recent reports showing P53 inhibition could reduce motor neuron loss in the $Smn^{-/-}$; *SMN2*; *SMNΔ7* mouse model of SMA, this finding is in agreement with previous work showing knockout of P53 has no beneficial effect on a mouse model of SMA[9,35]. There are also interesting parallels to work on the SOD^{G93A} mouse model of ALS, showing knockout of P53 has no effect upon motor neuron loss[36], despite the observation that P53 levels are elevated in postmortem tissue, cellular models and mouse models of ALS[16,17,19,37–40]. Whilst this could be due to a degree of redundancy between P53 and related pathways, it does demonstrate that motor neurons in SMA can die by a P53 independent mechanism.

Studies detailing apoptotic motor neurons in SMA are notably lacking. Although some have reported features consistent with apoptosis in postmortem and cellular and animal models, work using immunohistochemical approaches to label apoptotic revealed no difference between SMA and control patients in either fetal or newborn individuals with SMA[20,35,41,42]. However, knockout of the pro-apoptotic protein Bax in a mouse model of SMA did reduce motor neuron loss[43]. More work is required to define whether motor neurons in SMA are degenerating via a caspase dependant apoptosis, and investigate P53 independent up-stream regulators of this process. Identifying this mechanism will be of fundamental importance if we are to gain a thorough understanding of motor unit pathogenesis in SMA.

Materials and methods

Mouse maintenance

$Smn^{2B/2B}$ (originating from the Kothary Laboratory, Ottawa Hospital Research Institute) mice were crossed with $Smn^{+/-}$ (Strain: 10921, Jackson Laboratories) to produce $Smn^{2B/-}$ experimental mice and $Smn^{2B/+}$ controls. $Smn^{+/-}$ mice were crossed with mice carrying the $P53^{fl/fl}$ and *CAG-Cre* alleles (generously donated by Dr Luke Boulter, Kevin Myant and You-Ying Chou, University of Edinburgh) to obtain $Smn^{+/-}$; $P53^{fl/fl}$; *CAG-Cre* mice. $Smn^{2B/2B}$ mice were interbred with mice carrying the $P53^{fl/fl}$ allele to obtain $Smn^{2B/2B}$; $P53^{fl/fl}$ mice. $Smn^{+/-}$; $P53^{fl/fl}$; *CAG-Cre* and $Smn^{2B/2B}$; $P53^{fl/fl}$ mice were interbred to produce $Smn^{2B/+}$; $P53^{fl/fl}$; *CAG-Cre*, $Smn^{2B/+}$; $P53^{fl/fl}$, $Smn^{2B/-}$; $P53^{fl/fl}$; *CAG-Cre and* $Smn^{2B/-}$; $P53^{fl/fl}$ mice. All genotyping was performed using standard PCR protocols. Homozygosity for the $P53^{fl}$ allele was confirmed using q-PCR. All mice were maintained at the University of Edinburgh animal facilities on a C57Bl6 background. Mice aged over P10 were sacrificed by overdose of inhalation anaesthetic or a rising CO_2 and death was confirmed by exsanguination from the carotid artery. Mice under P10 were decapitated under terminal anaesthesia and death was confirmed by exsanguination from the carotid artery. Endstage of disease was defined by over 10% loss of weight over a period of 48 h. Since no phenotypic differences have been noted between male and female mice, experiments were not controlled for gender. All experiments were performed in accordance with the UK Home Office.

Tamoxifen

Tamoxifen (Sigma-Aldrich) was dissolved in corn oil to a concentration of 20 mg/ml. Tamoxifen solution was administered to litters of mice at P4 and P5 using oral gavage at a dose of 75 mg/kg.

Phenotypic analysis

The 'time to right' test was carried out on mice at P8 and P10. Mice were placed on their back and the time it took for them to right themselves (turn to be on all four paws) was noted, with a maximum of 30 sec and an average of three attempts.

The 'turn around test' was used on mice daily aged over P12. This test involved placing mice, head down on a gridded cage top that was at a 45° angle. The time it took for mice to turn 180° to face up was noted, with a maximum of 30 sec and an average of three attempts.

Neuromuscular junction labelling and quantification

Muscles were immediately dissected from recently sacrificed mice and fixed in 4% Paraformaldehyde (PFA; Electron Microscopy Science) in PBS for 15 min. Post-synaptic AChRs were labelled with α-bungarotoxin (BTX, 1:250; tetramethylrhodimine conjugate, Life Technologies) for 2 h. Muscles were permeabilised in 2% Triton X-100 in PBS for 30 min, then blocked in 4% bovine serum albumin (BSA)/1% Triton X-100 in PBS for 30 min before incubation overnight in primary antibodies [Neurofilament, 1:50 (NF; 2H3)—Developmental Studies Hybridoma Bank; synaptic vesicle protein 2, 1:100 (SV2)—Developmental Studies Hybridoma Bank] and visualised with secondary antibodies [AlexaFluor-488 rabbit anti-mouse at 1:250, Jackson]. Muscles were then whole-mounted in Mowiol (Sigma).

All images were quantified using a Leica inverted fluorescent microscope using single and dual wavelength filter sets allowing separate and simulations visualisation of red and green channels. The percentage of fully occupied endplates was determined by classifying each endplate in a given field of view either fully occupied (pre-synaptic terminal (SV2 and NF) completely overlies endplate (BTX)), partially occupied (pre-synaptic terminal only partially covers endplate (BTX)), or vacant (no pre-synaptic label overlies endplate). For pre-synaptic swelling, all NMJs were classified as having no swelling, mild (evidence of some axonal swelling and/or pre-synaptic swelling that does not obscure the endplate), moderate (evidence of clear axonal swelling and significant pre-synaptic swelling that is beginning to obscure the endplate) or severe (significant and obvious swelling along the length of the axon and severe swelling around the pre-synaptic terminal, which obscures the endplate). Endplate size was quantified using ImageJ software. Endplate maturation was quantified using a stage 1–4 categorisation, where stage 4 endplates are immature and have a plaque-like appearance, stage 3 endplates are developing from a plaque-like structure with folds visible on the plaque, stage 2 endplates are developing into a pretzel-like structure with folds and perforations visible and stage 1 endplates have a mature pretzel-like structure. At least three fields of view were analysed per muscle totalling >80 endplates per muscle. All Quantification was performed with researcher blind to genotype of material. All example images are z-stack projections and were obtained using a Nikon confocal microscope at ×40 magnification and images had pixel size of 1024 × 1024.

Motor neuron immuno-fluorescence and quantification

Spinal cords were removed from recently sacrificed mice and fixed in 4% PFA (Electron Microscopy Science) for 4 h. They were immersed in 30% sucrose for 48 h prior to embedding in 50% OCT; 15% Sucrose in PBS mixture. For temporal analysis of $Smn^{2B/-}$ mice, the ventral horn of thoracic (T1-T12) spinal cords were sectioned longitudinally at 10 µM and alternate sections were subjected to Nissl/ChAT labelling. For analysis of $P53^{fl/fl}$ mice, thoracic (T4-T8) spinal cords were sectioned coronally at 10 µM and every tenth section was subjected to Nissl/ChAT labelling.

Sections were washed in PBS, permeabilised in 0.3% Triton X-100 in PBS for 30 min and blocked in 0.1% Power Block (100×, Biogenex Laboratories, HK085–5K) in PBS for 10 min. Sections were incubated in ChAT (Goat anti-choline acetyl-transferase; Merck Millipore; 1:100) primary antibody in 0.3% Triton X-100; 1% Bovine Serum Albumin (BSA) in PBS at 4 °C, for three nights. Secondary antibody (AlexaFluor 555 Donkey anti-Goat; Life Technologies; 1:250) was applied for 2 h at a dilution of 1:250 at room temperature. Sections were then stained with DAPI (Life Technologies; 1:1000) and fluorescent Nissl stain (NeuroTrace; Life Technologies: 1:100). Sections were mounted in Mowiol (Sigma).

For quantification of motor neuron number, the number of ChAT positive cells with a visible nucleolus were quantified in each section. For Fig. 2, this was done on longitudinal section, quantifying every second section. For Fig. 5, this was done on coronal section, for every 30th section. For motor neuron cell body area, images were captured on a standard fluorescent microscope (Leica DM8) and the perimeter of each cell was traced using ImageJ software. All data was assembled in Microsoft Excel and analysed using GraphPad Prism.

qRT-PCR

RNA was extracted using a micro RNeasy Kit (Qiagen) and 1 µg of RNA was used to perform reverse

transcriptase using the RT[2] First Strand Kit (Qiagen). SYBR gene based Q-RT-PCR was performed using pre-optimised primers purchased from Qiagen. Amplification was performed using KAPA SYBR fast universal PCR mastermix as per manufacturer's instructions on a BioRad CFX connect real-time PCR detection system. Relative gene expression was calculated using the $2^{-\Delta\Delta cT}$ formula[44]. Relative levels are expressed normalised to Actin (F: CCGTCAGGCAGCTCATAGCTCTTC; R: CTGAACCCTAAGGCCAACCGT), GusB (F: GGCTGGTGACCTACTGGATTT; R: TTGGCACTGGGAACCTGAAGT) and YWHAZ (F: TTGATCCCCAATGCTTCGC; R:: CAGCAACCTCGGCCAAGTAA).

Acknowledgements
We are grateful to Luke Boulter, Kevin Myant and You-Ying Chau for generous donation of mice carrying CAG-Cre and floxed P53 alleles. This work was supported by grants from Cure SMA (grant number MU1415); Fight SMA; Muscular Dystrophy Association (grant number 417757); Tenovus Scotland (E15/4), Newlife foundation for disabled children (SG/14-15/08), and the Institute Strategic Support Fund (SSF3) at the University of Edinburgh, funded by the Wellcome Trust (ref IS3-R2.23). N.L.C. is a PhD student funded by the Euan McDonald Centre for Motor Neuron Disease Research. A.L.M. is a PhD student funded by the Anatomical Society.

Author details
[1]Centre for Discovery Brain Sciences, Edinburgh Medical School: Biomedical Sciences, Edinburgh, UK. [2]Euan MacDonald Centre for Motor Neurone Disease Research, University of Edinburgh, Edinburgh, Scotland EH8 9XD, UK

Conflict of interest
The authors declare that they have no conflict of interest.

Supplementary Information accompanies this paper at (https://doi.org/10.1038/s41419-019-1727-6).

Received: 19 October 2018 Revised: 23 April 2019 Accepted: 28 May 2019
Published online: 04 July 2019

References

1. Lefebvre, S. et al. Identification and characterization of a spinal muscular atrophy-determining gene. *Cell* **80**, 155–165 (1995).
2. Rodrigues, N. R. et al. Deletions in the survival motor neuron gene on 5q13 in autosomal recessive spinal muscular atrophy. *Hum. Mol. Genet.* **4**, 631–634 (1995).
3. Bebee, T. W., Dominguez, C. E. & Chandler, D. S. Mouse models of SMA: tools for disease characterization and therapeutic development. *Hum. Genet.* **131**, 1277–1293 (2012).
4. Goulet, B. B., Kothary, R. & Parks, R. J. At the "junction" of spinal muscular atrophy pathogenesis: the role of neuromuscular junction dysfunction in SMA disease progression. *Curr. Mol. Med.* **13**, 1160–1174 (2013).
5. Tisdale, S. & Pellizzoni, L. Disease mechanisms and therapeutic approaches in spinal muscular atrophy. *J. Neurosci.* **35**, 8691–8700 (2015).
6. Murray, L. M. et al. Selective vulnerability of motor neurons and dissociation of pre- and post-synaptic pathology at the neuromuscular junction in mouse models of spinal muscular atrophy. *Hum. Mol. Genet.* **17**, 949–962 (2008).
7. Cifuentes-Diaz, C. et al. Neurofilament accumulation at the motor endplate and lack of axonal sprouting in a spinal muscular atrophy mouse model. *Hum. Mol. Genet.* **11**, 1439–1447 (2002).
8. Murray, L. M., Beauvais, A., Gibeault, S., Courtney, N. L. & Kothary, R. Transcriptional profiling of differentially vulnerable motor neurons at pre-symptomatic stage in the Smn (2b/−) mouse model of spinal muscular atrophy. *Acta Neuropathol. Commun.* **3**, 55 (2015).
9. Simon, C. M. et al. Converging mechanisms of p53 activation drive motor neuron degeneration in spinal muscular atrophy. *Cell Rep.* **21**, 3767–3780 (2017).
10. Chaudhary, R. & Lal, A. Long noncoding RNAs in the p53 network. *Wiley Interdiscip. Rev. RNA* **8**, https://doi.org/10.1002/wrna.1410 (2017).
11. Marcel, V., Catez, F. & Diaz, J. J. p53, a translational regulator: contribution to its tumour-suppressor activity. *Oncogene* **34**, 5513–5523 (2015).
12. Mei, Y. & Wu, M. Noncoding RNAs regulating p53 and c-Myc signaling. *Adv. Exp. Med. Biol.* **927**, 337–365 (2016).
13. Marcel, V., Nguyen Van Long, F. & Diaz, J. J. 40 years of research put p53 in translation. *cancers* **10**, https://doi.org/10.3390/cancers10050152 (2018).
14. Chang, J. R. et al. Role of p53 in neurodegenerative diseases. *Neurodegener. Dis.* **9**, 68–80 (2012).
15. de la Monte, S. M., Sohn, Y. K. & Wands, J. R. Correlates of p53- and Fas (CD95)-mediated apoptosis in Alzheimer's disease. *J. Neurol. Sci.* **152**, 73–83 (1997).
16. Martin, L. J. p53 is abnormally elevated and active in the CNS of patients with amyotrophic lateral sclerosis. *Neurobiol. Dis.* **7**, 613–622 (2000).
17. Ranganathan, S. & Bowser, R. p53 and cell cycle proteins participate in spinal motor neuron cell death in ALS. *Open Pathol. J.* **4**, 11–22 (2010).
18. Szybinska, A. & Leniak, W. P53 dysfunction in neurodegenerative diseases - the cause or effect of pathological changes? *Aging Dis.* **8**, 506–518 (2017).
19. Vogt, M. A. et al. TDP-43 induces p53-mediated cell death of cortical progenitors and immature neurons. *Sci. Rep.* **8**, 8067 (2018).
20. Simic, G. et al. Ultrastructural analysis and TUNEL demonstrate motor neuron apoptosis in Werdnig-Hoffmann disease. *J. Neuropathol. Exp. Neurol.* **59**, 398–407 (2000).
21. Baumer, D. et al. Alternative splicing events are a late feature of pathology in a mouse model of spinal muscular atrophy. *PLoS Genet.* **5**, e1000773 (2009).
22. Jangi, M. et al. SMN deficiency in severe models of spinal muscular atrophy causes widespread intron retention and DNA damage. *Proc. Natl Acad. Sci. USA* **114**, E2347–E2356 (2017).
23. Staropoli, J. F. et al. Rescue of gene-expression changes in an induced mouse model of spinal muscular atrophy by an antisense oligonucleotide that promotes inclusion of SMN2 exon 7. *Genomics* **105**, 220–228 (2015).
24. Zhang, Z. et al. SMN deficiency causes tissue-specific perturbations in the repertoire of snRNAs and widespread defects in splicing. *Cell* **133**, 585–600 (2008).
25. Young, P. J. et al. A direct interaction between the survival motor neuron protein and p53 and its relationship to spinal muscular atrophy. *J. Biol. Chem.* **277**, 2852–2859 (2002).
26. Gilman, C. P. et al. p53 is present in synapses where it mediates mitochondrial dysfunction and synaptic degeneration in response to DNA damage, and oxidative and excitotoxic insults. *Neuromolecular Med.* **3**, 159–172 (2003).
27. Lau, D. & Bading, H. Synaptic activity-mediated suppression of p53 and induction of nuclear calcium-regulated neuroprotective genes promote survival through inhibition of mitochondrial permeability transition. *J. Neurosci.* **29**, 4420–4429 (2009).
28. Merlo, P. et al. p53 prevents neurodegeneration by regulating synaptic genes. *Proc. Natl Acad. Sci. USA* **111**, 18055–18060 (2014).
29. Bowerman, M., Murray, L. M., Beauvais, A., Pinheiro, B. & Kothary, R. A critical smn threshold in mice dictates onset of an intermediate spinal muscular atrophy phenotype associated with a distinct neuromuscular junction pathology. *Neuromuscul. Disord.* **22**, 263–276 (2012).
30. Thomson, S. R. et al. Morphological characteristics of motor neurons do not determine their relative susceptibility to degeneration in a mouse model of severe spinal muscular atrophy. *PLoS ONE* **7**, e52605 (2012).
31. Gould, T. W. et al. Complete dissociation of motor neuron death from motor dysfunction by Bax deletion in a mouse model of ALS. *J. Neurosci.* **26**, 8774–8786 (2006).
32. Maor-Nof, M. et al. Axonal degeneration is regulated by a transcriptional program that coordinates expression of pro- and anti-degenerative factors. *Neuron* **92**, 991–1006 (2016).
33. Geden, M. J. & Deshmukh, M. Axon degeneration: context defines distinct pathways. *Curr. Opin. Neurobiol.* **39**, 108–115 (2016).
34. Lassus, P., Ferlin, M., Piette, J. & Hibner, U. Anti-apoptotic activity of low levels of wild-type p53. *EMBO J.* **15**, 4566–4573 (1996).

35. Tsai, M. S., Chiu, Y. T., Wang, S. H., Hsieh-Li, H. M. & Li, H. Abolishing Trp53-dependent apoptosis does not benefit spinal muscular atrophy model mice. *Eur. J. Hum. Genet.* **14**, 372–375 (2006).
36. Kuntz, C., Kinoshita, Y., Beal, M. F., Donehower, L. A. & Morrison, R. S. Absence of p53: no effect in a transgenic mouse model of familial amyotrophic lateral sclerosis. *Exp. Neurol.* **165**, 184–190 (2000).
37. Barbosa, L. F. et al. Increased SOD1 association with chromatin, DNA damage, p53 activation, and apoptosis in a cellular model of SOD1-linked ALS. *Biochim. Biophys. Acta* **1802**, 462–471 (2010).
38. de la Monte, S. M., Sohn, Y. K., Ganju, N. & Wands, J. R. P53- and CD95-associated apoptosis in neurodegenerative diseases. *Lab. Invest.* **78**, 401–411 (1998).
39. Eve, D. J., Dennis, J. S. & Citron, B. A. Transcription factor p53 in degenerating spinal cords. *Brain Res.* **1150**, 174–181 (2007).
40. Wang, J. et al. TDP-43 interaction with the intracellular domain of amyloid precursor protein induces p53-associated apoptosis. *Neurosci. Lett.* **569**, 131–136 (2014).
41. Ito, Y., Shibata, N., Saito, K., Kobayashi, M. & Osawa, M. New insights into the pathogenesis of spinal muscular atrophy. *Brain Dev.* **33**, 321–331 (2011).
42. Piras, A. et al. Inhibition of autophagy delays motoneuron degeneration and extends lifespan in a mouse model of spinal muscular atrophy. *Cell Death. Dis.* **8**, 3223 (2017).
43. Tsai, M. S. et al. Abolishing Bax-dependent apoptosis shows beneficial effects on spinal muscular atrophy model mice. *Mol. Ther.* **13**, 1149–1155 (2006).
44. Livak, K. J. & Schmittgen, T. D. Analysis of relative gene expression data using real-time quantitative PCR and the 2(-Delta Delta C[T]) method. *Methods* **25**, 402–408 (2001).

1.37 *Appendix 4: Mitochondrial protein levels, number and activity at P15 versus P24 in central tissues*

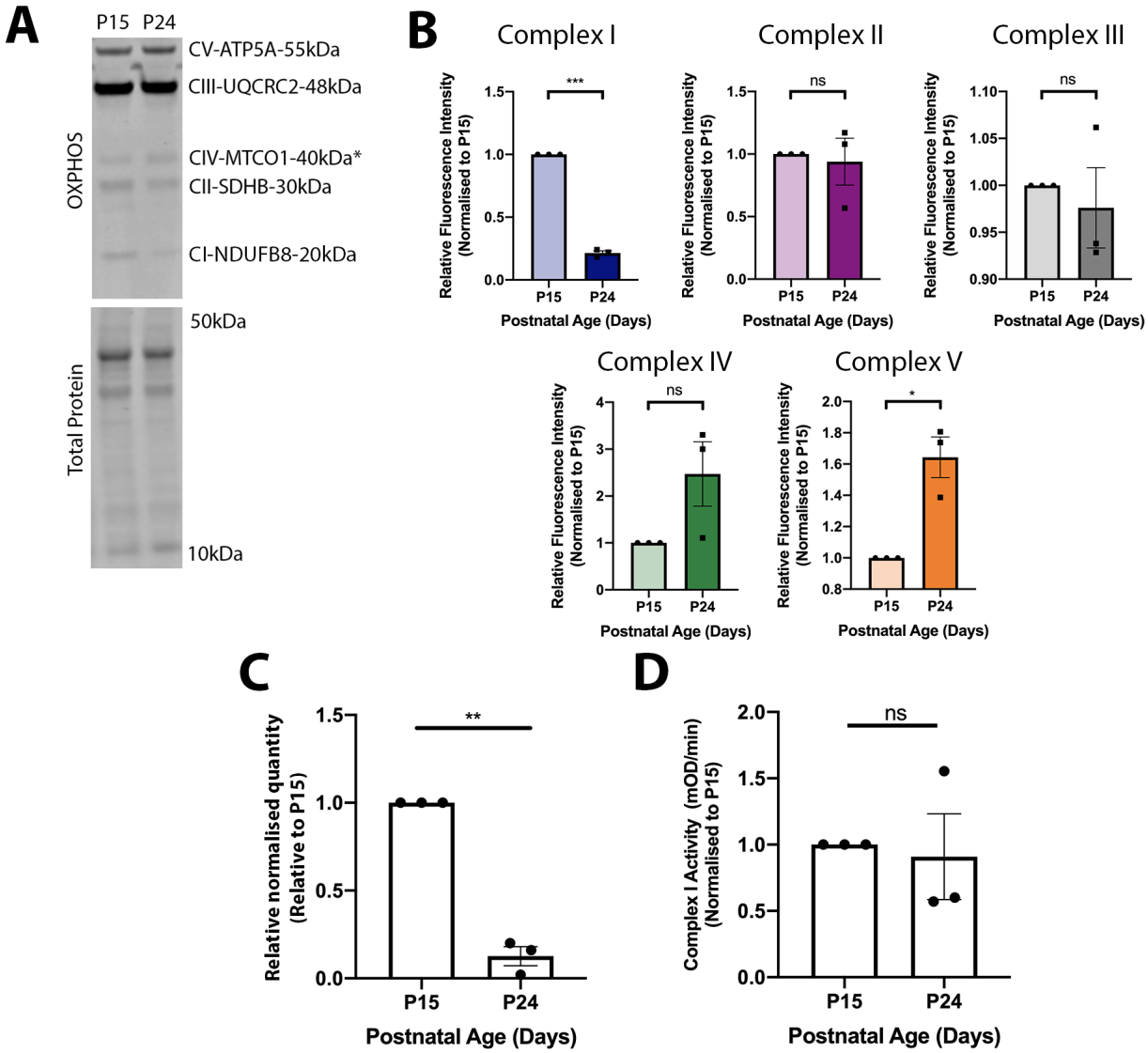

Figure A1: Mitochondrial protein levels, number and activity at P12 versus P24 in spinal cord. (**A**) Western blot result using antibodies against Complex I, II, III, IV and V subunits on spinal cord from P15 and P24 mice, with total protein staining used as a loading control. (**B**) Quantification of western blot against different complex subunits in spinal cord. Data is expressed normalised to loading control and relative to levels at P15. Ns = not significant, $p > 0.1$, * $p = 0.04$, *** $p = 0.0004$; one-sample t-test. (**C**) Relative normalised quantity of mtDNA as determined by qPCR and $2^{-\Delta\Delta CT}$ method in spinal cord at P15 versus P24. Note that no increase in mtDNA is seen. Data is normalised to H19 and expressed relative to P15. ** $P = 0.0039$; one-sample t-test (**D**) Complex I activity as determined by enzyme linked immunosorbent assay (ELISA) at P15 versus P24 in spinal cord. NADH dehydrogenase activity was measured kinetically over 60 min and the rate was determined as a change in optical density over time, and expressed normalised to P15. Ns = not significant, $p = 0.80$. In all cases, n=3 biological replicates. Error bars represent mean ± SEM.

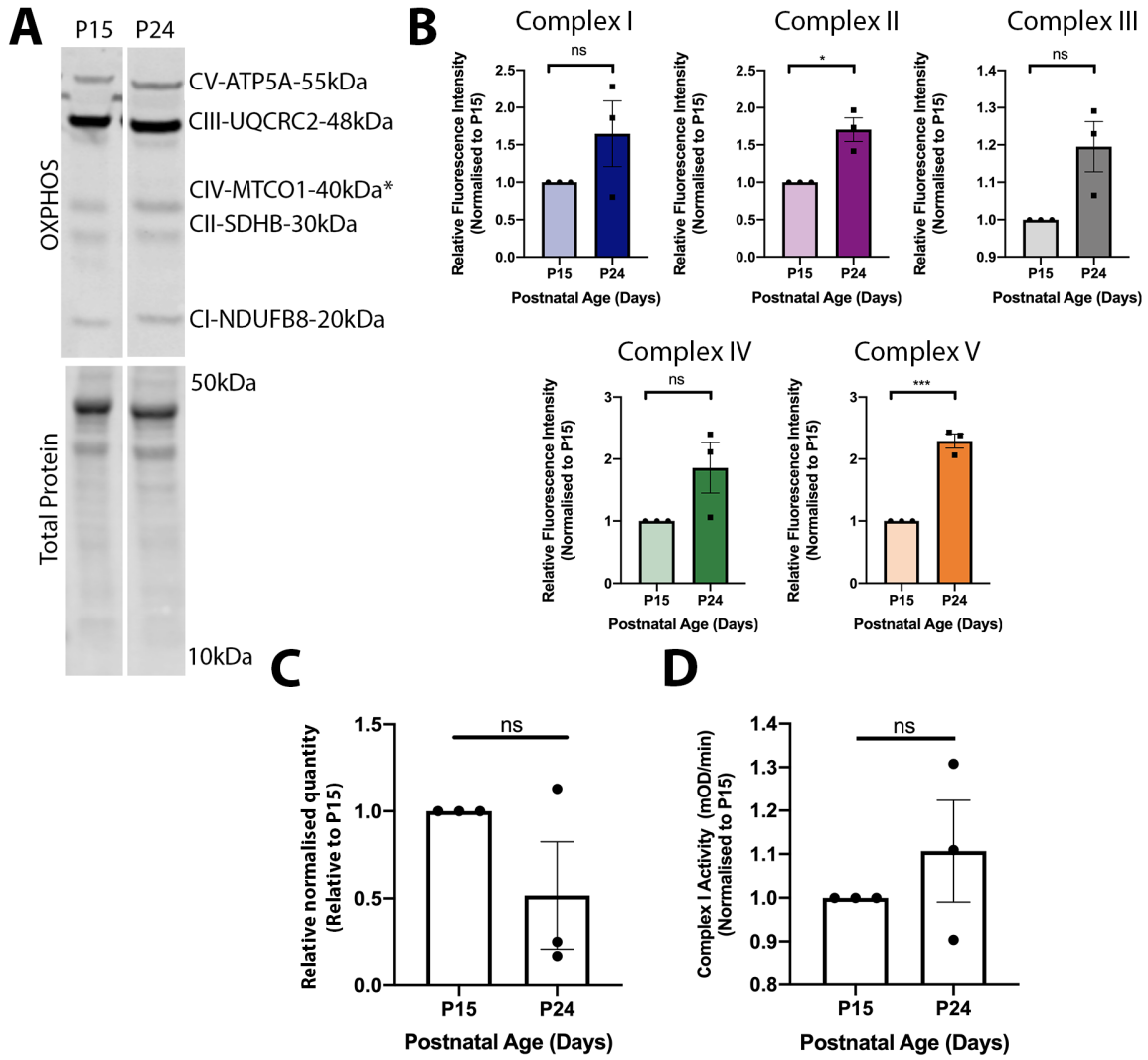
A
P15
P24
OXPHOS
CV-ATP5A-55kDa
CIII-UQCRC2-48kDa
CIV-MTCO1-40kDa*
CII-SDHB-30kDa
CI-NDUFB8-20kDa
Total Protein
50kDa
10kDa
B
Complex I
Complex II
Complex III
Complex IV
Complex V
Relative Fluorescence Intensity (Normalised to P15)
Postnatal Age (Days)
ns
*
***
C
Relative normalised quantity (Relative to P15)
D
Complex I Activity (mOD/min) (Normalised to P15)

Figure A2: Mitochondrial protein levels, number and activity at P12 versus P24 in brain. (**A**) Western blot result using antibodies against Complex I, II, III, IV and V subunits on brain from P15 and P24 mice, with total protein staining used as a loading control. (**B**) Quantification of western blot against different complex subunits in brain. Data is expressed normalised to loading control and relative to levels at P15. Ns = not significant, $p > 0.1$, * $p = 0.047$, ** $p = 0.008$; one-sample t-test. (**C**) Relative normalised quantity of mtDNA as determined by qPCR and $2^{-\Delta\Delta CT}$ method in brain at P15 versus P24. Note that no increase in mtDNA is seen. Data is normalised to H19 and expressed relative to P15. ** $P = 0.0039$; one-sample t-test (**D**) Quantification of Complex I activity as determined by enzyme linked immunosorbent assay (ELISA) at P15 versus P24 in brain. NADH dehydrogenase activity was measured kinetically over 60 min and the rate was determined as a change in optical density over time, and expressed normalised to P15. Ns = not significant, $p = 0.46$. In all cases, n=3 biological replicates. Error bars represent mean ± SEM.